

2019-07-09

Boron-Nitrogen Analogues of Indene Containing Hydrocarbons

Morgan, Matthew Michael

Morgan, M. M. (2019). Boron-Nitrogen Analogues of Indene Containing Hydrocarbons (Doctoral thesis, University of Calgary, Calgary, Canada). Retrieved from <https://prism.ucalgary.ca>.
<http://hdl.handle.net/1880/110608>

Downloaded from PRISM Repository, University of Calgary

UNIVERSITY OF CALGARY

Boron-Nitrogen Analogues of Indene Containing Hydrocarbons

by

Matthew Michael Morgan

A THESIS

SUBMITTED TO THE FACULTY OF GRADUATE STUDIES
IN PARTIAL FULFILMENT OF THE REQUIREMENTS FOR THE
DEGREE OF DOCTOR OF PHILOSOPHY

GRADUATE PROGRAM IN CHEMISTRY

CALGARY, ALBERTA

JULY, 2019

© Matthew Michael Morgan 2019

Abstract

Boron-nitrogen (BN) containing polycyclic aromatic hydrocarbons represent an important class of compounds of fundamental and applied interest. Despite their prevalence in main group chemistry, there remain few ways to efficiently synthesize large quantities of BN containing aromatic species.

We developed a method for the preparation of 3-bora-9aza-indene heterocycles based on zirconocene mediated functionalization of the *ortho*-CH bonds of pyridines. Unlike other methods, the boron center in these heterocycles remains functionalized with a chloride ligand allowing the compounds to be further elaborated through halide abstraction or reduction. The utility of the method was demonstrated by applying it towards the preparation of 1,5-dibora-4a,8a-diaza BN analogs of the intriguing hydrocarbon *s*-indacene starting from 2,5-dimethylpyrazine. This allowed us to experimentally and computationally compare the BN doped derivative to the all-carbon analogue, providing new knowledge on the effect of main group substitutions on bonding in aromatic compounds.

The developed synthetic method also provided us access to a new BN doped indenide species in large scale that allowed for its reactivity to be examined in depth. It was found that the reactivity of the nucleophilic indenide depended on which electrophile it was treated with. This divergent reactivity was investigated through reactions with alkyl halides and carbon dioxide and the mechanisms determined were supported through computational methods.

Inspired by the properties of the indacene species, we targeted derivatives of BN doped dihydroindeno[1,2-*b*]fluorene. They were synthesized via electrophilic borylation, a mildly air-sensitive technique, and the end products were handled readily under atmospheric conditions. Through transmetallation via diarylzinc reagents a series of derivatives were synthesized which

show broad absorption profiles and frontier energy levels amenable to their use in organic solar cell devices. Exploratory device parameters were studied and show moderate results with PCEs reaching 2% showing the possibility of molecules containing this framework in organic electronic devices.

Acknowledgements

I would first and foremost like to thank my supervisor Prof. Warren Piers without whom this thesis would not have been possible. From accepting me as a summer student with no research experience to providing me the opportunity to rejoin the group after my “break-year” your honesty and drive to produce high quality science has shaped me into the chemist I am today (for better or worse).

I would like to extend my thanks to my examination committee members, Prof. Roland Roesler, Prof. Todd Sutherland, Prof. Casey Hubert, and my external examiner Prof. Joe Gilroy for taking the time to read my thesis and attend my defense. I owe a great amount of this thesis to the great instrumental staff that we have at the University of Calgary, including Michelle Forgeron, Wade White, and Johnson Li. In addition, I have been fortunate to receive generous financial support from the National Sciences and Engineering Research Council of Canada (NSERC) and the University of Calgary which allowed me to focus on research without excessive financial stress.

Finishing a PhD is a task that no one should have to do on their own; fortunately, I had a network of amazing people around me the entire time. As one of the longest serving members of the Piers lab I have had the opportunity to work with countless amazing chemists, all of whom have had a great impact on my professional and personal growth. I would like to thank Drs. Adam Marwitz, Adrian Houghton, and Juan Araneda who taught me all the synthetic chemistry skills I would need for graduate school. I have spent my degree surrounded by great lab mates but must thank Joel Smith in particular, for his help and friendship from the first day we started in the lab together to today.

Finally, I would like to thank my family and friends who were by my side during the entire journey. From visiting me in Calgary, to filling the NMR with me on Christmas day, to many late nights spent playing video games I am grateful for the abundance of support I have received from outside of the lab. I am deeply thankful to my wife Melissa Wilson for your love, support, and amazing attitude that has kept me positive even through the difficult times over the course of this degree, and into the future.

*For Dawn and Randy Morgan,
always inspiring and developing my curiosity.*

Table of Contents

Abstract	ii
Acknowledgements	iv
Table of Contents	vii
List of Tables	ix
List of Figures	xi
List of Schemes	xvi
List of Symbols, Abbreviations, and Nomenclature	xviii
List of Numbered Compounds	xx
 CHAPTER 1: INTRODUCTION	 1
1.1 Main group element containing aromatic hydrocarbons	1
1.2 Boron-nitrogen containing aromatics	1
1.3 Established synthetic pathways to BN aromatics	3
1.3.1 Methods for 1,2-azaborine synthesis	3
1.3.2 Borylative cyclization	7
1.3.3 Electrophilic borylation	9
1.4 Zirconocene mediated synthesis of main group heteroaromatics	12
1.5 Aromaticity and antiaromaticity	15
1.6 Thesis Goals	18
 CHAPTER TWO: ZIRCONOCENE-BASED METHODS FOR THE PREPARATION OF BN INDENES: APPLICATION TO THE SYNTHESIS OF 1,5-DIBORA-4A,8A- DIAZA-1,2,3,5,6,7-HEXAARYL-4,8-DIMETHYL-S-INDACENES. ⁸⁹	 19
2.1 Preface	19
2.2 Author Contributions	19
2.3 Abstract	20
2.4 Introduction	20
2.5 Results and Discussion	21
2.6 Conclusions	53
 CHAPTER 3: DIVERGENT REACTIVITY OF NUCLEOPHILIC 1-BORA-7A- AZAINDENIDE ANIONS. ¹³²	 55
3.1 Preface	55
3.2 Author Contributions	55
3.3 Abstract	56
3.4 Introduction	56
3.5 Results and Discussion	58
3.5.1 Synthesis and Characterization of Indenide Species	58
3.5.2 Reactivity of 6 with Carbon Electrophiles	62
3.5.3 Reactivity of 6 with Carbon Dioxide	68
3.5.5 CO ₂ Functionalization	76
3.6 Conclusions	81
 CHAPTER 4: BORON-NITROGEN DOPED DIHYDROINDENO[1,2-B]FLUORENE DERIVATIVES AS ACCEPTORS IN ORGANIC SOLAR CELLS.	 82

4.1 Preface	82
4.2 Author Contributions	82
4.3 Abstract	83
4.4 Introduction.....	83
4.4.1 Organic Solar Cells.....	83
4.4.2 Boron-Nitrogen containing Active Species.....	87
Results.....	92
Conclusion	113
CHAPTER 5: CONCLUSIONS AND FUTURE WORK.....	115
5.1 Conclusion	115
5.2 Future Work	116
5.2.1 Purpose-built electron acceptor units	116
5.2.2 Synthesis of other isomers of indenofluorene	119
5.2.3 Pentacene derivatives synthesized by electrophilic borylation	122
CHAPTER 6 EXPERIMENTAL DETAILS	125
6.1 General Considerations	125
6.2 Experimental Details for Chapter 2	126
6.3 Experimental Details for Chapter 3	139
Experimental Details for Chapter 4	149
Crystallographic data collection and refinement parameters of isolated compounds	157
APPENDIX: PERMISSIONS.....	170
REFERENCES	171

List of Tables

Table 2-1. NICS Calculations of 4^H and 6^H	38
Table 2-2. Comparison of bond lengths from molecular structures of isomers 8.....	42
Table 2-3. NICS and GIMIC analysis on indacene species.....	46
Table 2-4. Integrated diatropic and paratropic magnetically induced current contributions to the net current strengths in inequivalent bonds of Π - C_{2h} and I^H [in nA T ⁻¹]. See Figures 2-8b and 2-8e, respectively, for color coding of bonds.	50
Table 2-5. Calculated low energy electronic transitions of 9^{tBu} and Π^{tBu} (1,3,5,7- <i>tert</i> -butyl- <i>s</i> -indacene) at TDDFT/BH-LYP/def-TZVP level of theory.....	51
Table 3-1. Nucleus independent chemical shifts (at PBE0/def-TZVP level of theory) for five-membered (A) and six-membered (B) rings of indenide, 6^H , 13^H , 10^H , and $10'$	59
Table 4-1. Electrochemical data for 15^{tBu} and 15^{NAr}	101
Table 4-2. Electrochemical data for 16^R and 17^R	108
Table 4-3. Organic solar cell data of the PTB7-Th, PBDB-T, PPDT2FBT: 16^{tBu} 10 mg/mL blends (1:1) cast from chlorobenzene. Average values are given with the best results in obtained in brackets	111
Table 6-1. Crystal Data Collection and Refinement Parameters for Complex $2B(C_6F_5)_4$	157
Table 6-2. Crystal Data Collection and Refinement Parameters for Complex 3.....	158
Table 6-3. Crystal Data Collection and Refinement Parameters for Complex 4^H	159
Table 6-4. Crystal Data Collection and Refinement Parameters for Complex 5^H	160
Table 6-5. Crystal Data Collection and Refinement Parameters for Complex 6^H	161
Table 6-6. Crystal Data Collection and Refinement Parameters for Complex 7^H	162
Table 6-7. Crystal Data Collection and Refinement Parameters for Complex <i>cis</i> - 8^H	163
Table 6-8. Crystal Data Collection and Refinement Parameters for <i>trans</i> - 8^H	164
Table 6-9. Crystal Data Collection and Refinement Parameters for Complex 9^{tBu}	165
Table 6- 10. Crystal Data Collection and Refinement Parameters for Complex 10^H	166
Table 6-11. Crystal Data Collection and Refinement Parameters for Complex 13^H	167
Table 6-12. Crystal Data Collection and Refinement Parameters for Complex 15^{tBu}	168

Table 6-13. Crystal Data Collection and Refinement Parameters for Complex 16 ^{tBu}	169
---	-----

List of Figures

Figure 1-1. Examples of BN containing aromatic compounds.....	2
Figure 1-2. Three possible isomers of azaborines	3
Figure 1-3. Bio-active molecules containing the 1,2-azaborine core.	7
Figure 1-4. The six possible isomers of contiguous BN substituted naphthalene.	9
Figure 1-5. Boron-nitrogen doped aromatics synthesized by electrophilic borylation.....	11
Figure 1-6. Diagram showing induced ring currents when benzene is exposed to an external magnetic field.....	17
Figure 2-1. Simplified structure of BN- <i>s</i> -indacene and the two bonding motifs discussed for the all-carbon analogue	21
Figure 2-2. Thermal ellipsoid (50%) diagram of the molecular structure of [Cp ₂ ZrMe(4- <i>t</i> BuPy)][B(C ₆ F ₅) ₄], hydrogen atoms removed for clarity.....	23
Figure 2-3. Thermal ellipsoid (50%) diagram of the molecular structure of diphenylacetylene inserted zirconocene 2•B(C ₆ F ₅) ₄ with the [B(C ₆ F ₅) ₄] counterion and hydrogen atoms removed for clarity. Selected bond lengths (Å): Zr1-N1 2.276(5), Zr1-C1 2.273(5).	25
Figure 2-4. Thermal ellipsoid diagram (50%) diagram of the molecular structure of 3, hydrogen atoms removed for clarity. Selected bond lengths (Å) Zr1-N1 2.447(3), Zr1-C1 2.403(3).	25
Figure 2-5. Thermal ellipsoid (50%) diagram of the molecular structure of Sn dimer species, hydrogen atoms removed for clarity.	26
Figure 2-6. Left: Normalized absorption and emission spectra of 4 ^H in dichloromethane and thin film. Right: image of a glass substrate coated with 4 ^H under ambient (top) and 365 nm irradiation (bottom), a blank side is shown next to the spin coated substrate for comparison.	29
Figure 2-7. Frontier molecular orbitals of 4 ^H calculated at the PBE0/TZVP level.	30
Figure 2-8. Thermal ellipsoid diagram (50%) of 5 ^H showing one of two equivalent molecules in the unit cell with hydrogen atoms removed for clarity. Selected bond lengths (Å) B1-N1 1.593(7), B1-C1 1.597(7), B1-O1 1.565(6), S1-O1 1.491(3), S1-O2 1.424(8).	32
Figure 2-9. ¹ H NMR (CD ₂ Cl ₂) spectra of 4 ^H (top) and 5 ^H (bottom), with ¹¹ B NMR spectra as inserts.	33
Figure 2-10. Cyclic voltammetry of a 1.16mM solution of 4 ^H in THF was measured using a three electrode setup using a CHI660D potentiostat. Glassy carbon, platinum wire, and	

- silver wire were used as the working, counter, and reference electrodes, respectively. Ionic strength of the solution was maintained by using a 0.1M solution of [nBu₄N][PF₆] in THF solvent. The sweep window was from -2.46V to 1.04V at 200 mV/s. 34
- Figure 2-11. ¹H NMR spectra of 4^H in CD₂Cl₂ (top) and 6^H in THF-D₈ (bottom), with ¹¹B NMR spectra as inserts. Two signals from the pyridyl ring have been highlighted in red... 36
- Figure 2-12. Thermal ellipsoid (50%) diagrams of the molecular structures of 4^H (left) and 6^H (right); hydrogen atoms have been removed for clarity in both structures and for 6^H, the [(2,2,2-cryptand)K]⁺ is omitted. Below each structure, the bond distances for the bonds of the 3-bora-9-aza rings are given; for clarity, the e.s.d. values are omitted, but none is greater than 4..... 37
- Figure 2-13. Thermal ellipsoid diagram (50%) of 7^H•B(C₆F₅)₄ with the [B(C₆F₅)₄]⁻ counterions and hydrogen atoms removed for clarity. Selected bond lengths (Å) Zr1-C1 2.287(3), Zr1-N1 2.323(2). 40
- Figure 2-14. Thermal ellipsoid (50%) diagrams of the molecular structures of *cis*-8^H (left) and *trans*-8^H (right); hydrogen atoms have been re-moved for clarity in both structures. ... 42
- Figure 2-15. ¹H NMR spectra (CD₂Cl₂) of *cis*-8^H (top) and a mixture of *cis/trans*-8^H (bottom). Diagnostic signals are highlighted in blue (*cis*-8^H) and red (*trans*-8^H)..... 43
- Figure 2-16. Thermal ellipsoid (50%) diagrams of the molecular structure of 9^{tBu}; hydrogen atoms have been removed for clarity. Below the structure, the bond distances for the bonds within the tricyclic ring system are given, along with those for the parent hydrocarbon as its 1,3,5,7-tert-butyl substituted derivative;¹²² for clarity, the e.s.d. values are omitted, but none is greater than 5..... 45
- Figure 2-17. Results from GIMIC analyses for II-C_{2h} (left) and I^H (right). (a,d): Isosurface (0.015) of the signed modulus of the calculated magnetically induced current density (blue, diatropic current; red, paratropic current); (b, e): color coding for inequivalent bonds; and (c, f): current strength profiles across the bonds. 48
- Figure 2-18. UV-Vis absorption and emission spectra of 9^{tBu} in CH₂Cl₂. Major absorption maxima at 314 and 458 nm. Emission maxima when excited at 458 nm at 600 nm. 51
- Figure 2-19. Diagram showing frontier molecular orbitals of 9^{tBu} and II^{tBu}. Structures were optimized at BH-LYP/def-TZVP level of theory. HOMO-LUMO difference from orbital energies calculated to be 5.1 eV for 9^{tBu} and 4.7 eV for II^{tBu}. Select orbitals shown for clarity. 52
- Figure 2-20. Cyclic voltammetry of a 1.14 mM solution of 9^{tBu} in THF was measured using a three electrode setup using a CHI660D potentiostat. Glassy carbon, platinum wire, and silver wire were used as the working, counter, and reference electrodes, respectively. Ionic strength of the solution was maintained by using a 0.1M solution of [nBu₄N][PF₆] in THF solvent. The current was swept in the negative direction with a sweep window from -3.1V to 0.3V at 200 mV/s. 53

Figure 3-1. Structure of the least substituted azaborine derivatives to date.	57
Figure 3-2. All 10 possible contiguous BN isomers of the indenide anion.	58
Figure 3-3. Highest occupied π orbitals of indenide (left) and 1-bora-7a-azaindenide (right).....	61
Figure 3-4. Electrostatic potential [atomic units (au)] of 6^H mapped on the electron density isosurface (0.005 au) at PBE0/def-TZVP level of theory.	62
Figure 3-5. 1H NMR Data for the reaction of 6^H with CH_2Cl_2 to form the product 10^H . signals on the 6-member pyridyl ring are highlighted.	63
Figure 3-6. Thermal ellipsoid (50%) diagram of the molecular structure of 10^H . Hydrogen atoms have been omitted for clarity. Selected bond lengths (Å): B(1)-N(1), 1.6198(16); B(1)-C(1), 1.6218(18); C(1)-C(2), 1.3599(18); C(2)-C(3), 1.4596(18); C(3)-C(4), 1.3962(18); C(4)-C(5), 1.379(2); C(5)-C(6), 1.388(2); C(6)-C(7), 1.3742(19); C(7)-N(1), 1.3404(17); N(1)-C(3), 1.3571(16).	65
Figure 3-7. Calculated Gibbs free energies ($kJ\ mol^{-1}$, PBE0/def-TZVP level of theory) for the reaction of 6^H with CH_2Cl_2 in dichloromethane to give either 10^H or $10'$	66
Figure 3-8. Reaction of 6^{Me} with an 80:20 <i>erythro:threo</i> mixture of 1-bromo-1,2-dideuterio-3,3-dimethylbutane. The $^1H\{^2H\}$ NMR spectra illustrate clean inversion to an 80:20 <i>threo:erythro</i> mixture in the 1:1 mixture of B-diastereomeric products of S_N2 alkylation, 12^{Me}	68
Figure 3-9. 1H NMR spectra for reaction of 6^H (top spectra) with CO_2 to give 13^H (bottom spectra). Relevant ^{11}B and ^{13}C NMR details are provided.	70
Figure 3-10. Thermal ellipsoid (50%) diagram of the molecular structure of the anion of 13^H . Hydrogen atoms and the (2,2,2-c) potassium ion have been omitted for clarity. Selected bond lengths (Å): B(1)-O(1), 1.562(3); B(1)-N(1), 1.534(4); B(1)-C(2), 1.665(4); C(2)-C(3), 1.525(3); C(3)-C(4), 1.371(4); C(4)-C(5), 1.447(4); C(5)-C(6), 1.354(4); C(6)-C(7), 1.420(5); C(7)-C(8), 1.363(4); C(8)-N(1), 1.355(4); N(1)-C(4), 1.405(3); C(1)-C(2), 1.530(3); C(1)-O(1), 1.334(3); C(1)-O(2), 1.208(3). Selected bond angles ($^\circ$): O(1)-B(1)-C(2), 86.01(18); C(1)-C(2)-B(1), 80.75(18); O(1)-C(1)-(C2), 100.3(2); B(1)-O(2)-(C1), 91.04(18); O(1)-C(1)-O(2), 125.9(2).	71
Figure 3-11. 1H NMR ($THF-d_8$) spectra of equilibrium reaction mixture.	74
Figure 3-12. Calculated Gibbs free energies ($kJ\ mol^{-1}$, PBE0/def-TZVP level of theory) for the reaction of 6^H with CO_2 in toluene to give either 13^H or $13^H'$	75
Figure 3-13. 1H (black) and $^{13}C[^1H]$ NMR spectra of $^{13}CO_2$ enriched 13^H and the reaction mixture after treatment with $B(C_6F_5)_3$	78
Figure 3-14. 1H NMR spectra of 10^H , 11^H , and proposed product 17^H	80

Figure 4-1. Development of donor molecules in Polymer-Fullerene cells.	85
Figure 4-2. Most well studied high performance NF acceptor materials.	86
Figure 4-3. Structures of boron-nitrogen containing species utilized in organic electronic devices.....	88
Figure 4-4. Boron-nitrogen doped indacene targets	89
Figure 4-5. Diarylpyrazine species synthesized for this study.	93
Figure 4-6. Representative ^1H NMR spectra of 14^{R} derivatives in CDCl_3 . Impurities are denoted as * CHCl_3 , x dioxane, δ H_2O	94
Figure 4-7. Normalized absorption and emission spectra of 14^{NAr} in a dichloromethane solution.....	95
Figure 4-8. ^1H NMR spectra in CDCl_3 of the borylated pyrazine species 15^{tBu} and 15^{NAr}	96
Figure 4-9. Thermal ellipsoid (50%) diagram of the molecular structure of 15^{tBu} . Hydrogen atoms have been omitted for clarity. Selected bond lengths (\AA) B(1)-N(1) 1.615(6), B(1)-C(1) 1.582(6), C(1)-C(2) 1.399(5), C(2)-C(3) 1.432(5), C(3)-C(4) 1.396(5), N(1)-C(3) 1.368(4), N(1)-C(5) 1.304(5).	97
Figure 4-10. Normalized absorption spectrum in dichloromethane solutions of 15^{tBu} and 15^{NAr}	98
Figure 4-11. HOMO, LUMO and LUMO+1 orbitals of 15^{tBu} based on calculations at the PBE0/Def-TZVP level.	99
Figure 4-12. Normalized absorption and emission spectra of 15^{tBu} in dichloromethane solutions.	99
Figure 4-13. Cyclic Voltammograms of 15^{tBu} (Left) and 15^{NAr} (Right). CV are recorded in dichloromethane with a 0.1M nBu_4NPF_6 electrolyte.....	100
Figure 4-14. Relevant bond lengths derived through X-Ray crystallography for 15^{tBu} and 16^{tBu} , E.S.D. have been removed for clarity.	104
Figure 4-15. Thermal ellipsoid (50%) diagram of the molecular structure of 16^{tBu} . Hydrogen atoms have been omitted for clarity.	104
Figure 4-16. Normalized absorption spectra for the arylated derivatives of 16 and 17 in dichloromethane solutions.	106
Figure 4-17. Absorption and Emission spectra of CH_2Cl_2 solutions of 16^{tBu} inset is an image of a vial of the compound under 365 nm light.	106

Figure 4-18. Frontier molecular orbitals of reported compounds calculated at the PBE0-DefTZVP level.	107
Figure 4-19. Frontier molecular orbitals and simulated absorption spectra of 17 ^{tBu} , with high frequency transitions highlighted by coloured arrows.	107
Figure 4-20. Cyclic Voltammograms of 16 ^{NAr} (Left) and 17 ^{NAr} (Right). CV are recorded in dichloromethane with a 0.1M nBu ₄ NPF ₆ electrolyte.	109
Figure 4-21. Top: Structures of the donor species utilized. Bottom Left: Frontier energy levels from CV of PTB7-Th and 16 ^{tBu} . Bottom Right: Device architecture used the organic solar cells.	110
Figure 4-22. Optical absorption spectra 16 ^{tBu} based film cast from C ₆ H ₅ Cl.	112
Figure 4-23. Current density-voltage curve of devices made form the donor species and 16 ^{tBu}	112
Figure 4-24. TOP = atomic force microscopy height images, BOTTOM = atomic force microscopy phase images. All films were spun-cast (1000 rpm) from C ₆ H ₅ Cl solutions at room temperature.	113
Figure 5-1. Top: example of best performing BN containing electron accepting species to date. Bottom, retrosynthetic approach for the synthesis of INCN functionalized BNindenofluorenes.	117
Figure 5-2. The five possible regioisomers of indenofluorene and the date they were synthesized.	120

List of Schemes

Scheme 1-1. Ring-closing metathesis pathway for the synthesis of 1,2-azaborine derivatives.	4
Scheme 1-2. Insertion reactions of antiaromatic boroles to generate 1,2-azaborine derivatives....	6
Scheme 1-3. Synthetic pathway for borylative cyclization reactions of amino styrenes.....	8
Scheme 1-4. Electrophilic borylation pathway by Hatekeyama and Nakamura, with helical species synthesized by same pathway below.....	10
Scheme 1-5. Zirconocene mediated synthesis of main group heteroles.	13
Scheme 1-6. Synthesis of phosphorous and boron containing heteroles.....	14
Scheme 2-1. Generation of BN-indene scaffolds from zirconocene chemistry.....	24
Scheme 2-2. Two step generation of BN-indenes.	27
Scheme 2-3. Murakami ¹⁰⁴ (top) and Wang ¹⁰⁵ (bottom) syntheses of BN-indenes.	28
Scheme 2-4. Reactions of 4 ^H	31
Scheme 2-5. Synthesis of 1,5-dibora-4a,8a-diaza-1,2,3,5,6,7-hexaaryl-4,8-dimethyl-s-indacenes.....	41
Scheme 3-1. Synthesis of 1-bora-7a-azaindenide anions 6.	59
Scheme 3-2. Bond lengths of ring bonds in optimized structures of 6 ^H , 13 ^H , 10, and 10'.	60
Scheme 3-3. Reactions of 1-bora-7a-azaindenide anions 6 with alkyl halides.....	64
Scheme 3-4. Reactions of 1-bora-7a-azaindenide anions 6 ^H /6 ^{Me} with carbon dioxide.....	69
Scheme 3-5. Examples of the diverse binding modes of CO ₂ reported for main group compounds.	72
Scheme 3-6. Equilibrium constant measurement at room temperature for CO ₂ binding to compounds 6 ^H and 6 ^{Me}	73
Scheme 3-7. Proposed Pathway for Catalytic Reduction of CO ₂	76
Scheme 3-8. Proposed mechanism for the reaction of 6 ^H and 13 ^H with B(C ₆ F ₅) ₃	79
Scheme 4-1. Electrophilic borylation pathways developed by the Ingleson group. ^{179, 180}	91
Scheme 4-2. Proposed synthetic pathway to access Ph ₂ Pz-BAr derivatives.	92
Scheme 4- 3. Electrophilic borylation of diarylpyrazine.	95

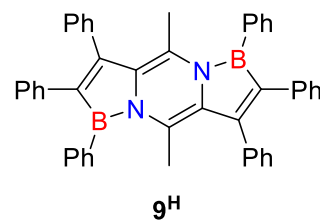
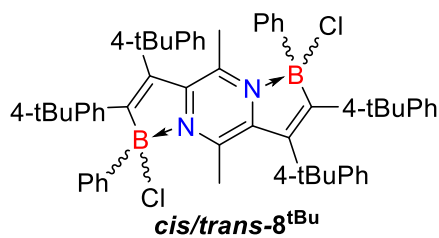
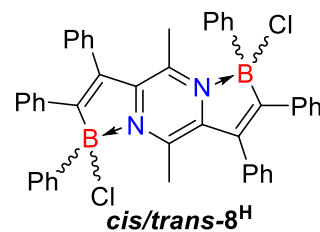
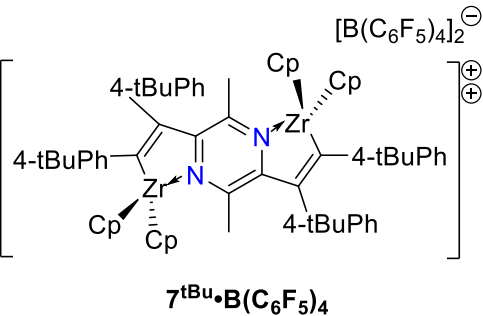
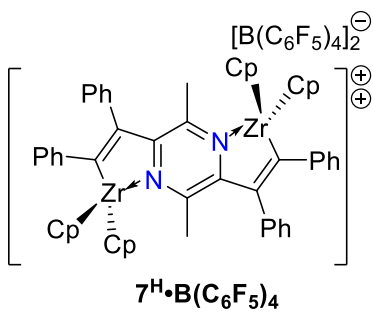
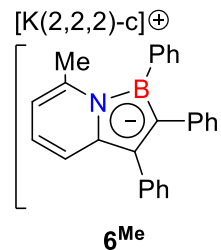
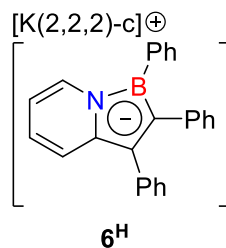
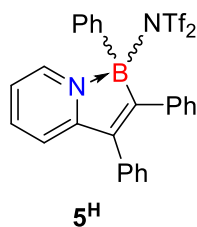
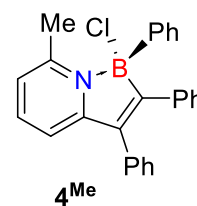
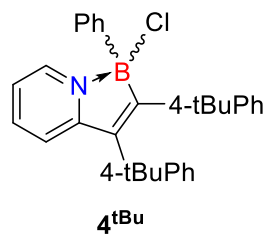
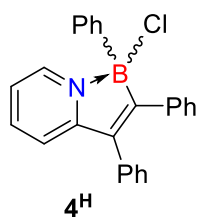
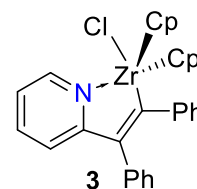
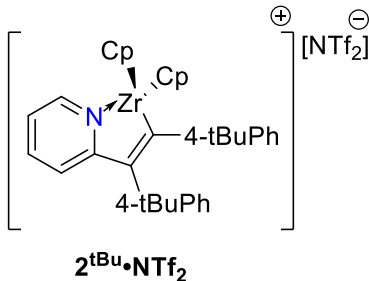
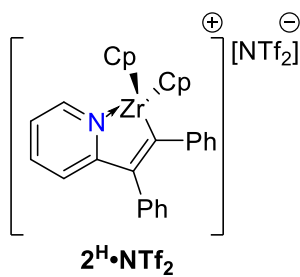
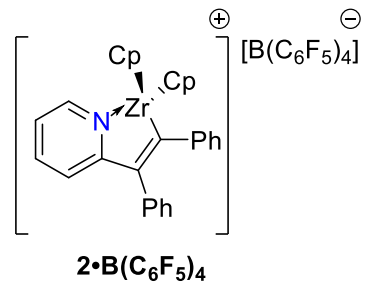
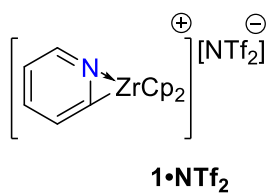
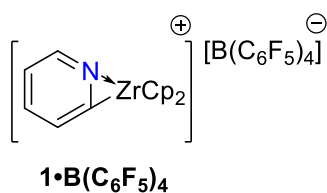
Scheme 4- 4. Attempted reduction reactions of 15 ^R	102
Scheme 4-5. Arylation reaction using diarylzinc reagents.	103
Scheme 5-1. Synthetic pathway to thiophene containing BN containing derivatives.	119
Scheme 5-2. Proposed synthetic pathway to access two new regioisomers of BN- indeno[1,2-b]fluorene, the [2,1-a] and [2,1-c] isomers.....	121
Scheme 5-3. Top: synthesis of BN anthracene by Liu. ²⁰⁸ Bottom: proposed synthesis of two derivatives of BN doped pentacene.	123

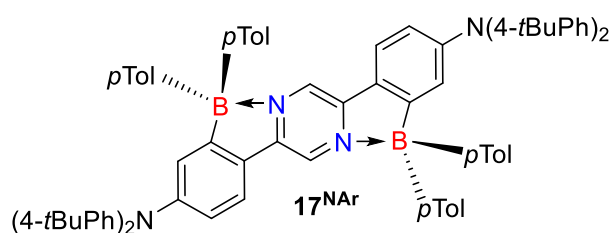
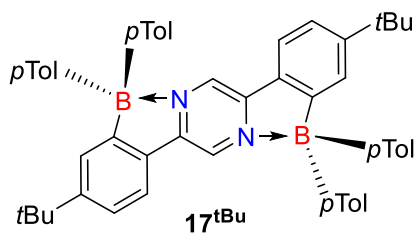
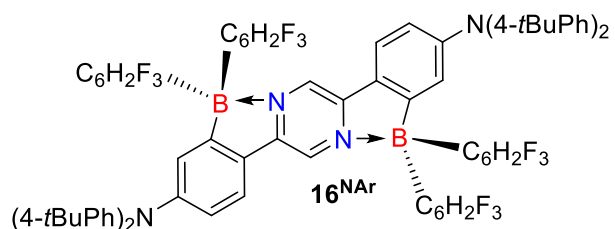
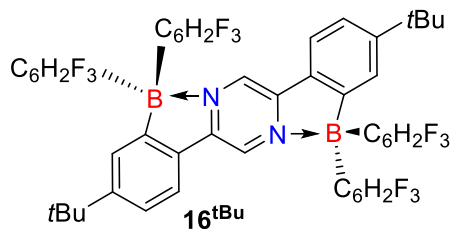
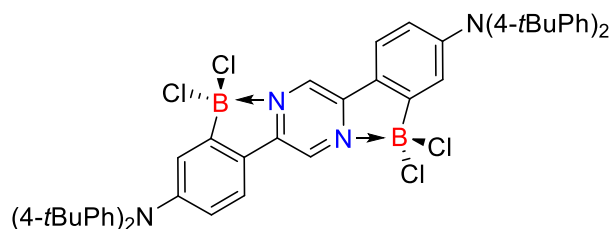
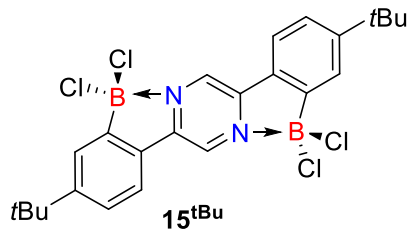
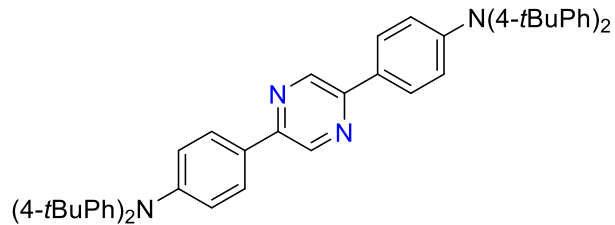
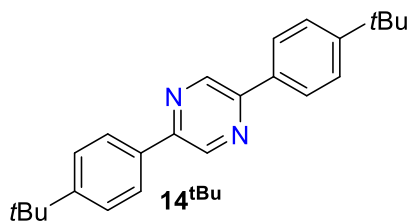
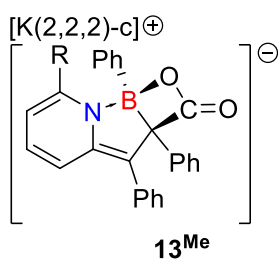
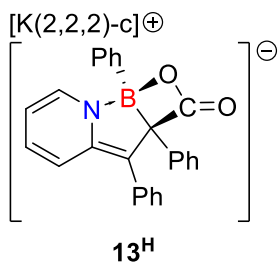
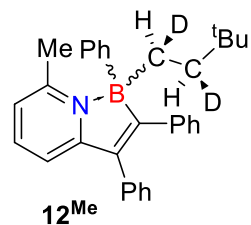
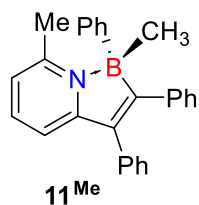
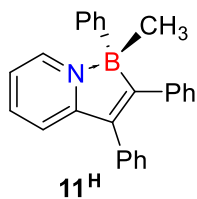
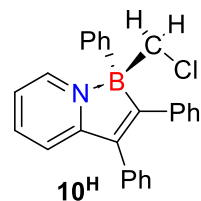
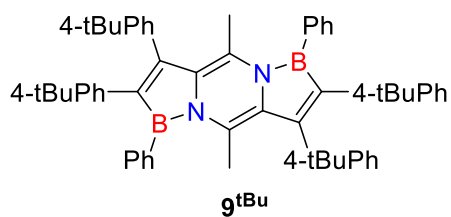
List of Symbols, Abbreviations, and Nomenclature

Symbol	Definition
Å	Angstrom
Ar	Aryl group
au	atomic units
°C	degrees Celsius
CDK2	Cyclin-dependent kinase 2
cm ⁻¹	inverse centimeters
COSY	homonuclear Correlation Spectroscopy
Cp	Cyclopentadienyl
<i>d</i>	doublet
DFT	Density Functional Theory
e.s.d	estimated standard deviation
E _{elec}	electrochemically determined band gap
E _{opt}	optically determined band gap
eV	electron volt
Fc ⁺	Ferrocenium
Fc	Ferrocene
FF	Fill Factor
FLP	Frustrated Lewis Pair
GIMIC	Gauge Including Magnetically Induced Current
HMBC	Heteronuclear Multiple Bond Correlation spectroscopy
HOMO	Highest Occupied Molecular Orbital
HSQC	Heteronuclear Single-Quantum Correlation spectroscopy
J _{sc}	short-circuit voltage
Kcal	kilocalorie
K _{eq}	equilibrium constant
LUMO	Lowest Unoccupied Molecular Orbital
M	Molarity (mole/litre)
m	multiplet
mol	mole
η ^x	hapticity of a ligand (x = 1,2,3,...etc.)
NF	Non-Fullerene
NICS	Nucleus Independent Chemical Shift
NMR	Nuclear Magnetic Resonance
OLED	Organic Light Emitting Diode
OPV	Organic Photovoltaic
OSC	Organic Solar Cell
PAH	Polycyclic Aromatic Hydrocarbon
PBE0	Perdew–Burke–Ernzerhof Exchange correlation functional

PCE	Power Conversion Efficiency
Ph	Phenyl group
ppm	parts per million
PSC	Polymer Solar Cell
<i>q</i>	quartet
R	alkyl group
rpm	rotations per minute
S _N 2	bimolecular substitution reaction
<i>t</i>	triplet
T ⁻¹	inverse Tesla
TBP	2,4,6-Tritertbutylpyridine
TDDFT	Time Dependent Density Functional Theory
tert	tertiary
Tf	triflate
THF	tetrahydrofuran
TLC	Thin Layer Chromatography
TMS	trimethylsilyl group
TS	Transition State
TZVP	Triple Zeta split Valence basis set
UV	ultraviolet
Vis	visible
Voc	open-circuit voltage
{ ¹ H}	proton decoupled
2,2,2-c	[2.2.2]Cryptand

List of Numbered Compounds





CHAPTER 1: INTRODUCTION

1.1 Main group element containing aromatic hydrocarbons

In the past 20 years modifying conjugated organic frameworks by incorporating main group heteroatoms has emerged as an effective method for developing new materials with properties that are unattainable in systems containing only carbon atoms.¹⁻⁵ By incorporating main group elements, the photophysical, electronic and solid-state properties of molecules can be readily tuned. From seminal early work on main group element containing small molecules and polymers the field has witnessed tremendous growth through incorporating elements such as boron,⁶⁻⁸ silicon,^{5,9} phosphorous^{10, 11} sulfur^{12, 13} or heavier atoms¹⁴ into conjugated systems.

1.2 Boron-nitrogen containing aromatics

One of the most prevalent substitutions made in organic compounds is the replacement of a C=C unit with B=N as the bonds are isosteric and isoelectronic, meaning that the overall electron count of the compound will remain the same, yet the insertion of BN creates a polar bond that can lead to new photophysical properties and reactivity.¹⁵⁻¹⁸ For example, the Piers group has shown that by replacing an aromatic CC bond with a BN bond in organic molecules such as pyrene,¹⁹ phenanthrene,²⁰ and picene,²¹ a significant bathochromic shift is observed in the fluorescence spectrum, shifting emission from the UV region to visible. The utility of BN bonds in traditionally organic substrates can be summarized into two key points of interest. The first benefit of the insertion of BN bonds is that the steric environment within the molecule will not change, but there

is now the introduction of a dipole, which is due to the differing electronegativities between boron (2.0) and Nitrogen (3.0).²²⁻²⁴ The introduction of a dipole has been shown to prompt some unique packing structures in the solid state as evidenced in the Piers synthesis of BN-pyrene (Figure 1-1) where the molecules stack alternatingly to line up boron in one molecule with the nitrogen of a second. The second key benefit is the access to structures previously unattainable as all-carbon molecules, as can again be highlighted in a report by the Piers group where a derivative of the previously unattainable dibenzo[*a,o*]picene was synthesized and several derivatives fully characterized.²¹

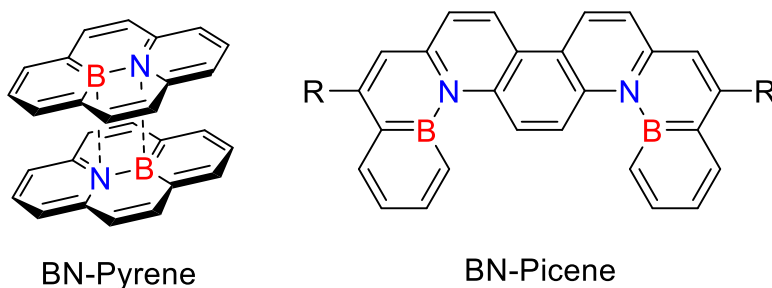


Figure 1-1. Examples of BN containing aromatic compounds.

Despite these advances, and the assertion in many reports of the potential applications for the BN isosteres in devices requiring organic semiconductors, until recently, few reports demonstrate their efficacy in this regard.⁸ Furthermore, real-world applications of such materials remain a futuristic proposition. A primary reason for this comes from the lack of general, high yielding synthetic routes to significant quantities of these materials. This is required not only to adequately assess the performance of these materials in device applications but also to give realistic hope for widespread applications even if only in niche markets. Indeed, many of the most fundamentally

interesting species can be synthesized in only milligram quantities, rendering exhaustive testing of properties impossible.²⁵ To assess and realize the potential of such materials, advances in synthesis are therefore required. Some of the best methods to date are highlighted in the following sections and illustrate the progress being made in addressing the problems of synthetic generality, scalability and scope.

1.3 Established synthetic pathways to BN aromatics

1.3.1 Methods for 1,2-azaborine synthesis

As benzene is the fundamental building block for all-carbon polycyclic aromatic hydrocarbons, the C₄BN core of azaborines can be regarded as the fundamental building block of larger BN substituted extended systems. There exist three possible isomers of azaborine (shown in Figure 1-2), with the most stable isomer (with BN in the 1,2 position) being the most studied. Access to the other two derivatives (1,3 and 1,4) has been very recently achieved²⁶⁻²⁸, but as the focus of this thesis is on systems containing direct B-N bonds, their properties will not be discussed in depth.

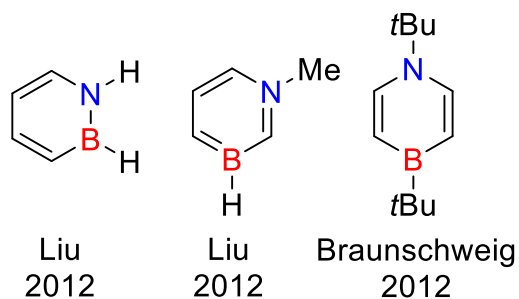
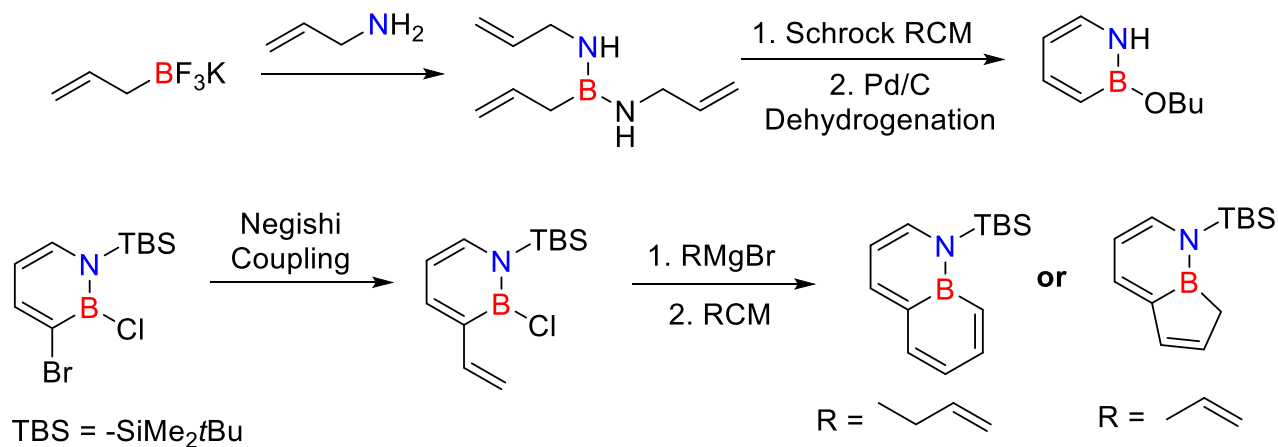


Figure 1-2. Three possible isomers of azaborines

Access to 1,2-azaborine heterocycles relies mainly on two synthetic methodologies. In the first, a ring closing metathesis reaction establishes the 6 membered ring and dehydrogenation using Pd/C aromatizes the ring system (Scheme 1-1 top). First developed by Ashe and Fang²⁹, the methodology was further refined by Liu and co-workers to the extent that it could be carried out with readily available starting materials on a multigram scale to give the cornerstone complex shown in Scheme 1-1.³⁰

Scheme 1-1. Ring-closing metathesis pathway for the synthesis of 1,2-azaborine derivatives.

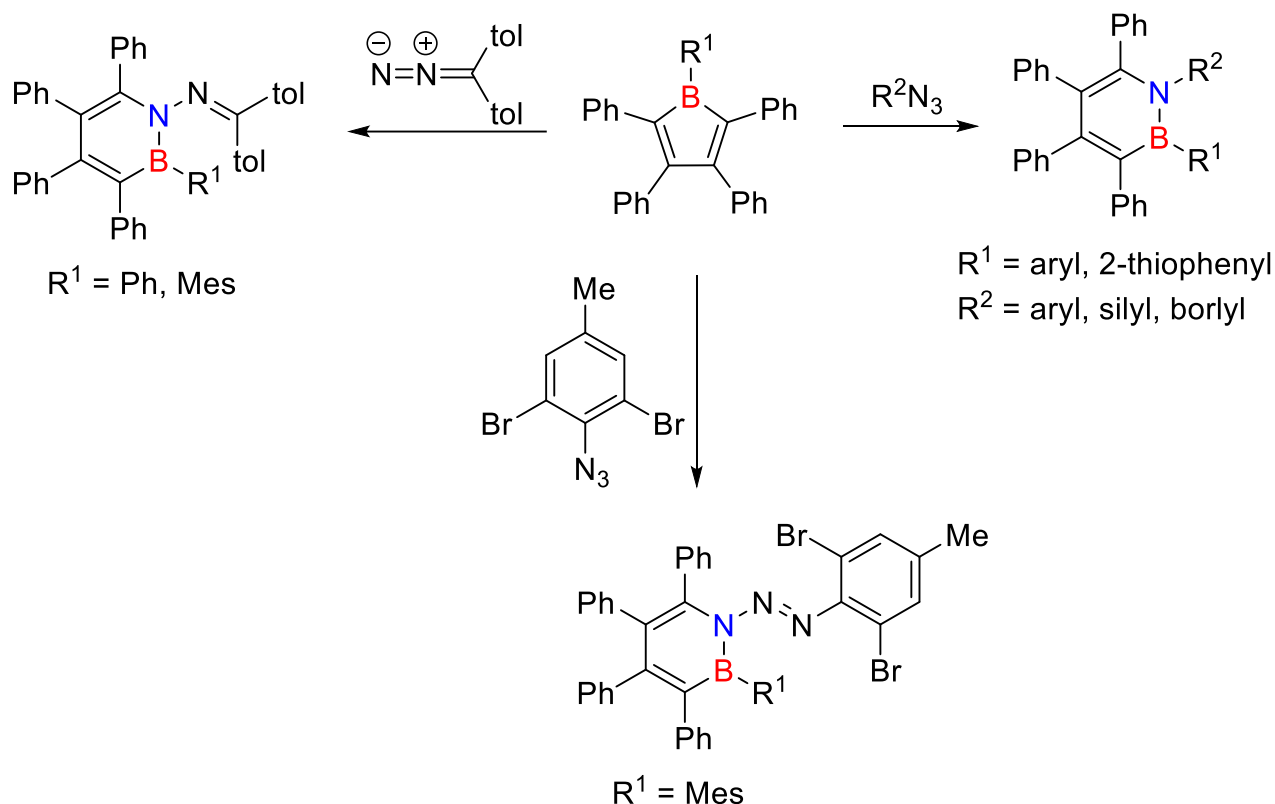


This compound is a convenient and versatile starting material for a wide range of derivatives with various groups at B in the 1,2-azaborine function. Post functionalization of azaborine represents a versatile strategy for expanding the range of derivatives available for BN analogs of cyclic aromatic hydrocarbons. Indeed, several reviews have been written on the functionalization of azaborines, with some more modern examples highlighted at the end of this section. One drawback of the RCM route shown in Scheme 1-1 is that functionalization of the carbon positions of the 1,2-azaborine ring is not readily accommodated. However, a report from

the Liu group has shown that iridium catalyzed borylation of the carbon adjacent to the nitrogen in the 1,2-azaborine ring is possible³¹ and the position next to boron is susceptible to electrophilic substitution.³² In addition, through resolution chemistry azaborines with boronic ester functionalities in the C4 and C5 positions can be isolated.³³ The Liu group has used the electrophilic substitution reactions reaction to elaborate 1,2-azaborines into bicyclic BN isosteres of naphthalene and the indenyl anion that are otherwise difficult to access (Scheme 1-1 bottom).³⁴ These methods for functionalizing the positions alpha to the heteroatoms have been combined to prepare a monomer suitable for the synthesis of regioregular azaborine oligomers and a polymer that is a 1,2-azaborine analog of a polyphenylene material through Suzuki–Miyaura polycondensation methodology.³¹ Thus, although still in its infancy, the elaboration of readily available 1,2-azaborine building blocks into more complex BN PAH molecules is an extremely promising strategy for accessing these materials.

Highly substituted derivatives of 1,2-azaborine can alternatively be prepared using a second synthetic route, the ring expansion reactions of antiaromatic borole rings via reaction with organic azides or diazoalkanes (Scheme 1-2). While this method is to some extent limited by the need to access the borole starting materials, recent progress in the chemistry of antiaromatic boroles has made their use as reagents more convenient.³⁵ This route allows for the synthesis of peraryl-substituted 1,2-azaborine derivatives exemplified by the hexaphenyl complex, prepared recently by the Braunschweig group.³⁶ The mechanism of this reaction has been explored by the Martin group,³⁷ and it has been further exploited to prepare novel BN-azo dye complexes through manipulation of the steric attributes of the reagents employed.³⁸ Completing the series, when a diazoalkane is reacted with boroles there is direct insertion into the ring system.³⁹

Scheme 1-2. Insertion reactions of antiaromatic boroles to generate 1,2-azaborine derivatives.



The potential for derivatives of these species is unfortunately still quite low, given the small number of readily accessible boroles. While not discussed in depth here, research is still plentiful on novel ways to access 1,2-azaborines.⁴⁰

Only ten years ago the mere synthesis of azaborines was ground-breaking, but because of the access to high yielding general routes, more “applied” research has been moving to the forefront. In addition to the fundamental studies on bonding and aromaticity one area that has become accessible is the study of bio-active molecules incorporating BN bonds. This has been pioneered by the Liu group and they have prepared BN derivatives of bioactive BN-biphenylcarboxamides and a BN substituted derivative of tryptophan (Figure 1-3).^{41, 42}

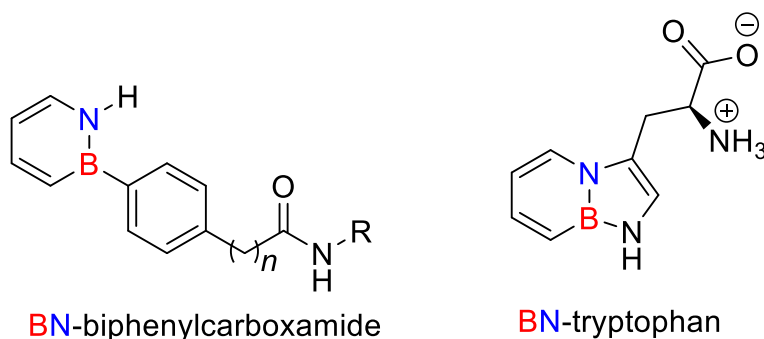


Figure 1-3. Bio-active molecules containing the 1,2-azaborine core.

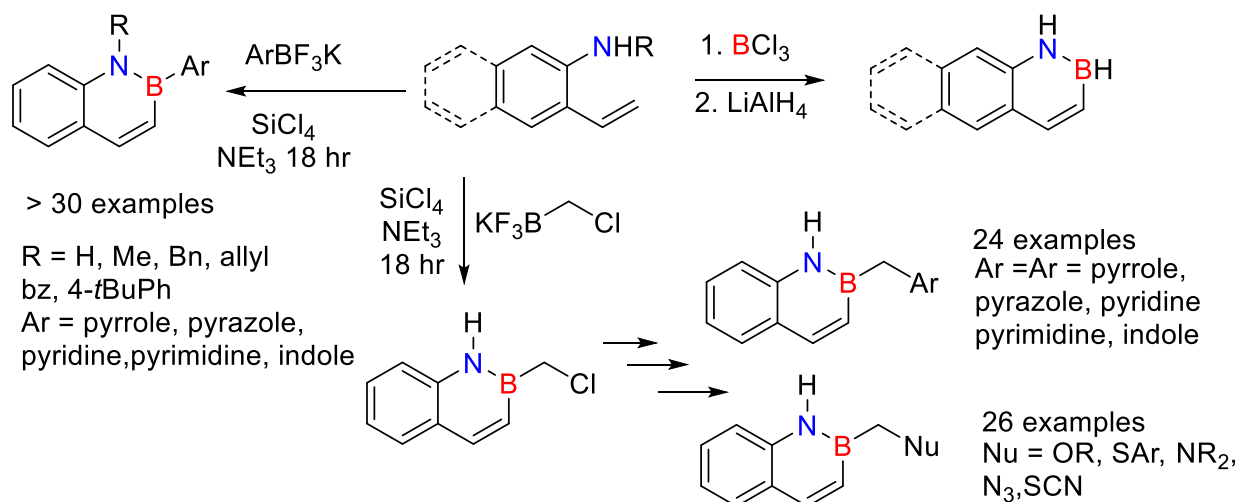
With the installation of the boron-nitrogen bond, the BN-biphenylcarboxamide derivatives have increased water solubility compared to the all-carbon derivative due to the increased polarity of the molecule. This property and the higher hydrogen bonding ability of the NH bond relative to CH yields improved biological activity as a CDK2 inhibitor, which slows the growth of cancerous cells.⁴¹ In the case of the ubiquitous amino acid tryptophan, the BN derivative shows a bathochromically shifted emission and is able to be incorporated into proteins within cells, suggesting it could be a useful probe for the examination of biological processes.⁴² While these are only two preliminary studies it is clear that 1,2-azaborines will see increased interest in many new fields due largely to their stability and synthetic accessibility.

1.3.2 Borylative cyclization

As shown above, synthetic endeavours toward small conjugated systems is well under way, but a reliance on ring-closing metathesis reactions can hamper the number of possible derivatives synthesized. A series of recent studies has expanded the scope of a method first introduced in Dewar's pioneering studies on BN analogs of aromatic hydrocarbons.⁴³⁻⁴⁵ The borylative

cyclization of ortho amino styrenes can lead directly to BN analogs of naphthalenes and anthracenes in reasonably high yielding reactions (Scheme 1-3).⁴⁶

Scheme 1-3. Synthetic pathway for borylative cyclization reactions of amino styrenes.



This is related to the electrophilic borylation strategies described in the next section in that the amine reacts with the boron halide reagent to establish and anchor the B–N linkage, and the Lewis acidity of the boron centre in this intermediate then facilitates the formation of the final BN heterocycle. One of the key discoveries in this synthetic pathway was that potassium trifluoroborate groups could be utilized,^{47, 48} many of which are already commercially available, and are much easier to handle than the reactive trichloroborane used by Dewar.^{49, 50} There is significant versatility in this synthesis in that a variety of R groups on the amine function can be accommodated, and the substituent on boron can also be manipulated. For example, the Molander group has prepared an extensive library of naphthyl azaborines by incorporating the chloromethyl function on boron as shown in the bottom of Scheme 1-3, this group may then be functionalized through nucleophilic substitution or coupling reactions.^{51, 52} Furthermore, they have demonstrated

that the position next to boron can be subjected to cross coupling reactions to institute both aromatic⁵³ and alkyl⁵⁴ substituents in this position. This again illustrates that post functionalization of a key building block can be an effective strategy to a range of BN materials.

1.3.3 Electrophilic borylation

The above methods are reliable but focus on relatively simple families of BN PAHs. Extended structures present more difficult synthetic challenges for which the above-described methods are generally not effective. Furthermore, as structures become more extensive, the number of possible BN isosteres grows dramatically and methodologies that target specific isomers become a potential issue. For example, even for the simplest bicyclic species, naphthalene, there are six possible isomers that contain BN units; to date only four of them have been synthesized and each of these derivatives took tremendous synthetic efforts.^{43, 55-57}

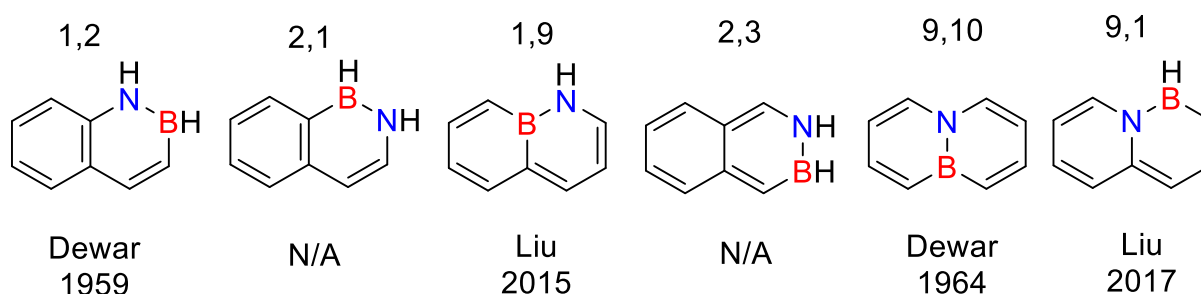
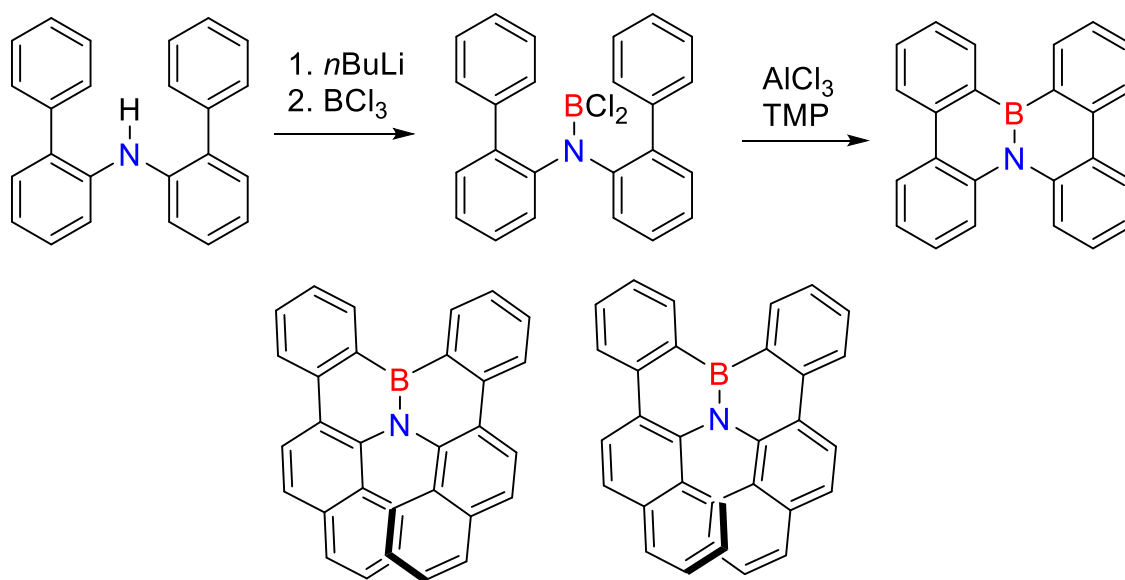


Figure 1-4. The six possible isomers of contiguous BN substituted naphthalene.

The positioning and orientation of BN units within a PAH framework has a large influence on the redox and photophysical properties of the isostere⁵⁸ and so as structures become more

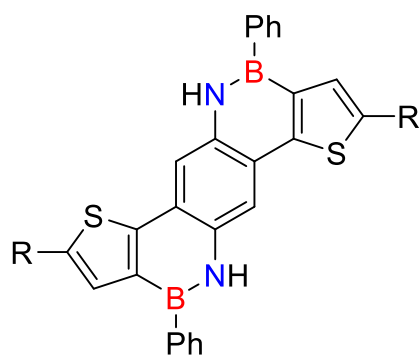
complex, the issue of selectively targeting a specific BN isomer becomes more important and remains a challenge. Electrophilic borylation is not a new methodology, having been employed by Dewar and co-workers in the early days of BN PAH chemistry.¹⁶ However, recent activity that creatively applies this electrophilic borylation strategy has resulted in significant progress for the assembly of large BN PAH molecules. Hatakeyama and Nakamura demonstrated the promise of this strategy in their gram scale synthesis of the BN-fused PAH molecule shown in Scheme 1-4.⁵⁹

Scheme 1-4. Electrophilic borylation pathway by Hatakeyama and Nakamura, with helical species synthesized by same pathway below.

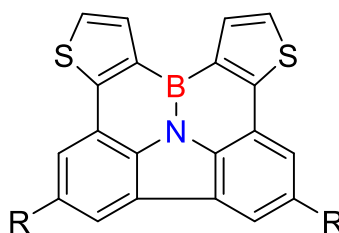


Although the conditions for the ring closure are fairly harsh (12 hours at 150 °C), the BN aromatic can be prepared in 67% yield in >3 g amounts. As a result, this was one of the first studies to report bulk conductivity measurements on a BN PAH. These authors subsequently adapted this strategy to prepare an azaboradibenzo[6]helicene derivative of whose conducting properties were dependent on the homochiral form of the compound.⁶⁰ The observed carrier inversion behaviour

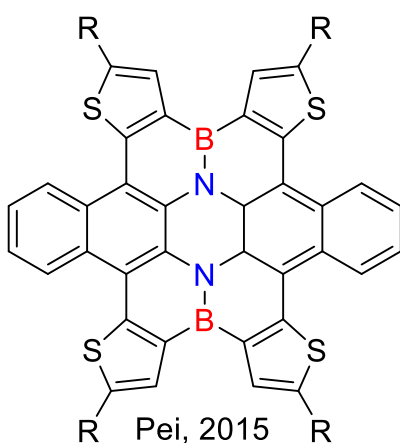
was attributed to the differences in crystal packing observed in the racemate vs. the single enantiomer of the compound. The thorough assessment of the properties of these compounds, and their performance in devices, were made possible by the efficient access to multigram quantities using this effective methodology. This synthetic strategy is now being used by other groups to access more complex BN PAHs with semi-embedded BN units (Figure 1-5). The embedding of the BN fragment is important because of the stability towards ambient air and moisture this engenders,¹⁹ and even partially embedded BN units are less prone to hydrolysis.²¹ Some recent examples of such materials are given in Figure 1-5.



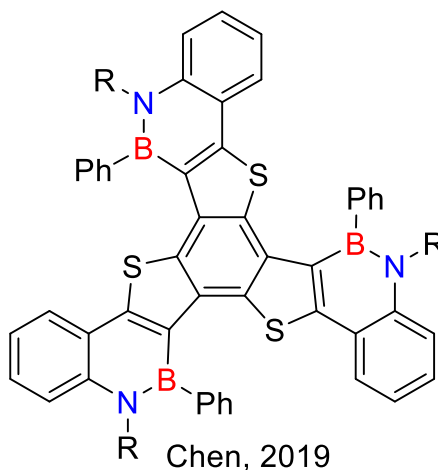
Feng, 2013



Pei, 2014



Pei, 2015



Chen, 2019

Figure 1-5. Boron-nitrogen doped aromatics synthesized by electrophilic borylation.

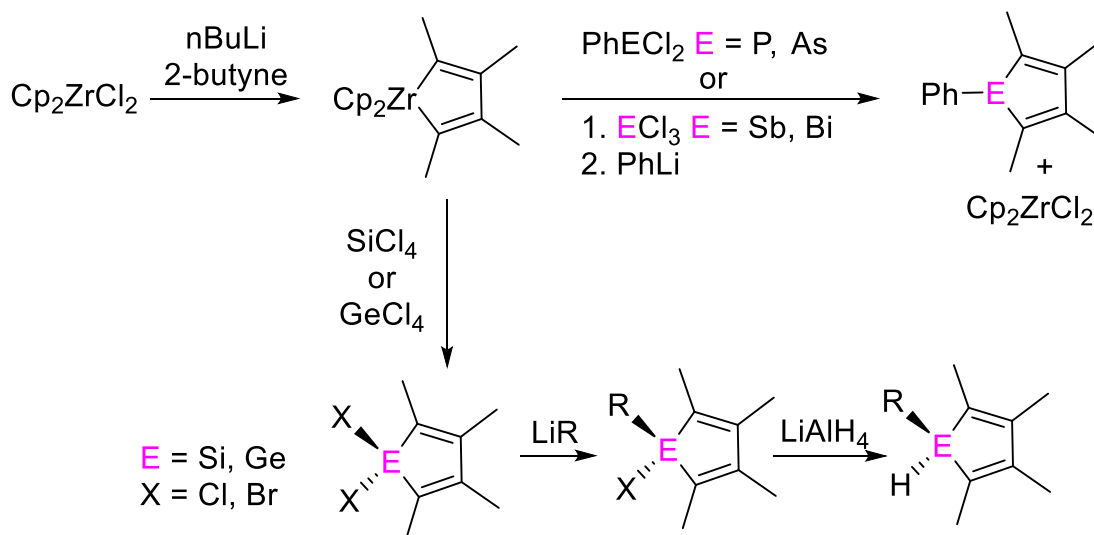
The frameworks necessary to enact electrophilic borylation are assembled using standard C–C coupling chemistry and the crucial B–C bond forming reaction sequence of Scheme 1-4 is applied in the last step to afford significant quantities of these relatively complex materials. The compound on the top left by Feng⁶¹ is a heteroacene compound, while the remaining three species are heterosuperbenzenes that model BN-doped graphene.⁶²⁻⁶⁴ The top right species in Figure 1-5 can be readily functionalized at the 2-positions of the thiophenes through bromination and C–C coupling chemistry, indicating that the partial embedding of the BN function allows it to withstand the conditions of these reactions. The facility and versatility of this electrophilic borylation reaction is illustrated by a growing number of examples of its application in the past year and offers much promise for the large-scale synthesis of large BN-doped PAH materials.⁶⁵⁻⁷⁰

1.4 Zirconocene mediated synthesis of main group heteroaromatics

The assembly of π systems with main group elements has been a focal point of organometallic chemists for decades. While the common methods for BN containing species are described above, a more general route to incorporate many main group elements is the transmetallation of zirconocene reagents. This was first applied by Fagan and Nugent as shown in Scheme 1-5. In their initial report, a variety of easily synthesized zirconacycles were used with main group containing halides (P, As, S, Sb, Ge, In, Sn, Bi,) to make substituted heteroles in good to excellent yields.^{71, 72} The synthesis starts from zirconocene dichloride, which is commercially available and builds up the ring system through insertion reactions. This zirconocyclobutane is then treated with main group halides resulting in a transmetallation, regenerating zirconocene dichloride and yielding the desired heterole. In a follow up report, more focus was placed on substituted element-

cyclobutadiene species, but interestingly applied this to boron also, although dimerization of the ring systems was observed in this case.⁷³ While these early reports were focused mainly on developing a synthesis to these species, follow up work by the Tilley group and others sought to investigate the chemistry of the heteroles.⁷⁴ Using the zirconacyclobutane starting material an array of silole and germole species were synthesized and their reactivity and properties investigated in depth, including the study of silolyl and germolyl anions and silole/germole dianions.

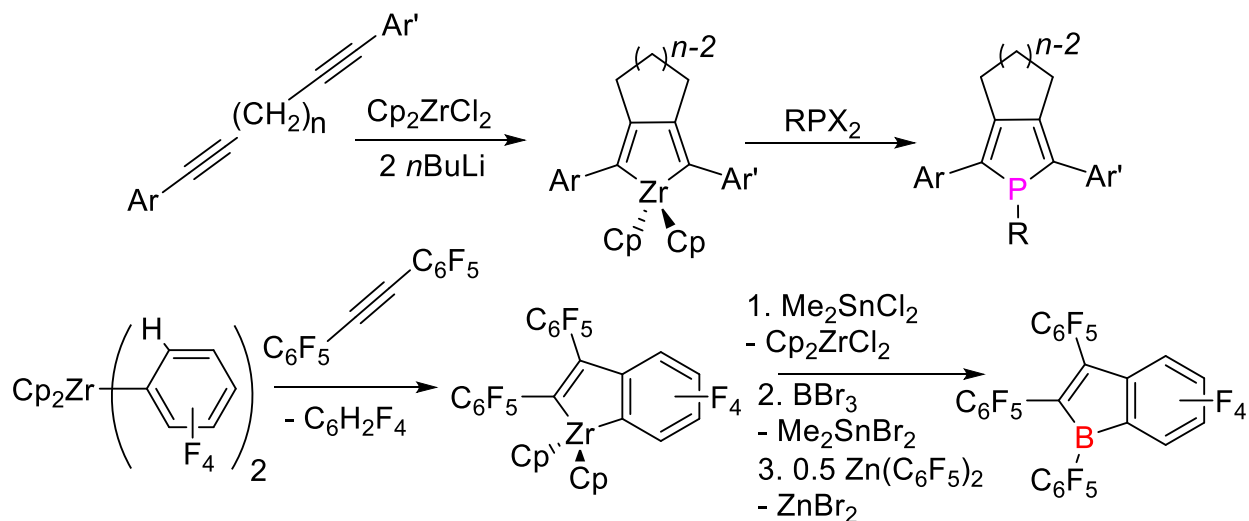
Scheme 1-5. Zirconocene mediated synthesis of main group heteroles.



This work has been elaborated to compounds containing phosphorous as highlighted in the top of Scheme 1-6.^{75, 76} The phospholes synthesized here showed promise as active components of OLEDs and due to the variety of zirconocycles that could be synthesized a large family of molecules were tested. Within our own lab the use of zirconocycles as transmetallation reagents has been used in the synthesis of two separate highly Lewis acidic borole species. In the first reported case of perfluoropentaphenylborole by Piers the synthesis started from Rosenthal's

pyridine supported zirconocene⁷⁷ instead of zirconocene dichloride but the principle remained the same where the goal was the generation of a zirconacyclobutane.⁷⁸ While direct transmetallation to boron was not possible, using tin as an intermediate step gave the substituted borole in the end. Following similar synthetic pathways, the Piers group synthesized a fused indene type borole as shown in the bottom of Scheme 1-6. Again, transmetallation from the zirconocyclobutane was not possible, but by going through tin the borole was isolated in good yields.^{79, 80}

Scheme 1-6. Synthesis of phosphorous and boron containing heteroles.



While there have certainly been tremendous efforts towards the synthesis of main group atom containing heteroles, the majority of the work has focused on the insertion of one single main group element. To the best of our knowledge no previous work has investigated using zirconocycle mediated pathways to synthesize BN doped aromatic species, despite the versatility of the synthetic pathway. This absence of a metallocene mediated synthetic method for BN organics will be the target of Chapters two and three in this thesis.

1.5 Aromaticity and antiaromaticity

Throughout this thesis a commonality of the synthesized compound is that their properties are dictated largely by their aromaticity, antiaromaticity, or lack of either. This makes it relevant to discuss what these phenomena are, how we measure them, and what impacts they can have on a molecule's properties. Aromaticity takes many forms in the literature, but in general occurs in organic molecules with a conjugated π -system and instills a special stability above that explained by resonance delocalization of electrons.⁸¹ This manifests itself in the equalization of bond lengths throughout the system, ring-current effects observable in NMR spectroscopy, and further magnetic properties.⁸²⁻⁸⁴ Contrary to this, antiaromaticity instills a special instability within the molecule, which is usually evidenced by a localization of single and double bonds within the molecule and ring-current effects opposite to those in aromatic systems. If a molecule does not possess the traits of either aromatic or anti-aromatic species it is said to be non-aromatic which is highlighted by not producing a ring current in an external magnetic field.

The most common, and straightforward method of assessing aromaticity within a molecule is Hückl's rule which has several parameters:

1. The molecule must have $4n+2$ electrons within a conjugated system (where n is some integer, i.e. $n=0,1,2,3\dots$)
2. The molecule (or section of interest) must be planar
3. The molecule must be cyclic (not-linear)
4. The molecule must have a continuous ring of p-orbitals

While this general set of rules provides a good starting point in understanding aromaticity, like many rules in chemistry it begins to fall apart in more complex (more than two adjoined rings) systems.⁸⁵

It is not possible to directly measure the degree of aromaticity within a molecule but several traits can be examined such as aromatic stabilization energy,⁸⁴ solid state geometry,^{82, 83} and magnetic properties. Unfortunately, since aromaticity depends on many factors, in varying amounts, these properties rarely align perfectly with one another.⁸⁴ This has prompted the development of computational methods to try and quantify the aromaticity of a molecule. The most common method for this is the nucleus independent chemical shift (NICS) calculation, due in large part to its low computational cost.⁸⁶

NICS provides a value representing the shielding or deshielding effects aromatic species experience in an external magnetic field. When a magnetic field is applied to a molecule, a ring-current is generated within aromatic compounds and this current induces an additional magnetic field as shown in Figure 1-6. When the induced magnetic field is in the same direction as the external field, a deshielding region is induced and the opposite is true when the induced magnetic field opposes the external. A similar phenomenon is observed for anti-aromatic compounds, but the generated magnetic field lines are reversed to those in aromatic species.

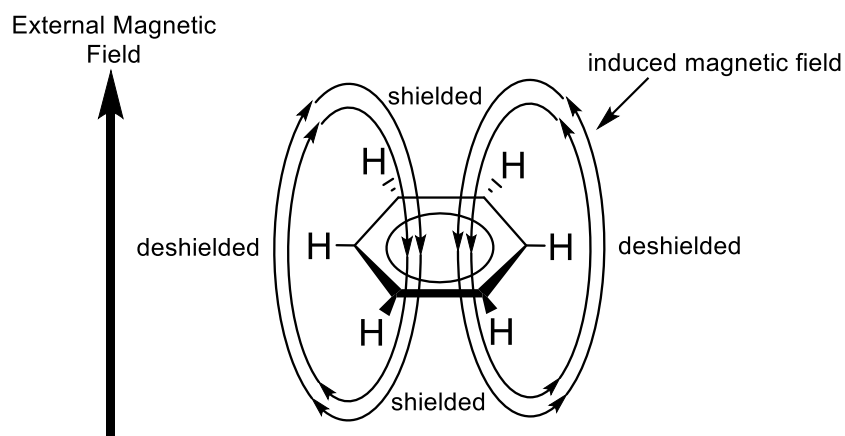


Figure 1-6. Diagram showing induced ring currents when benzene is exposed to an external magnetic field.

These fields can shield or deshield atoms in the molecule depending on their relative positions, with NICS representing the extent of shielding an imaginary atom experiences at the centre of a conjugated system. For aromatic systems the effect in the centre of the ring is shielding, giving a negative NICS value (diatropic) while for anti-aromatic species the centre of the ring is deshielding yielding a positive NICS (paratropic) value. If the molecule is non-aromatic, there is no ring-current generated, yielding a NICS value of near zero. The current standard method for measuring NICS values, places the dummy atom either in the plane (NICS(0)), or 1 Å above the centre of the plane (NICS(1)) of the ring in an effort to remove paratropic contributions from the sigma bonds. Both NICS(0) and NICS(1) values are presented in this thesis, as neither one is better in all scenarios and it is best to look for trends instead of focusing on the direct values. NICS calculations have been performed on hundreds of molecules and, like the Hückel rules presented above, NICS is not perfect and can have problems with more complex systems. While detailed methods have been developed (such as GIMIC which is highlighted in Chapter 2),^{87, 88} they are much more computationally expensive, making NICS the standard for a fast, reliable gauge of aromaticity.

1.6 Thesis Goals

This thesis discusses the synthesis, characterization and reactivity of conjugated boron-nitrogen containing compounds. With a desire to add to the library of synthetic methods available to make BN compounds, Chapter two describes the development of a zirconocene mediated synthetic pathway to generate BN doped indene and *s*-indacene containing species. This work gave us access to a derivative of the formally antiaromatic *s*-indacene albeit in low yields. The development of this synthetic pathway led to the discovery of a new BN containing aromatic five-member ring that showed unique reactivity toward electrophilic small molecules. Chapter three details the reactivity of the BN indenide anion and investigates the mechanism by which it reacts with varied electrophiles. Chapter four deviates from this synthetic pathway to examine further conjugated systems and tests them as electron accepting units in organic solar cells. Chapter five is a summary of the major findings in the thesis and provides a short proposal for future investigations on this chemistry.

CHAPTER TWO: ZIRCONOCENE-BASED METHODS FOR THE PREPARATION OF BN INDENES: APPLICATION TO THE SYNTHESIS OF 1,5-DIBORA-4A,8A-DIAZA-1,2,3,5,6,7-HEXAARYL-4,8-DIMETHYL-S-INDACENES.⁸⁹

(Adapted from reference ⁸⁹ with permission from the American Chemical Society)

2.1 Preface

There has been a large amount of work on the synthesis of main group containing heterocycles through zirconocene mediated synthetic routes, including within our own group on boron. Despite this, to the best of our knowledge these routes had not been employed for BN containing species. With the lack of versatile and scalable synthetic methods for BN containing organics it was a logical extension to test if similar routes would allow for facile synthesis of BN heterocycles. This chapter describes the development of a zirconocene mediated synthetic method and its application to several molecules of interest.

2.2 Author Contributions

Synthetic work on compounds **1-5** was performed jointly by Mr. Evan Patrick and Mr. Matthew Morgan, while synthetic work on remaining compounds was performed solely by Mr. Matthew Morgan. Crystallographic characterization for **2•B(C₆F₅)₄** and **3** were performed by Dr. Denis Spasyuk, while remaining compounds were performed by Mr. Matthew Morgan. Computational calculations were performed by Dr. Mikko Rautiainen and Prof. Heikki Tuononen. The manuscript was written collaboratively between Prof. Warren Piers, Dr. Mikko Rautiainen and Mr. Matthew Morgan.

2.3 Abstract

A method for the preparation of 3-bora-9-aza-indene heterocycles based on zirconocene mediated functionalization of the *ortho*-CH bonds of pyridines has been developed and used to make two such compounds. Unlike other methods, the boron centre in these heterocycles remains functionalized with a chloride ligand and so the compounds can be further elaborated through halide abstraction or reduction. The utility of the method was further demonstrated by applying it towards the preparation of 1,5-dibora-4a,8a-diaza BN analogs of the intriguing hydrocarbon *s*-indacene starting from 2,5-dimethylpyrazine. Gram quantities of one such compound were prepared and fully characterized, and both experimental and computational data is presented to compare its properties to the parent hydrocarbon *s*-indacene. This data indicates that the BN substituted derivative exhibits lowered aromaticity in relation to the hydrocarbon.

2.4 Introduction

The substitution of C-C with isoelectronic and isosteric BN building blocks within conjugated organic frameworks has been explored since the seminal work of Dewar, beginning in the late 1950s.¹⁶ These early studies, informed by the prior discovery of borazine,¹⁵ were motivated mainly by curiosity and shed light on the concept of aromaticity in heteroatom substituted conjugated systems. In the past decade, however, evaluating the effect of BN for CC substitution on the electronic properties of various conjugated hydrocarbon-based molecules,^{19-21, 46, 63, 90-96} polymers^{65, 97-99} and materials^{25, 59, 62, 63, 65, 70} has emerged as a primary goal of the field. Furthermore, the introduction of a significant dipole has implications for the BN analogs of

hydrocarbons as biological agents.^{51, 52, 100-102} There has therefore been a significant amount of activity in this field since its resurgence in the mid-2000s.^{17, 18, 22, 23, 30, 65, 103}

A corollary of the interest in these molecules is the need for new synthetic routes to such species that are efficient, modular and scalable.¹⁷ While much progress has been made, new methodologies are still of interest for preparing these materials and accessing BN frameworks for which current methods are not suited. Here we describe a zirconocene-based method for assembling 3-bora-9-aza-indene scaffolds^{104, 105} and its use to prepare 1,5-dibora-4a,8a-diaza BN analogs of the intriguing “quasi aromatic” hydrocarbon s-indacene (Figure 2-1).¹⁰⁶⁻¹⁰⁹

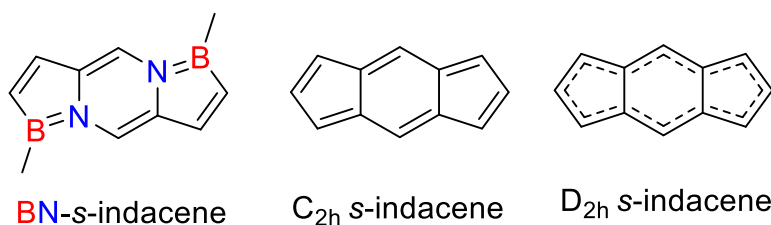


Figure 2-1. Simplified structure of BN-s-indacene and the two bonding motifs discussed for the all-carbon analogue

2.5 Results and Discussion

Our group has previously shown that zirconocycles are useful starting materials for the synthesis of boron containing heterocycles.^{78, 79} We hypothesized that by using well-established zirconocene chemistry in which the *ortho* C-H bonds of pyridine can be selectively functionalized,¹¹⁰⁻¹¹² these routes might be adaptable to preparing 3-bora-9-aza-indene functions with modular control over the substituents on the heterocyclic framework. Exploratory experiments (Scheme 2-1) showed that the zirconocene methyl cation generated by methide

abstraction using $[\text{Ph}_3\text{C}][\text{B}(\text{C}_6\text{F}_5)_4]^{113}$ reacted readily with pyridine to eliminate methane and give the expected η^2 -pyridyl cation $\mathbf{1}\cdot\text{B}(\text{C}_6\text{F}_5)_4$.¹¹⁰ Interestingly, if 4-*tert*-butylpyridine was employed in the synthesis instead of pyridine it was possible to isolate and crystallographically characterize the pyridine coordination compound $[\text{Cp}_2\text{ZrMe}(4\text{-}t\text{BuPy})][\text{B}(\text{C}_6\text{F}_5)_4]$ (Figure 2-2). Following the isolation of this coordination compound it was shown that upon heating to 40 °C in dichloromethane, insertion and concurrent release of methane proceeded readily to form the inserted compound analogous to $\mathbf{1}\cdot\text{B}(\text{C}_6\text{F}_5)_4$, but this *tert*-butyl derivative was not used in any further studies. Insertion of diphenyl acetylene into the Zr-C bond of $\mathbf{1}\cdot\text{B}(\text{C}_6\text{F}_5)_4$ was facile, selectively yielding the five-membered zirconacyclic cation $\mathbf{2}\cdot\text{B}(\text{C}_6\text{F}_5)_4$.¹¹¹ It was anticipated that reaction of this species with PhBCl_2 would yield the desired BN heterocycle, with “[Cp_2ZrCl][$\text{B}(\text{C}_6\text{F}_5)_4$]” as the by-product, but no reaction was observed between $\mathbf{2}\cdot\text{B}(\text{C}_6\text{F}_5)_4$ and the haloborane under any conditions we explored. However, if the cation was neutralized with the more coordinating chloride anion to give **3**, the transmetallation reaction proceeded smoothly to yield the desired product (vide infra). The synthetic intermediates shown in Scheme 1 ($\mathbf{1}\cdot\text{B}(\text{C}_6\text{F}_5)_4$, $\mathbf{2}\cdot\text{B}(\text{C}_6\text{F}_5)_4$, and **3**) were characterized via comparison with known compounds¹¹² and via spectroscopic and structural characterization (Figure 2-4).

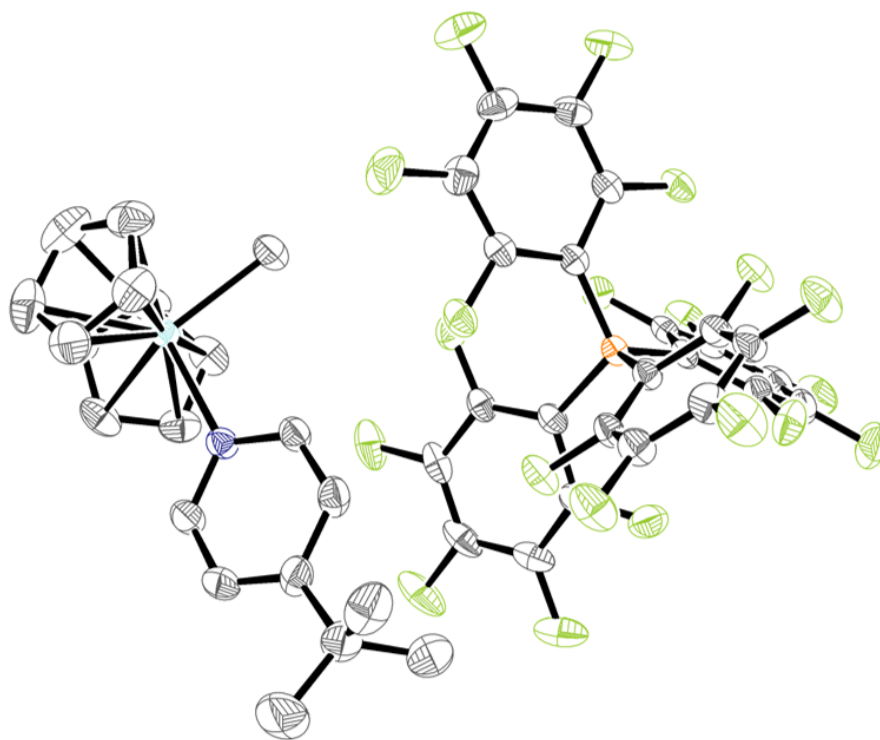
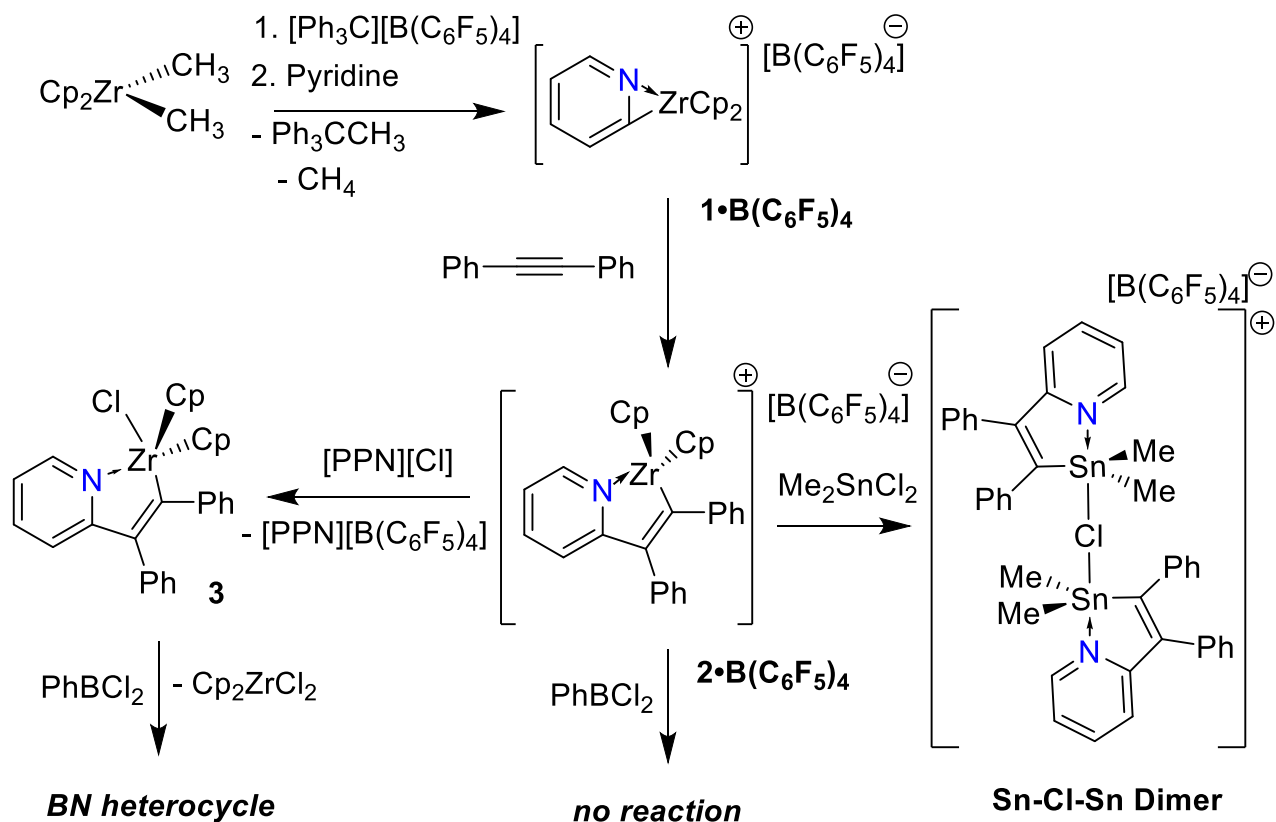


Figure 2-2. Thermal ellipsoid (50%) diagram of the molecular structure of $[\text{Cp}_2\text{ZrMe}(4\text{-}t\text{BuPy})][\text{B}(\text{C}_6\text{F}_5)_4]$, hydrogen atoms removed for clarity.

Although **3** was not isolated in analytically pure form due to contamination with the $[\text{PPN}][\text{B}(\text{C}_6\text{F}_5)_4]$ salt by-product, a structure determination was possible on carefully picked crystals. Analysis of the Zr-C and Zr-N distances in cation **2**• $\text{B}(\text{C}_6\text{F}_5)_4$ vs. neutral **3**, shows a significant lengthening of the bonds by 0.13-0.17 Å in the latter; this, coupled with the lowered Lewis acidity of the zirconium center makes **3** more reactive towards the haloborane reagent.

Scheme 2-1. Generation of BN-indene scaffolds from zirconocene chemistry.



The need to switch from cationic to neutral zirconocene chemistry makes the route shown in Scheme 2-1 somewhat atom extravagant and so efforts were made to streamline the synthesis as much as possible. One possible route to avoid going through neutral zirconocenes to exploit the transmetallation to Sn and then to boron. Several unsuccessful attempts at this were made, where a clean sample of **2•B(C₆F₅)₄** was treated with various alkyl tin halides, each time leading to an intractable mixture with the formation of several products in the NMR spectra. Eventually one of the products from the reaction with Me_2SnCl_2 was crystallized and confirmed to be a monocationic Sn-Cl-Sn dimeric species (Figure 2-5). Despite a low yield of this dimer, attempts at transmetallation with PhBCl_2 were attempted but led to an intractable mixture of products. The

protocol shown in Scheme 2-2 was developed and used to prepare the 3-bora-9-aza heterocycles **4^H** and **4^{tBu}** in a convenient, scalable (up to 5 grams) and high yielding two-step synthesis.

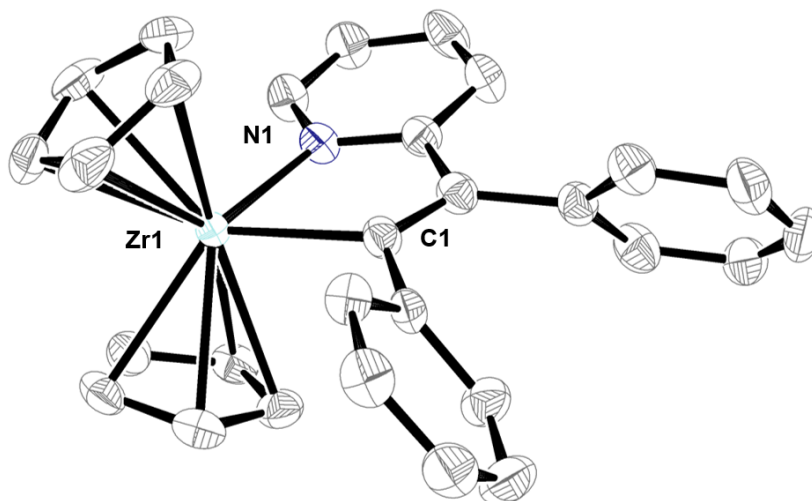


Figure 2-3. Thermal ellipsoid (50%) diagram of the molecular structure of diphenylacetylene inserted zirconocene **2•B(C₆F₅)₄** with the [B(C₆F₅)₄] counterion and hydrogen atoms removed for clarity. Selected bond lengths (Å): Zr1-N1 2.276(5), Zr1-C1 2.273(5).

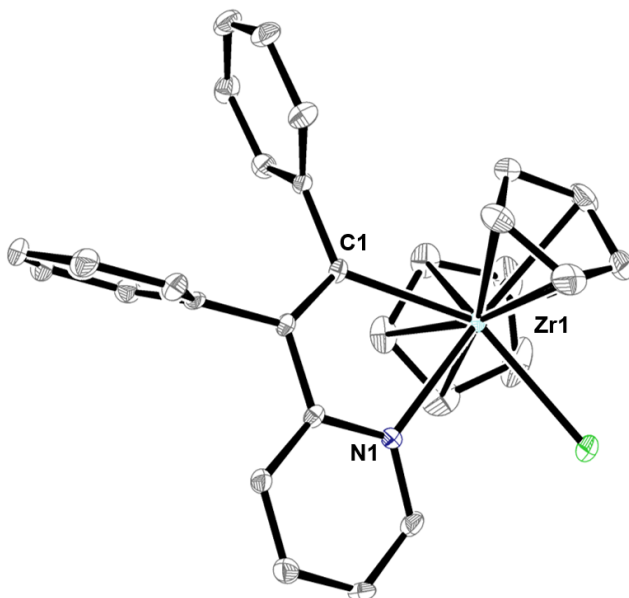


Figure 2-4. Thermal ellipsoid diagram (50%) diagram of the molecular structure of **3**, hydrogen atoms removed for clarity. Selected bond lengths (Å) Zr1-N1 2.447(3), Zr1-C1 2.403(3).

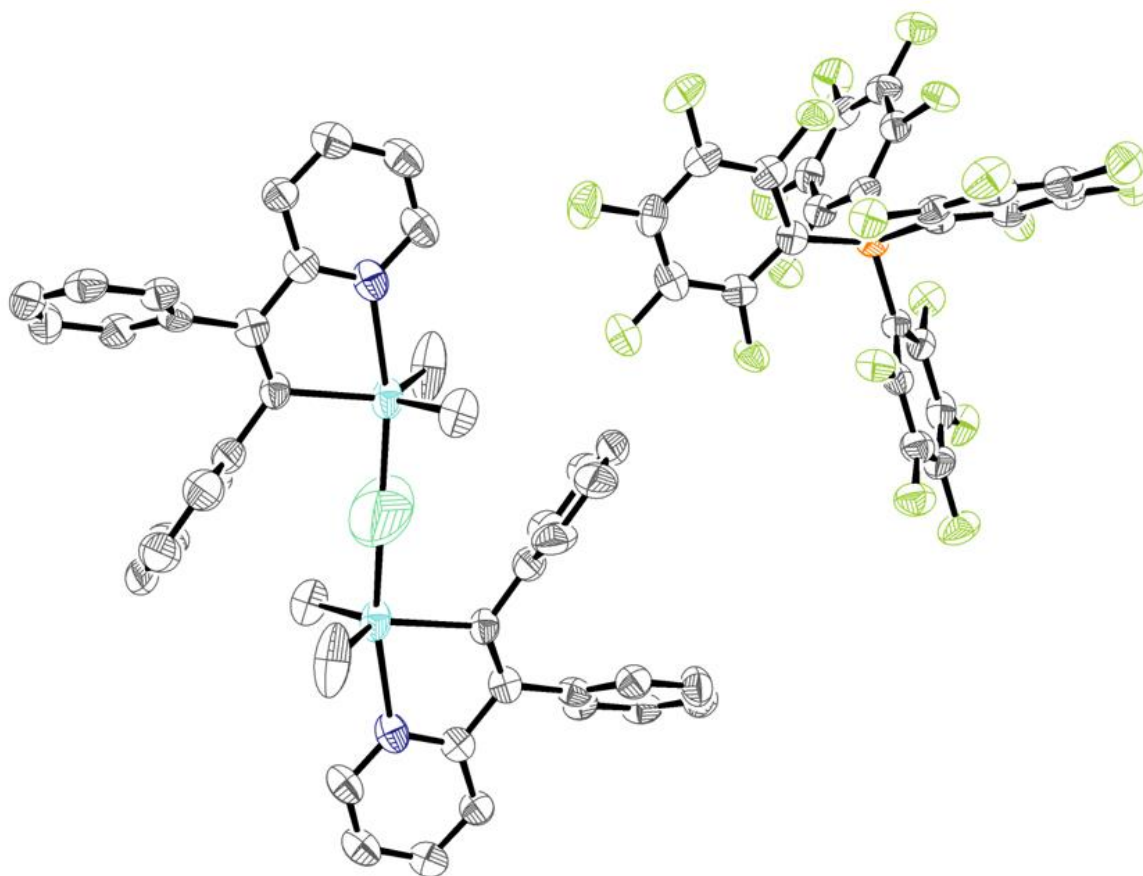


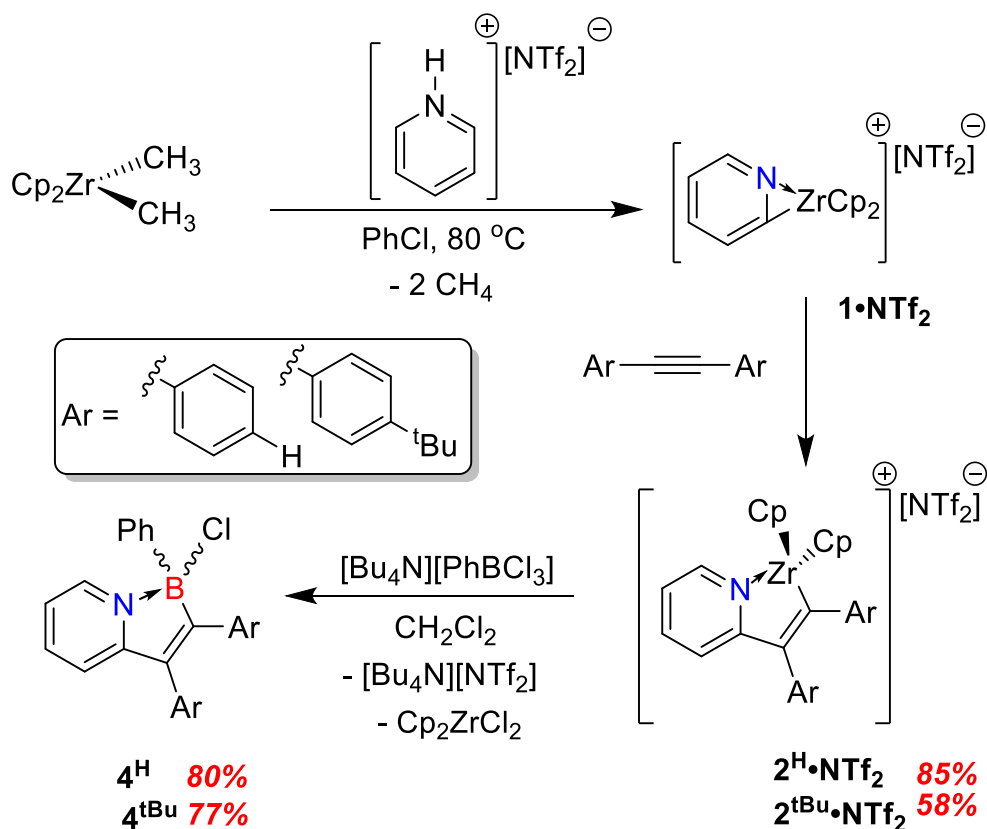
Figure 2-5. Thermal ellipsoid (50%) diagram of the molecular structure of Sn dimer species, hydrogen atoms removed for clarity.

In the first step, the η^2 -pyridyl complex **1**•NTf₂ was generated in situ via reaction of dimethyl zirconocene and the triflimato pyridinium salt,¹¹⁴ and used without isolation in further reactions with the diaryl acetylenes shown. Unfortunately, the analogous triflate salt **1**•OTf could not be prepared, probably due to the higher coordinating tendencies¹¹⁵ of OTf⁻ vs NTf₂⁻ in the Cp₂Zr(CH₃)ETf_n products of protonolysis. This was supported by the isolation of single crystals of Cp₂Zr(CH₃)(OTf) from the reaction of pyridinium triflate with dimethyl zirconocene. Pyridine is unreactive towards the triflate derivative,¹¹⁶ but for E = N, n = 2, the product zirconocycles **2**^H•NTf₂ and **2**^{Bu}•NTf₂ were isolated in good yields, the former on a multigram scale. Instead of

using [PPN][Cl] as the chloride source, cations **2**•NTf₂ were treated with [Bu₄N][PhBCl₃],¹¹⁷ and the required neutral zirconocenes **3**^H and **3**^{tBu} were generated in situ in the presence of PhBCl₂ leading directly to the BN indene products **4**^H and **4**^{tBu} in high yield as shown in Scheme 2-2.¹¹⁸

119

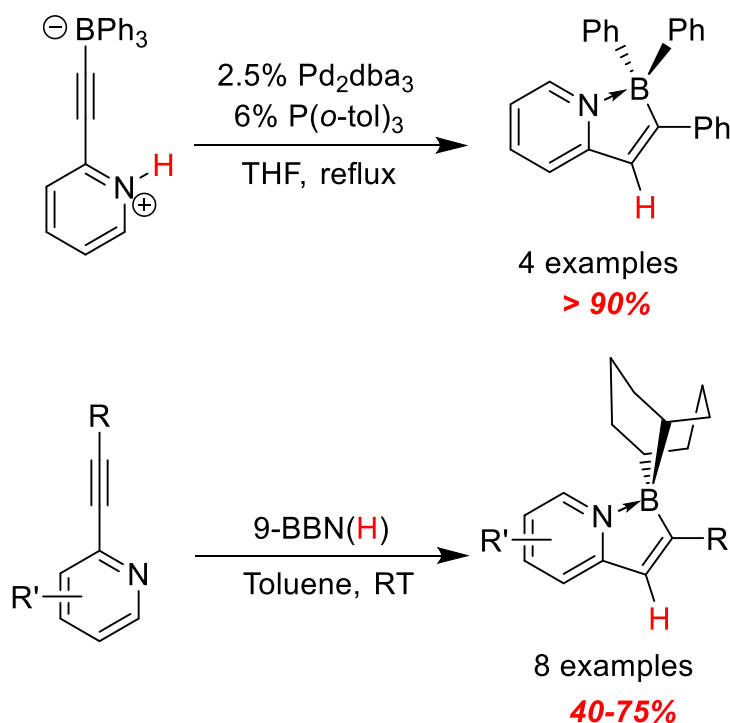
Scheme 2-2. Two step generation of BN-indenes.



This protocol provides an alternative, and potentially more versatile, route to these 3-bora-9-aza indenenes to those reported by Murakami¹⁰⁴ and Wang¹⁰⁵ (Scheme 2-3). In the Murakami method, palladium catalysis converts the zwitterionic alkynyl pyridinium borate substrates to the BN indenenes in a high yielding reaction that allows for hydrocarbyl substituents on the pyridinium

ring, and some variation in the aryl substituents on the borate. In the Wang synthesis, an unusual trans hydroboration is observed when the 2-alkynyl pyridine substrates are treated with stoichiometric 9-borabicyclo[3.3.1]nonane (9-BBN). Here, the yields are somewhat lower, and the R group is restricted to being an aryl group or a silyl substituent. In both previous methods, the boron atom of the BN indene ring is substituted by two aryl or alkyl groups, making further chemical derivatization at the boron center difficult.

Scheme 2-3. Murakami¹⁰⁴ (top) and Wang¹⁰⁵ (bottom) syntheses of BN-indenes.



Compounds **4^R** are isolable as air and moisture tolerant yellow powders by filtering the reaction mixtures through a plug of silica to remove the by-products. Vacuum line techniques are not required for these manipulations. The two derivatives were fully characterized spectroscopically and via an X-ray structural analysis on **4^H** (vide infra). In addition to the expected

resonances in the ^1H NMR spectra, the compounds are characterized by ^{11}B chemical shifts of 5.8 (4^{H}) and 6.3 (4^{tBu}) ppm, consistent with four coordinate, neutral boron centers. Like the previous examples reported, compound 4^{H} exhibits blue fluorescence at 481 nm when excited at its lowest energy absorption band of 369 nm ($\epsilon = 9.4 \times 10^3 \text{ M}^{-1} \text{ cm}^{-1}$) with an observed Stokes shift of 112 nm (6310 cm^{-1}). Spin-coating a film of the compound onto a glass substrate shows that the solid also fluoresces, albeit with a slightly reduced Stokes shift of 99 nm (6299 cm^{-1}) as shown in Figure 2-6. The lowest energy absorbance has been attributed to a π - π^* transition from the HOMO, to the LUMO which is largely associated with the five-membered ring with significant localization on the B-N bond.¹⁰⁵

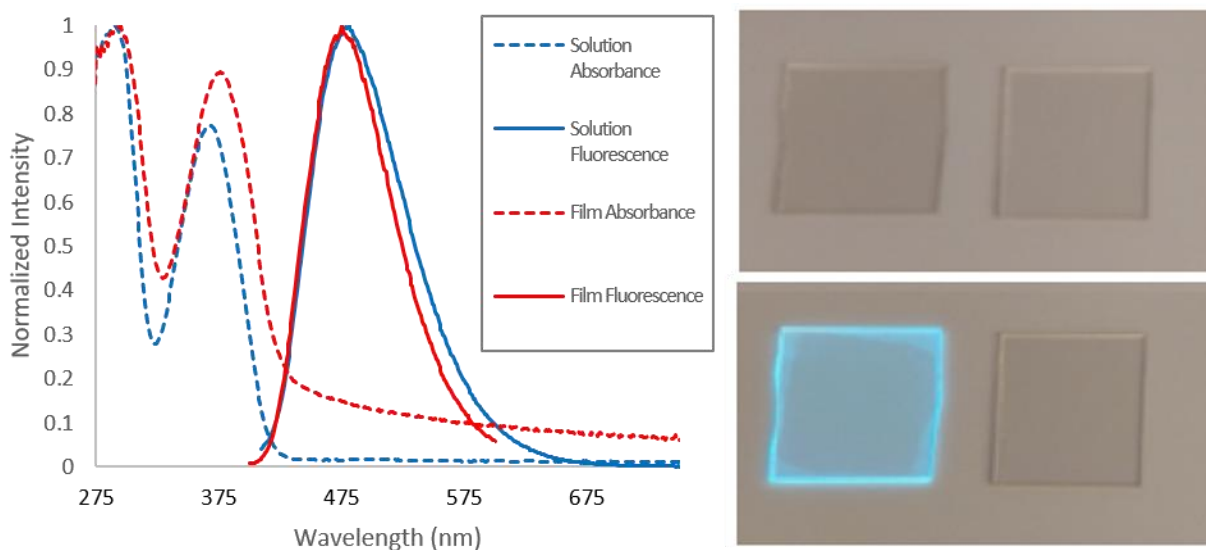


Figure 2-6. Left: Normalized absorption and emission spectra of 4^{H} in dichloromethane and thin film. Right: image of a glass substrate coated with 4^{H} under ambient (top) and 365 nm irradiation (bottom), a blank side is shown next to the spin coated substrate for comparison.

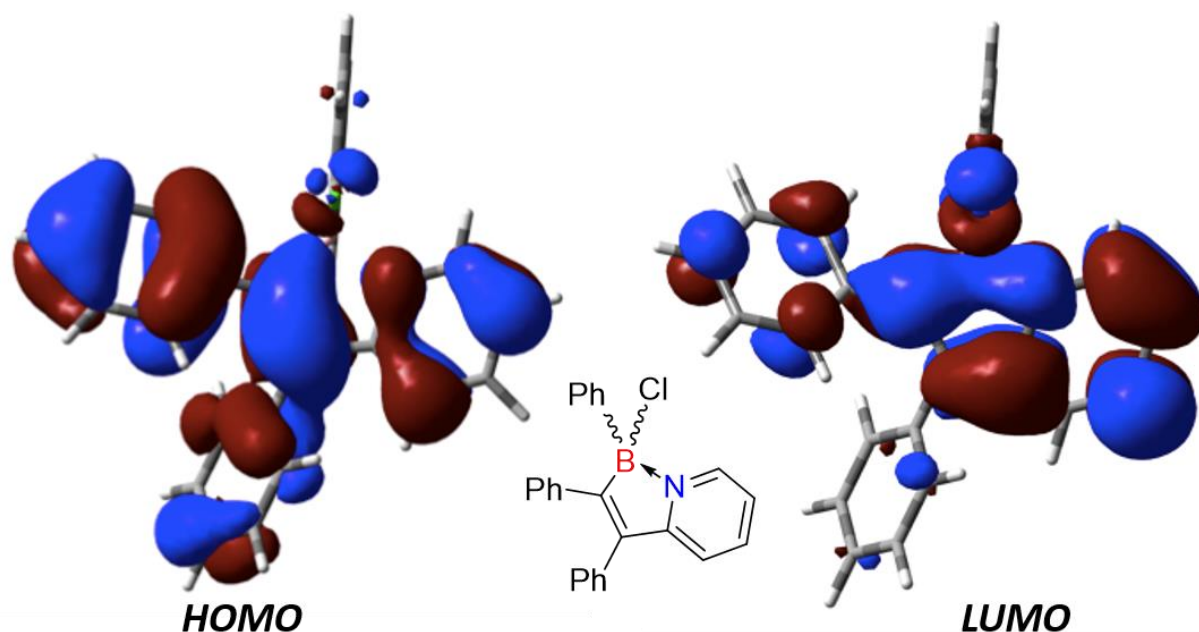
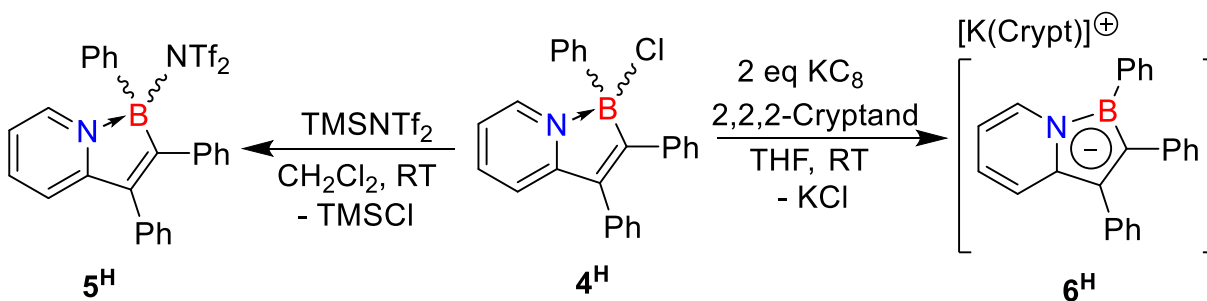


Figure 2-7. Frontier molecular orbitals of **4^H** calculated at the PBE0/TZVP level.

Even though the by-product of the reaction from this second synthetic pathway is a smaller percentage of the total molecular weight it is still not very atom economical. Due to the method of work up through a silica plug, the Cp_2ZrCl_2 was never re-isolated as it stuck to the top of the plug. Fortunately, the large molecular weight salts $[\text{PPN}][\text{B}(\text{C}_6\text{F}_5)_4]$ and $[\text{nBu}_4\text{N}][\text{NTf}_2]$ could be isolated by passing excess dichloromethane through the silica plug. Both by-product salts were isolated in high purity and could conceivably be converted to several other useful products within our laboratory. One area of interest is as an electrolyte for electrochemical measurements instead of the difficult to purify $[\text{nBu}_4\text{N}][\text{B}(\text{C}_6\text{F}_5)_4]$ employed in many electrochemical measurements. Potential variation in the diaryl acetylene employed, the ArBX_2 reagent utilized, and substitution on the pyridyl component makes this route a modular strategy for assembling 3-bora-9-aza indene ring systems. In addition, and distinct from the previously reported methods, in this route the boron

retains a halogen function in the products, allowing for further derivatization of the core framework. For example, as shown in Scheme 2-4, this halide can be exchanged for other anions via abstractive protocols or removed via two electron reduction to form a BN-indenide anion. Treatment of **4^H** with trimethylsilyl triflamide, TMSNTf₂, rapidly produces TMSCl and a new 3-bora-9-aza indene, **5^H**, in which the NTf₂ anion has replaced the chloride ion. The X-ray structure of **5^H** was determined (Figure 2-8) and despite some disorder in the NTf₂ anion, it is apparent that in the solid state it remains coordinated to the boron center through one of the oxygen atoms (B1-O1 = 1.565(6)Å).

Scheme 2-4. Reactions of **4^H**.



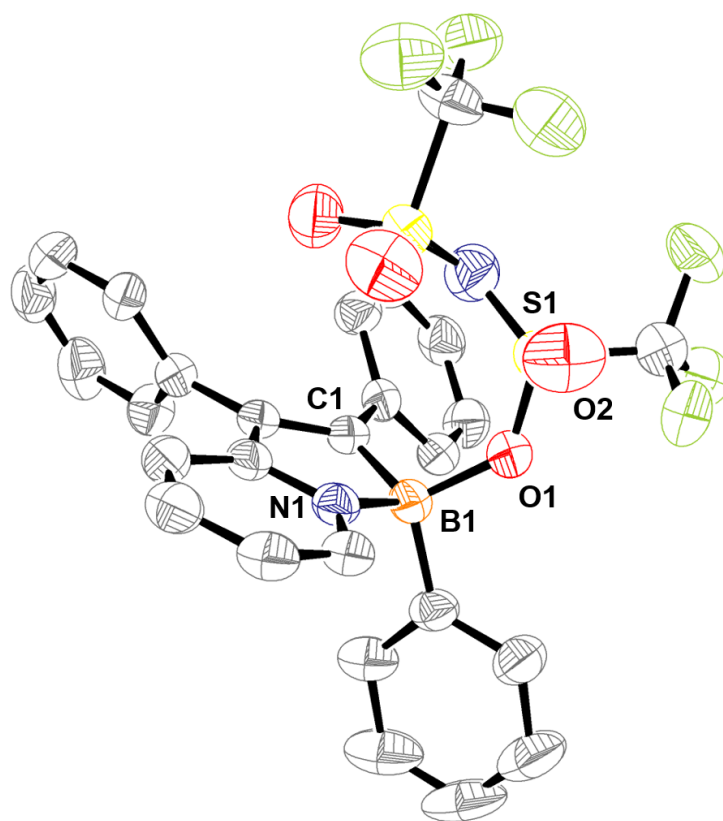


Figure 2-8. Thermal ellipsoid diagram (50%) of **5^H** showing one of two equivalent molecules in the unit cell with hydrogen atoms removed for clarity. Selected bond lengths (Å) B1-N1 1.593(7), B1-C1 1.597(7), B1-O1 1.565(6), S1-O1 1.491(3), S1-O2 1.424(8).

The bond distances within the BN-indene ring of **5^H** do not differ significantly from those seen in **4^H** and the ^{11}B NMR resonance for **5^H** (10.5 ppm) compared to **4^H** (6.4 ppm), although slightly downfield shifted suggests that the borenium ion character in this compound is low. This is further supported by the small changes in chemical shifts observed in the ^1H NMR spectra suggesting little change in the overall electronic structure (Figure 2-9). Still, in the ^{19}F NMR spectrum, the CF_3 groups appear as a single resonance even at low temperatures, suggesting some lability in the anion and the potential for **5^H** to serve as a borocation¹²⁰ synthon.

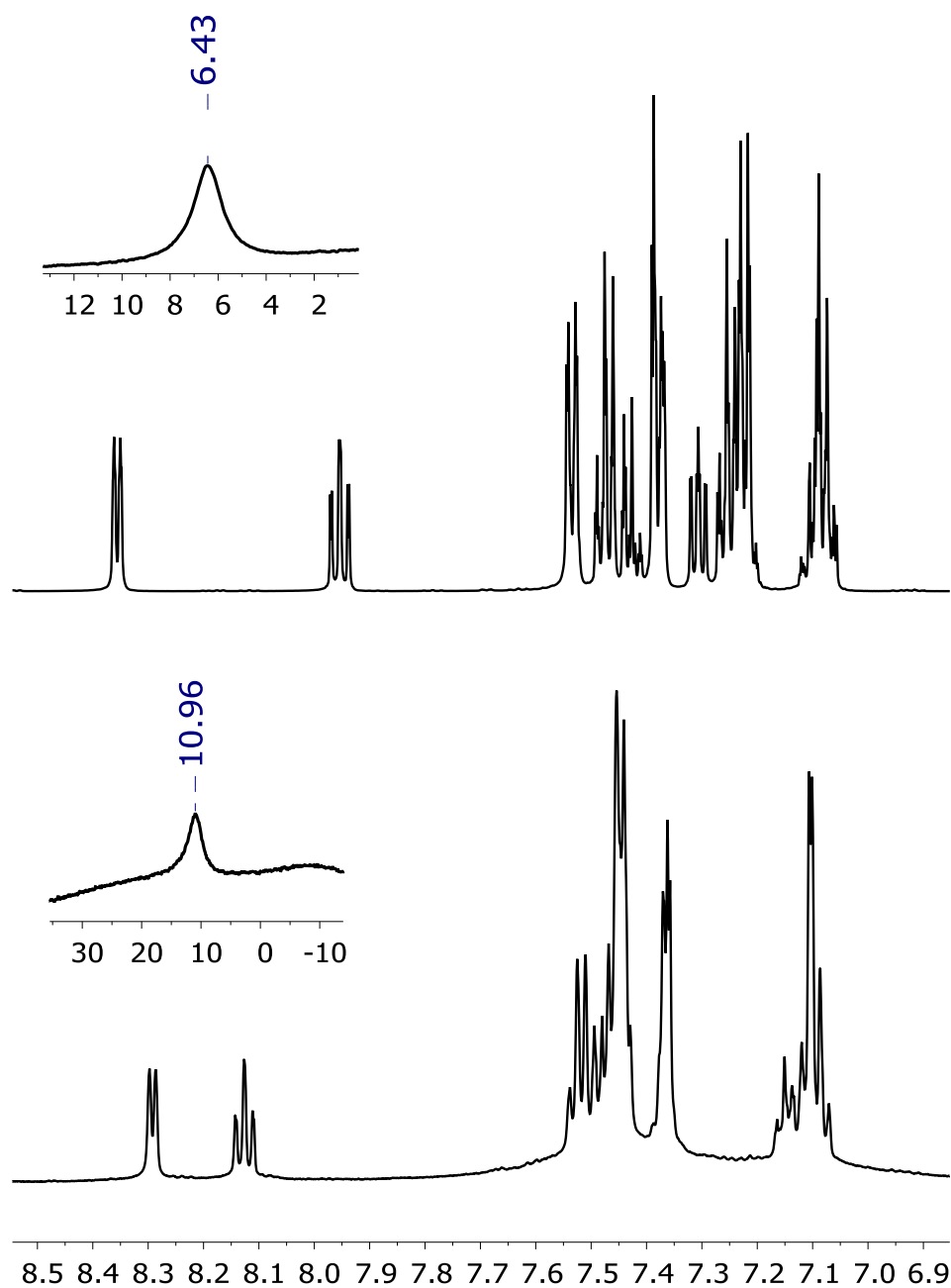


Figure 2-9. ¹H NMR (CD₂Cl₂) spectra of **4^H** (top) and **5^H** (bottom), with ¹¹B NMR spectra as inserts.

Electrochemical measurements on **4^H** (Figure 2-10) suggest that it can be reduced, as evidenced by the irreversible reduction waves present at -1.3 and -2.0 V vs Fc/Fc⁺. While efforts

were undertaken to reduce 4^{H} by one electron using one equivalent of either cobaltocene or potassium graphite, a non-isolable product was generated showing broad aromatic signals in the ^1H NMR spectra and the disappearance of any ^{11}B NMR signal. Treatment of THF solutions of the chloroborane with two equivalents KC_8 led to a rapid yellow to red color change and after workup, the potassium salt of 6^{H} could be isolated as an orange powder. Use of 2,2,2-cryptand allowed us to obtain crystals suitable for X-ray diffraction, but for reactivity studies, the cryptand is not necessary.

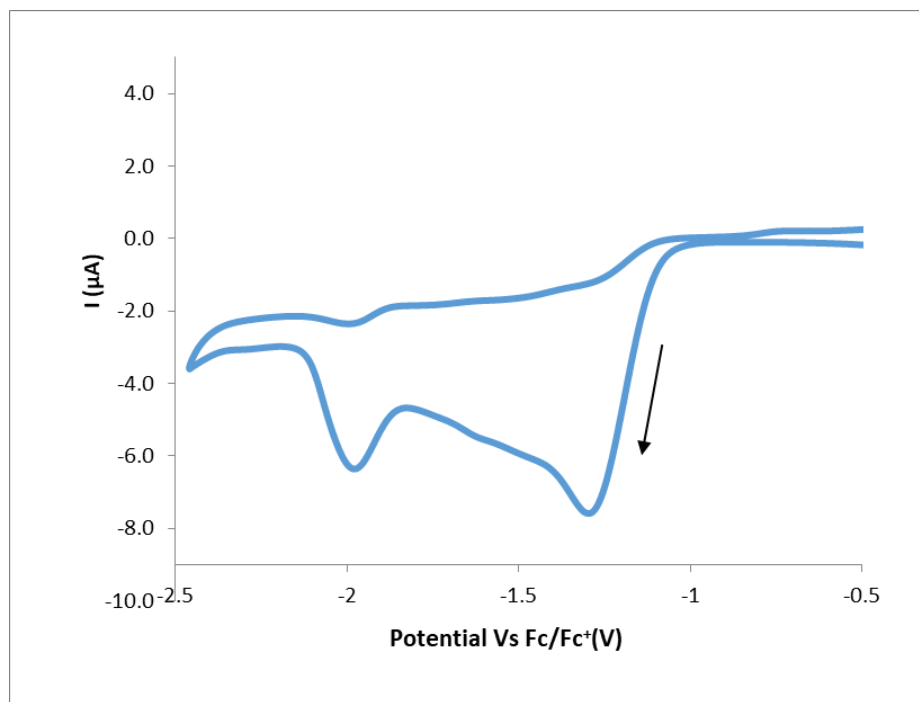


Figure 2-10. Cyclic voltammetry of a 1.16mM solution of 4^{H} in THF was measured using a three electrode setup using a CHI660D potentiostat. Glassy carbon, platinum wire, and silver wire were used as the working, counter, and reference electrodes, respectively. Ionic strength of the solution was maintained by using a 0.1M solution of $[\text{nBu}_4\text{N}][\text{PF}_6]$ in THF solvent. The sweep window was from -2.46V to 1.04V at 200 mV/s.

The structures of both **4^H** and **6^H** are depicted in Figure 2-12 for easy comparison. It is apparent that the boron center goes from tetrahedral to planar and this is reflected in the downfield shift of the boron resonance for **6^H** to 24.5 ppm. A comparison of the bond distances within the fused BN framework shows that in **4^H** there is bond alternation in the five-membered ring, while in the six-membered pyridyl ring the congruent distances indicate delocalization. The situation is reversed in the 10 π anion **6^H**, where bond equalization is apparent in the BN containing ring, while localization occurs in the pyridyl ring. This is supported by Nucleus Independent Chemical Shift (NICS) computations using Density Functional Theory (DFT), which show that the five membered ring is aromatic with NICS(0) and NICS(1) values of -12.5 and -11.4 respectively, while the six membered ring is non-aromatic with NICS values near zero (Table 2-1). This change in bonding is further supported by examining the ¹H NMR spectra of **6^H** compared to **4^H**. As shown in Figure 2-11 two diagnostic signals are highlighted in red and correspond to two of the hydrogens on the pyridyl ring. There is a clear shift from the aromatic region (signals at ~ 8.4 and 7.9 ppm) to the area one would expect to find alkene signals (~ 5.6 and 5.5 ppm). A more detailed discussion of the bonding within this molecule and its reactivity is discussed in Chapter three of this thesis.

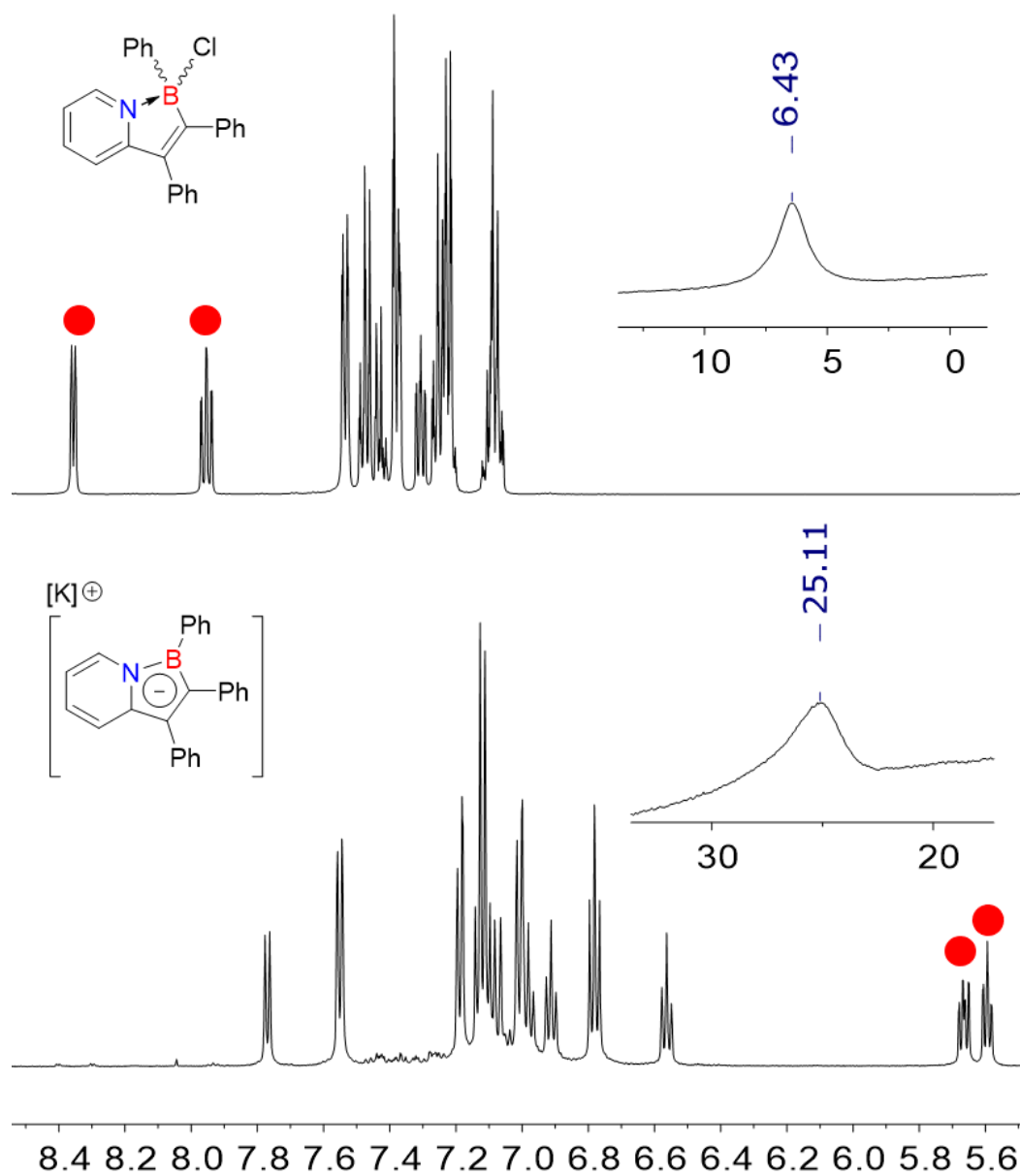


Figure 2-11. ^1H NMR spectra of **4^H** in CD_2Cl_2 (top) and **6^H** in THF-D_8 (bottom), with ^{11}B NMR spectra as inserts. Two signals from the pyridyl ring have been highlighted in red.

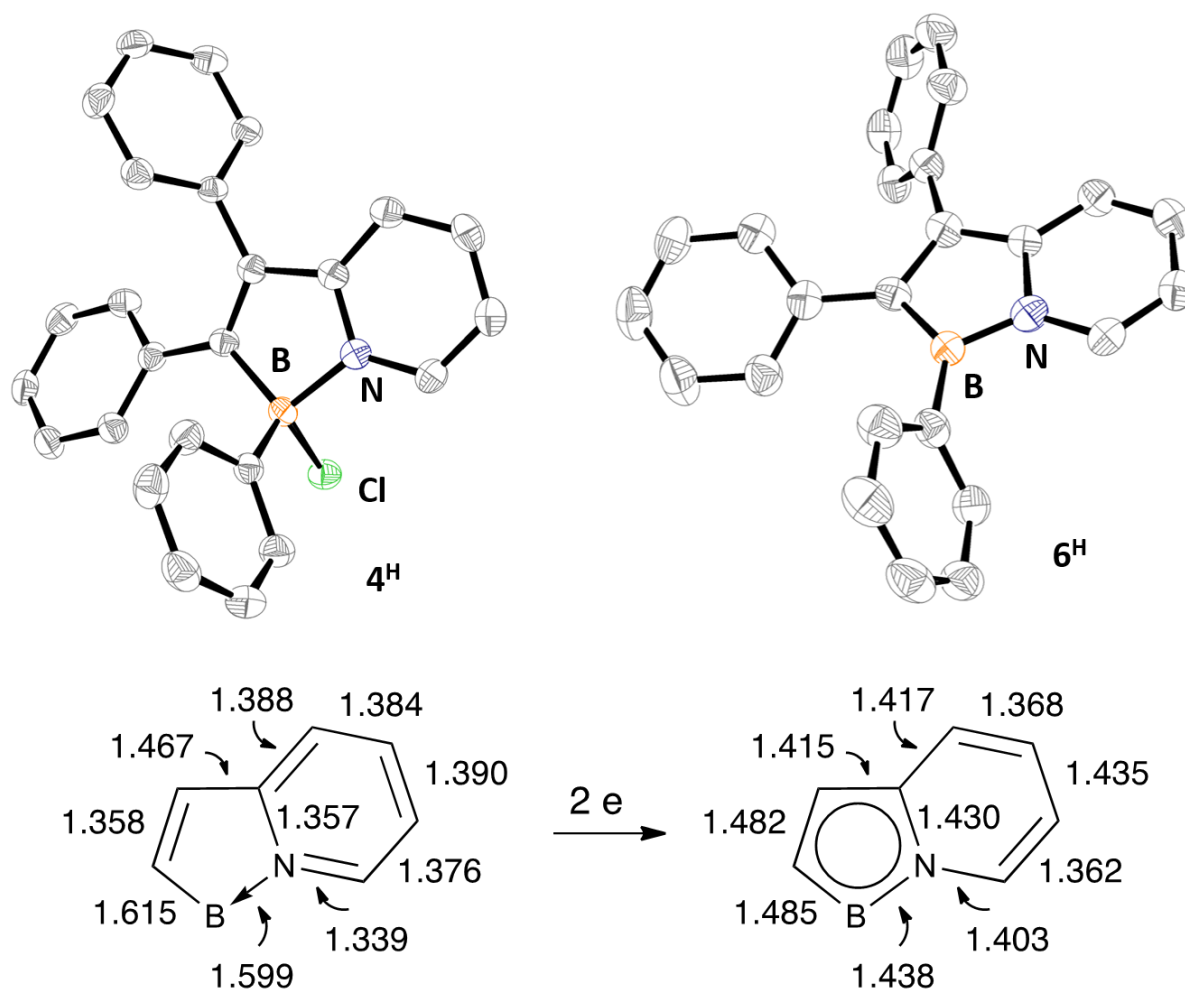
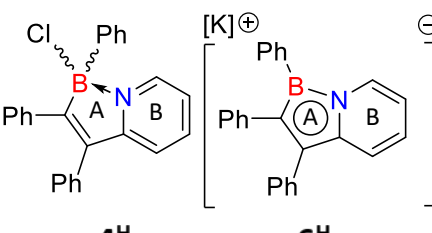


Figure 2-12. Thermal ellipsoid (50%) diagrams of the molecular structures of **4^H** (left) and **6^H** (right); hydrogen atoms have been removed for clarity in both structures and for **6^H**, the [(2,2,2-cryptand)K]⁺ is omitted. Below each structure, the bond distances for the bonds of the 3-bora-9-aza rings are given; for clarity, the e.s.d. values are omitted, but none is greater than 4.

Table 2-1. NICS Calculations of **4^H** and **6^H**.



4^H

6^H

NICS(0)	A	0.9	-12.5
	B	-6.5	0.0
NICS(1)	A	-1.9	-11.4
	B	-8.0	-1.8

Having demonstrated the efficacy of the zirconocene-based methodology for assembling 3-bora-9-aza indenenes, we sought to apply it to the synthesis of a new BN heterocyclic framework. *s*-Indacene (Figure 2-1) is an interesting conjugated hydrocarbon due to its ambiguous aromaticity. Although it is a 12 π system, and therefore formally antiaromatic, experimental^{106, 121, 122} and computational studies^{107, 123, 124} show that there is significant carbon-carbon bond equalization on the perimeter of the molecule, leading to its description as a “quasi-aromatic” system. These studies thus suggest that it assumes a D_{2h} structure instead of a C_{2h} isomer (Figure 2-1) in which the C=C bonds are more localized. Nonetheless, the synthesis of *s*-indacene derivatives is a challenge,¹⁰⁸ and must include sterically bulky substituents in the 1,3,5,7-positions,¹⁰⁶ or electron donating groups in the 4,8-positions¹²⁵ to prevent decomposition pathways that arise because of the considerable diradical character of the ground state D_{2h} structure.¹²³ Suitably substituted derivatives can be reduced by one¹²⁶ or two¹²⁷ electrons and have promise as structural subunits in conductive organic materials.^{128, 129} Readily accessible BN-*s*-indacenes,¹³⁰ therefore, may be of

interest for incorporation into devices that utilize such materials, but are also of fundamental significance in addressing the effect of BN substitution on bond delocalization within the cyclic framework. Accordingly, we sought to apply our methodology to this problem. In order to direct the synthesis to the desired 1,5-dibora-4a,8a-diaza BN indacene, 2,5-dimethyl pyrazine was selected as the substrate for C-H activation with $[\text{Cp}_2\text{ZrCH}_3]^+$ (Scheme 2-5). Unfortunately, the pyrazine could not be doubly protonated to prepare a suitable NTf_2 salt and so $[\text{Cp}_2\text{ZrCH}_3][\text{B}(\text{C}_6\text{F}_5)_4]$ had to be employed for this synthesis for direct reaction with the pyrazine. The dimeric η^2 -pyridyl dication expected from double C-H activation of the pyrazine substrate (not shown in Scheme 2-5) formed smoothly, and in the optimized syntheses was used without isolation to generate the two zirconocycles $7^{\text{H}}\cdot\text{B}(\text{C}_6\text{F}_5)_4$ and $7^{\text{tBu}}\cdot\text{B}(\text{C}_6\text{F}_5)_4$ in excellent yields as deep purple solids on scales of up to 2 grams. Both compounds have been fully characterized, including via X-ray crystallography in the case of $7^{\text{H}}\cdot\text{B}(\text{C}_6\text{F}_5)_4$ (Figure 2-13).

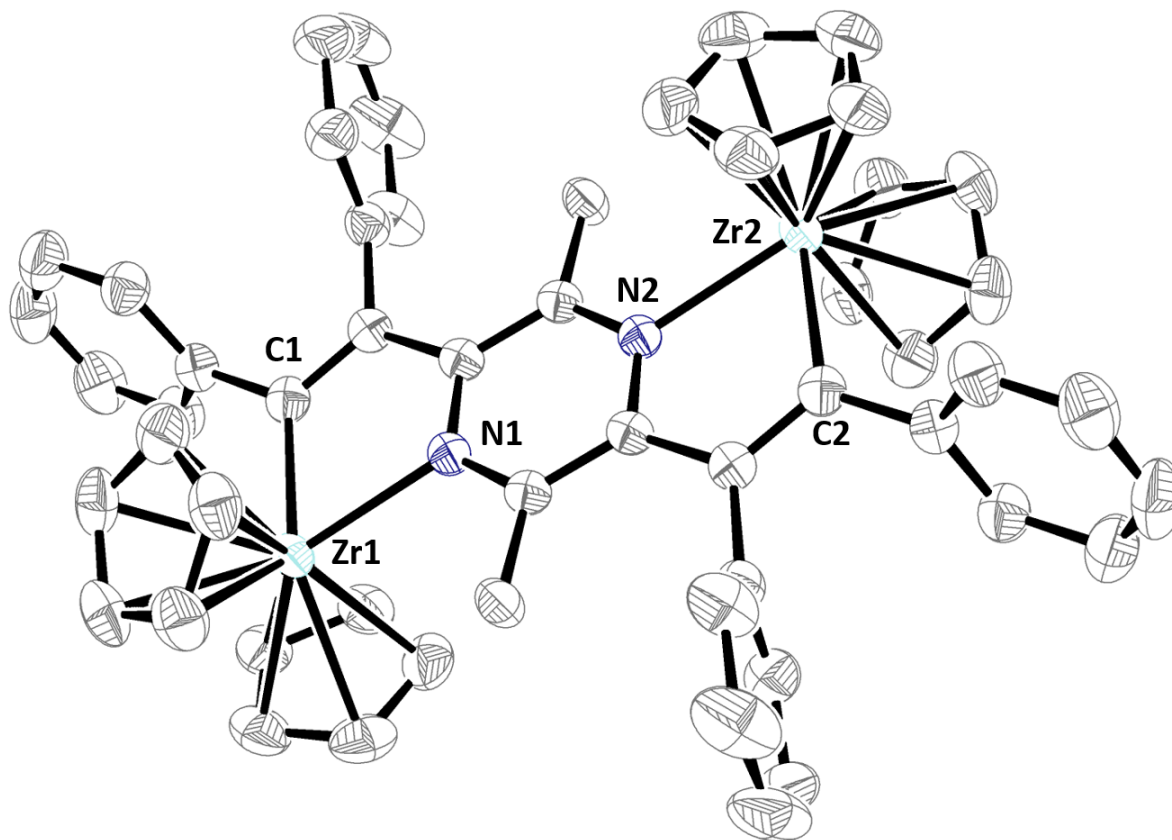
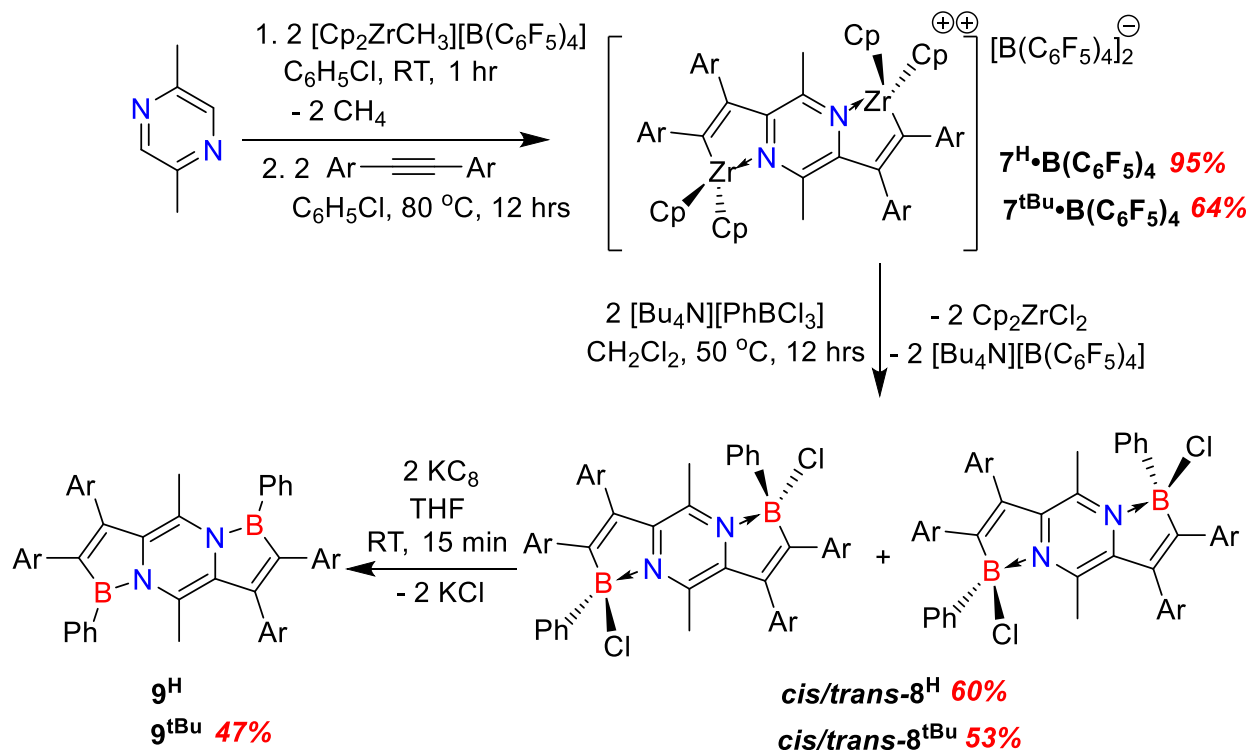


Figure 2-13. Thermal ellipsoid diagram (50%) of $7^{\text{H}}\cdot\text{B}(\text{C}_6\text{F}_5)_4$ with the $[\text{B}(\text{C}_6\text{F}_5)_4]^-$ counterions and hydrogen atoms removed for clarity. Selected bond lengths (Å) Zr1-C1 2.287(3), Zr1-N1 2.323(2).

The structure is similar in nature to that found for $2^{\text{H}}\cdot\text{B}(\text{C}_6\text{F}_5)_4$ and the purple color in comparison to the orange hue of $2^{\text{H}}\cdot\text{B}(\text{C}_6\text{F}_5)$ is presumably due to the more extended conjugation in $7^{\text{H}}\cdot\text{B}(\text{C}_6\text{F}_5)$. As shown in Scheme 2-5, the zirconocycles were carried forward to the pink colored boracycles 8^{R} via treatment with $[\text{Bu}_4\text{N}][\text{PhBCl}_3]$; compounds 8^{R} are produced as essentially 1:1 mixtures of the cis and trans isomers as defined by the disposition of the substituents on boron across the plane of the polycyclic framework. The isomers are distinguishable by NMR spectroscopy, and they can be enriched by careful fractional crystallization methods because the cis isomer is more soluble in CH_2Cl_2 /hexanes mixtures than the trans. In this way, the molecular

structures of both *cis*-**8^H** and *trans*-**8^H** were determined (Figure 2-14) and the nature of the isomers produced in this reaction confirmed. In terms of bond distances within the heterocyclic framework, the two isomers are very similar (Table 2-2), and since separation of these isomers is not necessary for the next step, they will not be discussed in detail here. Interestingly, a *cis* enriched sample of **8^H** (95:5) could be equilibrated back to a 50:50 mixture by heating to 50 °C for several hours, indicating that this is the thermodynamic ratio of the *cis* and *trans* isomers. The mechanism of equilibration is unknown, but involvement of borenium ions¹²⁰ accessible via chloride dissociation is the most likely scenario.

Scheme 2-5. Synthesis of 1,5-dibora-4a,8a-diaza-1,2,3,5,6,7-hexaaryl-4,8-dimethyl-s-indacenes.



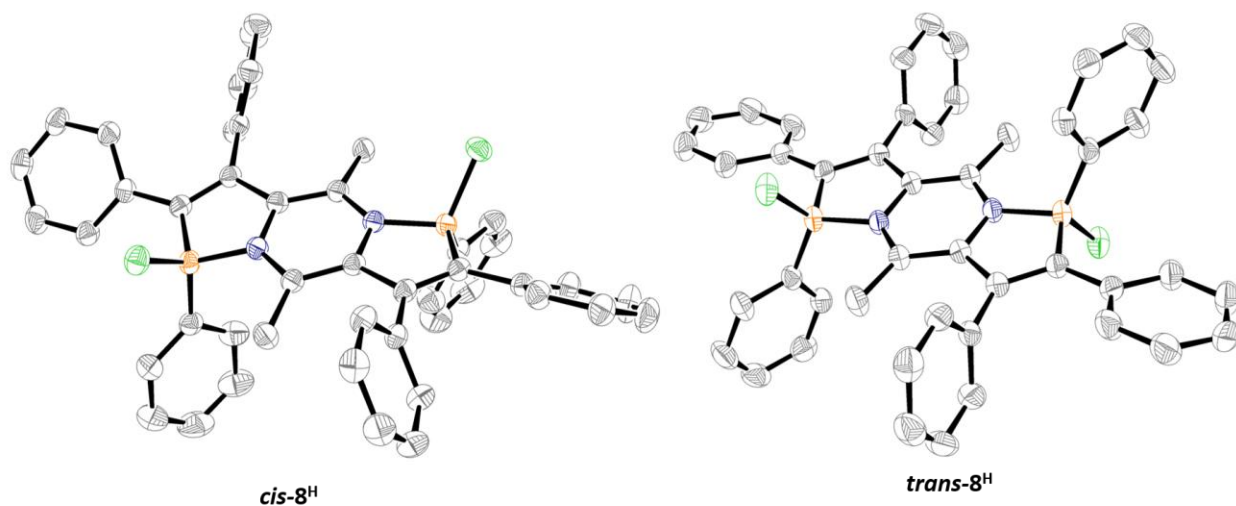
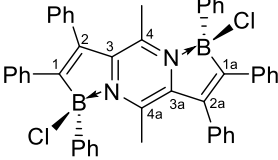
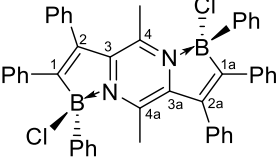


Figure 2-14. Thermal ellipsoid (50%) diagrams of the molecular structures of *cis-8^H* (left) and *trans-8^H* (right); hydrogen atoms have been re-moved for clarity in both structures.

Table 2-2. Comparison of bond lengths from molecular structures of isomers **8**.

Bond		
	<i>cis-8^H</i>	<i>trans-8^H</i>
B1-N1	1.633(2)	1.625(3)
B1-C1	1.599(2)	1.602(3)
C1-C2	1.357(2)	1.369(3)
C2-C3	1.471(2)	1.465(3)
C3-C4	1.407(2)	1.412(3)
C3-N1	1.364(2)	1.363(3)
C4-N1a	1.345(2)	1.341(3)
B1a-N1a	1.625(2)	1.625(3)
B1a-C1a	1.604(2)	1.602(3)
C1a-C2a	1.356(2)	1.369(3)
C2a-C3a	1.471(2)	1.465(3)
C3a-C4a	1.405(2)	1.412(3)
C3a-N1a	1.365(2)	1.363(3)
C4a-N1	1.344(2)	1.341(3)

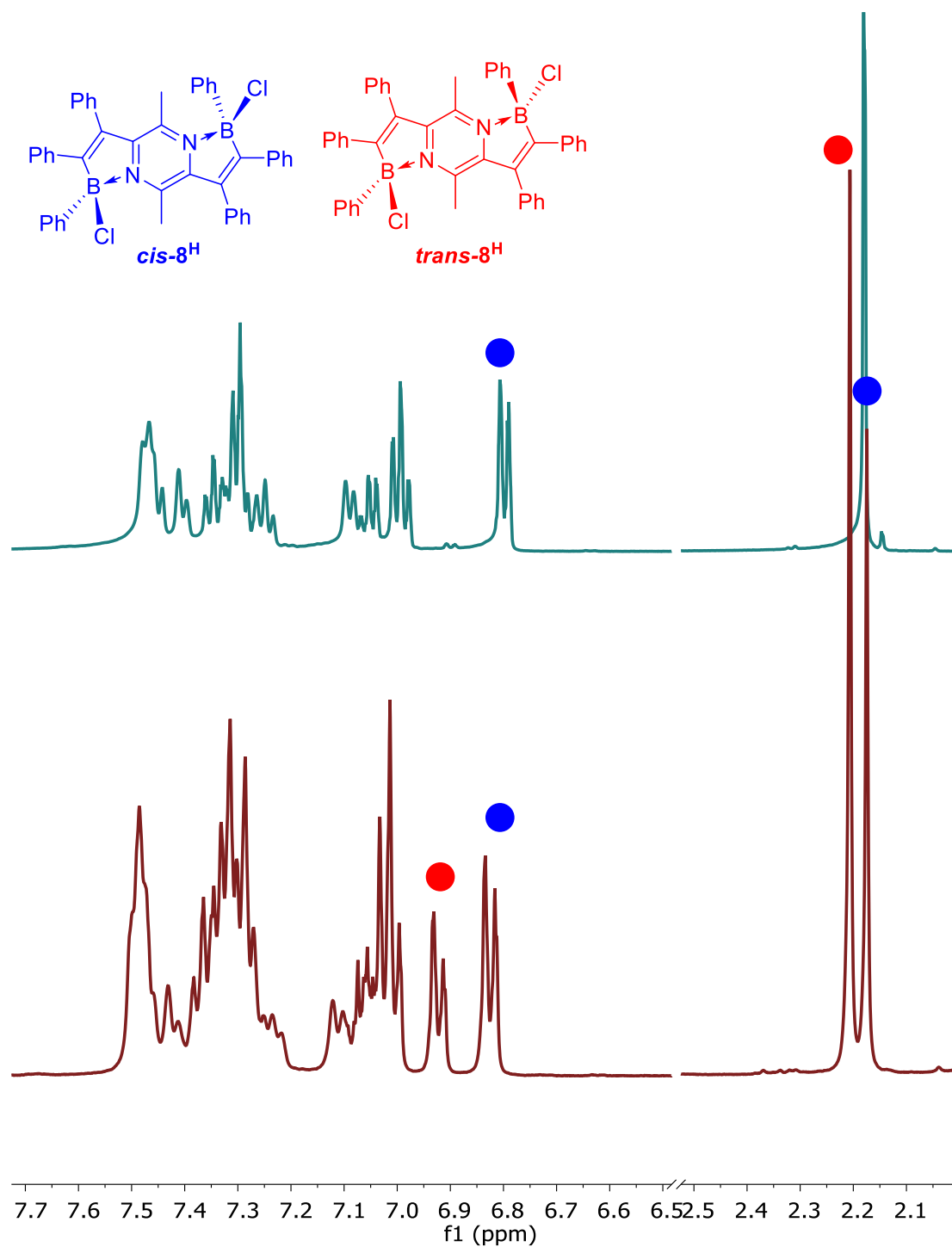


Figure 2-15. ^1H NMR spectra (CD_2Cl_2) of *cis*-**8^H** (top) and a mixture of *cis*/*trans*-**8^H** (bottom). Diagnostic signals are highlighted in blue (*cis*-**8^H**) and red (*trans*-**8^H**).

Compounds **8^R** serve as ideal precursors to the target 1,5-dibora-4a,8a-diaza BN indacenes via reduction by two electrons using KC₈. These reactions proceed efficiently at room temperature in THF. For the reduction of *cis/trans*-**8^H**, the product **9^H** precipitates as a yellow powder from the reaction mixture and was found to be sparingly soluble in all common solvents. It was therefore difficult to purify and obtain NMR data on this species. A molecular structure with poor bond precision was obtained and established the connectivity of the structure conclusively. The compound **9^{tBu}**, however, was more well-behaved and fully characterized by all the usual means. A resonance at 42.3 ppm was observed in the ¹¹B NMR spectrum and the patterns of resonances in both the ¹H and ¹³C{¹H} NMR spectra were fully consistent with the proposed structure. The compounds were not stable when exposed to ambient atmosphere, with both solutions and solid samples returning to a dark pink color in the presence of O₂/H₂O. The nature of the products was not determined. Single crystals of **9^{tBu}** were obtained from THF/pentane and the molecular structure is depicted in Figure 2-16.

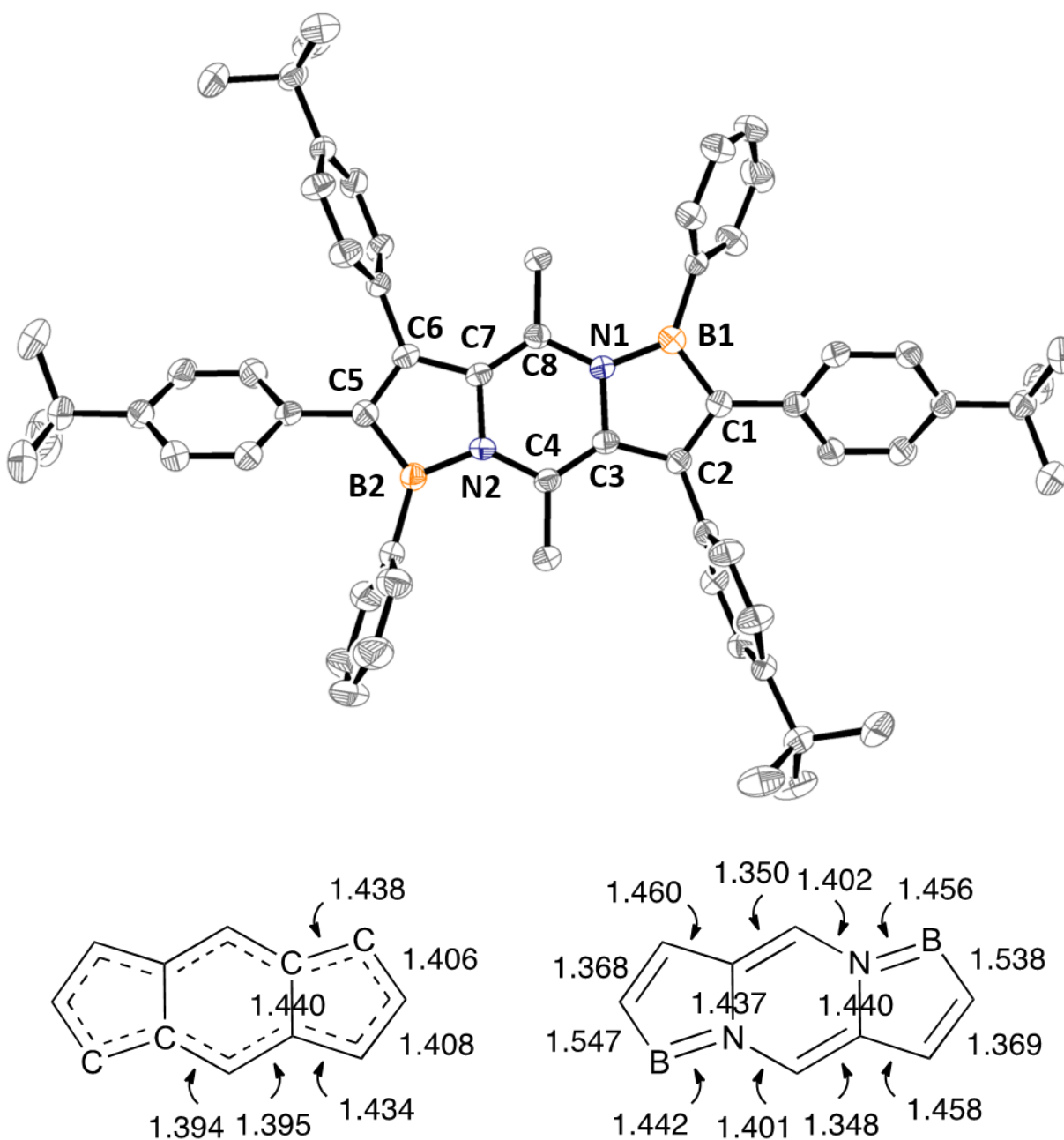
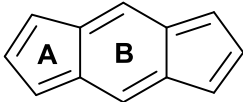
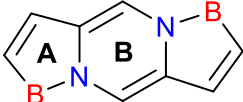
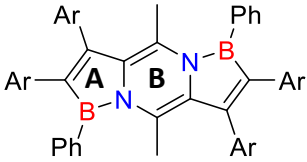


Figure 2-16. Thermal ellipsoid (50%) diagrams of the molecular structure of **9tBu**; hydrogen atoms have been removed for clarity. Below the structure, the bond distances for the bonds within the tricyclic ring system are given, along with those for the parent hydrocarbon as its 1,3,5,7-tert-butyl substituted derivative;¹²² for clarity, the e.s.d. values are omitted, but none is greater than 5.

The C₈B₂N₂ heterocyclic ring system is planar, with the range of deviation from the least squares plane defined by these atoms at 0.008-0.070 Å. The bond distances within the tricyclic framework are depicted below the structure, along with the values found for 1,3,5,7-tert-butyl-s-indacene (**II**^{tBu}).¹²² It can be seen that the bond alternation in **9**^{tBu} is pronounced in comparison to the delocalization observed in the all-carbon tricycle. In particular, short B-N distances of 1.442(5) and 1.456(5) Å are suggestive of double bond character, and the distances of 1.369(5) Å for C1-C2 and 1.368(5) Å for C5-C6 indicate localized C=C bonds.

DFT level NICS computations are consistent with this picture as the NICS(1) and NICS(0) values for both the 5 membered ring (-3.2; -2.0) and the central 6 membered ring (-0.3, 1.4) indicate that they are non-aromatic (Table 2-3). Thus, in comparison, the 12 π BN-*s*-indacene ring system is significantly more localized than the all-carbon analog. In order to further compare the electronic structures of **9**^R and *s*-indacene, gauge-including magnetically induced current (GIMIC) calculations were performed at the DFT level.^{87, 88}

Table 2-3. NICS and GIMIC analysis on indacene species.

Ar = p-^tBuPh

	A	B	A	B	A	B
NICS(1)	8.8	8.1	-4.8	0.3	-3.2	-0.3
NICS(0)	12.9	11.9	-3.1	1.9	-2.0	1.4
NICS(1) _{zz}	30.2	28.4	-9.3	3.4	-4.2	-2.5
GIMIC	-7.6	-5.6	2.6	-1.0		

In short, GIMIC analysis allows for the determination and visualization of magnetically induced diatropic (clockwise) and paratropic (anti-clockwise) ring-currents (Figure 2-17) that are associated with aromaticity and antiaromaticity, respectively.⁸⁸ Specifically, for aromatic molecules, diatropic current on the outside of the rings (depicted by blue surface in Figure 2-17a and Figure 2-17d) dominates over the paratropic current (red surface in Figure 2-17a and Figure 2-17d) that lies mostly inside the rings, while the relative strengths of the currents are reversed for anti-aromatic molecules. For comparative purposes, a net ring current can be calculated for each ring in the molecule by averaging the net currents of individual bonds in the ring (calculated by integrating the diatropic and paratropic currents through a cross section of the bond). In the case of *s*-indacene, the **II-D_{2h}** symmetric structure with a broken symmetry singlet ground state was calculated to be the global minimum, in agreement with the diradical character of **II**.¹²³ Although the **II-C_{2h}** structure was found to be a local minimum 3.1 kcal mol⁻¹ higher in enthalpy than **II-D_{2h}**, it was nevertheless used in the GIMIC analysis to represent a formally anti-aromatic reference system. Furthermore, instead of employing **9^H** or **9^{tBu}** in the GIMIC analysis, the parent 12 π BN-*s*-indacene **I^H** (Figure 2-17e) was used to simplify the interpretation of results.

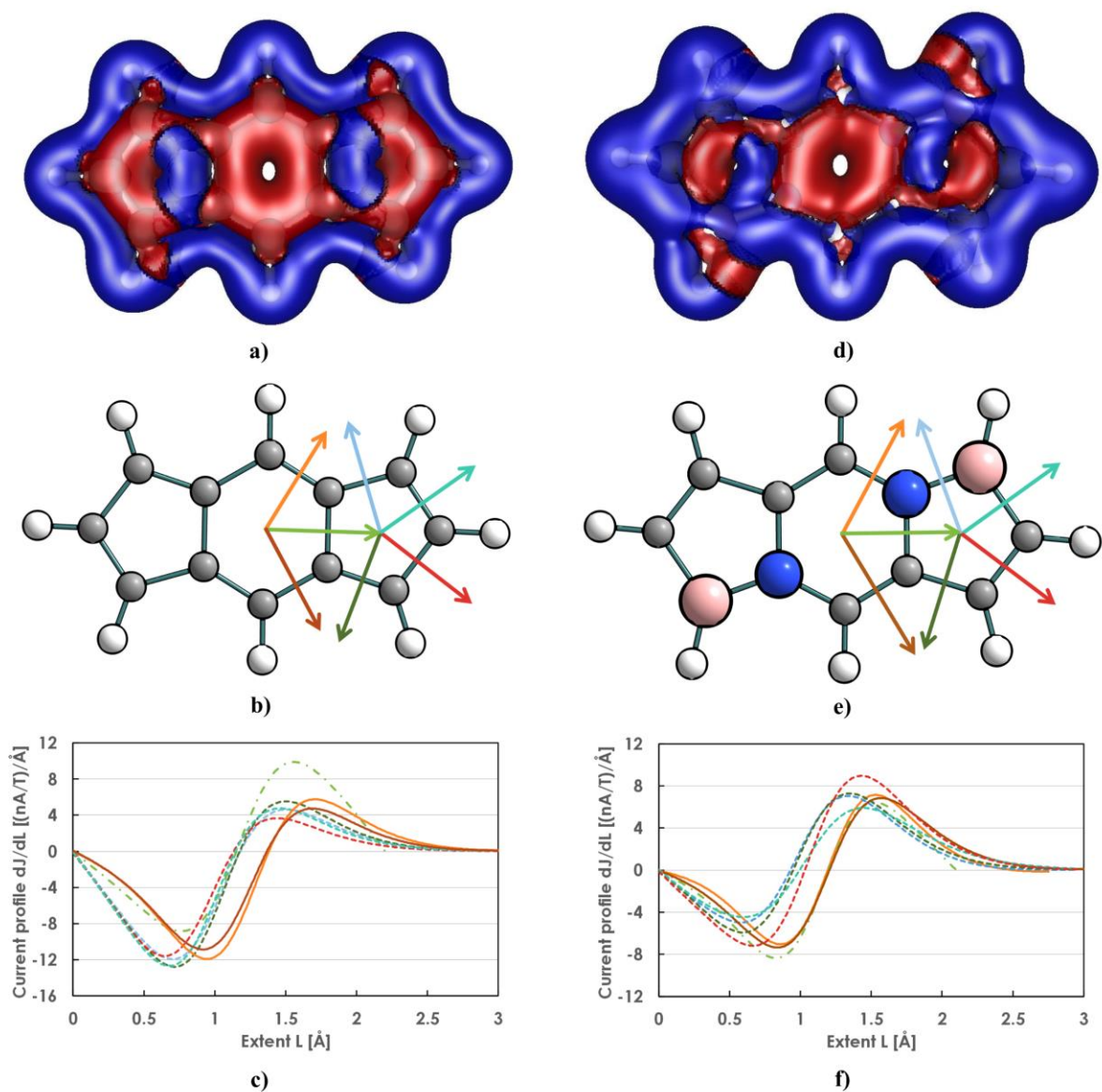
















Figure 2-17. Results from GIMIC analyses for **II-C_{2h}** (left) and **I^H** (right). (a,d): Isosurface (0.015) of the signed modulus of the calculated magnetically induced current density (blue, diatropic current; red, paratropic current); (b, e): color coding for inequivalent bonds; and (c, f): current strength profiles across the bonds.

For **II-C_{2h}**, the magnetically induced current profiles across inequivalent bonds (Figure 2-17c) and integrated current contributions (Table 2-1) indicate that paratropic (negative) contributions to the net current are much stronger than diatropic contributions for all of the bonds

apart from the bond connecting the 5 and 6 membered rings. Consequently, the net ring currents calculated as averages of the integrated current strengths of individual bonds were found to be strongly paratropic for both the 5 (-7.6 nA T^{-1}) and 6 membered (-5.6 nA T^{-1}) rings, in line with the 12π antiaromatic nature of the structure. By comparison, the current strength profiles of **I^H** bonds (Figure 2-17f) indicate comparable contributions from both paratropic and diatropic parts of the magnetically induced current that result in weak net ring currents for both the 5 (2.6 nA T^{-1}) and 6 membered rings (-1.0 nA T^{-1}). The weak net currents are consistent with the non-aromatic nature inferred for **9^{tBu}** from NICS calculations and bond distance analysis. The observed change towards non-aromaticity upon BN for CC substitution is reminiscent of the decrease in the degree of aromaticity in 1,2-dihydro-1,2-azaborine¹⁰¹ and BN substituted fused polyaromatic hydrocarbons¹³¹ compared to their all-carbon analogs.

Looking at the individual contributions from diatropic and paratropic currents to the net current (Table 2-4), the GIMIC analysis shows that the strengths of diatropic bond currents increase only slightly going from **II-C_{2h}** to **I^H** whereas the paratropic currents decrease significantly. The analysis also reveals distinct fluctuations in the strengths of diatropic and paratropic currents going from one bond to the next, but the net currents across the perimeter bonds of a particular ring in **II-C_{2h}** or **I^H** stay roughly the same regardless of the atoms involved in the bonds. This demonstrates that the BN for CC substitution in **I^H** affects the net currents across all the bonds in the molecule and the observed differences in ring currents between **II-C_{2h}** and **I^H** are not simply due to localized contributions from the BN heteroatom bonds.

Table 2-4. Integrated diatropic and paratropic magnetically induced current contributions to the net current strengths in inequivalent bonds of **II-C_{2h}** and **I^H** [in nA T⁻¹]. See Figures 2-8b and 2-8e, respectively, for color coding of bonds.

		Bond	Diatropic	Paratropic	Total
II-C_{2h}		C-C	7.8	-16.6	-8.8
		C-C	12.1	-11.3	0.8
		C-C	6.8	-16.4	-9.6
		C-C	6.6	-15.4	-8.8
		C-C	7.7	-17.3	-9.6
		C-C	7.0	-16.9	-9.9
I^H		C-C	5.8	-15.7	-9.9
		C-N	8.4	-8.2	0.2
		C-N	6.8	-10.3	-3.5
		B-N	9.9	-5.6	4.3
		C-C	9.3	-8.9	0.4
		C-C	10.6	-6.5	4.1
		C-C	9.8	-5.5	4.3
		C-C	12.9	-8.7	4.2

The differences observed in the GIMIC analysis of **II-C_{2h}** and **I^H** are also borne out in the electronic structure of the two compounds. The UV-vis spectrum of **9^{tBu}** (Figure 2-18) exhibits two main absorptions at 314 and 458 nm, the latter being ascribed to a HOMO to LUMO excitation by TDDFT analysis (Table 2-5). When excited at 465 nm **9^{tBu}** shows an emission signal at 600 nm, and when an excitation spectrum was recorded, it matched well with the reported absorption spectra.

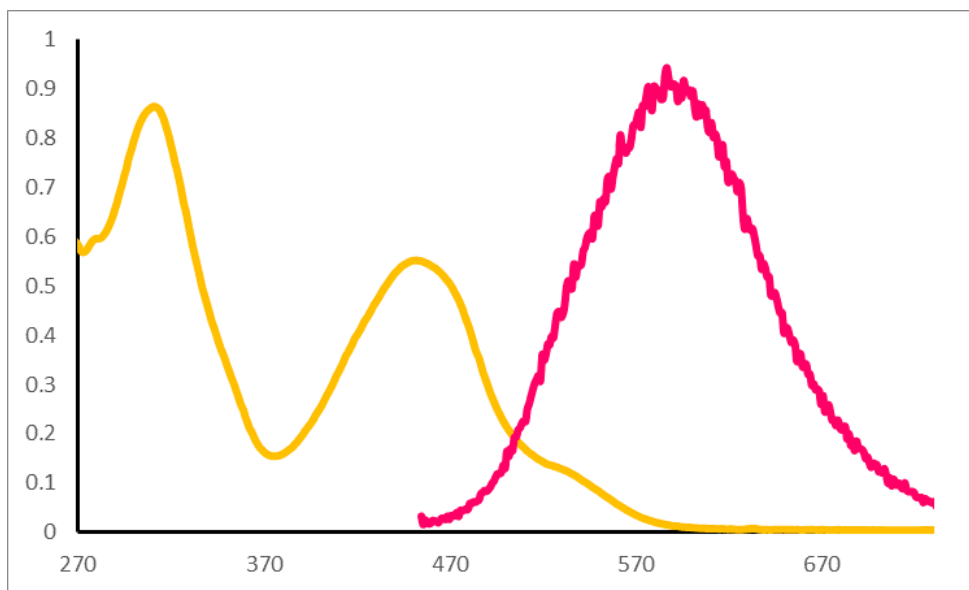


Figure 2-18. UV-Vis absorption and emission spectra of **9^tBu** in CH₂Cl₂. Major absorption maxima at 314 and 458 nm. Emission maxima when excited at 458 nm at 600 nm.

Table 2-5. Calculated low energy electronic transitions of **9^tBu** and **II^tBu** (1,3,5,7-*tert*-butyl-*s*-indacene) at TDDFT/BH-LYP/def-TZVP level of theory.

	Excitation energy [nm]	Oscillator strength	Dominant contributions to transition
9^tBu	360	0.875	HOMO → LUMO (94%)
	283	0.644	HOMO-2 → LUMO (60%) HOMO-1 → LUMO+1 (32%)
	256	0.464	HOMO-3 → LUMO (58%) HOMO-1 → LUMO+1 (16%)
	253	0.510	HOMO-1 → LUMO+1 (39%) HOMO-2 → LUMO (23%) HOMO-3 → LUMO (21%)
II^tBu	449	0.249	HOMO → LUMO (86%)
	254	0.241	HOMO-2 → LUMO (66%) HOMO → LUMO+1 (20%)
	249	0.748	HOMO-1 → LUMO+1 (82%)

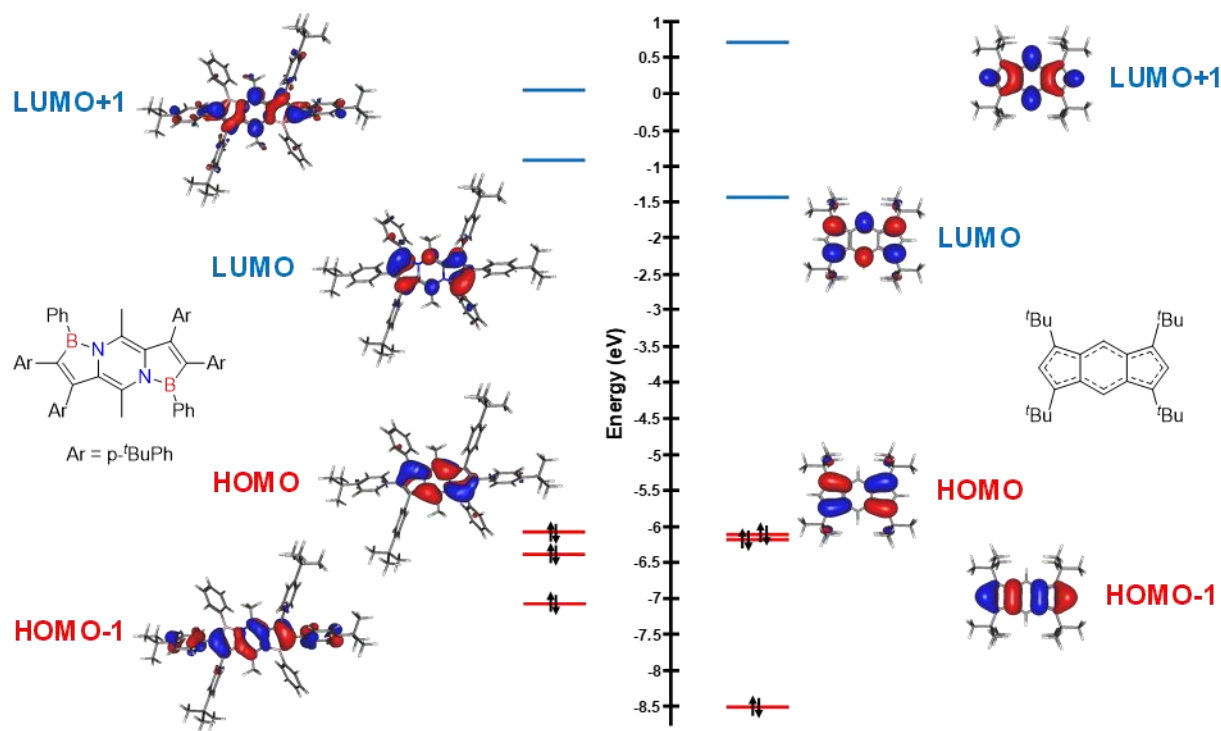


Figure 2-19. Diagram showing frontier molecular orbitals of **9tBu** and **II^{tBu}**. Structures were optimized at BH-LYP/def-TZVP level of theory. HOMO-LUMO difference from orbital energies calculated to be 5.1 eV for **9tBu** and 4.7 eV for **II^{tBu}**. Select orbitals shown for clarity.

Cyclic voltammetry (CV) measurements showed that the compound undergoes two irreversible reductions at -2.28 V and -2.67 V (vs Fc/Fc⁺) and an irreversible oxidation at -0.73 V (Figure 2-20). From the intersection of the normalized UV-vis absorption and emission data, a HOMO/LUMO gap of 2.43 eV was obtained, which compares reasonably well with the computed value of 3.44 eV obtained from the TDDFT analysis. This gap is substantially larger than that calculated for the hydrocarbon **II^{tBu}** (2.76 eV), which is more readily and reversibly reduced to its radical anion¹²⁶ or dianion¹²⁷ than the BN-s-indacene compounds reported here. NICS computations on the putative dianion of **9tBu** indicated that this 14 π species exhibits similar levels of aromaticity in the flanking 5 membered rings as **6^H**, but it is 26.3 kcal mol⁻¹ less stable than the neutral species in the gas phase. Although such energy difference could be offset by anion-cation

interactions in the solid state, attempts to chemically reduce $\mathbf{9^{tBu}}$ with KC_8 or potassium naphthalenide did not lead to isolable products. This is attributed to the apparent instability of reduced $\mathbf{9^{tBu}}$ seen in CV measurements, presumably due to the high energy LUMO of $\mathbf{9^{tBu}}$. Interestingly, the anion $\mathbf{6^H}$ is highly reactive towards electrophiles at the boron center, and it may be that the dianion of $\mathbf{9^{tBu}}$ is even more reactive and also a strong reducing agent.

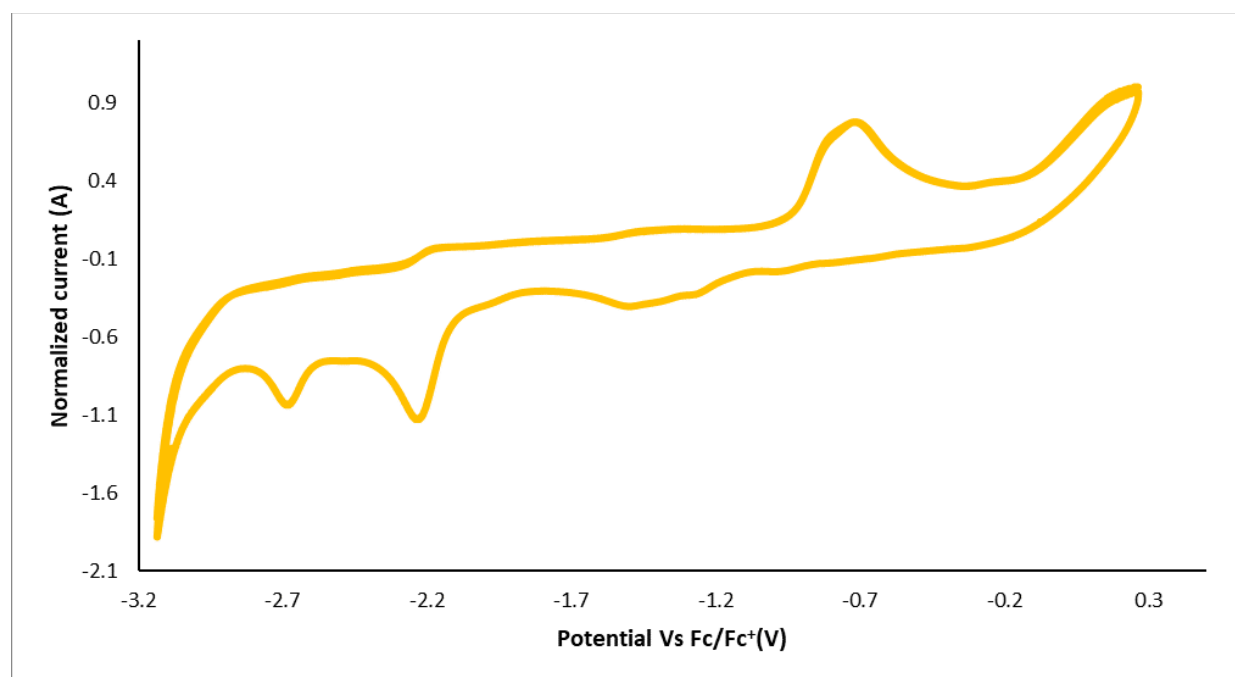


Figure 2-20. Cyclic voltammetry of a 1.14 mM solution of $\mathbf{9^{tBu}}$ in THF was measured using a three electrode setup using a CHI660D potentiostat. Glassy carbon, platinum wire, and silver wire were used as the working, counter, and reference electrodes, respectively. Ionic strength of the solution was maintained by using a 0.1M solution of $[\text{nBu}_4\text{N}][\text{PF}_6]$ in THF solvent. The current was swept in the negative direction with a sweep window from -3.1V to 0.3V at 200 mV/s.

2.6 Conclusions

This study reports a scalable new method for assembling BN heterocycles using established zirconocene mediated pyridyl C-H functionalization chemistry. The methodology was optimized

in the preparation of examples of 3-bora-9-aza-indenes and then applied to the more interesting 1,5-dibora-4a,8a-diaza BN analogs of the unique hydrocarbon *s*-indacene, which were fully characterized using spectroscopic, structural and computational tools. These investigations reveal that the BN substitution favors a more localized bonding framework, as would be found in the C_{2h} isomer of *s*-indacene, which has been shown to be less favoured than the more delocalized D_{2h} isomer. The BN substituted material also features a larger HOMO-LUMO gap than the all-carbon framework.

CHAPTER 3: DIVERGENT REACTIVITY OF NUCLEOPHILIC 1-BORA-7A-AZAINDENIDE ANIONS.¹³²

(Reproduced from Ref ¹³² with Permission from the Royal Society of Chemistry)

3.1 Preface

Concurrent with the work in Chapter Two, some unusual reactivity of the reduced indenide **6^H** towards dichloromethane was noted. This observation prompted the study presented in this chapter where the reactivity of a rare class of nucleophilic boron centres was examined with several electrophiles. Due to the inherent electron poor nature of boron, cases where it can act as a nucleophile are of interest from both a fundamental point of view and from a practical sense for the development of novel reactions for the formation of B-X bonds.

3.2 Author Contributions

All synthetic work was performed by Mr. Matthew Morgan. Crystallographic characterization for **11^H** was performed by Mr. Chris Gendy, and **13^H** was performed by Mr. Matthew Morgan. Computational calculations were performed by Dr. Mikko Rautiainen and Prof. Heikki Tuononen. The manuscript was written collaboratively between Prof. Warren Piers, Dr. Mikko Rautiainen, and Mr. Matthew Morgan.

3.3 Abstract

The reactions of 1-bora-7a-azaindenide anions, prepared in moderate to excellent yields by reduction of the appropriate 1-bora-7a-azaindenyl chlorides with KC_8 in THF, with alkyl halides and carbon dioxide were studied. With alkyl halides (CH_2Cl_2 , CH_3I and $\text{BrCH(D)CH(D)}^t\text{Bu}$), the anions behave as boron anions, alkylating the boron center via a classic $\text{S}_{\text{N}}2$ mechanism. This was established with DFT methods and via experiments utilizing the neo-hexyl stereoprobe $\text{BrCH(D)CH(D)}^t\text{Bu}$. These reactions were in part driven by a re-aromatization of the six membered pyridyl ring upon formation of the product. Conversely, in the reaction of the 1-bora-7a-azaindenide anions with CO_2 , a novel carboxylation of the C-2 carbon alpha to boron was observed. Computations indicated that while carboxylation of the boron center was kinetically feasible, the products of B-carboxylation were not thermodynamically favored relative to the observed C-2 carboxylated species, which were formed preferably due to the generation of both C-C and B-O bonds. In these products, the pyridyl ring remains non-aromatic, in part accounting for the observed reversibility of carboxylation

3.4 Introduction

The synthesis and evaluation of BN isosteres of archetypical aromatic hydrocarbons has been a fruitful and active area of research in main group and organic materials chemistry in the past decade.^{17, 18, 30, 58, 94, 103} The substitution of a C=C double bond with the more polarized B-N unit within a larger aromatic framework can have beneficial effects on the solid state packing,^{19, 91} light absorption^{20, 96} and electron transporting^{60, 63} properties of the molecules and materials

compared to the all-carbon frameworks.²² As such, there has also been significant interest in defining the differences between all-carbon and BN compounds at a more fundamental level in the most basic building units of polycyclic aromatic hydrocarbons (PAHs). The groups of Liu and Braunschweig,¹³³ for example, have developed general syntheses of all three possible isomers of azaborines, BN analogs of benzene, and evaluated the physical properties and reactivity of these compounds in detail (Figure 3-1).^{26-28, 32, 134-137} The undertaking of similar studies on even simple polycyclic building blocks becomes more complex due to heightened numbers of possible BN isomers, but investigations into the exhaustive evaluation of BN analogs of naphthalene^{51, 54, 57} and other PAHs^{46, 138} have been initiated.

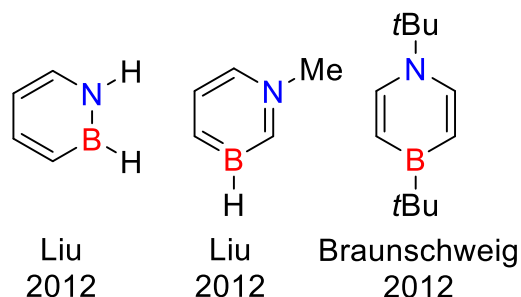


Figure 3-1. Structure of the least substituted azaborine derivatives to date.

Indene and the indenide anion constitute another basic building block in PAH chemistry^{109, 129, 139-141} and there has also been recent interest in BN isosteres of this unit.^{34, 89, 104, 105, 142} Here, even only considering 1,2 BN compounds, there are 10 possible BN indenide isomers, (Figure 3-2) and so the mapping of properties and stabilities of each isomer is a complex endeavour just from a synthetic perspective.

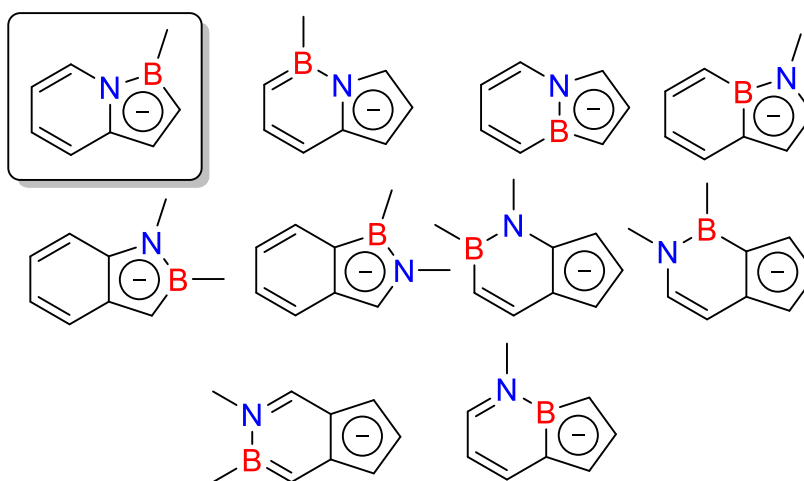


Figure 3-2. All 10 possible contiguous BN isomers of the indenide anion.

Chapter 2 describes a zirconocene mediated synthesis of the 1-bora-7a-azaindene framework represented by compounds **4^H** and **4^{Me}** (Scheme 3-1)⁸⁹ which is one of the possible 1,2-BN analogs of indene. Our synthesis differs from others reported^{104, 105} in that the boron centre remains functionalized with a halide, and so the compound can be readily reduced by two electrons to form the 1-bora-7a-azaindenide anions **6^H** and **6^{Me}** as shown. The synthesis can be carried out in gram quantities which has made it possible to conduct reactivity studies of these anions with electrophiles. Here we report two different reaction paths for these BN indenides, highlighting how aromaticity changes can dictate reaction paths and lead to unique reactivity in comparison to that observed in analogous reactions in the all-carbon reaction manifold.

3.5 Results and Discussion

3.5.1 Synthesis and Characterization of Indenide Species

Compounds **4^H** and **6^H** were reported previously, and the methylated derivatives **4^{Me}** and **6^{Me}** were prepared analogously using 2-methyl pyridine in the zirconocene synthetic sequence. The 1-bora-7a-azaindenides **6** can be prepared without using the cryptand potassium ion sequestering agent but the K(2,2,2-c) salts are more easily handled and were therefore used throughout this study (Scheme 3-1).

Scheme 3-1. Synthesis of 1-bora-7a-azaindenide anions **6**.

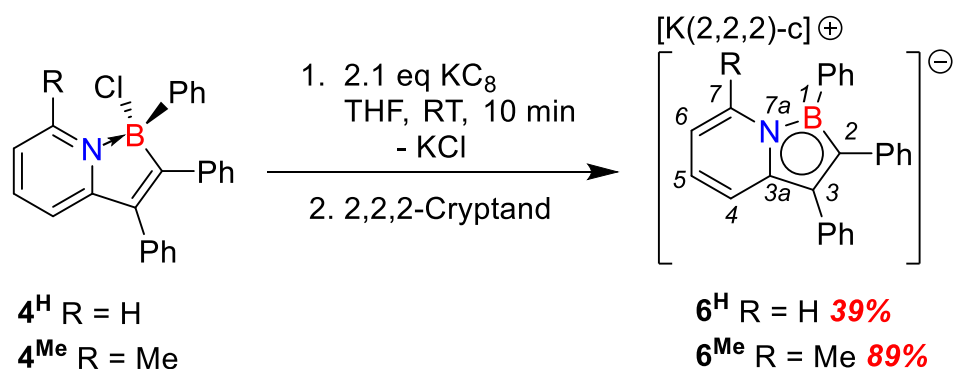
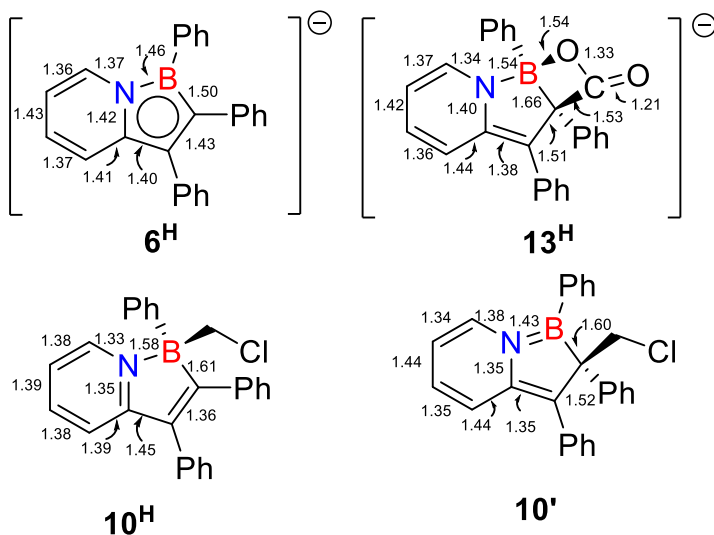


Table 3-1. Nucleus independent chemical shifts (at PBE0/def-TZVP level of theory) for five-membered (A) and six-membered (B) rings of indenide, **6^H**, **13^H**, **10^H**, and **10'**.

	Ring	NICS(1)	NICS(0)	NICS _{zz} (1)
indenide	A	-13.6	-15.8	-40.0
	B	-9.3	-9.1	-27.1
6^H	A	-11.4	-12.5	-29.5
	B	-1.8	0.0	-3.6
13^H	A	-1.0	-1.7	-2.3
	B	0.2	3.5	-0.4
10^H	A	-1.9	0.7	0.2
	B	-8.2	-5.9	-2.4
10'	A	0.3	0.2	-2.8
	B	2.5	5.9	-1.7

As reported previously,⁸⁹ NICS calculations on these anions indicate that the five-membered C₃BN ring has significant aromaticity associated with it (the NICS(1) and NICS(0) values are -11.4 and -12.5, respectively, for **6^H**; a complete listing of NICS values computed for all compounds reported here can be found in Table 3-1). Conversely, the six-membered ring, with NICS values near 0, is essentially non-aromatic. This is reflected in the chemical shifts associated with the C-H protons of this ring in **6^H** and **6^{Me}**, which are shifted significantly up-field in the ¹H NMR spectrum. In particular, the C-*H*₅ and C-*H*₆ protons of **6^H** appear at 5.66 and 5.59 ppm, respectively, while in **6^{Me}**, they arise at 5.49 and 5.28 ppm. These shifts are more consistent with a diene moiety than a pyridyl group. As reported earlier,⁸⁹ the striking bond length alternation in the structure of **6^H** is consistent with the molecule illustrated in Scheme 3-2. Molecular orbital analysis of the occupied π orbitals of an unsubstituted model of **6^H** in comparison to the all-carbon indenide anion (Figure 3-3) also supports the description of delocalized bonds in five-membered BN-containing ring.

Scheme 3-2. Lengths of ring bonds in optimized structures of **6^H**, **13^H**, **10**, and **10'**.



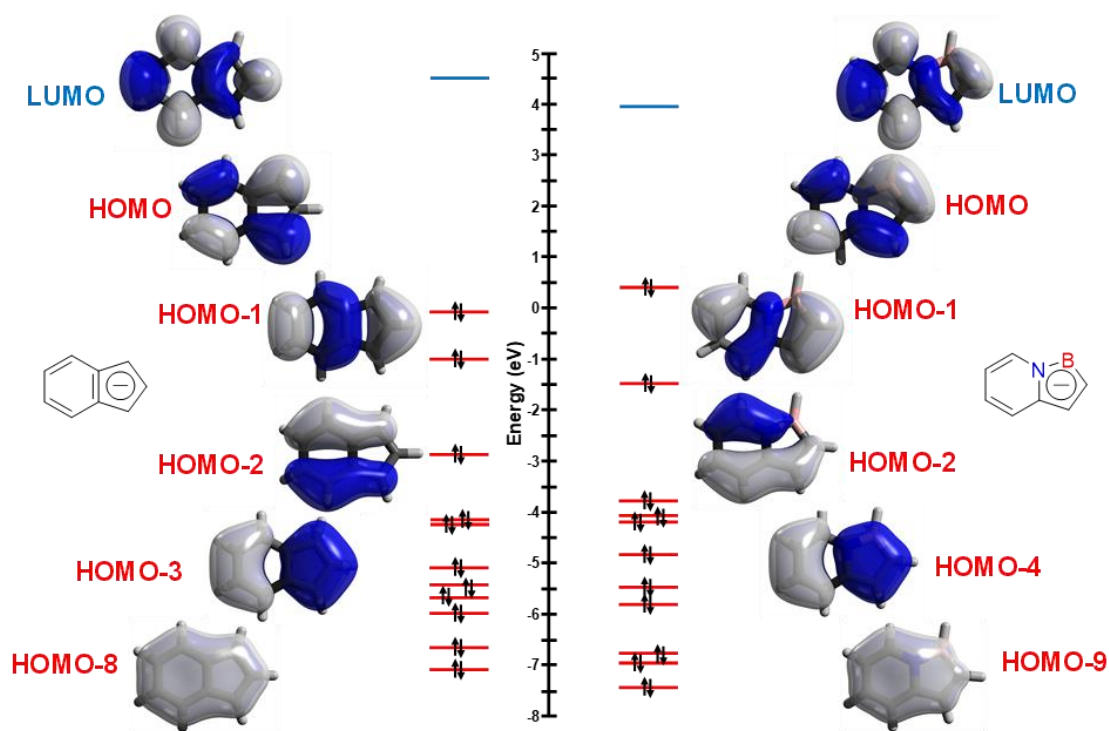


Figure 3-3. Highest occupied π orbitals of indenide (left) and 1-bora-7a-azaindenide (right).

Four of the π orbitals are bonding and one is anti-bonding with respect to each of the bonds of the five-membered ring, apart from the transannular C-N bond for which only three π orbitals are bonding and two are anti-bonding. Similarly, the π orbitals support the localization of π electrons to two double bonds C4-C5 and C6-C7 in the six-membered ring.

Given this analysis, it is perhaps not surprising that an evaluation of the charge distribution (electrostatic potential) within the 1-bora-7a-azaindenide anion (Figure 3-4) indicates that the negative charge is mainly associated with the five-membered ring, with C-2 and the boron atom bearing most of the charge. This contrasts with the all-carbon indenide ion, wherein the locus of charge is mainly associated with the C-1/C-3 positions. We thus explored the reactions of anions

6^H and **6^{Me}** with simple electrophiles to ascertain the impact of this unusual charge distribution on the outcome of the reactions.

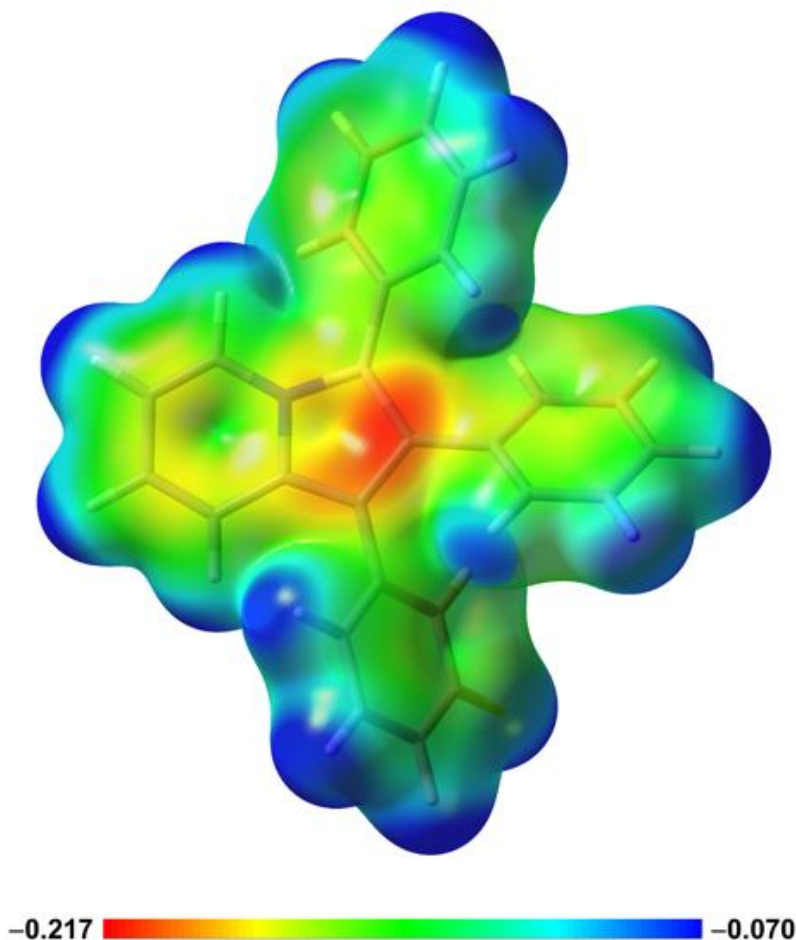


Figure 3-4. Electrostatic potential [atomic units (au)] of **6^H** mapped on the electron density isosurface (0.005 au) at PBE0/def-TZVP level of theory.

3.5.2 Reactivity of **6** with Carbon Electrophiles

It was apparent early in our investigations that **6^H** was not stable in the presence of alkyl halides; attempts to obtain the ¹H NMR spectrum of **6^H** in CD₂Cl₂ resulted in immediate and clean

conversion to a new product as judged by a dark orange to pale yellow colour change and NMR spectroscopy. The characteristic ^{11}B NMR chemical shift of 24.5 ppm for **6^H** shifted upfield to 1.9 ppm, in the range of neutral, four-coordinate borane compounds, and the C-H4-7 protons of the pyridyl unit all shifted downfield significantly, indicating a re-aromatization of this ring in comparison to **6^H** (Figure 3-5)

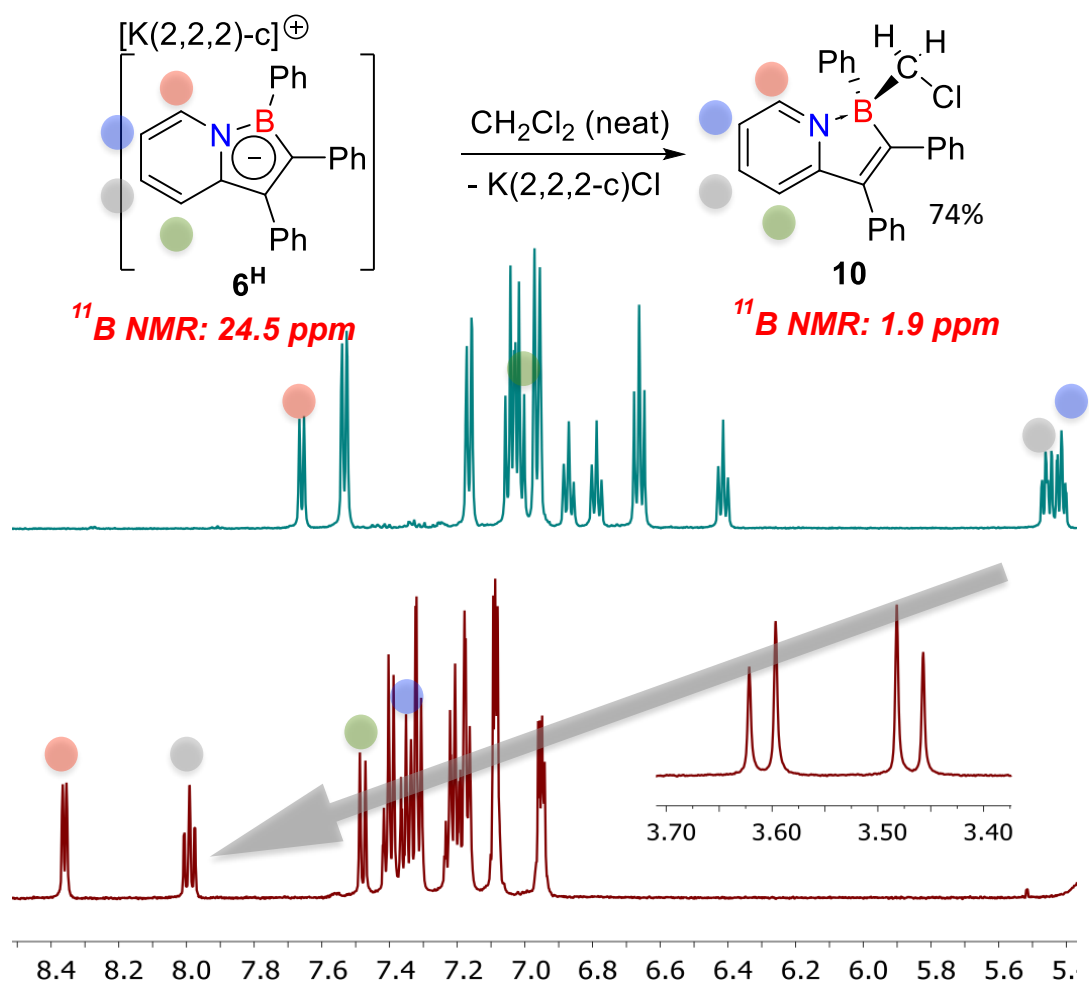
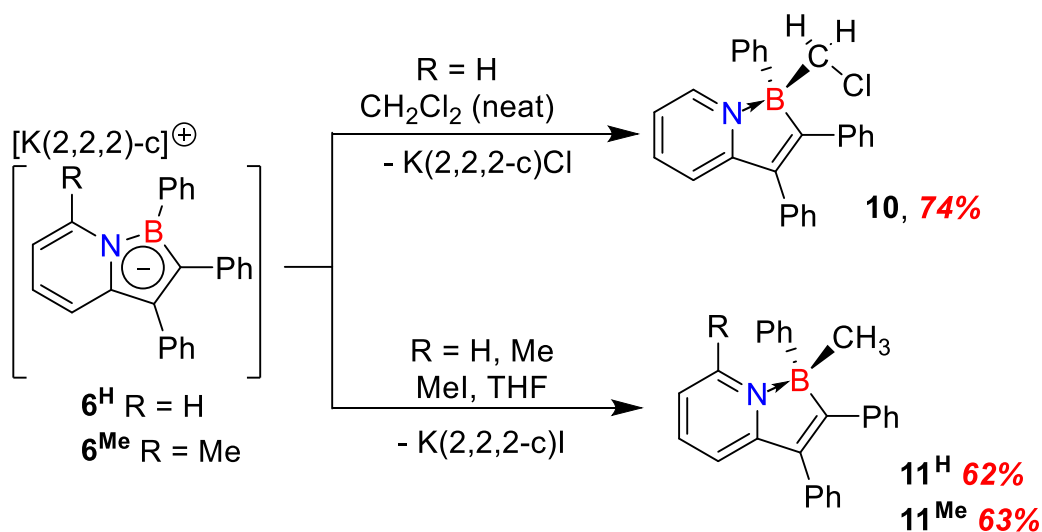


Figure 3-5. ^1H NMR Data for the reaction of **6^H** with CH_2Cl_2 to form the product **10^H**. signals on the 6-member pyridyl ring are highlighted.

Furthermore, when CH_2Cl_2 was employed, an AB quartet at 3.62 and 3.48 ppm ($^2J_{\text{HH}} = 12.5$ Hz) was observed for the diastereotopic protons deriving from the aliphatic methylene unit in the product. While the electrostatic map in Figure 1 suggests that C-2 might be the most nucleophilic site in the ring, subsequent investigations showed the product of this reaction to be the 1-chloromethyl-1-bora-7a-azaindenyl derivative **10** (Scheme 3-3).

Scheme 3-3. Reactions of 1-bora-7a-azaindenide anions **6** with alkyl halides.



This was confirmed via a partial structural determination (connectivity only) on single crystals, and by the synthesis of the analogous methyl compounds, **11^H** and **11^{Me}**, prepared by reaction of **6^H/6^{Me}** with methyl iodide in good yields. For derivative **11^H**, the molecular structure was determined (Figure 3-6) and clearly establishes that the alkyl groups in these reactions add to the boron centre. The metrical parameters for **11^H** support the notion that the pyridyl ring has re-aromatized, and a longer B1-N1 bond of 1.6198(16) Å compared to the distance of 1.438(4) Å in **6^H** is also consistent with conversion from a 1-bora-7a-azaindenide to an indenyl derivative.

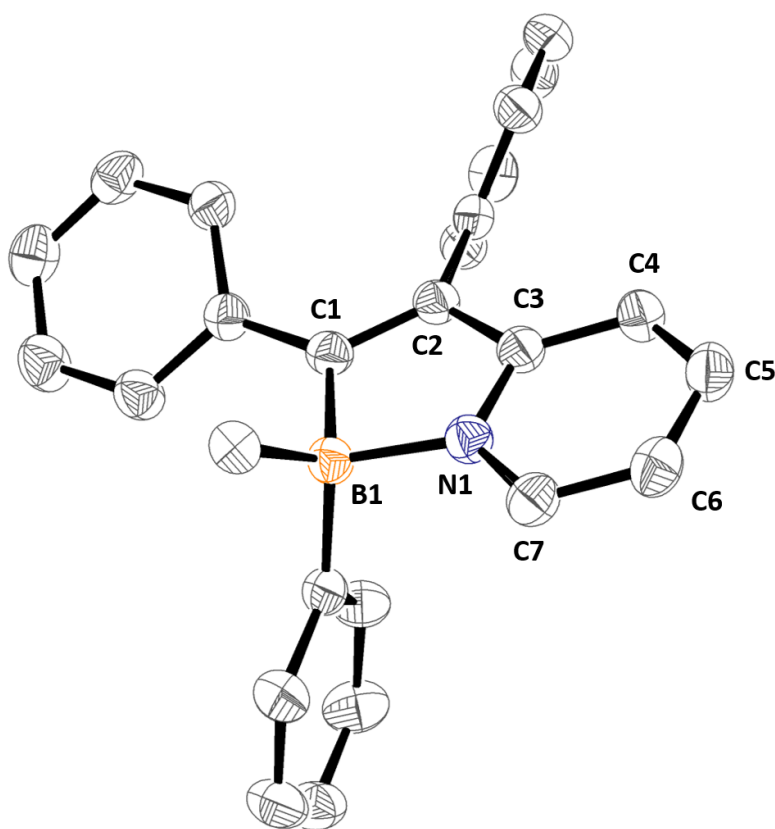


Figure 3-6. Thermal ellipsoid (50%) diagram of the molecular structure of **10^H**. Hydrogen atoms have been omitted for clarity. Selected bond lengths (Å): B(1)-N(1), 1.6198(16); B(1)-C(1), 1.6218(18); C(1)-C(2), 1.3599(18); C(2)-C(3), 1.4596(18); C(3)-C(4), 1.3962(18); C(4)-C(5), 1.379(2); C(5)-C(6), 1.388(2); C(6)-C(7), 1.3742(19); C(7)-N(1), 1.3404(17); N(1)-C(3), 1.3571(16).

These observations indicate that **6^H** functions as a rare example of anionic boron nucleophile¹⁴³⁻¹⁴⁷ in its reactions with alkyl halides, despite the more pronounced localization of negative charge on the C-2 carbon of the 1-bora-7a-azaindenide anion. Given that the indenide anion itself alkylates exclusively at the C-1/C-3 positions,¹⁴⁸ it is notable that no evidence for alkylation of the C-3 position in anions **6^H**/**6^{Me}** was observed. Density functional theory investigation of the reaction of **6^H** with CH₂Cl₂ shows that the lowest energy reaction path involves direct S_N2 type attack of the boron on the alkyl halide (Figure 3-7) while attempts to locate a

transition state involving C-2 attack on the substrate were not successful. The boron displacement of chloride and B-C bond formation occurs through a transition state (TS1) with a barrier of 71 kJ mol⁻¹ to yield product **10^H** in a strongly exergonic reaction (-200 kJ mol⁻¹).

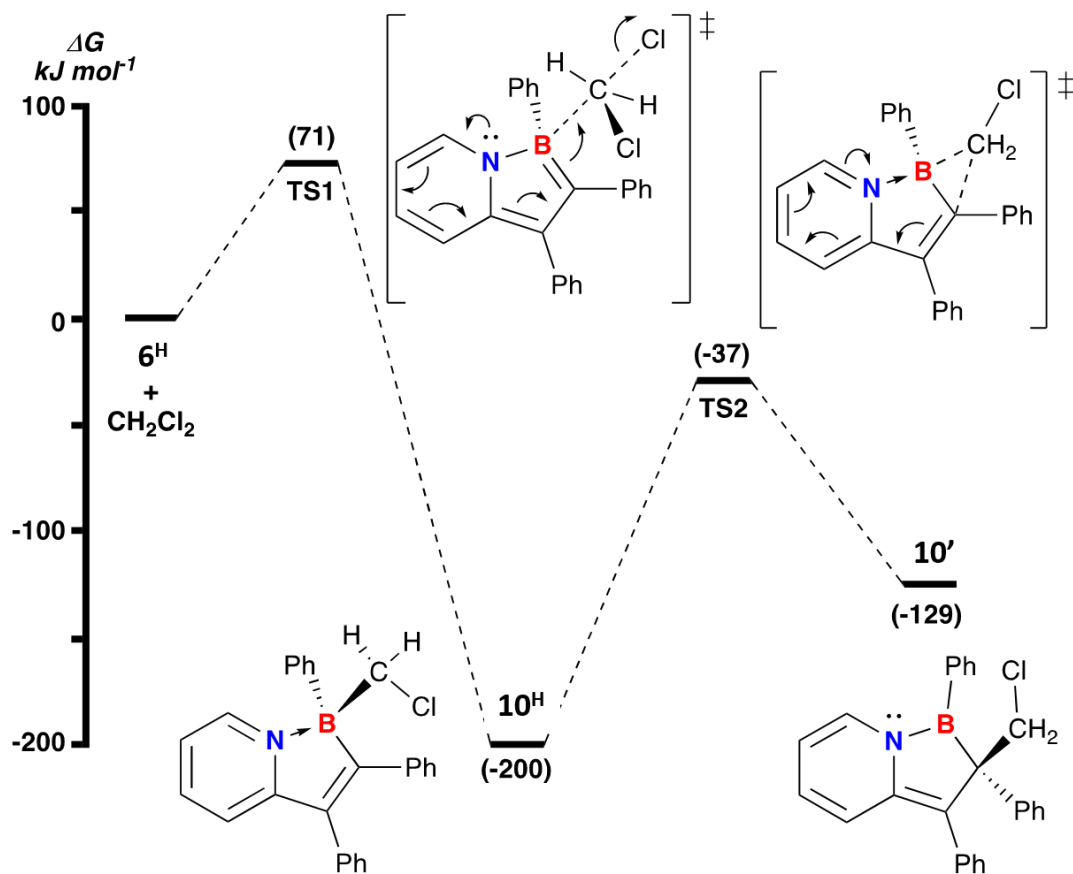


Figure 3-7. Calculated Gibbs free energies (kJ mol⁻¹, PBE0/def-TZVP level of theory) for the reaction of **6^H** with CH₂Cl₂ in dichloromethane to give either **10^H** or **10'**.

Although it was possible to locate a transition state (TS2) for transfer of a CH₂Cl⁺ fragment to C-2 starting from **10^H**, it had a very high activation barrier (163 kJ mol⁻¹) and the product of the reaction, **10'**, is less stable than **10^H** by 71 kJ mol⁻¹. We attribute this to the fact that, for **10^H**, the formation of the B- C bond is accompanied by re-aromatization of the pyridine ring (a NICS(1)

value of -8.2 is calculated for this ring in compound **3**, see Table 3-1) while in **10'**, the ring remains non-aromatic (NICS(1) = 2.5) and the five membered ring also loses aromaticity (NICS(1) = 0.3) as compared to **6^H**. Thus, the overall regiochemistry of this alkylation is determined to a large degree by the changes in aromaticity in **10^H/10'** vs the starting materials.

To provide experimental support for the computed transition state, the 7-methyl-1-bora-7a-azaindenide **6^{Me}** was treated with the alkyl bromide 1-bromo-1,2-dideuterio-3,3-dimethylbutane. The dideuterated neo-hexyl group is a useful stereoprobe for acquiring mechanistic information because the change in stereochemistry at C-1 is easily monitored by ¹H NMR spectroscopy.¹⁴⁹ The bromo alkyl substrate was prepared via hydrozirconation methodology as an 80:20 mixture of erythro:threo diastereomers using a literature procedure¹⁵⁰ and reacted with **6^{Me}**. A clean reaction to a new product (**12^{Me}**) was observed but required heating at 60°C for 3 hours to go to completion due to the greater steric bulk of this substrate. For an S_N2 mechanism, inversion of stereochemistry would be expected¹⁵⁰ in the alkylborane product, while mechanisms involving, for example, electron transfer¹⁵¹ from **6** to the substrate, would lead to racemization. The experiment is somewhat complicated by the fact that the boron center in the alkylated product **12^{Me}** is also a stereocentre. There is no diastereoselectivity observed in the formation of this stereocentre, so four signals are observed for the protons of the stereoprobe in the product's ¹H{²H}NMR spectrum. As can be seen in Figure 3-8, the ¹H NMR signal associated with the proton in the 2-position of the probe is well resolved and indicates that the probe has cleanly undergone conversion to an 80:20 mixture of threo:erythro isomers, as would be expected for an S_N2 mechanism and therefore completely consistent with the computations presented above. Thus, these 1-bora-7a-azaindenides behave as pure S_N2 nucleophiles to alkyl halides and the involvement of SET reaction mechanisms¹⁵¹ is negligible for this class of boron anions.

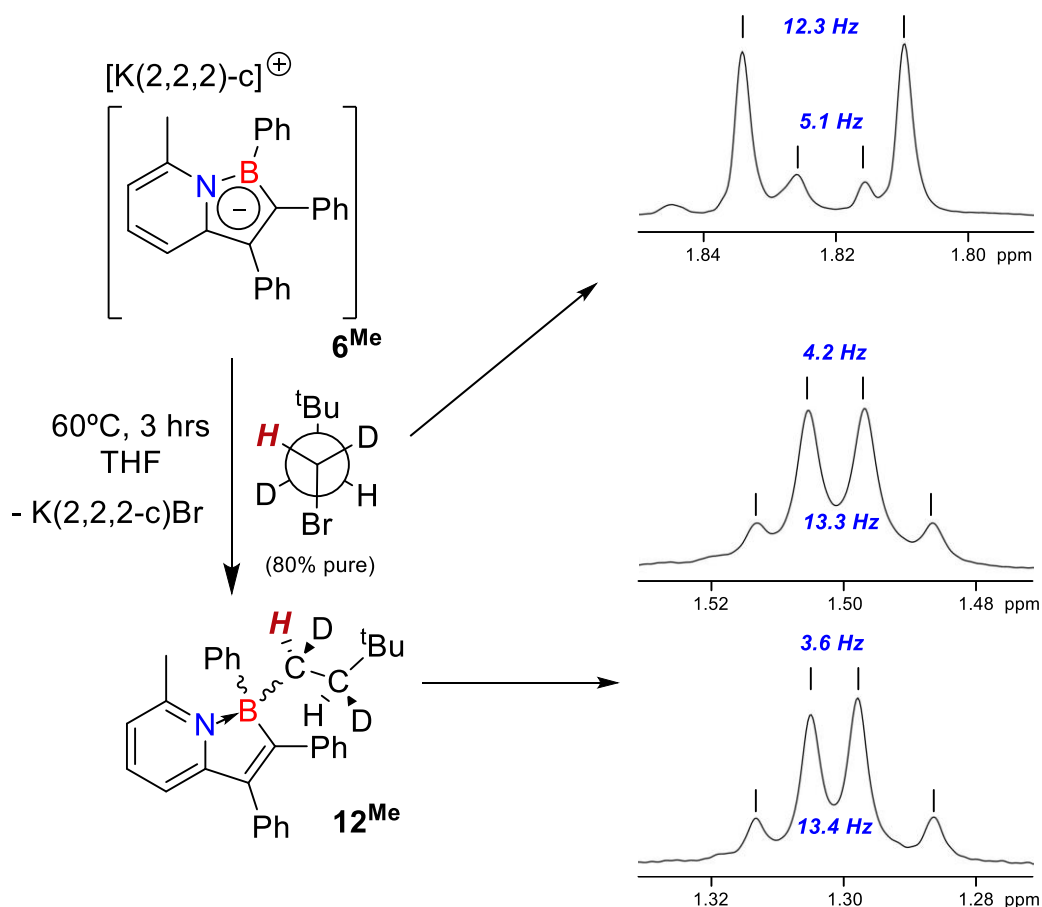


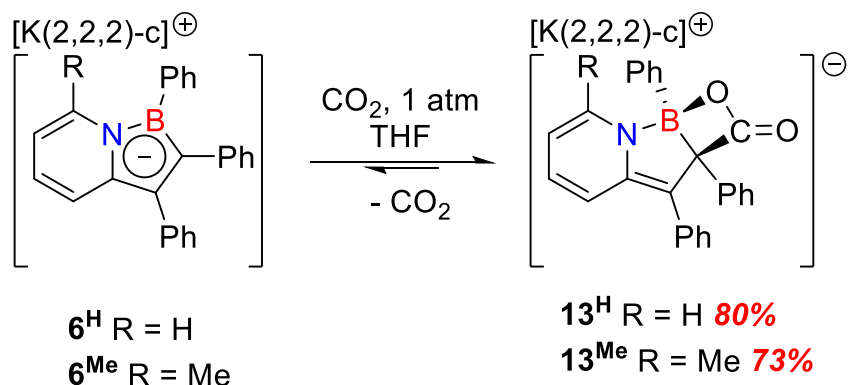
Figure 3-8. Reaction of **6^{Me}** with an 80:20 *erythro:threo* mixture of 1-bromo-1,2-dideuterio-3,3-dimethylbutane. The ¹H{²H} NMR spectra illustrate clean inversion to an 80:20 *threo:erythro* mixture in the 1:1 mixture of B-diastereomeric products of S_N2 alkylation, **12^{Me}**.

3.5.3 Reactivity of **6** with Carbon Dioxide

Another topical area of research in main group chemistry involves the “metal-free” binding and activation of small molecules, particularly carbon dioxide¹⁵²⁻¹⁵⁸ (CO₂). Compounds **6** do not react with H₂ or silanes, but undergo an immediate reaction with the electrophile CO₂, as indicated by a dark orange to deep red colour change upon exposure of THF solutions to 1 atm of CO₂. In

situ NMR spectroscopy indicates that the reaction proceeds cleanly to one product (Figure 3-9); by analogy to the reactions with alkyl halides, initially it was postulated that the boron nucleophile attacked the electrophilic carbon of CO₂. However, while the ¹¹B NMR spectrum exhibited a signal at 5.3 ppm, consistent with four-coordinate boron, the ¹³C{¹H} NMR spectrum contained a sharp signal at 176.0 ppm for the carbon in the product derived from CO₂. This was confirmed by using ¹³CO₂. If bonded to boron, this signal would be expected to be significantly broadened due to proximity to the quadrupolar boron centre. Furthermore, in the ¹H NMR spectrum, the signals for the pyridyl ring C-H groups remain upfield shifted (C-H₅ = 6.21 ppm; C-H₆ = 4.94 ppm), suggesting that re-aromatization of the pyridyl ring is not featured in the product of this reaction. X-ray crystallography on the product of the reaction of **6^H** with CO₂ revealed the structure of the products **13^H**/**13^{Me}** to be as depicted in Scheme 3-4 and Figure 3-10, wherein the electrophilic carbon of CO₂ has been attacked by C-2 of the 1-bora-7a-indenide ring.

Scheme 3-4. Reactions of 1-bora-7a-azaindenide anions **6^H**/**6^{Me}** with carbon dioxide.



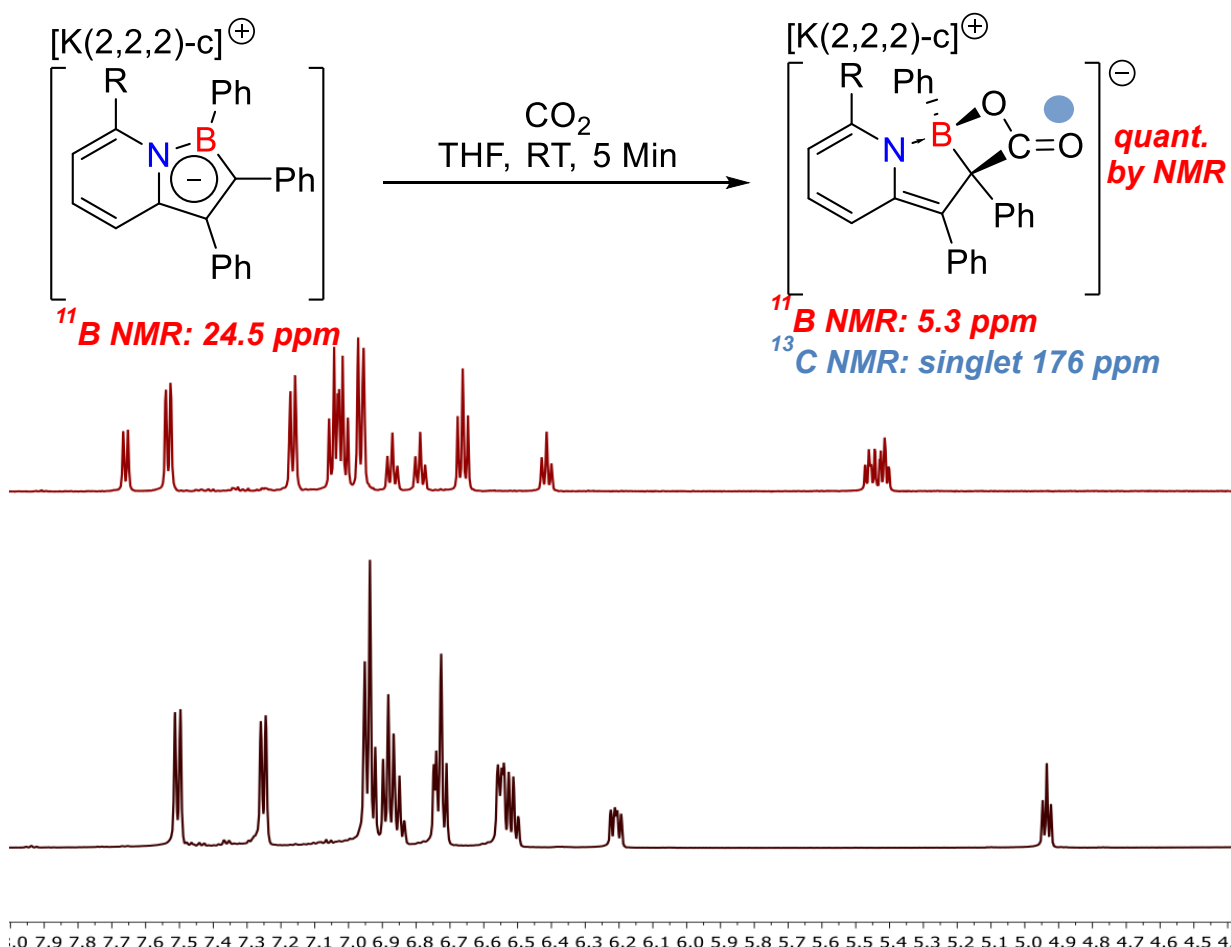


Figure 3-9. ¹H NMR spectra for reaction of **6^H** (top spectra) with CO₂ to give **13^H** (bottom spectra). Relevant ¹¹B and ¹³C NMR details are provided.

The ions in compound **13^H** are well separated in the solid state; Figure 3-10 shows only the anion, and reveals that the CO₂ has added across the C(2)-B(1) bond. The C(1)-O(1) bond length of 1.334(3)Å is significantly lengthened compared to the 1.208(3)Å distance for C(1)-O(2); a stretching vibration of 1709 cm⁻¹ in the IR spectrum of **13^H** is also consistent with a C(1)-O(2) double bond. Short bond lengths for C(3)-C(4), C(5)-C(6) and C(7)-C(8) alternate with longer lengths C(4)-C(5) and C(6)-C(7), indicating bond localization within the bicyclic framework and non-aromaticity within both rings. NICS(1) values of 0.2 for the pyridyl and -1.0 for the five-

membered ring (Table 3-1) support this notion; upon addition of CO₂ to compounds **6**, the aromaticity of the five-membered ring is disrupted, while the pyridyl ring remains non-aromatic.

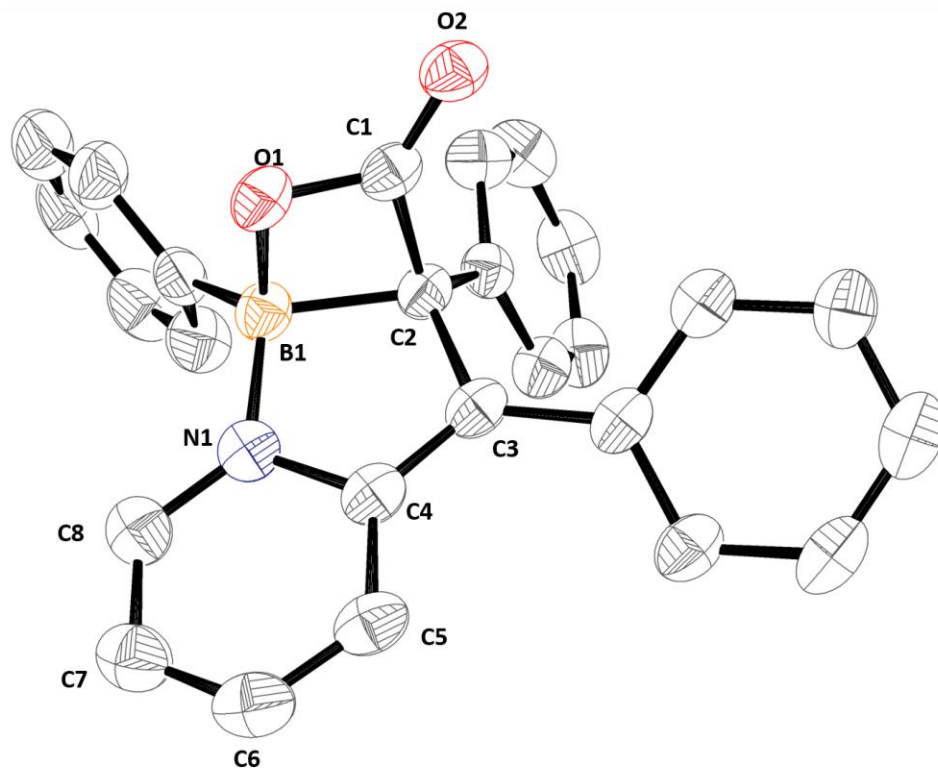
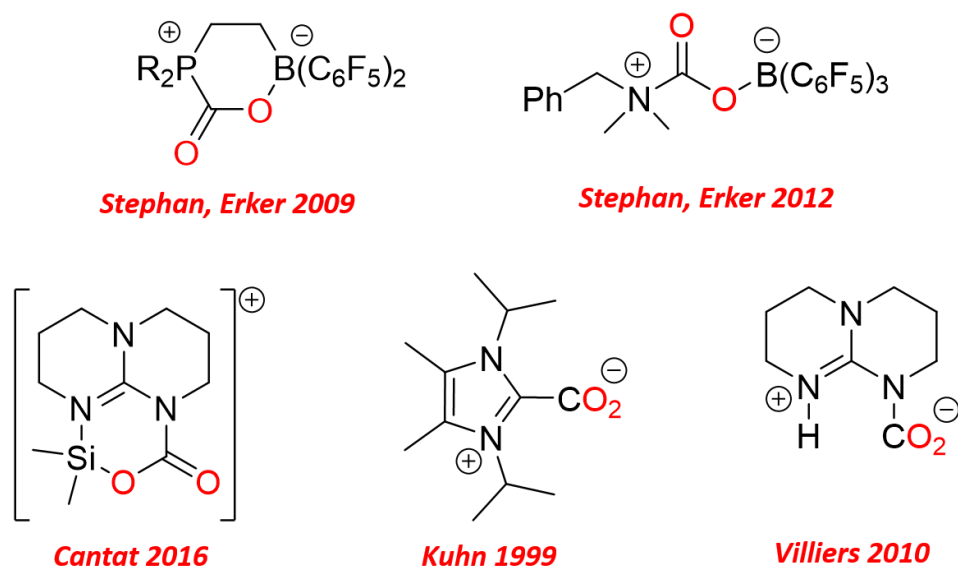


Figure 3-10. Thermal ellipsoid (50%) diagram of the molecular structure of the anion of **13^H**. Hydrogen atoms and the (2,2,2-c) potassium ion have been omitted for clarity. Selected bond lengths (Å): B(1)-O(1), 1.562(3); B(1)-N(1), 1.534(4); B(1)-C(2), 1.665(4); C(2)-C(3), 1.525(3); C(3)-C(4), 1.371(4); C(4)-C(5), 1.447(4); C(5)-C(6), 1.354(4); C(6)-C(7), 1.420(5); C(7)-C(8), 1.363(4); C(8)-N(1), 1.355(4); N(1)-C(4), 1.405(3); C(1)-C(2), 1.530(3); C(1)-O(1), 1.334(3); C(1)-O(2), 1.208(3). Selected bond angles (°): O(1)-B(1)-C(2), 86.01(18); C(1)-C(2)-B(1), 80.75(18); O(1)-C(1)-(C2), 100.3(2); B(1)-O(2)-(C1), 91.04(18); O(1)-C(1)-O(2), 125.9(2).

The generation of this binding mode for CO₂ within main group molecules was to the best of our knowledge previously unobserved. The most common mechanism for binding of CO₂ is through the insertion into an “FLP” system yielding a ring or linear chain such as those by Stephan and Erker shown below in Scheme 3-5. There have been previous examples of binding using a

highly Lewis basic NHC or nitrogen containing bases such as those shown by Kuhn, Cantat and Villiers below. Despite the large amount of literature there is no binding similar to the “2+2” type addition observed in **13**.

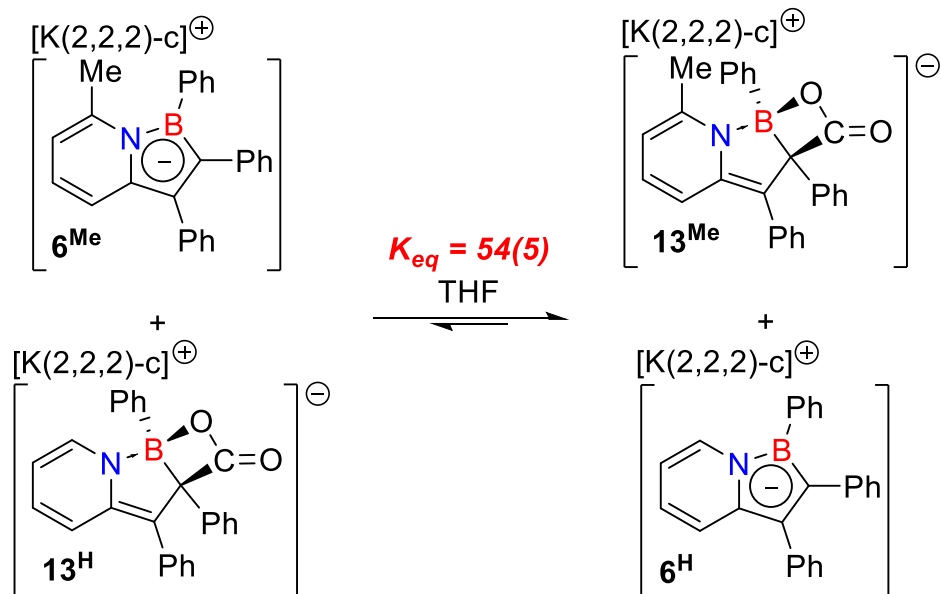
Scheme 3-5. Examples of the diverse binding modes of CO₂ reported for main group compounds.



The binding of CO₂ to these compounds was found to be reversible in solution. When solutions of **13^H** were exposed to ¹³CO₂, incorporation of the labelled carbon dioxide into **13^H** was facile. Furthermore, when **13^H** was treated with excess CH₂Cl₂, slow, irreversible conversion of the compound to compound **10^H** was observed. Presumably, the CO₂ is released from **13^H** and **6^H** is trapped by the DCM via the S_N2 reaction discussed above. This reversibility enabled us to probe the relative affinity of **6^H** and **6^{Me}** for binding CO₂ (Scheme 3-6, and Figure 3-11). When freshly isolated **13^H** or **13^{Me}** was dissolved in THF with one equivalent of **6^{Me}** or **6^H**, respectively, the

equilibrium established over the course of a few hours indicated that the CO₂ adduct **13^{Me}** is strongly favoured over **13^H**; K_{eq} at 298 K was measured by ¹H NMR spectroscopy to be 54(5).

Scheme 3-6. Equilibrium constant measurement at room temperature for CO₂ binding to compounds **6^H** and **6^{Me}**.



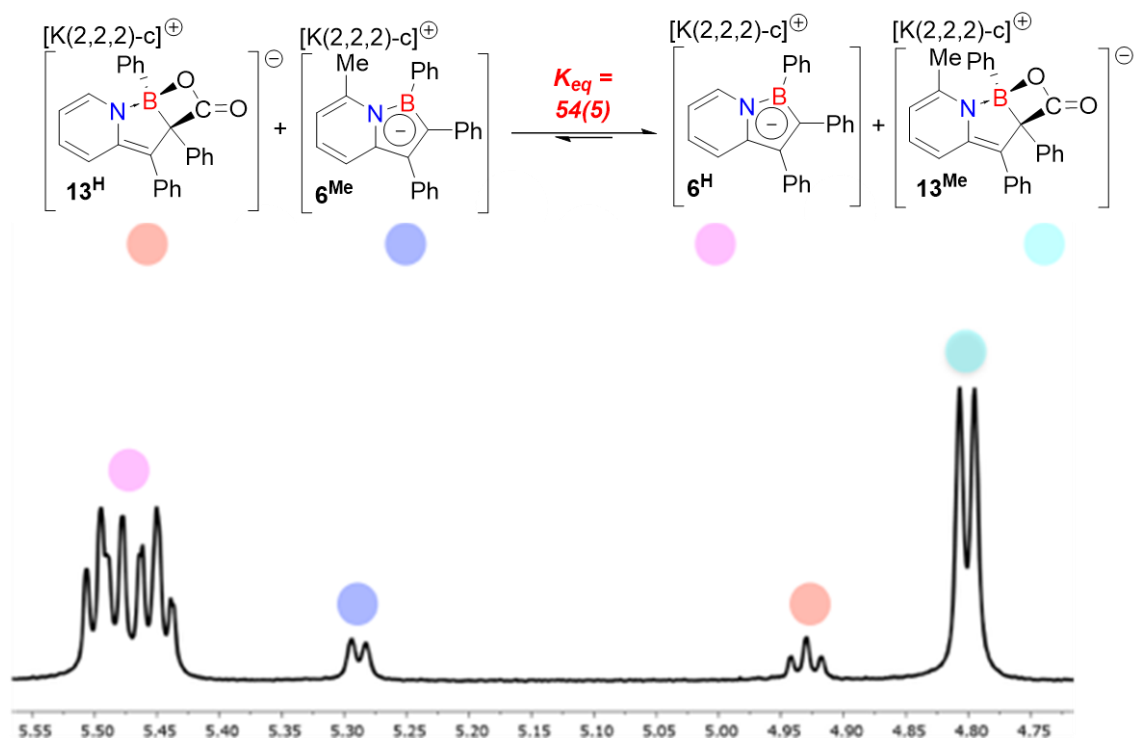


Figure 3-11. ^1H NMR (THF-d_8) spectra of equilibrium reaction mixture.

This is in keeping with the notion that methyl substituted $\mathbf{6}^{\text{Me}}$ is a more electron rich anion that acts as a stronger nucleophile to RX or CO_2 electrophiles. The addition of CO_2 to C-2 in compounds $\mathbf{6}^{\text{H}}/\mathbf{6}^{\text{Me}}$ directly contrasts with what is observed when the all-carbon indenide anion is trapped with CO_2 . Here, CO_2 adds exclusively to the C-1 position resulting in indene-1-carboxylic acid or indene-3-carboxylic acid, depending on the nature of the work up procedure.^{159, 160} The reaction of $\mathbf{6}^{\text{H}}$ with CO_2 was probed computationally (Figure 3-12) and while a transition state (TS4) was located for attack of the CO_2 by the nucleophilic boron centre, the product of this reaction ($\mathbf{13}^{\text{H}}$ in Figure 3-12) is 34 kJ mol^{-1} less stable than the starting materials. Hence, the reverse reaction is essentially barrierless and the equilibrium favours $\mathbf{6}^{\text{H}}$ and CO_2 . The transition state TS3 for attack of CO_2 by C-2 (TS3), while slightly higher than TS4, is nonetheless readily accessible with an energy of only 59 kJ mol^{-1} above the starting materials.

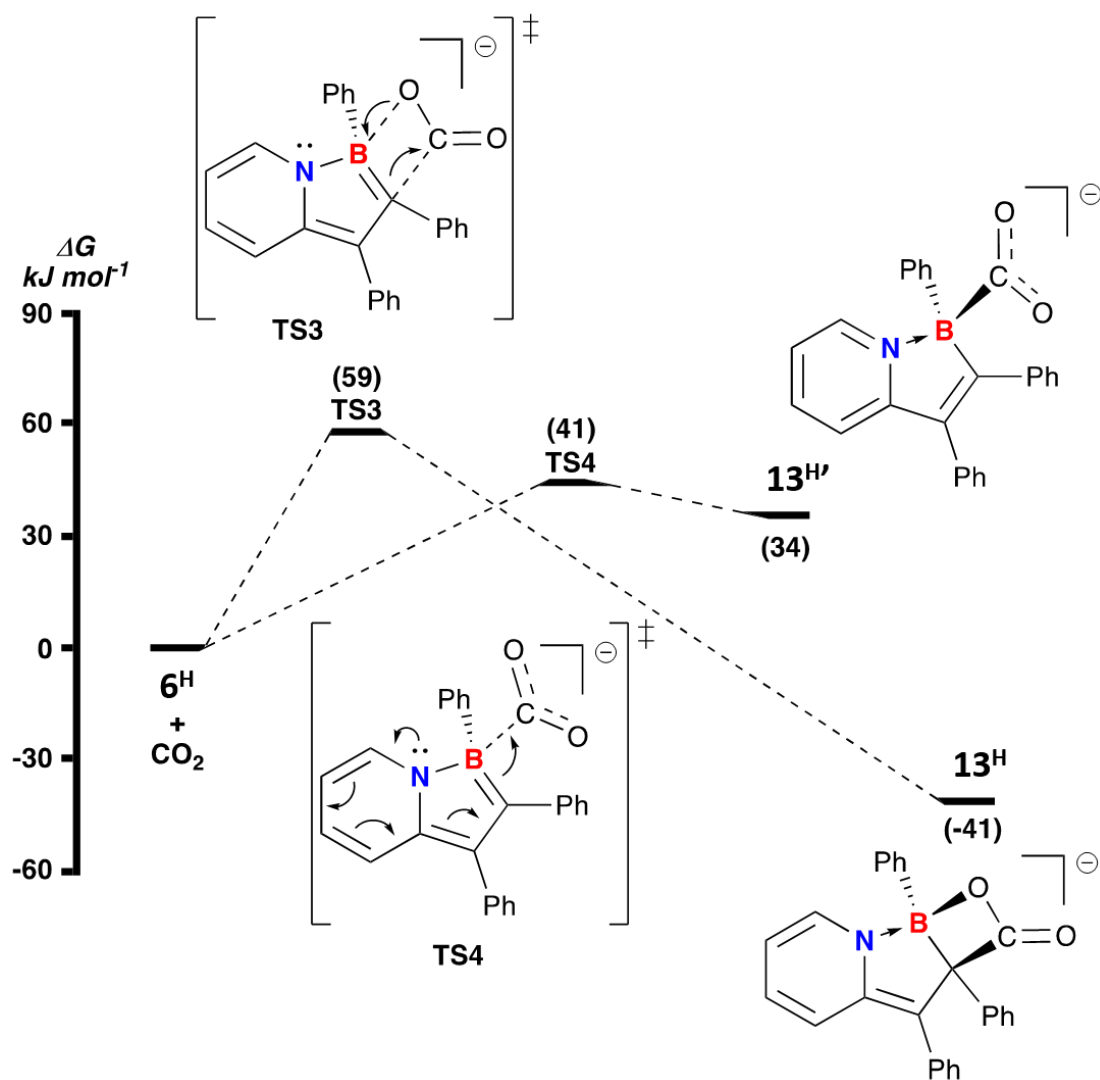


Figure 3-12. Calculated Gibbs free energies (kJ mol^{-1} , PBE0/def-TZVP level of theory) for the reaction of 6^{H} with CO_2 in toluene to give either **13^H** or **13^{H'}**.

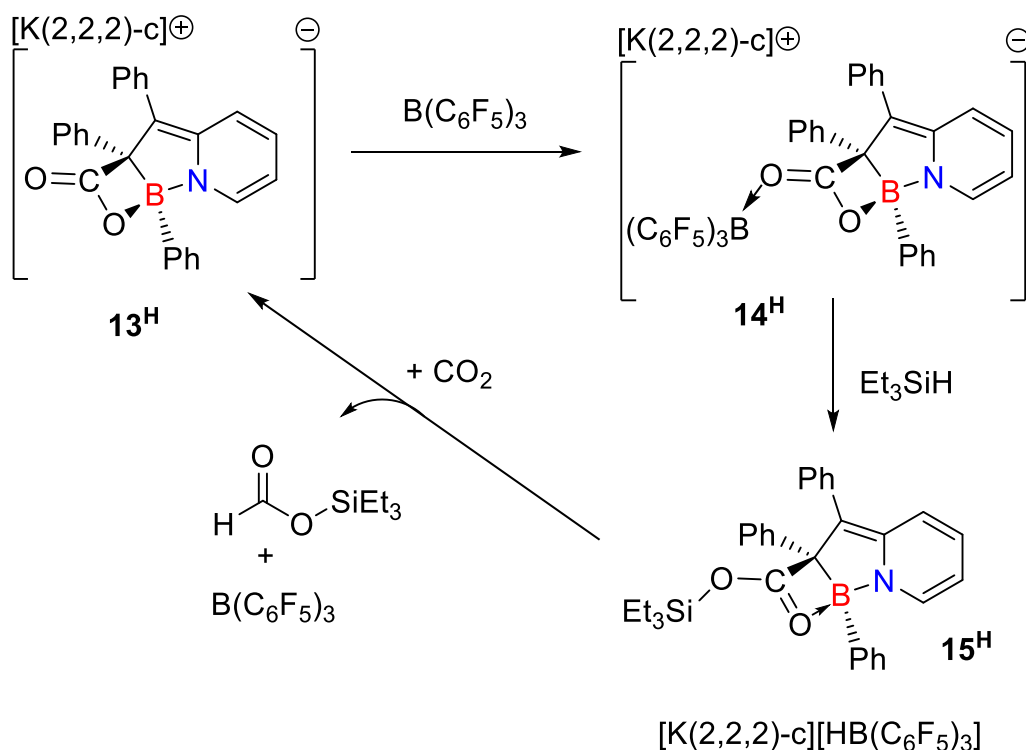
This transition state leads directly to product **13^H** in a moderately exergonic reaction (41 kJ mol^{-1}) which, despite the non-aromatic character of both rings and the absence of re-aromatization as a driving force is favoured by the formation of both new C-C and B-O bonds.

Still, the barrier to CO₂ loss is only 100 kJ mol⁻¹ which is consistent with the observed tendency of **13^H** to lose CO₂ at room temperature.

3.5.5 CO₂ Functionalization

While reversible binding of CO₂ is interesting from a fundamental perspective there is a large desire to transform carbon dioxide into more useful molecules. Therefore, several efforts were made to reduce the bound CO₂ in **13**, which are highlighted in this section.

Scheme 3-7. Proposed Pathway for Catalytic Reduction of CO₂.



Upon discovering the unique binding mode of CO₂, we devised what seemed like a reasonable catalytic cycle shown in Scheme 3-7. We proposed that upon binding of CO₂ the addition of one equivalent of B(C₆F₅)₃ should be able to bind to the pendant oxygen atom of CO₂, forming a compound of the form **14^H**. Attempts to synthesize this intermediate species were met with mixed success. Upon the addition of one equivalent of B(C₆F₅)₃ to a solution of **13^H** there was the clear formation of at least two new products, with the major one being proposed as the borane adduct **14^H**. As shown in Figure 3-13 there is a drastic change in the ¹H NMR spectrum of the product and the ¹³C{¹H} NMR signal corresponding to CO₂ has split into two signals at 189 and 168 ppm, where the peak at 189 ppm is broad, suggestive of a dynamic binding of the Lewis acid. Unfortunately, there is also a second compound that forms in varying degrees depending on the reaction conditions. Upon further investigation, it was found that this same by-product is formed upon the addition of one equivalent of B(C₆F₅)₃ to **6^H**. This aligns with the reversible nature of the CO₂ bonding, where some **13^H** may have converted to **6^H** which was able to react with the borane in solution.

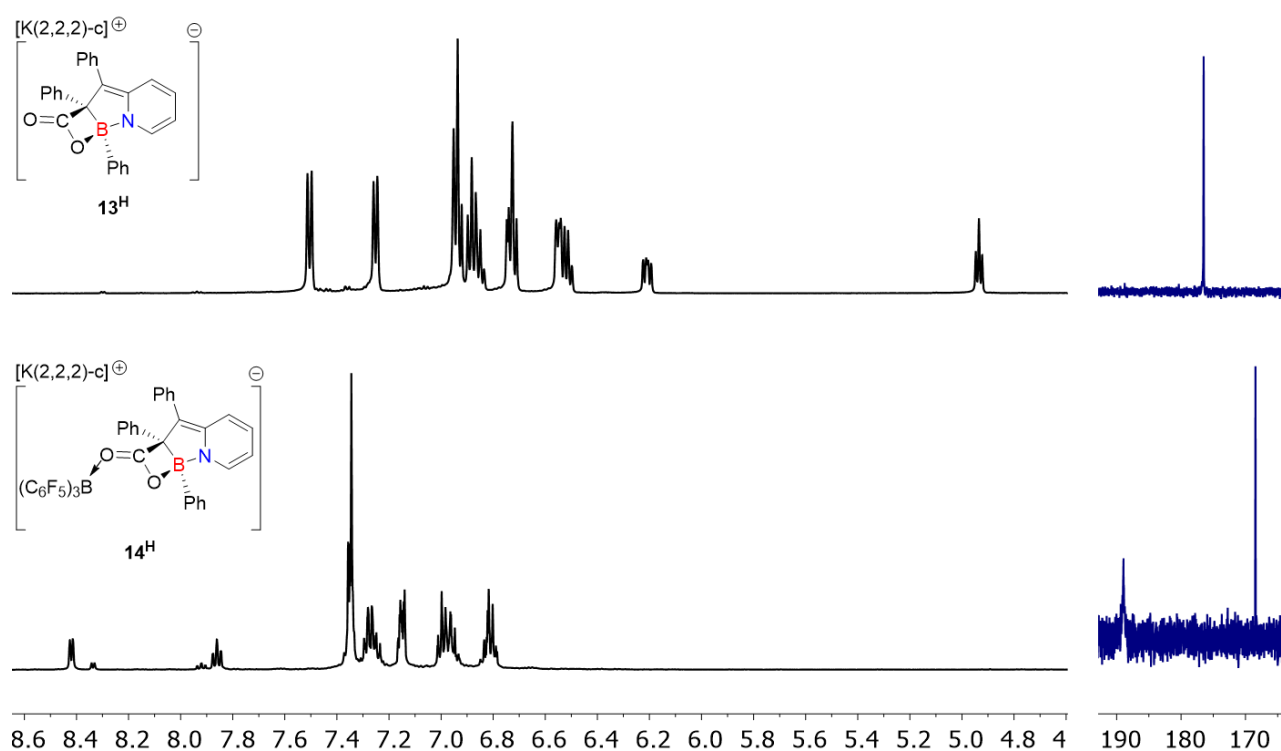
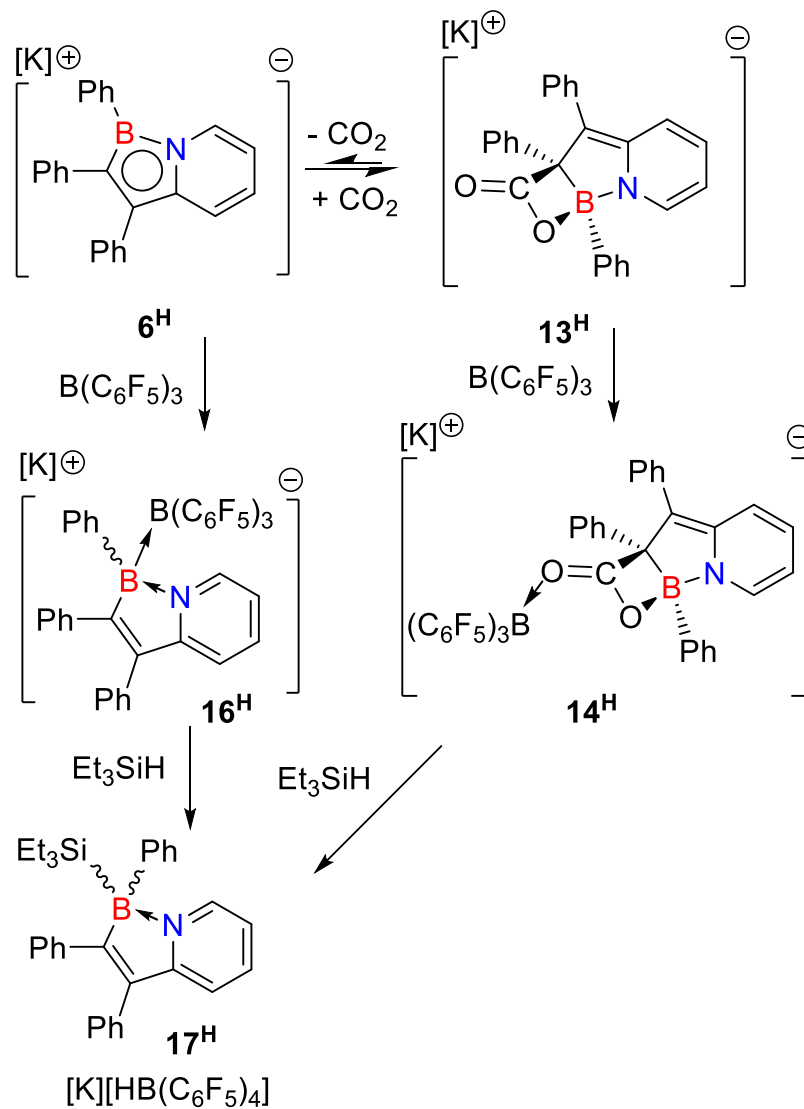


Figure 3-13. ¹H (black) and ¹³C[¹H] NMR spectra of ¹³CO₂ enriched **13^H** and the reaction mixture after treatment with B(C₆F₅)₃

Despite the formation of a side product the reaction mixture was further treated with one equivalent of Et₃SiH. Interestingly, the same product was formed upon the addition of Et₃SiH to solutions of the proposed structures of either **14^H** or **16^H** as shown below in Scheme 3-8. While it was not possible to characterize the proposed product **17^H** the ¹H NMR spectra does compare well with the previously synthesized derivatives **10^H** and **11^H** as shown in Figure 3-14.

Scheme 3-8. Proposed mechanism for the reaction of **6^H** and **13^H** with B(C₆F₅)₃.



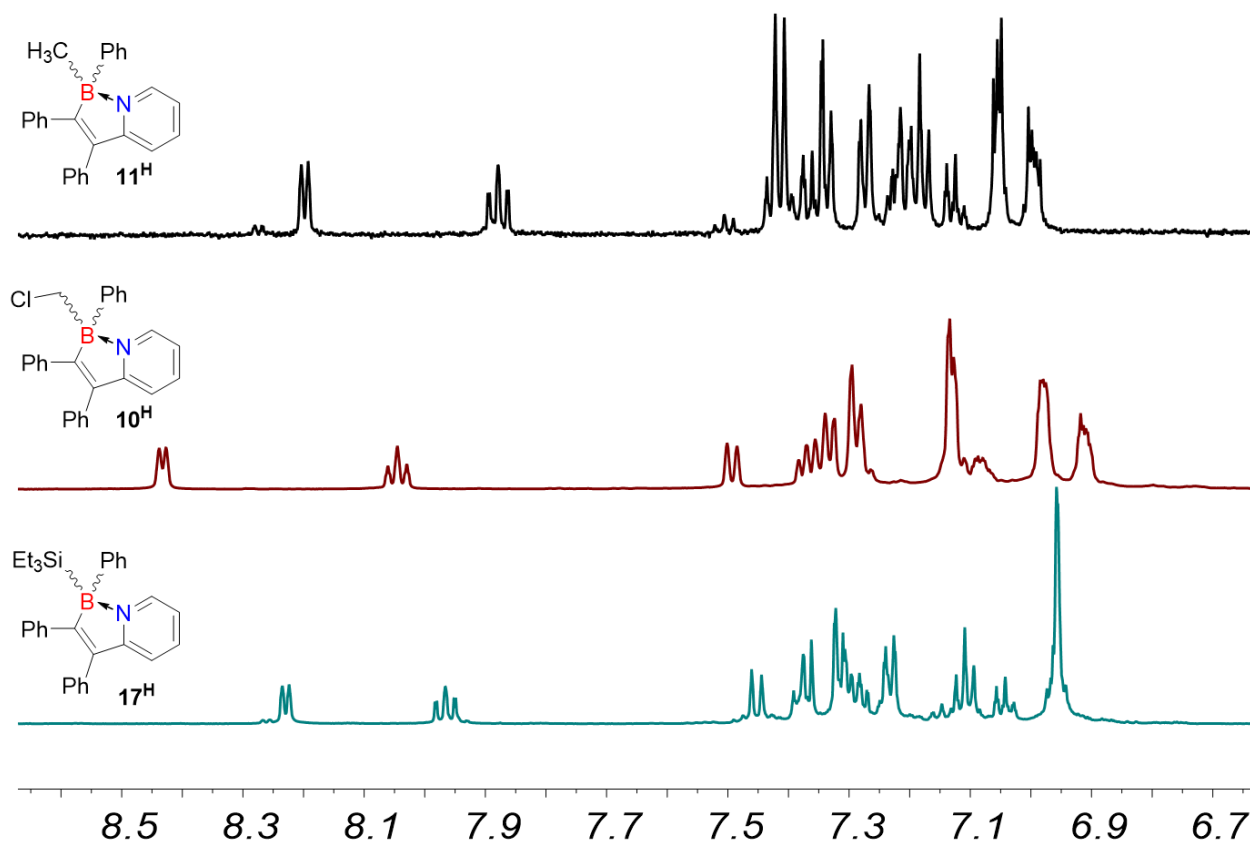


Figure 3-14. ^1H NMR spectra of 10^{H} , 11^{H} , and proposed product 17^{H} .

The only product of the reaction that could be unambiguously characterized was the potassium hydridoborate by-product, and it was found both with and without the encapsulating cryptand ligand on potassium. While it seems quite unlikely that catalytic or even stoichiometric reduction of carbon dioxide can be achieved with this system there is still chemistry to be explored, as the nature of the reactivity with silanes is still not yet fully understood.

3.6 Conclusions

The study described here was aimed at examining the effects of BN substitution within the indenide framework on the course of reactions with simple electrophiles. We specifically utilized 1-bora-7a-azaindenide anions, prepared using organozirconocene based methods, one of ten possible BN indenide isomers. We found that the locus of electrophilic attack was confined to the five-membered BN containing ring, but that the regiochemistry observed was dependent on the nature of the electrophile. Alkyl halides reacted at the boron atom to give neutral BN-indenyl products in which the six-membered pyridyl ring is re-aromatized, a strong factor in determining the outcome of the reaction. This reactivity bears some similarity to what is observed in the reactions of the all-carbon indenide anion with alkyl halides, which alkylate at the C-1/3 positions. The reactions of **6^H**/**6^{Me}** with CO₂, however, differs from the analogous reactivity in the indenides in that the CO₂ electrophile adds to the C-2 carbon of the 1-bora-7a-azaindenides. Here, the Lewis base/Lewis acid nature of these BN compounds conspires to bind the CO₂ without re-aromatizing the pyridyl ring. For this reason, the bonding of CO₂ to compounds **6** is reversible at room temperature.

CHAPTER 4: BORON-NITROGEN DOPED DIHYDROINDENO[1,2-B]FLUORENE DERIVATIVES AS ACCEPTORS IN ORGANIC SOLAR CELLS.

4.1 Preface

Despite the interesting properties of the indacene species described in Chapter 2, the compounds were too air and moisture sensitive to easily make a variety of derivatives and test their properties in devices. In addition, the synthetic pathway produced large amounts of high molecular weight by-products that when making gram-scale BN materials generated significant waste. With these considerations in mind we sought to target similar molecules using more atom economical synthetic pathways.

4.2 Author Contributions

All synthetic work, characterization and crystallographic characterization were performed by Mr. Matthew Morgan. Computational calculations were performed collaboratively by Dr. Mikko Rautiainen, Prof. Heikki Tuononen and Mr. Matthew Morgan during an international exchange term at the University of Jyväskylä, Finland. Fabrication and testing of devices were performed by Ms. Maryam Nazari.

4.3 Abstract

The electrophilic borylation of 2,5-diarylpyrazines results in the formation of boron-nitrogen doped dihydroindeno[1,2-b]fluorene which can be synthesized via mildly air-sensitive techniques and the end products handled readily under atmospheric conditions. Through transmetallation via diarylzinc reagents a series of derivatives were synthesized which show broad absorption profiles that highlight the versatility of this backbone to be used in organic solar cell devices. These compounds can be synthesized in large yields, in a low number of steps and functionalized at many stages along the way providing a large depth of possibilities. Exploratory device parameters were studied and show moderate results with PCEs reaching 2%

4.4 Introduction

4.4.1 Organic Solar Cells

As mentioned in Chapter One, a large amount of focus has been placed on designing BN containing polycyclic aromatic hydrocarbons for use in organic devices. A very active area within organic materials research is organic photovoltaics, which are proposed as good alternatives to inorganic silicon cells due to their synthetic tunability and solution processability. To date organic (OSC) or polymer (PSC) cells that contain only one active species have yielded poor device performances due to poor charge carrier generation and unbalanced charge transport.¹⁶¹ To

improve this, a bilayer bulk heterojunction architecture has been adopted where there are separate hole transport (p-type) species and electron transporting (n-type) materials.^{162, 163}

Organic solar cell operation can be described in several stages. The first step is the absorption of a photon of light, exciting an electron from the HOMO to the LUMO of the material generating an electron-hole pair, referred to as an exciton. This is followed by the diffusion of the exciton to the interface between the donor and acceptor species of the active layer.¹⁶⁴ From this point the energetics of the active layer have the largest impact. If acceptable energy levels are met, the electron can travel from the LUMO of the donor species to the LUMO of the acceptor. Concurrently, the hole travels “uphill” from the HOMO of the acceptor to the HOMO of the donor species. The free electron and hole charges can then flow within the device towards the respective electrodes and then to the load attached to the cell. This transportation of charge is the second key consideration for the use of donor and acceptor molecules, as the efficiency of the device is impacted by the physical characteristics of the active species.

The key measure of OSC device performance is the power conversion efficiency (PCE) which is a measure of the ratio of energy put into the cell over the energy output from the device.¹⁶⁵ This is given by equation 4-1 (below) where the energy output is equal to the product of the voltage and current at the maximum power output, and are defined by three parameters, the open circuit voltage (V_{oc}), the short-circuit current (J_{sc}) and the fill factor (FF).^{165, 166} These factors are affected by the blend of active layer materials employed and device engineering. In general, research efforts have focused on developing novel active layer materials that lead to higher PCEs and V_{oc} than previous systems.¹⁶⁷

Equation 4-1.

$$PCE(P_{Max}) = \frac{V_{oc} \times J_{sc} \times FF}{P_{in}}$$

To date, the field of organic solar cells has been dominated by work on polymer donor and fullerene acceptor systems. This research all grew from the benchmark performance of P3HT with PC₇₁BM (Figure 4-1) which show PCEs from 3-5%.^{168, 169} Over years, this led to the development of a family of similar polymer systems which has evolved to use the more complex PTB7-Th donor molecule capable of PCEs of 9%.¹⁷⁰

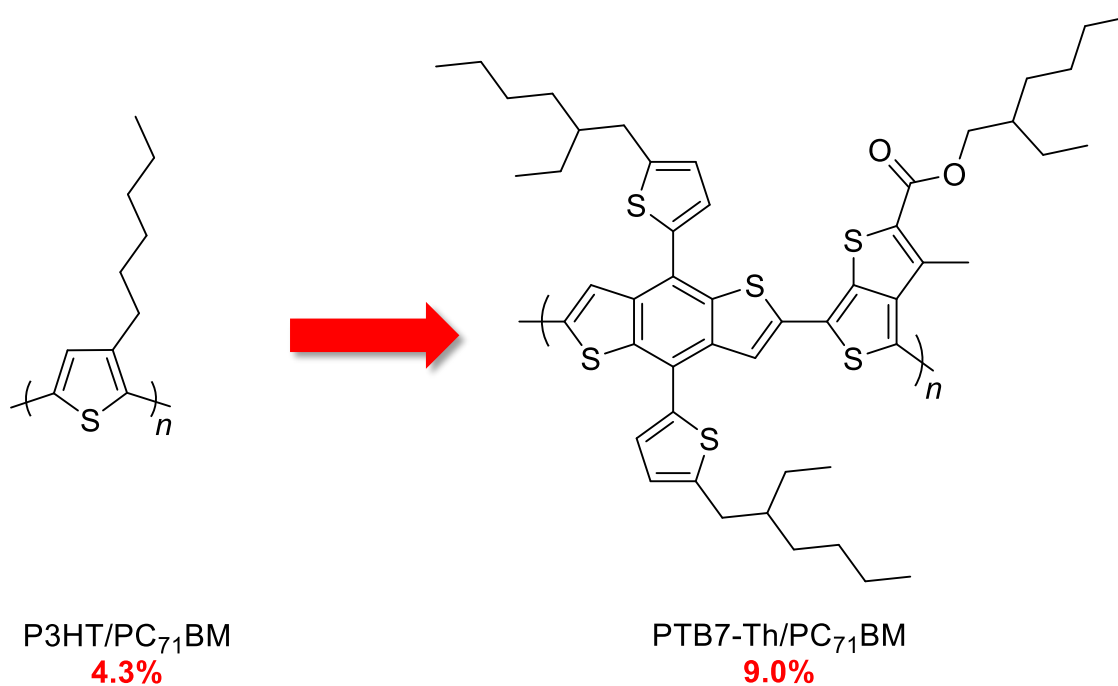


Figure 4-1. Development of donor molecules in Polymer-Fullerene cells.

Despite these increases in performance, it became clear that the polymer-fullerene system had some problems that could no longer be overcome by tuning. The fullerenes themselves do not

efficiently absorb light and in addition to their generally poor stability are difficult to access synthetically, making them quite costly.¹⁷¹ This kickstarted work into the field of non-fullerene (NF) accepting molecules which since ~ 2013 has grown into a massive area of research. Two of the most successful NF acceptor systems are the perylene diimide (PDI) and indacenedithiophene motifs highlighted in Figure 4-2. They have allowed for PCEs of as high as 13% which are even higher than many of the top performing fullerene containing systems.¹⁷²⁻¹⁷⁴

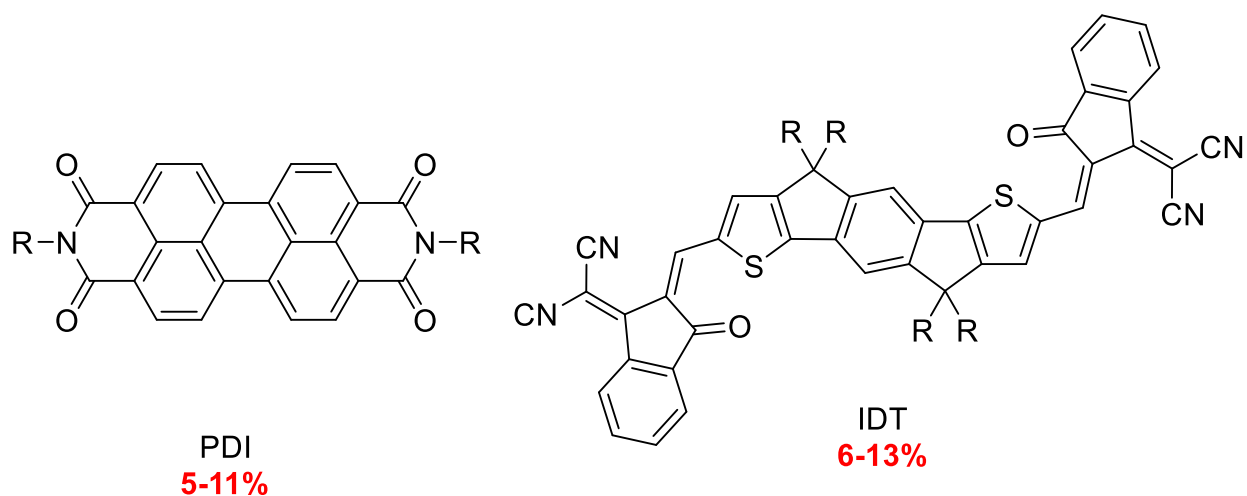


Figure 4-2. Most well studied high performance NF acceptor materials.

One of the major advantages of NF acceptors is the ability to tune the electronics of the molecule to more closely match the donor species of interest, yielding a larger V_{oc} and therefore a higher PCE. While research into the above-mentioned acceptors is ongoing there is also a need for the discovery of new accepting molecules to pair with less expensive or higher efficiency donors as they are discovered to allow for better device properties.

4.4.2 Boron-Nitrogen containing Active Species

Boron-nitrogen containing aromatics have been studied extensively for their optoelectronic properties. Despite the large number of molecules synthesized, testing in devices is still quite rare for new systems. This holds especially true for their use in OPVs. To date most work has focused on testing materials for their hole or electron transport properties likely due to the simpler device architecture required. Despite this, some recent examples of molecules used as active components in OPVs are presented in Figure 4-3. Compound **I** represents the first heteroaromatic species with an imbedded BN to be tested in an OPV.⁶² When this molecule was used as a donor with PC₇₁BM as the acceptor a PCE of 3.12% and a V_{oc} of 0.96 eV were observed. In addition, when **I** was used as an additive to a standard PTB7/PC71BM cell, the ternary cells displayed an enhanced PCE of 4.75% compared to the binary device (3.91%).

Due to the ease of synthesis and tunability, BODIPY functionalities have been one of the most studied systems for OPVs. They have been used with electron rich subunits appended such as carbazole as highlighted by compound **II**. A device made with **II** as the donor species and PC71BM as the acceptor, gave PCE and V_{oc} values of 5.05% and 0.90 V respectively.¹⁷⁵ In addition, due to the strong electron affinity, BODIPY based materials should be suitable as the electron accepting materials within devices. Indeed when the DPP bridged BODIPY dimer **III** was synthesized and tested as the acceptor with PTB7-Th as the donor a PCE of 2.84% was observed, which is the highest performance to date for BODIPY based acceptor materials.¹⁷⁶

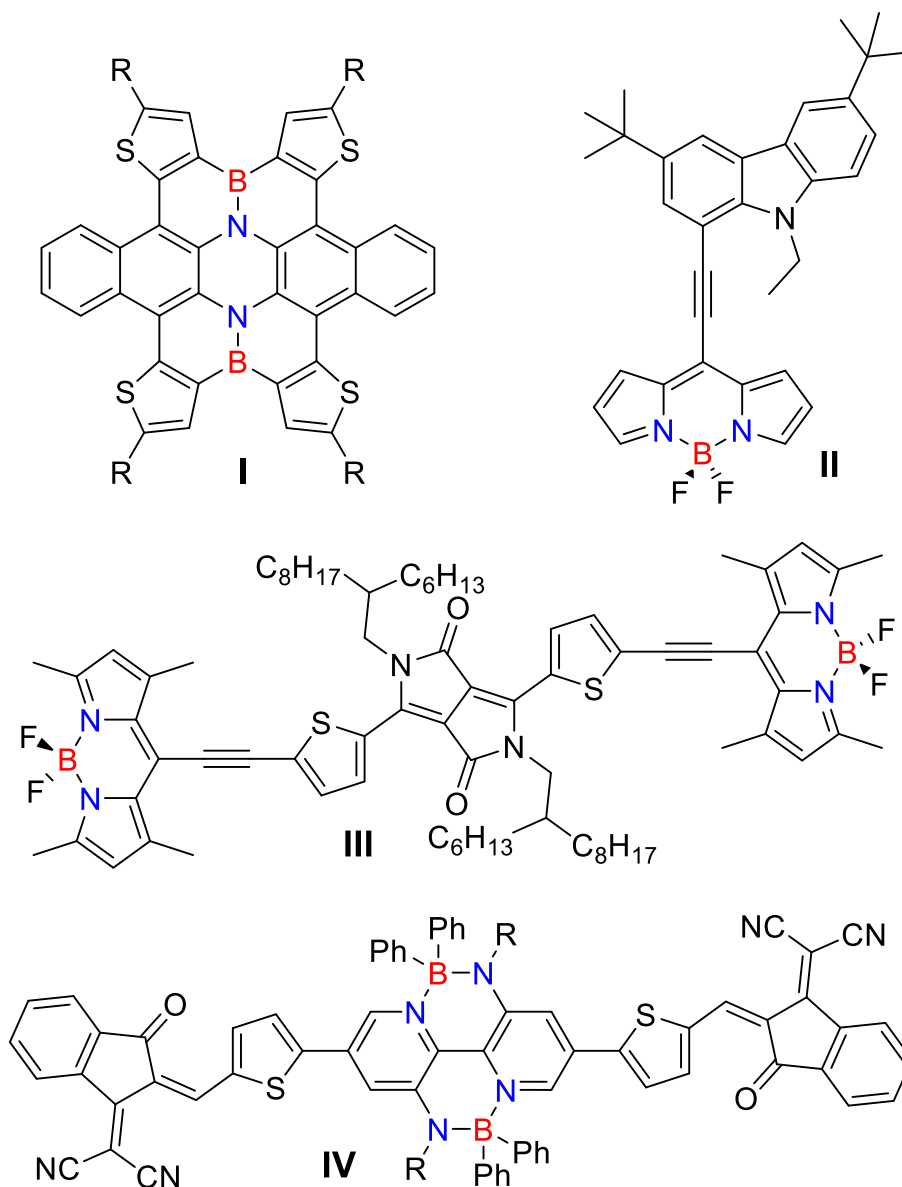


Figure 4-3. Structures of boron-nitrogen containing species utilized in organic electronic devices.

Recently the Liu group has been focused on the synthesis of a novel BN bipyridine subunit (BNBP) and have tested it with a variety of substituents.^{56, 177} The best performing molecular species to date (**IV** in Figure 4-3) has been used as the acceptor with PTB7-Th and yielded a

competitive PCE of 7.06% which is quite similar to those observed with traditional organic acceptors.⁵⁷ The immense amount of study on this single new core highlights the need for novel subunits and shows the promise of units containing BN bonds.¹⁷⁸

While these species based around the BN subunit show good promise there is a need for novel cores that are easy to synthesize and can be readily functionalized to tune frontier orbital energies to match donor species. Following the work described in Chapter Two, we were prompted by the photophysical properties of BN s-indacene derivatives to target extended systems such as dihydroindeno[1,2-*b*]fluorene derivatives (**Ph₂PzB(R)₂**) or the reduced fully planar analogue **Ph₂PzBAr** depicted in Figure 4-4. Due to the extended pi system the indenofluorene species should be more stable to ambient conditions and can be synthesized utilizing electrophilic borylation chemistry which is well studied and known to produce high yields. The all-carbon indenofluorene systems have been studied recently by the Haley group and have shown a number of interesting properties both from a fundamental understanding of aromaticity, and application to OFETs.^{109, 129, 139} Once a synthetic pathway to these derivatives is developed they can be easily tuned to give backbones similar to the IDT species in Figure 4-2. which are among the highest performing NF acceptors to date.

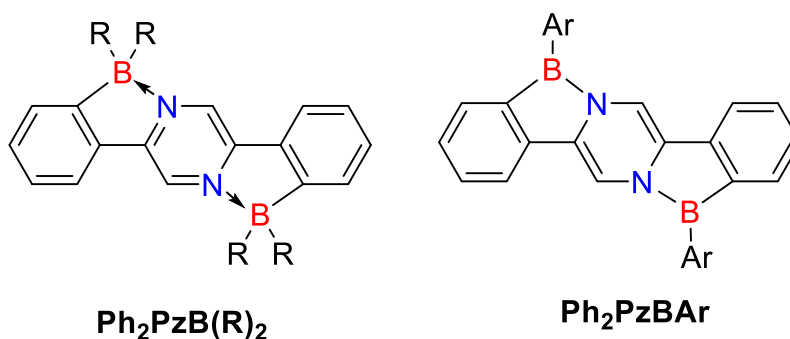
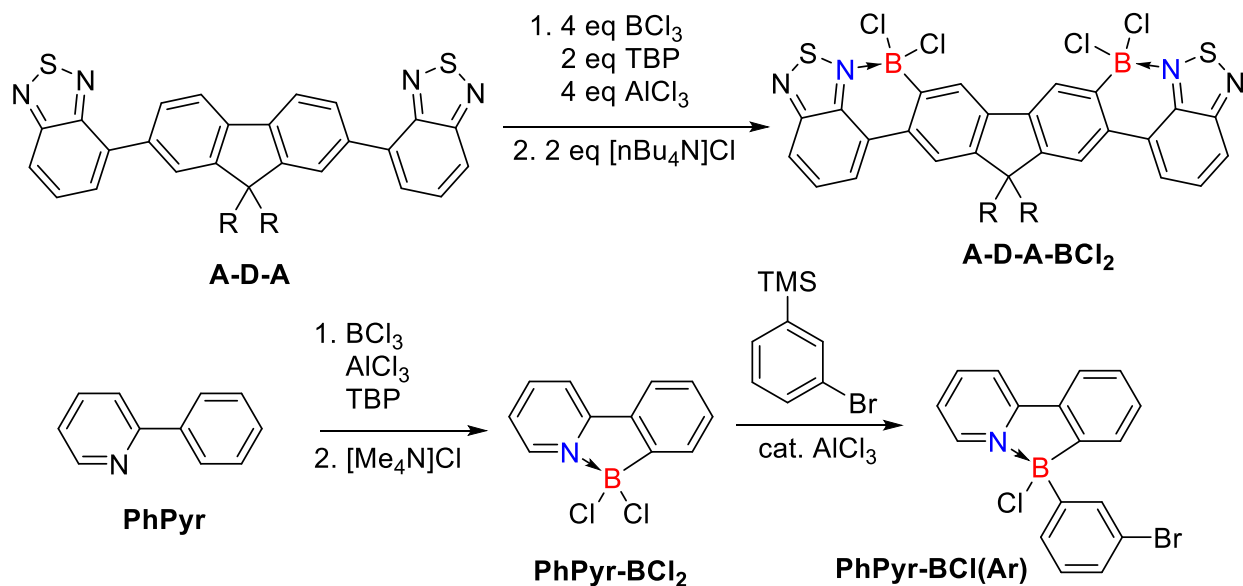


Figure 4-4. Boron-nitrogen doped indacene targets

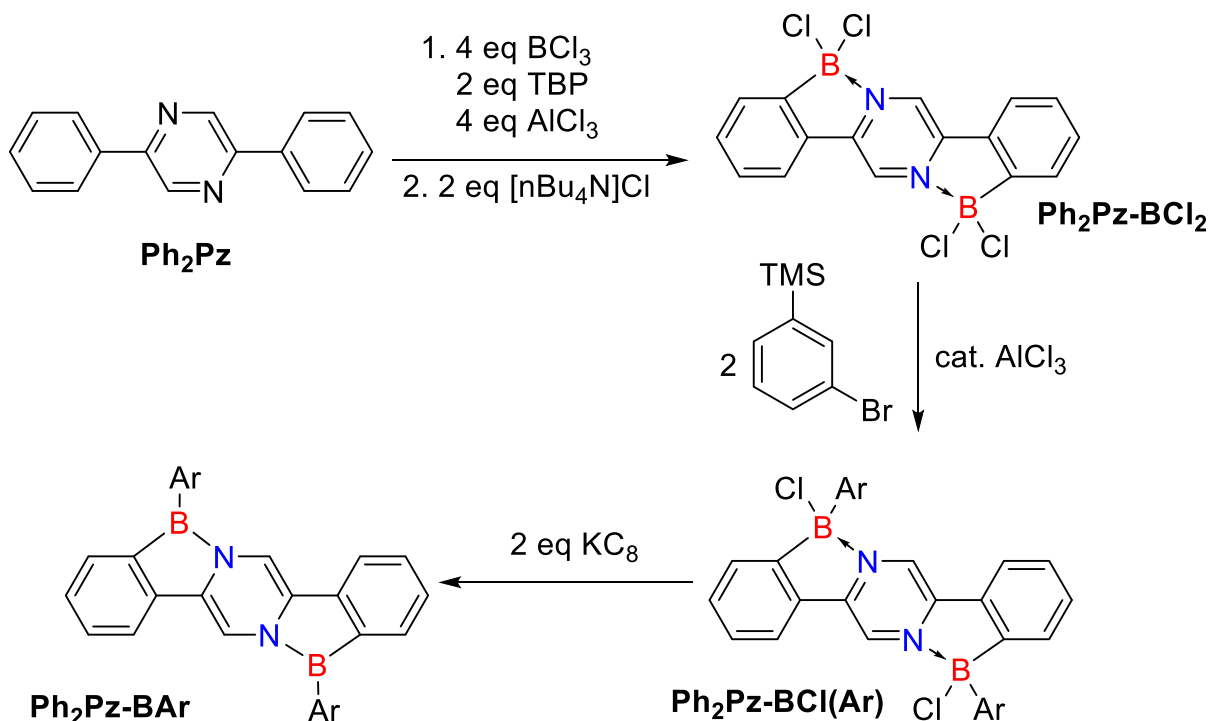
We were inspired by the work of the Ingleson group on the borylation of electronically interesting molecules shown below in Scheme 4-1.¹⁷⁹ In 2015, the Ingleson group utilized electrophilic borylation on an acceptor-donor-acceptor organic molecule (**A-D-A** in Scheme 4-1) to yield **A-D-A-BCl₂**.¹⁸⁰ The starting material has an electron rich fluorene flanked by two electron accepting benzothiadiazole moieties. Upon treatment with BCl₃, AlCl₃ and the bulky base TBP (2,4,6-tritertbutylpyridine) electrophilic borylation was successful in good yields. It is noteworthy that the bulky base was necessary as when the synthesis was attempted with triethylamine no reaction occurred, the BCl₃ simply coordinated to the small amine base. Following borylation, transmetallation to arylated derivatives was possible through treatment of the dihaloboranes with diaryl zinc reagents, to yield several derivatives which showed good performances as red emitters in organic light emitting diodes. One of the major issues with this and similar synthetic pathways is the need for highly reactive organozinc reagents to functionalize the borane formed. In a follow-up report, the Ingleson group showed a synthetic pathway that allowed for more selective functionalization at the boron using milder organo-tin and organo-silane reagents.¹⁷⁹ In this report 2-phenylpyridine (**PhPyr** in Scheme 4-1) is borylated in the same fashion to yield **PhPyr-BCl₂** in good yields. The authors were then able to arylate the dichloroboranes atom in a variety of manners, but the most relevant example is shown below where the haloborane was treated with one equivalent of an electron poor arylsilane to afford the monoarylated product **PhPyr-BCl(Ar)**.

Scheme 4-1. Electrophilic borylation pathways developed by the Ingleson group.^{179, 180}



We sought to employ this synthetic method to make a variety of indenofluorene species as described in our proposed synthesis below in Scheme 4-5. Starting from the readily synthesized diphenylpyrazine the electrophilic borylation should proceed easily to yield **Ph₂Pz-BCl₂**. This haloborane could then be subjected to a variety of systems to yield the monoarylated species and analogously to the work on *s*-indacene presented earlier to yield the fully planar indenofluorene derivative shown. This Chapter describes the facile synthesis of a new family of B-N doped dihydroindeno[1,2-*b*]fluorene derivatives which show promising device properties when utilized as the electron accepting layer in organic solar cells. In addition, efforts towards the synthesis of fully planar derivatives with three-coordinate boron centres is described.

Scheme 4-2. Proposed synthetic pathway to access **Ph₂Pz-BAr** derivatives.



Results

The first step of the synthetic pathway was to synthesize the diarylpyrazine reagents, which could easily be accomplished through a palladium catalyzed Suzuki coupling reaction between commercially available dibromopyrazine and substituted arylboronic acids. Due to solubility issues previously observed in the indacene systems we sought to synthesize substituted aryl pyrazines and targeted several derivatives shown in Figure 4-5. In addition to solubilizing groups, the ease of synthesis prompted us to target the both electron deficient (**14^F** and **14^{CF₃}**) and electron rich (**14^{OMe}** and **14^{NAr}**) end caps to gain an understanding of the influence of electron density on the optoelectronic properties of the synthesized BN compounds.

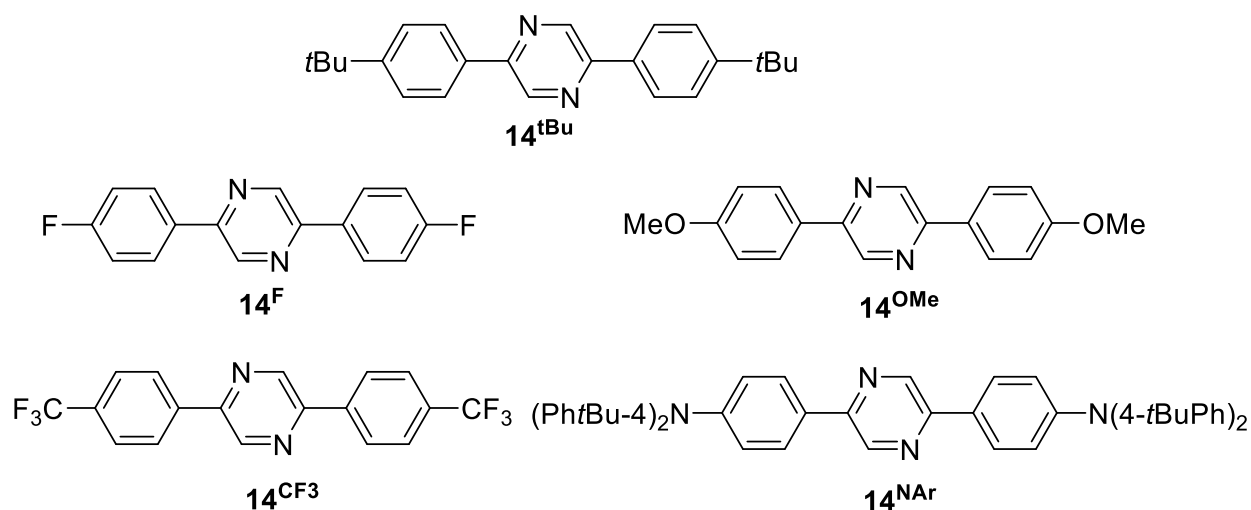


Figure 4-5. Diarylpyrazine species synthesized for this study.

Each of these derivatives was synthesized following literature preparations and were purified on gram scale without the need for column chromatography. They were all recrystallized from hot ethanol after filtering from the reaction mixture. Representative ¹H NMR spectra of these recrystallized products are shown below in Figure 4-6. The pyrazines are white crystalline solids with the exception of **14^{NAr}** which is a bright fluorescent yellow crystalline solid. This property is retained in solution and representative absorption and emission spectra are shown in Figure 4-7. The bright fluorescence and synthetic accessibility could make **14^{NAr}** interesting on its own as it adds to the number of tunable donor-acceptor-donor dyes available.^{181, 182}

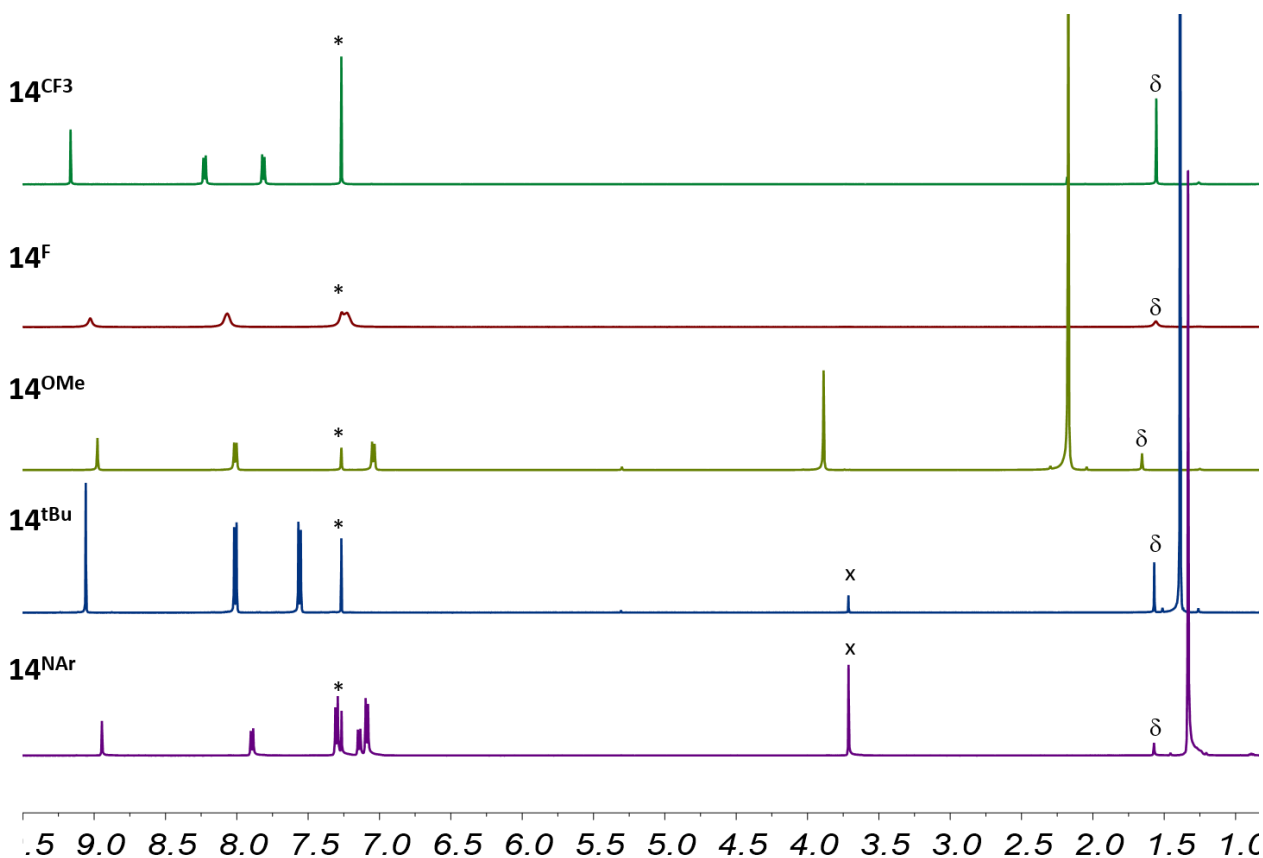


Figure 4-6. Representative ^1H NMR spectra of **14**^R derivatives in CDCl_3 . Impurities are denoted as * CHCl_3 , x dioxane, δ H_2O .

Utilizing the electrophilic borylation conditions reported by Crossley *et al.*,¹⁸⁰ the prepared pyrazines (**14**) were treated with BCl_3 , AlCl_3 and the bulky base TBP (2,4,6-tri-*tert*-butylpyridine) in dichloromethane to yield the borylated species. For the fluorinated derivative **14**^F there was no reaction as starting material was simply isolated from the reaction mixture. For **14**^{CF3}, trifluoromethyl groups are known to react with aluminum trichloride¹⁸³⁻¹⁸⁵ and the only isolated product was the starting material with all the fluorine atoms replaced by chlorine. Similarly, to **14**^F, the methoxy derivative only yielded starting material under these reaction conditions, even if

excess of either trichloroborane or aluminum chloride were added to coordinate to the Lewis basic oxygen atoms on the alkoxy functional group.

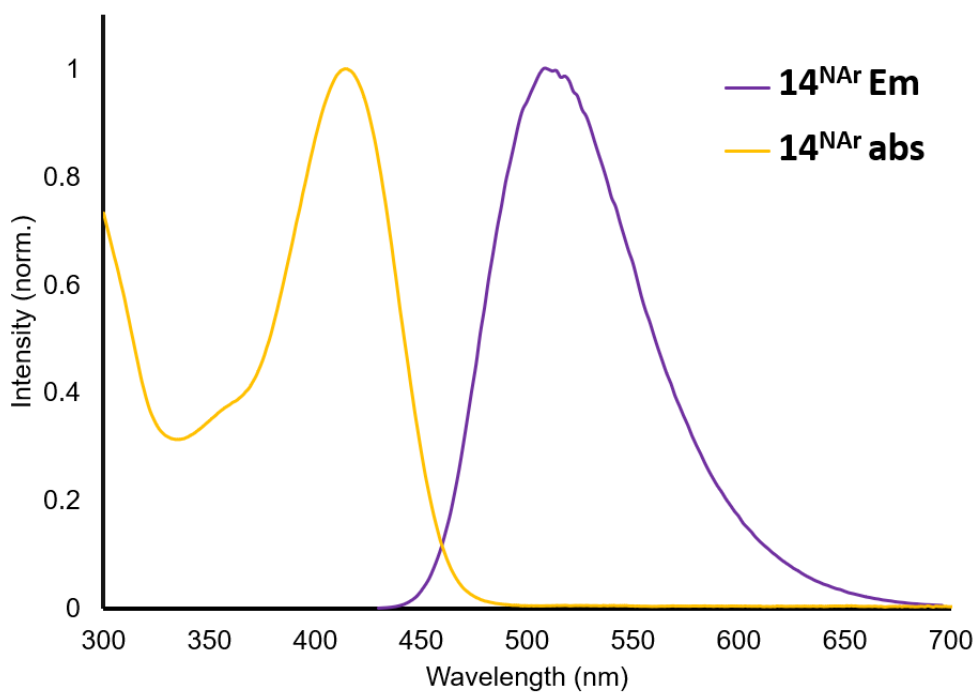
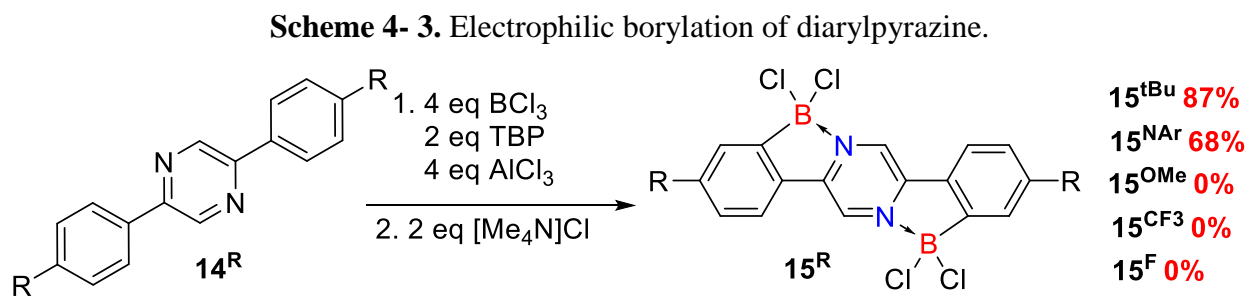


Figure 4-7. Normalized absorption and emission spectra of 14^{NAr} in a dichloromethane solution.



This procedure did work well for **14^{tBu}** and **14^{Nar}**, as **15^{tBu}** and **15^{Nar}** were synthesized in 87% and 68% yields, respectively. These compounds were isolated in atmospheric conditions by washing the solids obtained from the reaction mixture with water and hexanes; we observed no decomposition due to hydrolysis of the B-Cl bonds. This simple work up yielded almost completely pure product as indicated by the ¹H NMR spectra shown below in Figure 4-8. The synthesis of these species is easily repeatable and can be performed with only moderate considerations to remove air and moisture from the system.

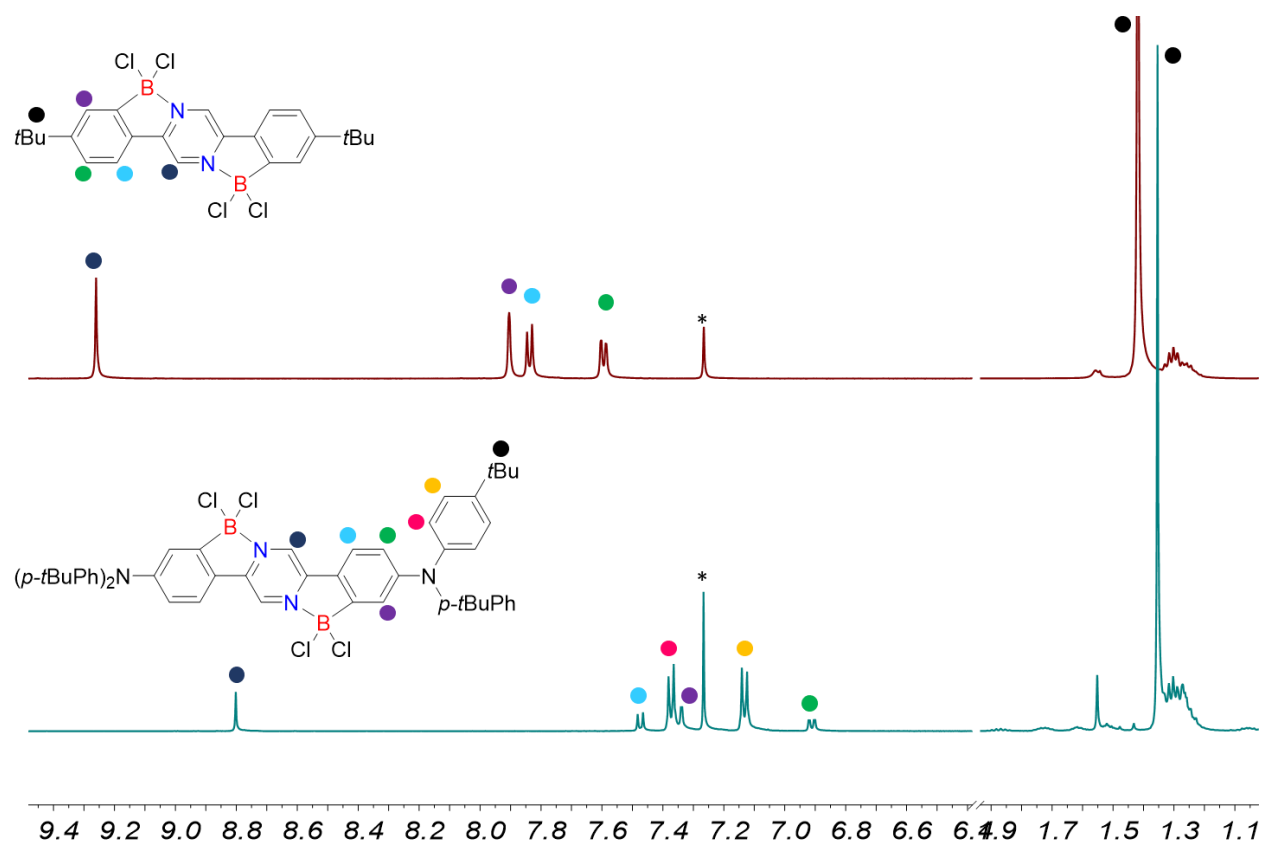


Figure 4-8. ¹H NMR spectra in CDCl₃ of the borylated pyrazine species **15^{tBu}** and **15^{Nar}**.

reported with a B-N bond length of 1.615 Å.^{118, 180}

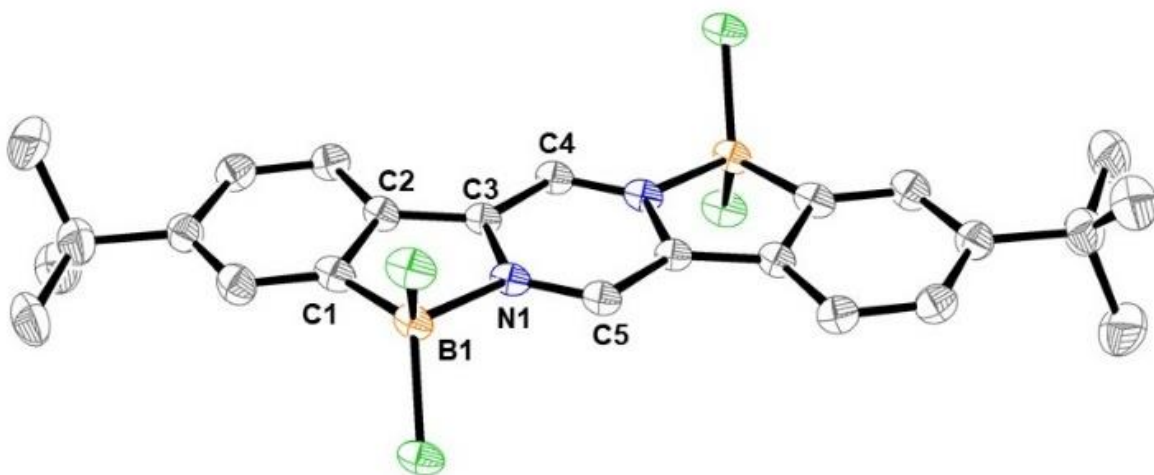


Figure 4-9. Thermal ellipsoid (50%) diagram of the molecular structure of **15^{tBu}**. Hydrogen atoms have been omitted for clarity. Selected bond lengths (Å) B(1)-N(1) 1.615(6), B(1)-C(1) 1.582(6), C(1)-C(2) 1.399(5), C(2)-C(3) 1.432(5), C(3)-C(4) 1.396(5), N(1)-C(3) 1.368(4), N(1)-C(5) 1.304(5).

Both **15^{tBu}** and **15^{Nar}** are highly coloured (orange and green respectively) and have broad absorption profiles with two major peaks (336, 505 nm and 471, 800 nm respectively) as shown in Figure 4-10. These wide absorption spectra are promising for OSC device efficiency, as it likely indicates superior light harvesting ability which is ideal in photovoltaic applications.

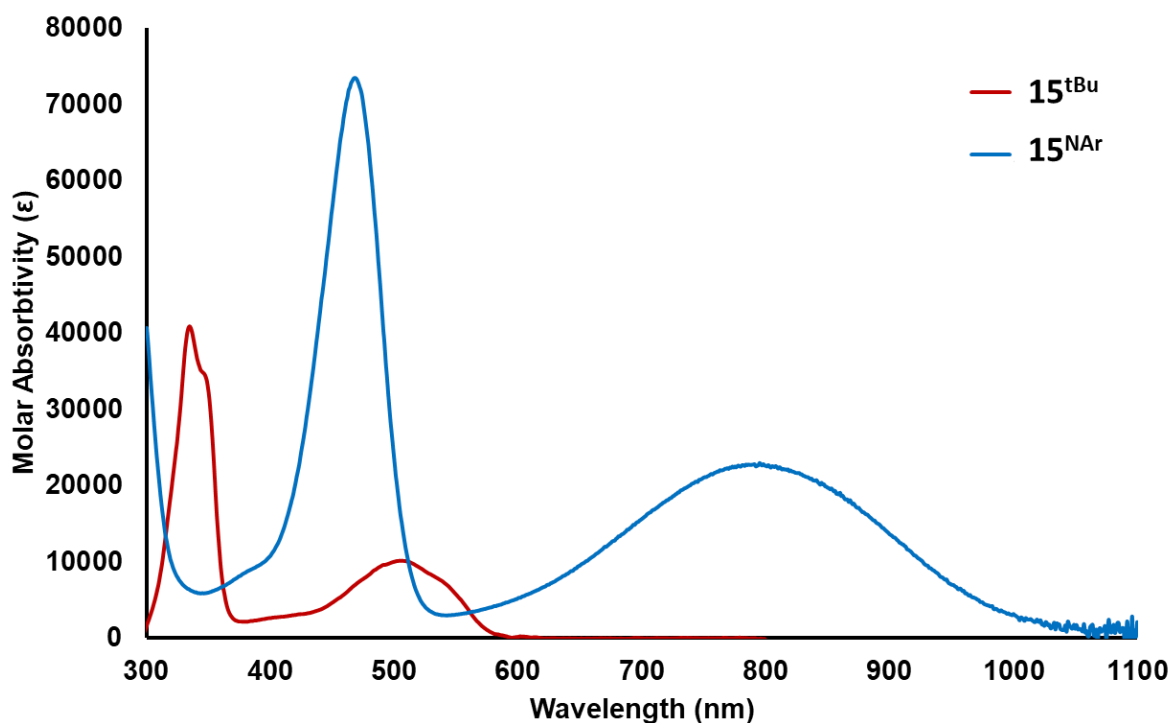


Figure 4-10. Normalized absorption spectrum in dichloromethane solutions of **15^{tBu}** and **15^{NAr}**.

Through TD-DFT (PBE0/Def-TZVP) analysis of these species it is apparent that the longer wavelength absorption band is from the HOMO-LUMO transition, while the shorter wavelength band is primarily from the HOMO-LUMO+1 transition. Looking at the localization of the frontier orbitals Figure 4-11 it is noteworthy that the HOMO is localized primarily on the outer aryl rings of the molecule, while the LUMO and to a lesser extent the LUMO+1 are localized on the central pyrazine core. While only the orbitals for **15^{tBu}** are highlighted here the trend is maintained for **15^{NAr}**, as will be discussed later in this chapter. In addition, **15^{tBu}** has an emission maximum at 598 nm (Figure 4-12) giving a Stokes shift of 89 nm (2870 cm^{-1}), which is unexpectedly large for such a rigid planar system and is likely due to the charge transfer nature of the HOMO-LUMO transition which causes significant bond length rearrangements in the excited state. Compound **15^{NAr}** does

not appear to be emissive which could be due to our inability to measure emission past ~ 900 nm or due to competing pathways of non-radiative decay within the molecule. This was surprising as the exceptionally bright fluorescence in 14^{Nar} was completely lost in the borylation procedure.

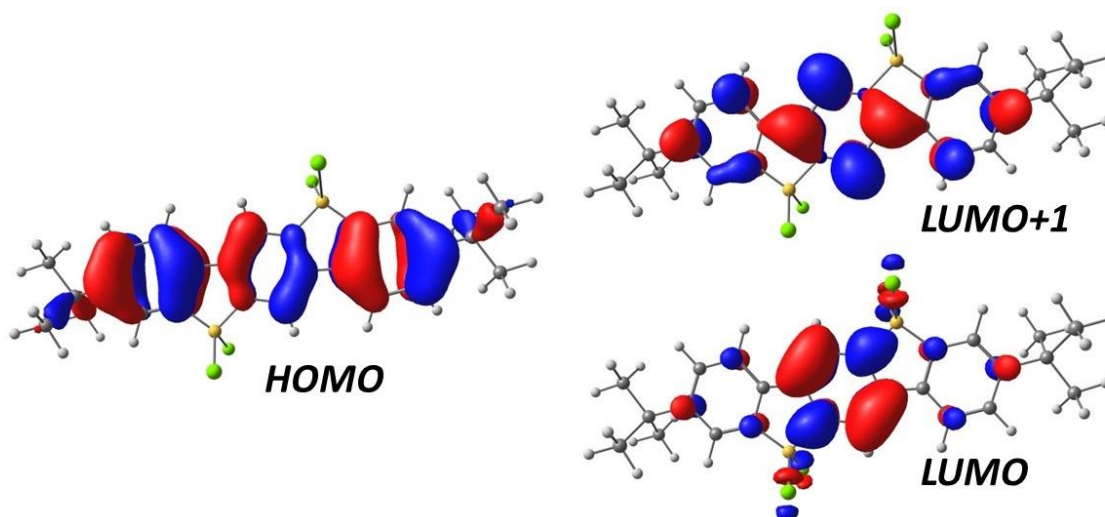


Figure 4-11. HOMO, LUMO and LUMO+1 orbitals of 15^{tBu} based on calculations at the PBE0/Def-TZVP level.

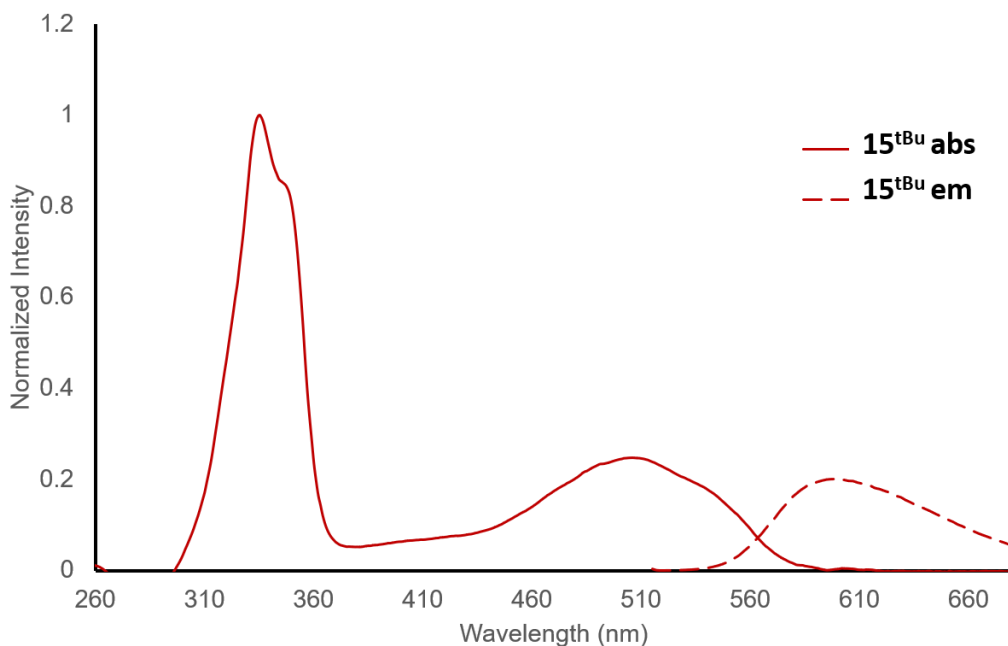


Figure 4-12. Normalized absorption and emission spectra of 15^{tBu} in dichloromethane solutions.

To further understand the electronic structure of these chlorinated derivatives, cyclic voltammetry experiments were performed and are shown in Figure 4-13. It is possible to estimate the HOMO and LUMO energy levels using the onset of oxidation and reduction potentials respectively. The electrochemical data is presented in Table 4-1 and the electrochemical band gap can be compared to that derived through UV-Vis spectroscopy. There is good agreement in the tert-butyl derivative as the electrochemical band gap (E_{elec}) and optical band gap (E_{opt}) are 2.1 and 2.2 eV respectively. While **15^{tBu}** shows mainly one reduction and oxidation peak, there are clearly additional signals at higher voltages in the **15^{NAr}** derivative which are likely due to the oxidation of the external diarylamino groups. The seemingly reversible (or at least quasi-reversible) reduction waves showed promise that the reduction to the fully planar system should be possible chemically and this will be discussed later in the chapter.

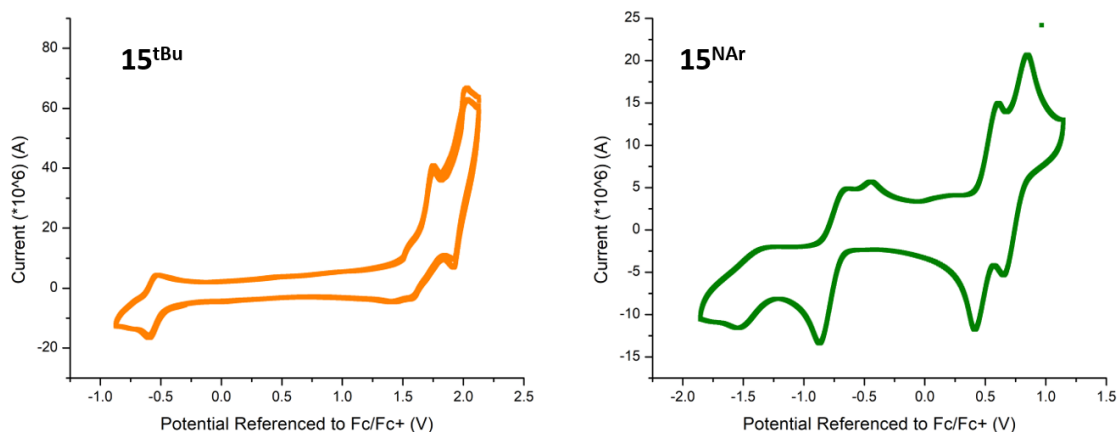


Figure 4-13. Cyclic Voltammograms of **15^{tBu}** (Left) and **15^{NAr}** (Right). CV are recorded in dichloromethane with a 0.1M nBu₄NPF₆ electrolyte.

Table 4-1. Electrochemical data for **15^{tBu}** and **15^{NAr}**.

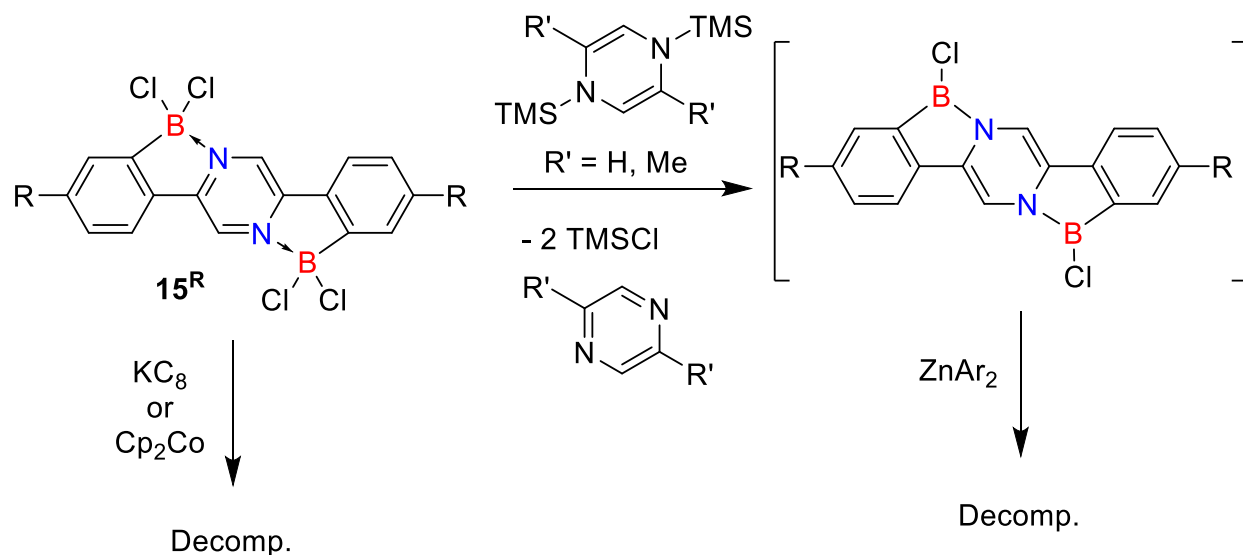
	Red _{On} (V)	Ox _{On} (V)	HOMO (eV)	LUMO (eV)	E _{elec} (eV)	E _{Optical} (eV)
15^{tBu}	1.61	-0.43	-6.41	-4.31	2.1	2.2
15^{NAr}	0.42	-0.44	-5.22	-4.18	1.0	1.3

With these chlorinated derivatives in hand we sought to functionalize them further at the boron centres as outlined in the proposed synthesis in Scheme 4-2. Initial attempts focused on applying the borenium cation mediated desilylation or destannylation reported by Ingleson to install aryl groups on boron.¹⁸⁰ While these procedures work well for their systems, in our hands no substitution was observed when **15^{tBu}** or **15^{NAr}** were treated with phenylSiMe₃ or phenylSnBu₃ with catalytic or stoichiometric AlCl₃. Despite varying temperature (20-80 °C), solvent (dichloromethane, chlorobenzene) and amount of aryl stannane or silane no transmetallation was observed, and only starting material was recovered. It is worth noting that we were able to reliably reproduce the synthesis reported for the phenyl pyridine system, just not with these pyrazine derivatives.

Attempts were made to reduce the chlorinated species **15^{tBu}**/**15^{NAr}** using a variety of methods with the idea that a planar haloborane would be more susceptible to arylation reactions. The reduction was attempted with standard reducing agents such as KC₈ and Cp₂Co, which led to intractable mixtures. Following up on some recent chemistry by the Yamashita group with bis(trimethylsilyl)pyrazines.¹⁸⁶⁻¹⁸⁸ the chloroboranes were treated with two bis(silyl)pyrazine derivatives as shown in Figure 4-12. While initial attempts were promising (one compound apparent in the NMR spectra) whatever compound was being made was not isolable in our hands. Attempts to arylate the reduced chloroboranes with diarylzinc reagents also led to decomposition.

Despite this, work in the future still needs to be done on isolating the reduced species, perhaps just with different groups on the core to impart further stability.

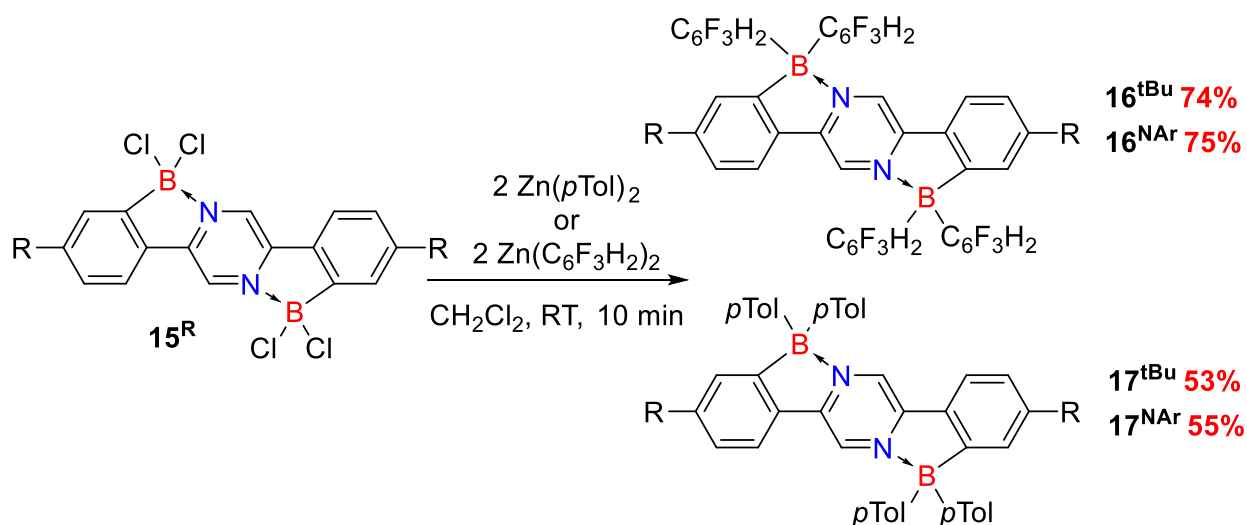
Scheme 4- 4. Attempted reduction reactions of **15^R**.



Since mild conditions could not produce the arylated products we turned to the use of diaryl zinc reagents which have been reported in other cases to readily transmetallate with B-X bonds. The arylated products **16^R** and **17^R** were synthesized in moderate to good yields by stirring a solution of the haloboranes **15^R** with a small excess (~2.1 equivalents) of diarylzinc reagents as shown in Scheme 4-5. It is important to note that this reaction only progressed in good yields if the diarylzinc reagents were base (ether and THF) free, which was accomplished through sublimation. In an effort to generate the monoarylated species **15^{tBu}** was treated with one equivalent of diarylzinc reagent, unfortunately the reaction proceeded to a seemingly statistical mixture of mono-, di-, tri-, and terta-substitued products in addition to remaining starting material. This reaction was attempted with both slow addition of diarylzinc reagent and through controlling

the temperature of the reaction to drive the reaction towards the disubstituted species ideal for subsequent reduction. When the reaction temperature was maintained at -78°C , the reaction did not proceed at all and not until $\sim -40^{\circ}\text{C}$ did a reaction occur which again led to a mixture of products as confirmed through TLC analysis of the reaction mixture.

Scheme 4-5. Arylation reaction using diarylzinc reagents.



While access to the desired disubstituted indeno[1,2-b]fluorene species was not afforded through this synthetic method, the tetra-arylated species **16^{tBu}** showed extremely bright yellow fluorescence in solution and prompted us to study these arylated species further. X-Ray diffraction analysis was performed on single crystals of **16^{tBu}** confirming the connectivity within the molecule (Figure 4-15). The bond parameters remain consistent to those of **15^{tBu}** with little change in bonding throughout the molecule, and the planarity of the indeno[1,2-b]fluorene core is maintained. The most significant change is the increase in the bond lengths of the $\text{B-C}_{\text{phenyl}}$ and B-N bonds which go from 1.582 and 1.615 to 1.618 and 1.642 Å in **15^{tBu}** to **16^{tBu}**, respectively.

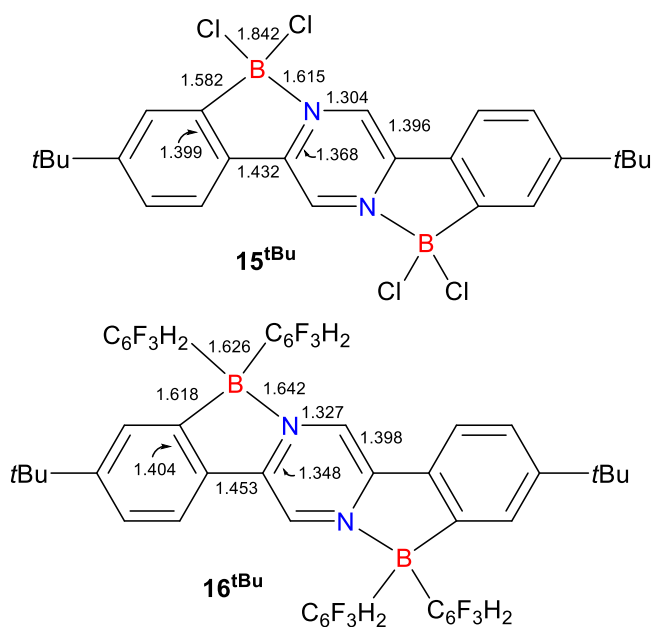


Figure 4-14. Relevant bond lengths derived through X-Ray crystallography for **15^{tBu}** and **16^{tBu}**, E.S.D. have been removed for clarity.

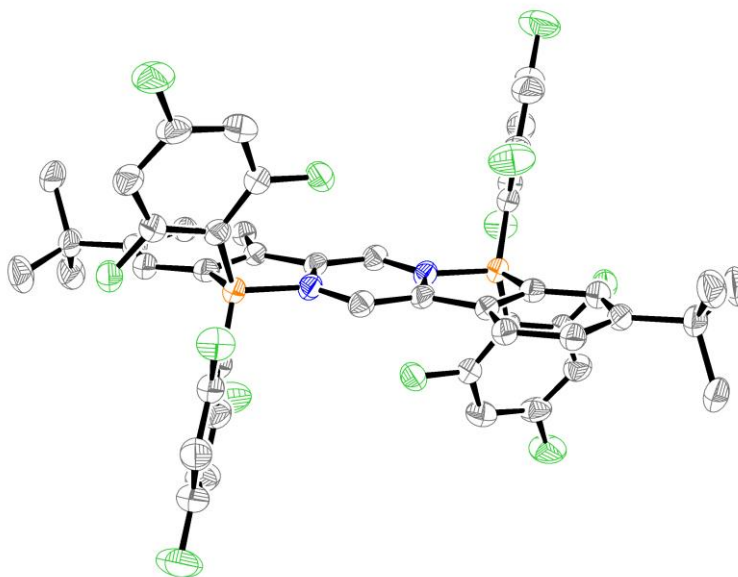


Figure 4-15. Thermal ellipsoid (50%) diagram of the molecular structure of **16^{tBu}**. Hydrogen atoms have been omitted for clarity.

As expected, the optical properties of the dihydroindenofluorene species change drastically with the substitution of the halides by aryl groups. This is especially apparent in the diarylamino substituted systems where the long wavelength absorption maxima change over 150 nm across the series from **15**^{NAr} to **17**^{NAr}, with a smaller variation of 60 nm for the tert-butyl series (Figure 4-16). With both the tert-butyl and diarylamino functionalized derivatives there is a blue shift in both absorption maxima going from **16** to **17** which is expected going from a more electron deficient substituents on boron to more electron donating aryl groups. Like **15**^{NAr} neither of the diarylamino functionalized species are emissive but, as mentioned **16**^{tBu} shows bright fluorescence (Figure 4-17) and possesses a large fluorescence quantum yield of 0.85. Interestingly, **17**^{tBu} shows no fluorescence in a dichloromethane solution, which can be explained by looking at the frontier orbitals calculated by TD-DFT shown in Figure 4-19. Unlike the other reported species, with frontier orbitals shown in Figure 4-18, **17**^{tBu} has a HOMO that lies primarily on one of the tolyl groups attached to boron. The calculated transition from HOMO-LUMO has a very small frequency, and the major transition observed experimentally is due to a combination of the HOMO-2 to LUMO and HOMO-4 to LUMO.

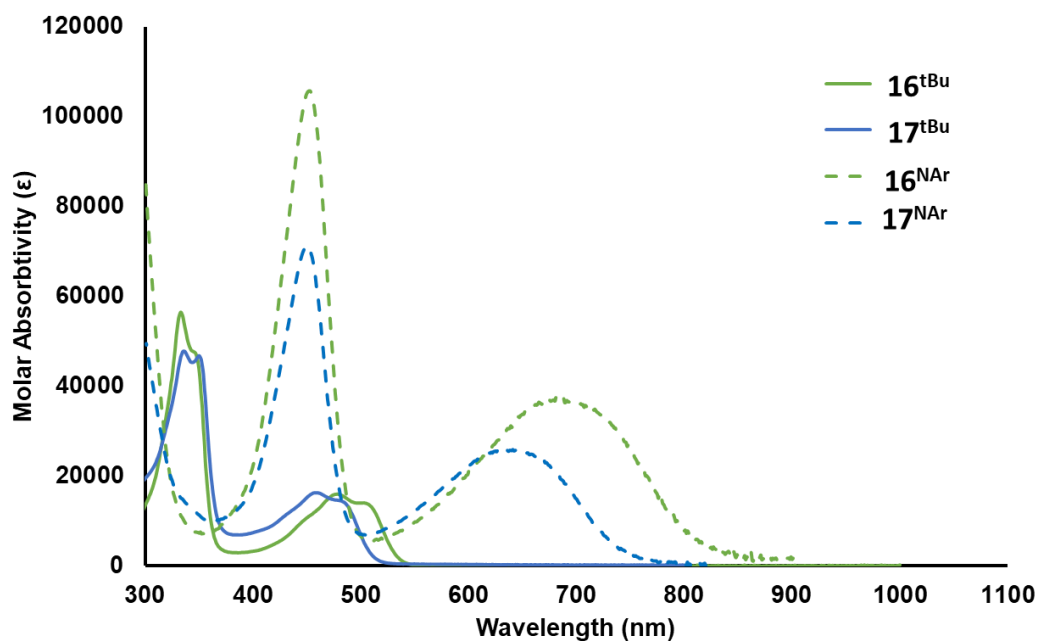


Figure 4-16. Normalized absorption spectra for the arylated derivatives of **16** and **17** in dichloromethane solutions.

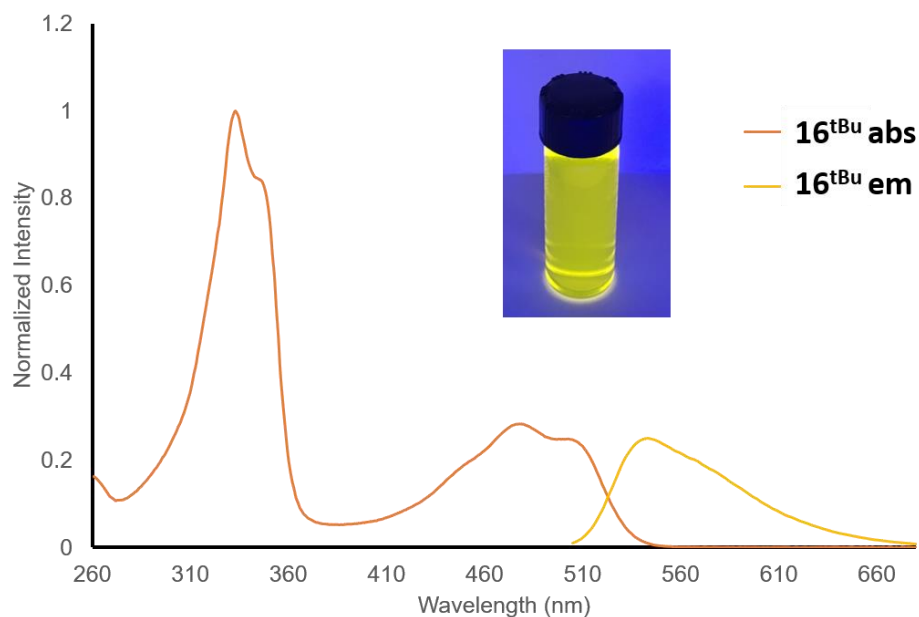


Figure 4-17. Absorption and Emission spectra of CH₂Cl₂ solutions of **16^{tBu}** inset is an image of a vial of the compound under 365 nm light.

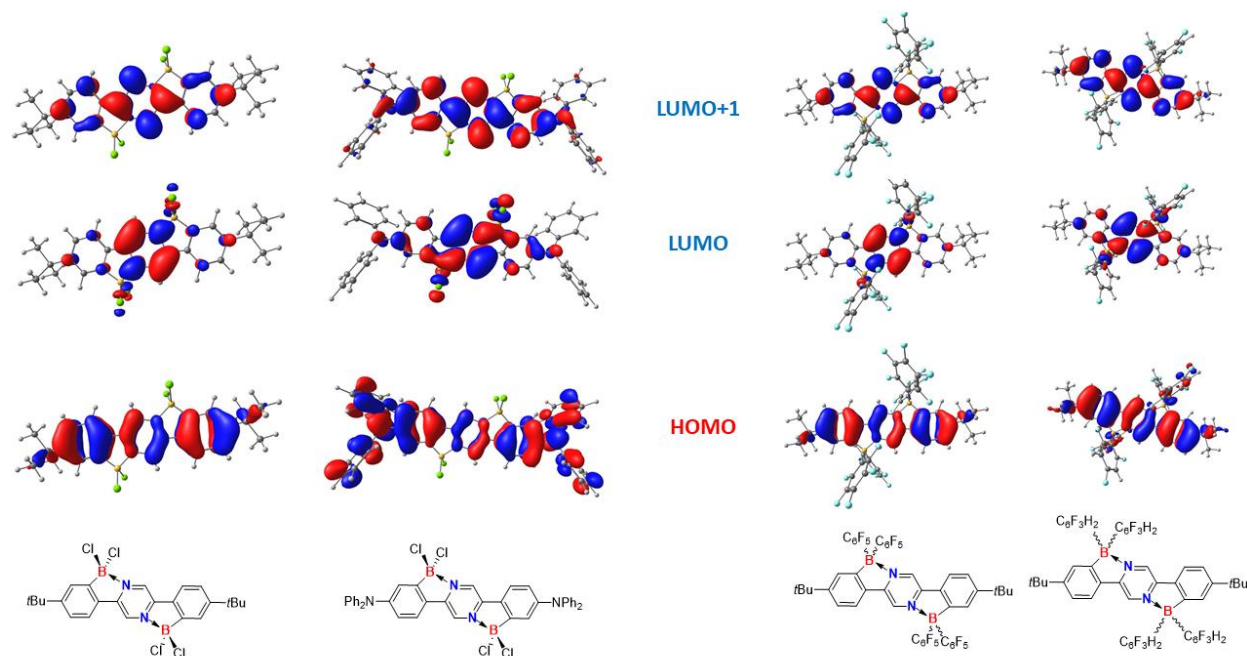


Figure 4-18. Frontier molecular orbitals of reported compounds calculated at the PBE0-DefTZVP level.

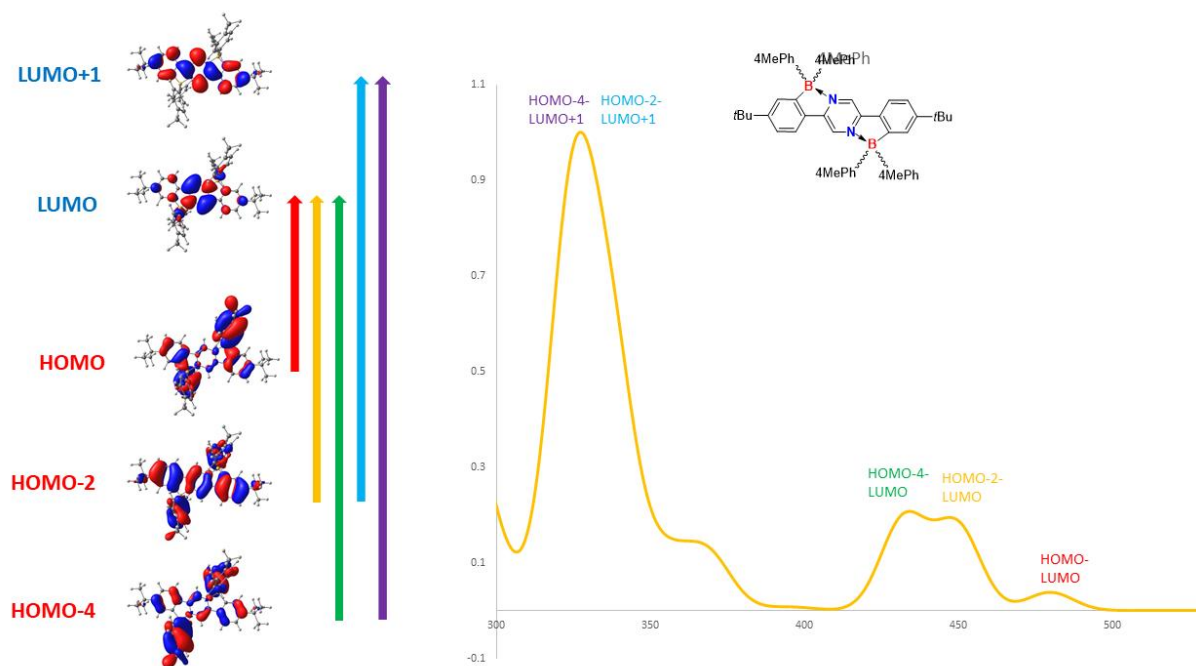


Figure 4-19. Frontier molecular orbitals and simulated absorption spectra of **17^{tBu}**, with high frequency transitions highlighted by coloured arrows.

The modification of the electronic nature across the series is further supported by the electrochemical data. Like for compounds **15^R** the HOMO and LUMO energy levels of these molecules are estimated by cyclic voltammetry and the results summarized in Table 4-2. Using **16^{tBu}** as an example, the HOMO and LUMO energy levels are -6.24 eV and -3.88 eV respectively giving an electrochemical band gap of 2.4 eV which matches closely with the photophysical gap of 2.3 eV. Across most of the series the optical and electrochemical band gaps are in good agreement, except **17^{NAr}** where the electrochemical oxidation peak could not be observed. This lack of oxidation wave could be due to the low solubility as even for **16^{NAr}** which shows higher solubility, the oxidative couple is significantly smaller in magnitude than the reduction (Figure 4-15).

Table 4-2. Electrochemical data for **16^R** and **17^R**.

	Red _{On} (V)	Ox _{On} (V)	HOMO (eV)	LUMO (eV)	Eg _{elec} (eV)	Eg _{Opt} (eV)
16^{tBu}	1.44	-0.92	-6.24	-3.88	2.4	2.3
16^{NAr}	0.38	-1.11	-5.18	-3.66	1.5	1.5
17^{tBu}	1.21	-1.09	-6.01	-3.71	2.3	2.4
17^{NAr}	0.33	N/A	-5.13	N/A	N/A	1.6

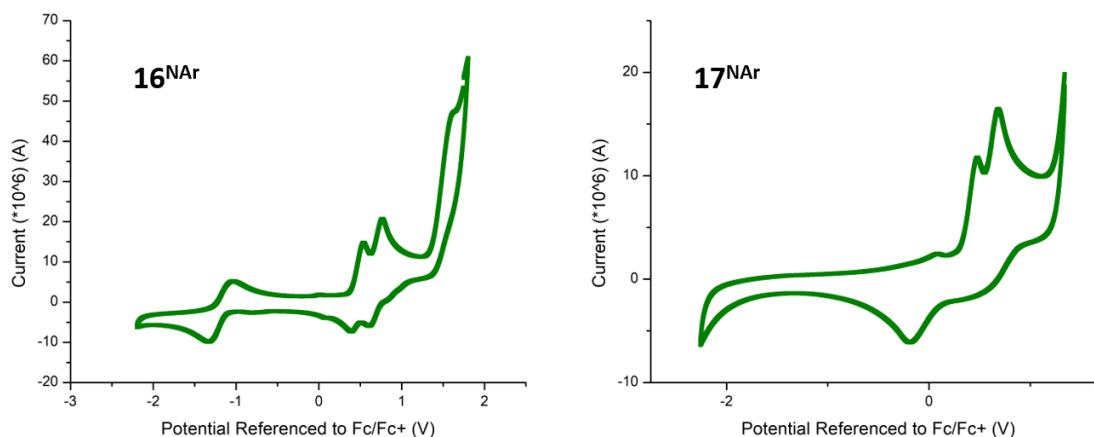


Figure 4-20. Cyclic Voltammograms of **16^{NAr}** (Left) and **17^{NAr}** (Right). CV are recorded in dichloromethane with a 0.1M nBu₄NPF₆ electrolyte.

Considering the appropriately placed frontier molecular orbitals we sought to test the efficacy of the arylated derivatives for their performances as non-fullerene acceptors in organic solar cells. After initial proof of concept devices were made, with PTB7-Th as the donor species and **16^R**/**17^R** as the accepting species in bulk heterojunction cells it was determined that the most promising compound was **16^{tBu}** so it was used for all further testing. One of the main criteria for good device performance is the effective matching of frontier energy levels of the donor and acceptor pair. Taking the values gained from cyclic voltammetry the HOMO/LUMO levels of both the PTB7-Th donor species along with **16^{tBu}** are shown in Figure 4-21.

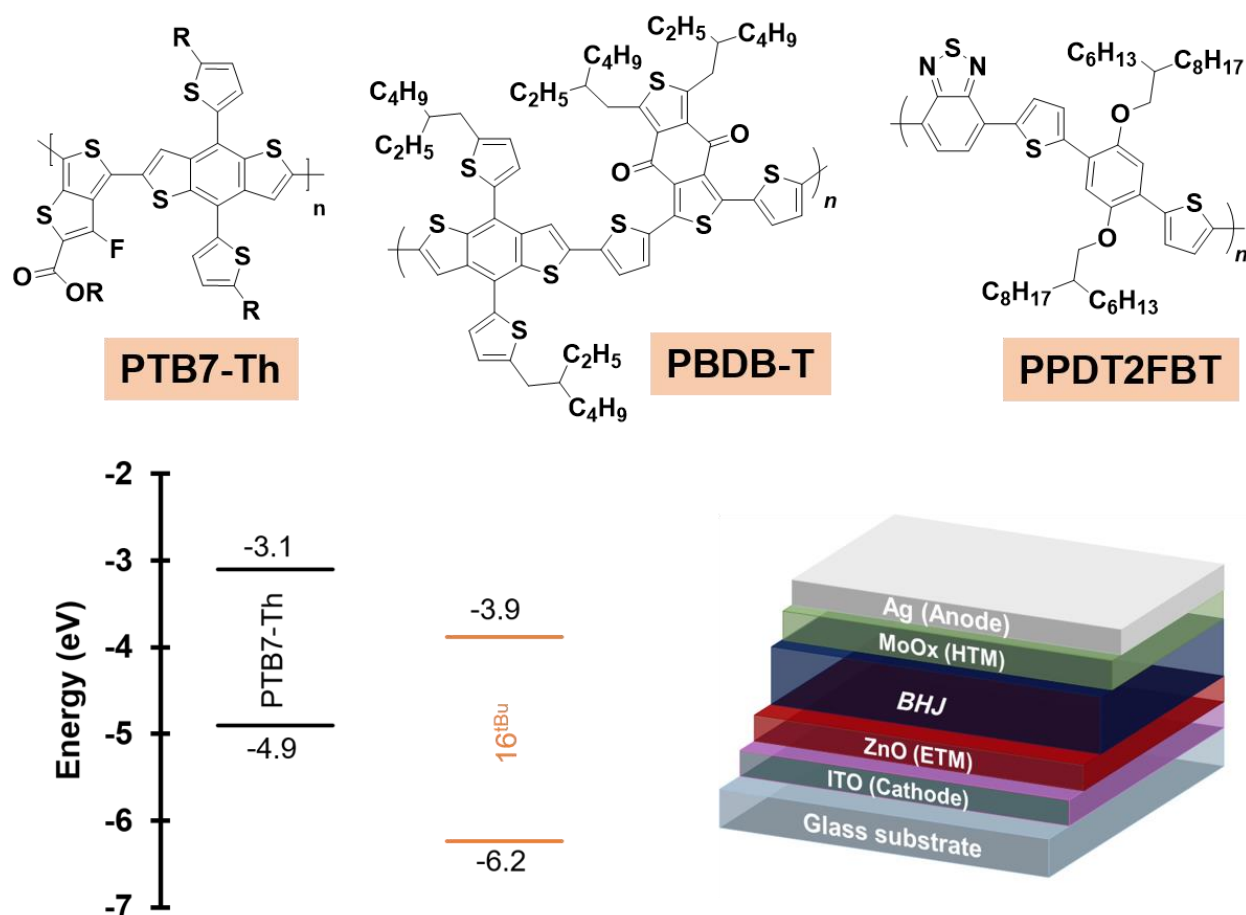


Figure 4-21. Top: Structures of the donor species utilized. Bottom Left: Frontier energy levels from CV of PTB7-Th and **16^{tBu}**. Bottom Right: Device architecture used the organic solar cells.

Since the LUMO of the donor is higher than the acceptor, and the HOMO of the acceptor, lower than the donor, the levels are aligned for proper device performance. While only the energy levels for PTB7-Th are shown, devices were made with a series of other donors, but as discussed later they all gave similar performances. The architecture of the solar cells made is presented in Figure 4-21, and follows the standard method for inverted bulk-heterojunction cells.¹⁸⁹⁻¹⁹¹ The films were made by processing the active layers from chlorobenzene in air. The device performances are summarized with the various donors in Table 4-3.

Table 4-3. Organic solar cell data of the PTB7-Th, PBDB-T, PPDT2FBT: **16^{tBu}**10 mg/mL blends (1:1) cast from chlorobenzene. Average values are given with the best results in obtained in brackets

Donor	V _{oc} (V)	J _{sc} (mA/cm ²)	FF (%)	PCE (%)
PTB7-Th	0.85 (0.89)	4.8 (5.6)	38 (40)	1.5 (2.0)
PBDB-T	0.85 (0.86)	2.7 (2.7)	38 (39)	0.9 (0.9)
PPDT2FBT	0.78 (0.78)	3.4 (3.6)	38 (39)	1.0 (1.1)

The three architectures tested resulted in working devices with good photodiode behavior. Interestingly the device performances remain quite constant across the donors tested, with the only variations really being in the short circuit currents (J_{sc}). Since the short-circuit voltage depends on the optical absorption profile of the bulk material, it makes sense that the different donors with different absorption profiles yield varying J_{sc} values with the same acceptor and the difference is evident when examining the film absorption profiles (Figure 4-22). There is a large variance in the devices tested since much of the absorption profile comes from the donor species, with the acceptor (**16^{tBu}**) enhancing primarily the higher energy area. The device performance is also shown in the current density-voltage (JV) curves of the devices (Figure 4-23).

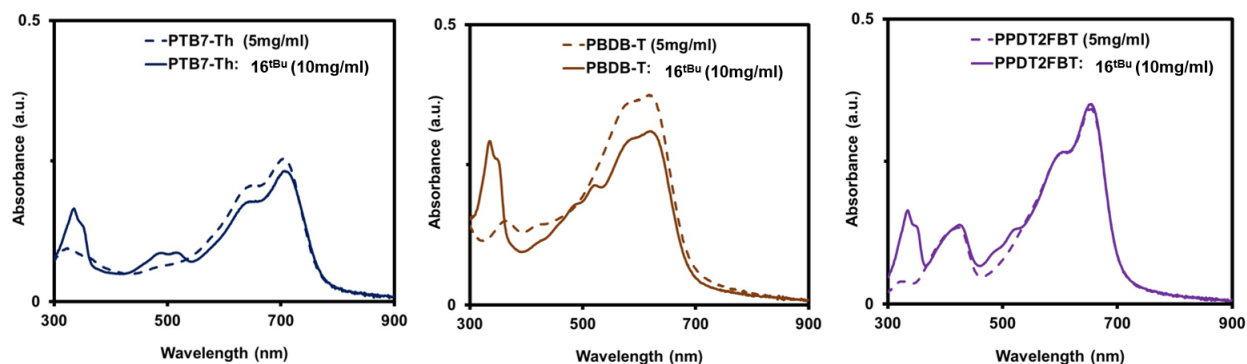


Figure 4-22. Optical absorption spectra 16^{tBu} based film cast from $\text{C}_6\text{H}_5\text{Cl}$.

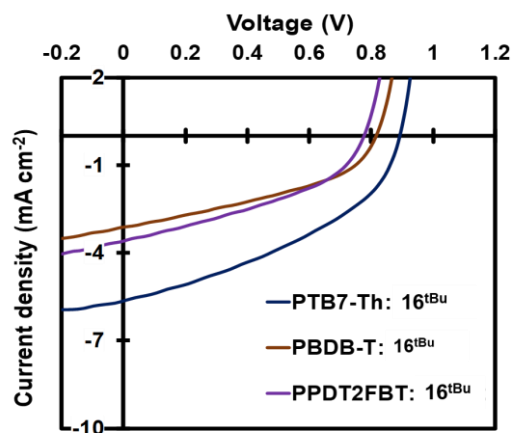


Figure 4-23. Current density-voltage curve of devices made from the donor species and 16^{tBu} .

Examination of the active layer surfaces using atomic force microscopy revealed uniform films with smooth surfaces and little phase separation (Figure 4-24). This prompted further optimization of the PTB7-Th: 16^{tBu} architecture. Unfortunately, despite thorough investigation into changing donor-acceptor ratios, using various annealing methods and additives none of these improved the PCE of the devices.

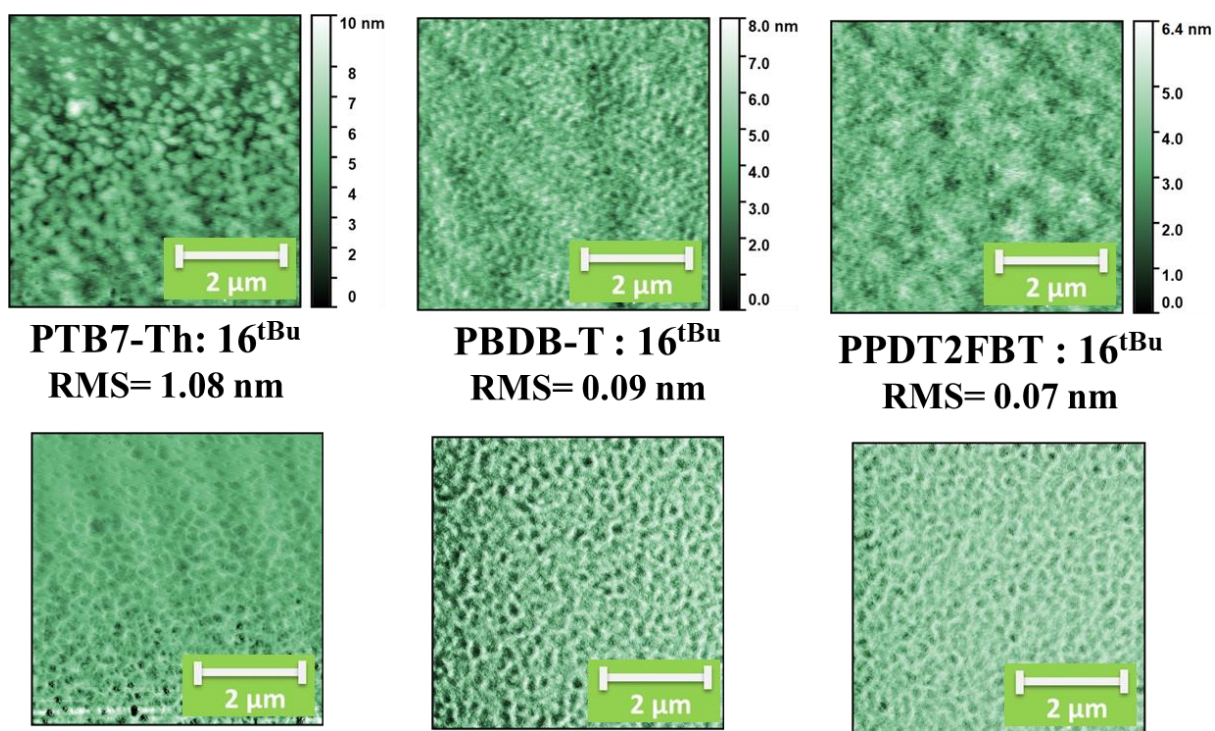


Figure 4-24. TOP = atomic force microscopy height images, BOTTOM = atomic force microscopy phase images. All films were spun-cast (1000 rpm) from C₆H₅Cl solutions at room temperature.

While PCEs are not spectacular, the fact that **16^{tBu}** performs consistently with a variety of donors lends evidence that it is a good starting point for the design of molecular non-fullerene acceptors. With the rapid advancements in the field of organic electronics it is feasible that tuning of the BN doped indenofluorene core could yield device performances competitive with other acceptors.

Conclusion

In conclusion, electrophilic borylation was utilized to synthesize a new family of B-N containing organic molecules. The synthetic pathway is versatile and allows for steric and

electronic properties to be readily tuned. In addition, several derivatives were tested as electron acceptors in organic solar cells and showed moderate performance results with PCEs up to 2%. While these device performances are not high enough for application, the synthetic pathway described should be able to yield a vast array of systems tailored for use in solar cells. Efforts towards higher performance derivatives are currently underway.

CHAPTER 5: CONCLUSIONS AND FUTURE WORK

5.1 Conclusion

Chapter two of this thesis detailed the development of a zirconocene mediated pathway for the synthesis of BN containing indene species. This synthetic pathway yielded a unique derivative of a boron-nitrogen doped indene in addition to the isolation of a BN substituted derivative of *s*-indacene. The indacene species was found to have drastically different aromaticity properties when compared to the all-carbon analogue, showing the large impact BN for CC substitution has on bonding within a molecule.

Chapter three investigated the chemistry of the BN-indene species synthesized in Chapter two. It was found that the reduced indenide species had interesting reactivity when treated with differing electrophiles. When the BN indenide was treated with carbon electrophiles, an S_N2 type reaction occurred where the boron atom acted as the nucleophile. When treated with CO_2 , the indenide species underwent a formal “2+2” addition with the formation of a four-member CCBO ring not previously observed in main group systems. The differing reactivity was examined computationally and the changes in aromaticity in the ring systems was a large driving force for the observed reactivity.

Chapter four strayed from the zirconocene mediated synthetic pathways and instead targeted a family of BN doped indenofluorene derivatives which were stable to ambient conditions. Due to the synthetic tuneability and overall stability of the molecules they could be tested as electron accepting units in organic solar cells, showing modest performances with a variety of donor molecules. These species represent a framework that can be expanded upon to yield much

higher device performances in the future through careful consideration of functional group appended.

Overall this thesis has provided a novel zirconocene mediated synthetic pathway to access BN doped aromatics and explored the photophysical properties and reactivity of the synthesized species. Using the knowledge gained from the indacene compound a family of easily synthesized BN doped indenofluorene derivatives were tested in organic solar cells. All the chemistry presented in this dissertation was made possible through the development of versatile, high yielding synthetic pathways.

5.2 Future Work

The work presented in this thesis has provided a platform for new chemistry to be developed in the field of boron-nitrogen containing polycyclic aromatic hydrocarbons. In the following sections, a research proposal building from these chemistries will be outlined.

5.2.1 Purpose-built electron acceptor units

The chemistry explored in Chapter four showed the ability of the BN indenofluorene core to be used as an electron accepting material in OSCs with a variety of donor species. While the device performances were poor at best, there is still great promise in the framework, as the molecules tested were not specifically designed to be used as molecular acceptor species. With a more thoughtful design, materials that are more active could be synthesized, and due to the versatility of the synthetic pathway should be easy to explore. The focus of the synthesized

indenofluorenes to date was on modifications of the electronic nature and to impart solubility such that characterization would be possible via traditional means. Now that proper synthetic pathways are in hand, focus can be placed on the addition of units known to yield good solid state-packing or to be active sub-units for organic solar cell performance. In many of the highest performing devices there are common end units that should be easily added to the BN-indenofluorene core. In fact, examining the best performing BN acceptor material (BNBP in Figure 5-1) to date there are many design ideas that could be adapted from this system.^{56, 57, 177, 192} As highlighted in the retrosynthetic analysis, the installation of strongly electron withdrawing 2-(3-oxo-2,3-dihydroindenylidene)malonitrile (INCN) groups should be possible by starting from commercially available reagents and following the electrophilic borylation conditions discussed previously.^{179,}

180, 193

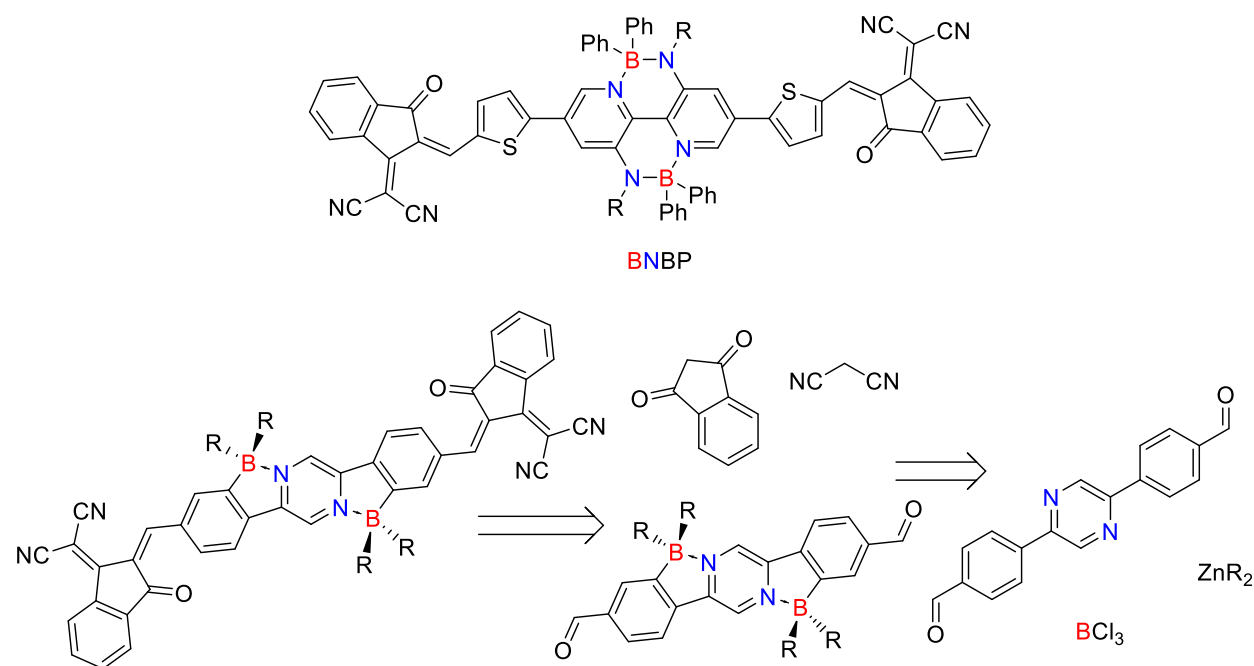
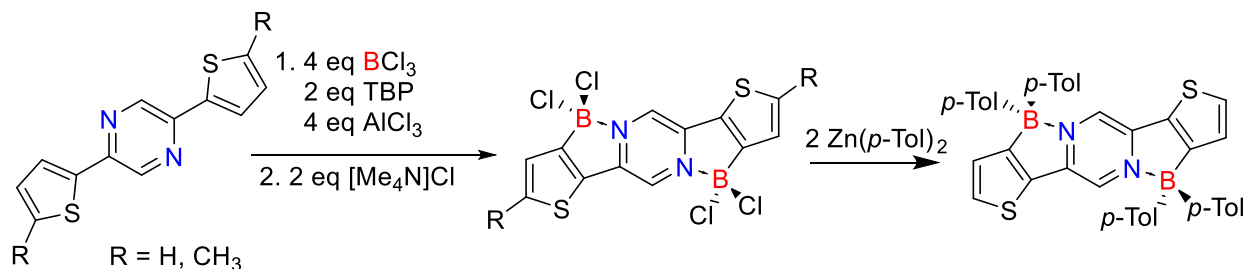


Figure 5-1. Top: example of best performing BN containing electron accepting species to date. Bottom, retrosynthetic approach for the synthesis of INCN functionalized BNindenofluorenes.

To date, we have only examined the use of diarylzinc reagents in installing functionality to the boron atoms, but branched alkyl substituents could be interesting as well. As they allow for efficient packing in the solid state.^{194, 195} Due to the accessibility of dialkylzinc reagents it should prove easy to iteratively design a good accepting material using concepts studied in depth in the top performing species.^{196, 197}

With material applications a clear possibility, another suitable direction for this chemistry is to move away from the tested indenofluorene core and examine other frameworks, such as the replacement of flanking phenyl groups with thiophene units (Scheme 5-1). Preliminary work into this has been undertaken in our lab and shows promise that interesting molecules could indeed be synthesized via this method. To date, two different pyrazines have been synthesized, the dithiophenepyrazine and the methyl substituted derivatives. Both allowed for facile borylation, but without the methyl substituents the species is completely insoluble in common organic solvents. Despite this low solubility it can be reacted with $\text{Zn}(p\text{-Tol})_2$ to yield the arylated species shown in Scheme 5-1.

Scheme 5-1. Synthetic pathway to thiophene containing BN containing derivatives.



Unlike the *tert*-butylaryl derivatives, the thiophene species shows fluorescence in solution even when the electron-rich tolyl groups are bound to boron, suggesting that the more electron donating thiophene units localize the HOMO on the planar core as opposed to the aryl groups on boron. These thiophene linkers allow for further derivatives to be targeted as significant work has been performed on functionalizing the 2-position of thiophene linkers in organic materials, and presents a good framework to build upon.¹⁹⁸ Once more of these compounds are synthesized it should be possible to tune the frontier orbital energies to allow for superior performances in organic solar cells.

5.2.2 Synthesis of other isomers of indenofluorene

In addition to the application focused proposal outlined above, through the expansion of the synthetic scope of the electrophilic borylation pathway we can further explore the fundamental bonding within BN aromatics. One of the key concepts within the field of BN doping of aromatic which has been mentioned throughout his thesis is the focus on orientation and location of BN bonds within the molecule. While the species discussed thus far are certainly of interest, there exist several other structural isomers of indenofluorene as shown in Figure 5-2. If one wants to target

BN substituted versions of these, an additional layer of complexity exists, as the five indenofluorene regioisomers need to be considered along with the dozens of possible orientations of BN bonds within the molecule. While the best studied isomer is indeno[1,2-*b*]fluorene, the groups of Haley,^{139, 199} Tobe¹⁰⁸ and others²⁰⁰⁻²⁰² have put extensive work into expanding the scope of regioisomers synthetically accessible, with the fifth and final primary isomer only recently being synthesized.²⁰³ The electronic structure of each regioisomer is different, possessing differing degrees of singlet vs triplet ground-state. Computational techniques based on these findings allowed for extended thiophene containing derivatives to be designed and targeted and some interesting triplet ground state species to be isolated.²⁰⁴

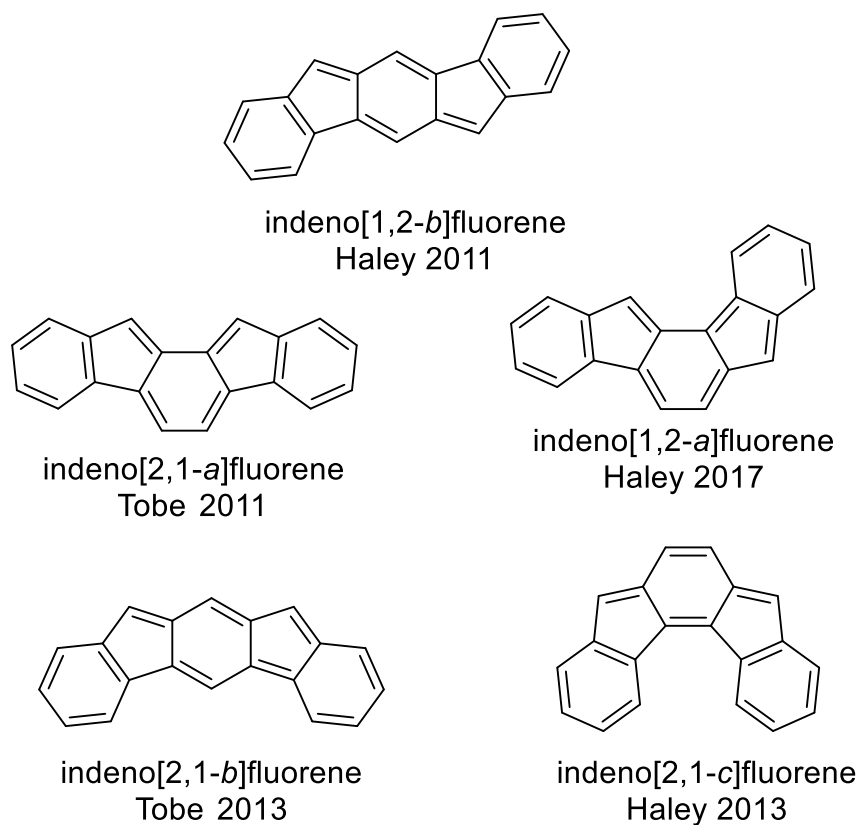
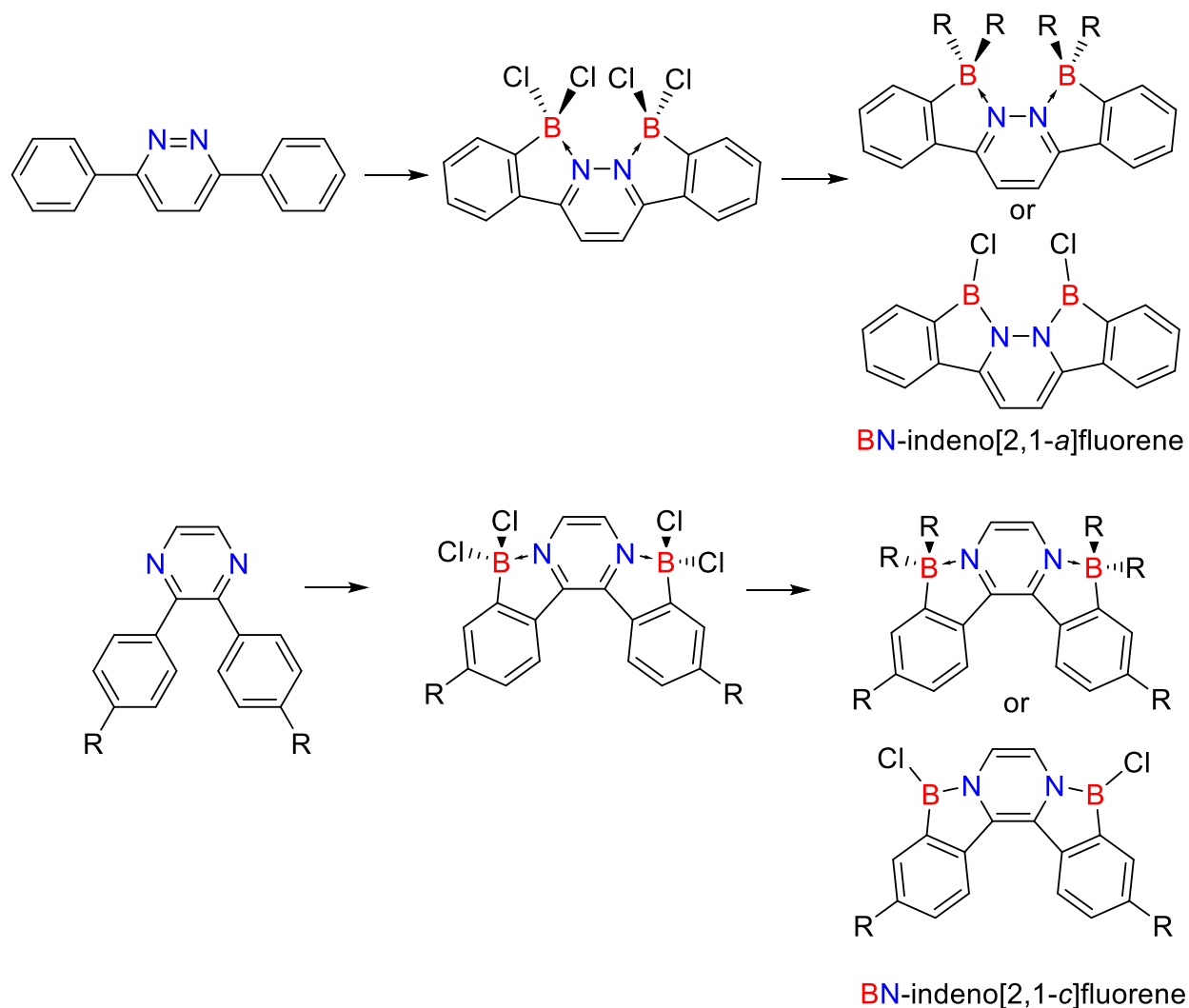


Figure 5-2. The five possible regioisomers of indenofluorene and the date they were synthesized.

While it may seem like a task akin to stamp-collecting, there is great utility in exploring BN doped derivatives of systems already isolated and characterized in the all-carbon forms. As described in a recent review on azaborine chemistry by Liu, the fundamental knowledge on bonding within these molecules has allowed for new synthetic methods, and new properties previously unexpected to be discovered.^{33, 205}

Scheme 5-2. Proposed synthetic pathway to access two new regioisomers of BN-indenofluorene, the [2,1-a] and [2,1-c] isomers.



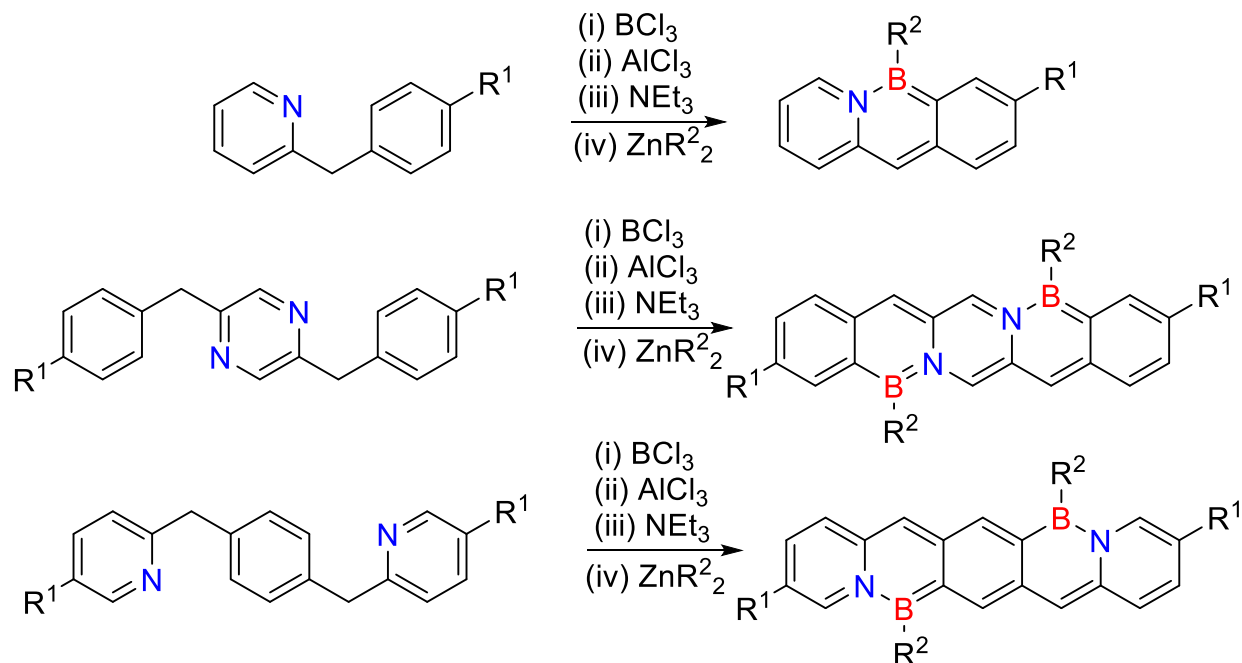
Following the electrophilic borylation techniques described, it should be easy to synthesize two other regioisomers of BN doped indenofluorene (Scheme 5-2). The synthesis for these derivatives starts from readily accessible diarylpyridazine or pyrazine species and should follow similar workup and functionalization procedures as the parent system in Chapter Four. The pathway will also be highly adaptable as changes can be easily made to the starting heteroaromatics to install electron rich/poor or solubilizing groups. A short-term possibility of this proposal is that one of the new isomers will be more amenable to the reduction chemistry attempted in Chapter four, which would allow for a good comparison to the planar all-carbon indenofluorene species. In addition to the fundamental interest, this project has the potential to yield even better electron accepting units for use in device applications.

5.2.3 Pentacene derivatives synthesized by electrophilic borylation

One of the most ubiquitous materials for organic device applications is pentacene. This is due to the extended pi system within the molecule which imparts exceptional photophysical and electrochemical properties.²⁰⁶ Due to its high charge transport capabilities it has found success when used in thin film transistors and organic solar cells as a p-type material.²⁰⁷ One downfall of pentacene is the relatively low stability when exposed to atmospheric conditions, which is usually overcome by attaching large groups to prevent oxidation or dimerization reactions. It would be interesting to examine boron-nitrogen doped derivatives of this to see if stability can be improved without the need for tremendous steric bulk. With the recent work by Liu on the synthesis of BN

anthracene shown in the top of Scheme 5-3, it should be possible to extend the chemistry to larger systems like pentacene.²⁰⁸

Scheme 5-3. Top: synthesis of BN anthracene by Liu.²⁰⁸ Bottom: proposed synthesis of two derivatives of BN doped pentacene.



The synthetic route should be amenable to changes in functionality on the flanking phenyl (middle Scheme 5-3) or pyridine (bottom of Scheme 5-3) to increase solubility or tune the electronics of the molecule. While not trivial to synthesize there is precedent for the synthesis of both the dibenzylpyrazine and bispyridine starting materials. These molecules can also be easily functionalized at the boron centre using the same diarylzinc reagents discussed previously.

The research projects described within this chapter would complement the work described in this dissertation. The versatility of the synthetic methods examined in this thesis have tremendous possibilities in the synthesis of molecules of fundamental and application-based

research. Furthermore, through the examination of novel aromatics, properties that are wholly unexpected may be discovered and improve our knowledge of bonding in boron-based materials.

CHAPTER 6 EXPERIMENTAL DETAILS

6.1 General Considerations

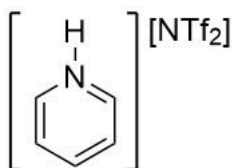
Storage and manipulation of all compounds were performed under an argon atmosphere either in a VAC glove box or using a double manifold high vacuum line using standard techniques. Passage of argon through an OxisorBW scrubber (Matheson Gas Products) removed any residual oxygen and moisture. Toluene and tetrahydrofuran were dried and purified using a Grubbs/Dow solvent purification system and stored in 500 mL thick-walled glass pressure flasks over sodium/benzophenone ketal. *n*-Pentane was purified using a M-Braun solvent purification system, dried over sodium/benzophenone ketal and stored in a 100 mL thick-walled glass pressure flask. Benzene-*d*₆ was dried over sodium/benzophenone ketal and stored in a 100 mL thick-walled glass pressure flask. Dichloromethane and chlorobenzene were stored in the same manner except dried over calcium dihydride instead of sodium/benzophenone ketal. Dichloromethane-*d*₂ was dried over CaH₂ and stored in a 50 mL thick-walled glass pressure flask. All dried solvents were degassed and vacuum distilled prior to use. bis(4-*t*Butylphenyl)aminophenylboronic acid,²⁰⁹ KC₈,²¹⁰ Zn(*p*-Tol)₂,²¹¹ Zn(C₆F₃H₂)₂²¹¹ were prepared according to literature procedures and all other chemicals were acquired from commercial sources. ¹H and ¹³C NMR chemical shifts were referenced to residual solvent protons and naturally abundant ¹³C resonances for all deuterated solvents. Chemical shift assignments are based on ¹H, ¹¹B, ¹³C{¹H}, ¹H-¹H-COSY, ¹H-¹³C-HSQC and ¹H-¹³C-HMBC NMR experiments performed on Avance III 400, Ascend-500, or Avance-600 MHz spectrometers. X-ray crystallographic analyses were performed on a Bruker system equipped

with a Bruker Apex-II CCD using samples coated in Paratone 8277 oil (Exxon) and mounted on a glass fibre.

UV-Vis spectra were obtained on a Varian Carey 5000 UV-Vis-NIR spectrophotometer operating in single-beam mode. Fluorescence spectra were obtained on a Horiba Jobin Yvon FluoroMax-4. Infrared spectra were obtained on a Nicolet Avatar IR spectrophotometer. Calculations were conducted using the Gaussian 09 program. Whenever possible input geometries were derived from X-ray data in the form of .pdb files. Building or modification of input files was conducted on Gauss View. All structures were optimized until frequency calculations gave only positive values and then used for TD-DFT and NICS calculations. Elemental analyses were performed by staff at the Instrumentation Facility in the Department of Chemistry, University of Calgary

6.2 Experimental Details for Chapter 2

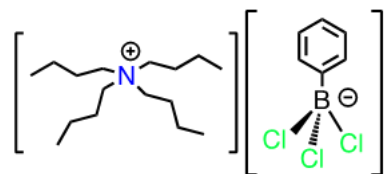
Synthesis of Pyridinium Triflamide:



Was prepared as previously reported by Montavon et al. in the literature.¹¹⁵ A swivel frit with a 100 mL two-neck round bottom flask was charged with N,N-bis(trifluoromethanesulfonyl)imide (1.02g, 3.6mmol), dichloromethane (20ml), and a Teflon stirbar. A solution of pyridine (0.29ml, 3.6mmol) in dichloromethane (2 ml) was then added drop-wise using a syringe under a flow of argon with stirring. The solution was stirred for 45 min., yielding a faintly pink-colorless solution.

Hexanes (20 ml) was then vacuum transferred into the flask producing a white precipitate. The solid was then filtered and washed using the swivel frit apparatus. The solvent was then removed *in vacuo*, and the solid washed again with additional hexanes (20ml). The white crystalline product was then dried under vacuum with a yield of 95% (1.241g, 3.4mmol). NMR spectra were matched to previous literature and the product used without further purification. ^1H NMR (500 MHz, THF- d_8) δ 14.67 (s, 1H, NH), 8.96 – 8.86 (m, 2H, o-CH), 8.69 (tt, J = 7.9, 1.6 Hz, 1H, p-CH), 8.20 – 8.10 (m, 2H, m-CH). ^{13}C NMR (126 MHz, Methylene Chloride- d_2) δ 148.10 (p-CH), 141.75 (o-CH), 128.34 (m-CH), 120.05 (q, J = 320.6 Hz, -CF $_3$). ^{19}F NMR (471 MHz, THF- d_8) δ -81.06 .

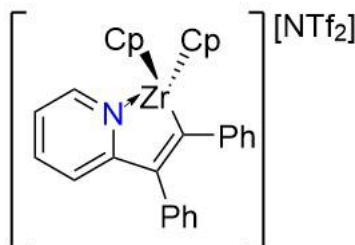
Synthesis of tetrabutylammonium trichlorophenylborate:



Was prepared similarly to that which was reported by Sheikh.²¹² A 100ml round bottom flask was charged with [nBu $_4$ N][Cl] (1.000g, 3.60mmol), PhBCl $_2$ (0.571g, 3.60mmol), dichloromethane (20ml), and a Teflon stirbar, and stirred for 16h at room temperature. Pentane (~20ml) was then vacuum transferred into the flask, and stirred for 5 min. The solvent was then removed *in vacuo*, yielding the product as a white powder (1.540g, 3.53mmol, 98%). NMR spectra were matched to previous literature and the product used without further purification. ^1H NMR (500 MHz, Methylene Chloride- d_2) δ 7.75 (d, J = 7.0 Hz, 2H, *ortho* Ar-**H**), 7.21 (t, J = 7.6 Hz, 2H, *meta* Ar-**H**), 7.13 (t, J = 7.3 Hz, 1H, *para* Ar-**H**), 3.07 – 2.95 (m, 8H, N-CH $_2$ -CH $_2$ -CH $_2$ -CH $_3$), 1.59 – 1.47 (m, 8H, N-CH $_2$ -CH $_2$ -CH $_2$ -CH $_3$), 1.38 (h, J = 7.3 Hz, 8H, N-CH $_2$ -CH $_2$ -CH $_2$ -CH $_3$), 0.99 (t, J = 7.3 Hz, 12H, N-CH $_2$ -CH $_2$ -CH $_2$ -CH $_3$). ^{13}C NMR (126 MHz, Methylene Chloride- d_2) δ 131.89 (*ortho*

C-H), 126.96 (*meta* C-H), 126.29 (*para* C-H), 58.94 (N-CH₂-CH₂-CH₂-CH₃), 24.13 (N-CH₂-CH₂-CH₂-CH₃), 19.92 (N-CH₂-CH₂-CH₂-CH₃), 13.72 (N-CH₂-CH₂-CH₂-CH₃). ¹¹B NMR (161 MHz, Methylene Chloride-*d*₂) δ 10.27 (br s).

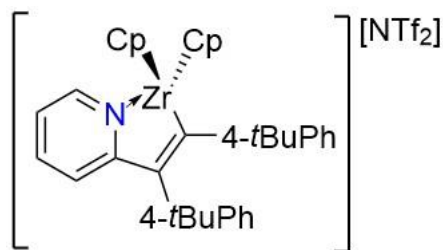
Synthesis of 2^H•NTf₂.



A 100ml round bottom flask was charged with pyridinium triflamide (2.545g, 7.06mmol), dimethylzirconocene (1.776g, 7.06mmol), PhCl (25ml), and a Teflon stirbar, immediately producing a yellow solution with effervescence. The flask was then attached to a reflux condenser apparatus under flow of argon creating an open system to accommodate the loss of methane, and stirred for 1.5h. The mixture was then heated at 80°C for 24h yielding an amber colored solution. A slight excess of diphenylacetylene (1.385g, 7.77mmol) was then added and the mixture heated at 110°C for 24h producing an orange solution. Pentane (25ml) was then vacuum transferred into the flask with stirring producing an orange precipitate, and the supernatant decanted off via cannula transfer. The solid was then washed with pentane again (2x15ml), after which it was dried *in vacuo*, yielding the product 2^H•NTf₂ as an orange solid (4.549g, 6.00mmol, 85%). Crystals suitable for X-ray were grown from a solution of 2^H•NTf₂ dissolved in PhCl and layered with pentane at -35°C. ¹H NMR (500 MHz, Toluene-*d*₈) δ 8.53 (ddd, *J* = 5.9, 1.7, 0.8 Hz, 1H, Py-**H**), 7.07 – 7.02 (m, 2H, Ar-**H**), 6.96 – 6.90 (m, 3H, Ar-**H**), 6.87 (ddd, *J* = 8.1, 7.4, 1.7 Hz, 1H, Py-**H**), 6.85 – 6.82 (m, 2H, Ar-**H**), 6.78 – 6.71 (m, 2H, Py-**H** & 1x Ar-**H**), 6.70 (ddd, *J* = 8.1, 1.5, 0.8 Hz, 1H, Py-**H**), 6.68 –

6.64 (m, 2H, Ar-**H**), 6.01 (s, 10H, 2xCp). ^{13}C NMR (126 MHz, Toluene- d_8) δ 211.61 , 164.38 , 150.13 (C-H_a) , 149.60 , 141.92 , 140.84 (C-H_c) , 139.70 , 130.50 , 128.47 , 128.01 , 126.97 , 125.94 , 124.84 , 123.68 , 120.85 , 120.53 (q, J = 321.5 Hz, -CF₃) , 114.63 (2xCp) . ^{19}F NMR (471 MHz, Toluene- d_8) δ -79.31. Elemental analysis calculated for C₃₁H₂₄F₆N₂O₄S₂Zr (%):C, 49.13; H, 3.19; N, 3.70. Found: C, 48.77; H, 3.52; N, 3.69.

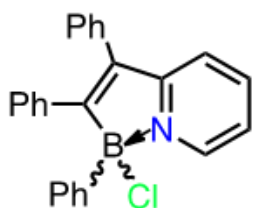
Synthesis of **2^{tBu}•NTf₂**.



A 100ml thick walled glass vessel was charged with pyridinium triflamide (143mg, 0.40mmol) and dimethylzirconocene (100mg, 0.40mmol), PhCl (25ml), and a Teflon stirbar, immediately producing a yellow solution with effervescence. The headspace of the vessel was evacuated, and stirred for 1.5h. The headspace was evacuated a second time, and the mixture was heated at 80°C for 24h yielding a colorless solution. A slight excess of 1,2-bis(4-(tert-butyl)phenyl)ethyne (131mg, 0.45mmol) was then added and the mixture heated at 110°C for 21h producing a red solution. The mixture was then transferred to a 50ml two-necked round bottom flask, to which pentane (25ml) was vacuum transferred, producing an orange precipitate. The supernatant was decanted off via cannula transfer, and the solid washed with additional pentane (2x10ml). The solid was then dried *in vacuo*, yielding the product **2^{tBu}•NTf₂** as an orange solid (201mg, 0.23mmol, 58%). ^1H NMR (500 MHz, Toluene- d_8) δ 8.65 (dt, J = 5.6, 1.2 Hz, 1H), 7.17 – 7.11 (m, 2H), 6.99 (d, J = 8.4 Hz, 2H), 6.82 (d, J = 8.2 Hz, 2H), 6.81 – 6.77 (m, 2H), 6.71 – 6.64 (m,

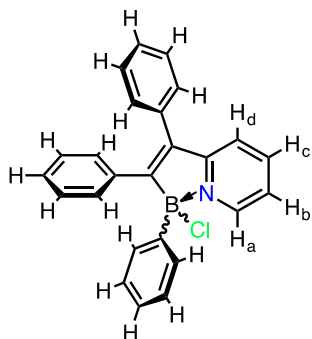
3H), 5.97 (s, 10H), 1.19 (s, 9H), 1.15 (s, 9H). ^{13}C NMR (126 MHz, Toluene- d_8) δ 212.20, 165.09, 150.53, 149.42, 147.73, 147.29, 142.07, 140.57, 130.33, 128.24, 125.98, 125.16, 123.56, 120.56, 120.37 (q, $J=321$ Hz, $-\text{CF}_3$), 114.08, 34.48, 34.24, 31.34, 31.32. ^{19}F NMR (471 MHz, Toluene- d_8) δ -79.28. Elemental analysis calculated for $\text{C}_{39}\text{H}_{40}\text{F}_6\text{N}_2\text{O}_4\text{S}_2\text{Zr}$ (%): C, 53.84; H, 4.63; N, 3.22. Found: C, 53.55; H, 4.52; N, 3.28.

Synthesis of 4^{H} :

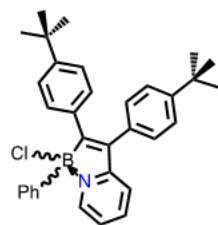


A 50ml round bottom flask was charged with $2^{\text{H}}\cdot\text{NTf}_2$ (248mg, 0.33mmol), $[\text{nBu}_4\text{N}][\text{PhBCl}_3]$ (144mg, 0.33mmol), dichloromethane (15ml), and a Teflon stirbar, producing an orange solution. The mixture was stirred for 16h producing a yellow solution. The mixture was then run through a silica/dichloromethane plug under atmospheric conditions, where a faint yellow band passed through and was collected. The solvent of the collected solution was then removed *in vacuo*, yielding the product as a yellow powder (99mg, 0.26mmol, 79%). Crystals suitable for X-ray were grown from a solution of 4^{H} dissolved in dichloromethane and layered with pentane at -35°C . ^1H NMR (500 MHz, Methylene Chloride- d_2 , 295K) δ 8.36 (dt, $J = 5.7, 1.2$ Hz, 1H H_a), 7.95 (td, $J = 7.9, 1.5$ Hz, 1H H_c), 7.58 – 7.50 (m, 2H, Ar-H), 7.52 – 7.44 (m, 2H, Ar-H), 7.47 – 7.39 (m, 1H, Ar-H), 7.42 – 7.35 (m, 3H, $\text{H}_d + 2x$ Ar-H), 7.31 (ddd, $J = 7.2, 5.7, 1.2$ Hz, 1H, H_b), 7.30 – 7.17 (m, 5H, Ar-H), 7.15 – 7.04 (m, 3H, Ar-H). ^{13}C NMR (126 MHz, Methylene Chloride- d_2) δ 168.76, 160.47, 144.60, 143.44 (C- H_a), 142.98 (C- H_c), 138.06, 135.77, 135.24, 132.27, 130.13,

129.95 , 129.50 , 128.37 , 128.04 , 127.99 , 127.82 , 127.39 , 121.80 (C-H_b) , 119.69 (C-H_d). ¹¹B NMR (128 MHz, Methylene Chloride-*d*₂) δ 5.79 (br s). Elemental analysis of C₂₅H₁₉BClN Calcd. (%): C, 79.08; H, 5.04; N, 3.69. Found: C, 78.88; H, 5.13; N, 3.56.

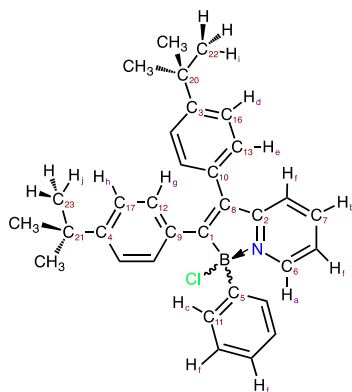


Synthesis of (E)-2-(2-(chloro(phenyl)boryl)-1,2-bis(4-(tert-butyl)phenyl)vinyl)pyridine 4^{tBu} :

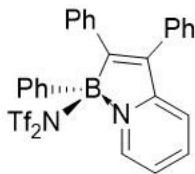


A 50ml round bottom flask was charged with **4^{tBu}** (100mg, 0.12mmol), [nBu₄N][PhBCl₃] (50mg, 0.12mmol) and dichloromethane (15ml) producing an orange solution. The mixture was stirred for 41h producing a yellow/green solution. The mixture was then run through a silica/dichloromethane plug under atmospheric conditions, where a faint yellow/green band passed through and was collected. The solvent of the collected solution was then removed *in vacuo*, yielding the product as a yellow/green powder (43mg, 0.09mmol, 77%). ¹H NMR (500 MHz, Methylene Chloride-*d*₂) δ 8.30 (ddd, *J* = 5.8, 1.5, 0.9 Hz, 1H, H_a), 7.91 (ddd, *J* = 8.2, 7.4, 1.6 Hz, 1H, H_b), 7.56 (dt, *J* = 6.8, 1.5 Hz, 2H, H_c), 7.55 – 7.51 (m, 2H, H_d), 7.35 – 7.30 (m, 2H, H_e), 7.30 – 7.22 (m, 5H, H_f), 7.22 – 7.19 (m, 2H, H_g), 7.13 – 7.08 (m, 2H, H_h), 1.40 (s, 9H, H_i), 1.21 (s, 9H, H_j). ¹³C NMR (126 MHz,

Methylene Chloride- d_2) δ 167.38 (C₁), 161.09 (C₂), 151.49 (C₃), 151.17 (C₄), 145.19 (C₅), 143.14 (C₆), 142.76 (C₇), 135.17 (C₈), 134.72 (C₉), 132.71 (C₁₀), 132.23 (C₁₁), 130.15 (C₁₂), 129.63 (C₁₃), 128.06, 127.35, 126.59 (C₁₆), 124.99 (C₁₇), 121.40, 119.65, 35.02 (C₂₀), 34.79 (C₂₁), 31.51 (C₂₂), 31.25 (C₂₃). ¹¹B NMR (161 MHz, Methylene Chloride- d_2) δ 6.32. HRMS (EI-TOF) m/z : [M +] Calcd for C₃₃H₃₅B³⁵ClN 491.2551; Found 491.2557. [M +] Calcd for C₃₃H₃₅B³⁷ClN 493.2522; Found 493.2569.



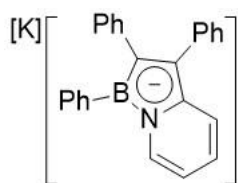
Synthesis of 5^H:



Chloroborane **4^H** (50 mg, 0.132 mmol) was taken up in 5 mL of CH₂Cl₂, and to this a solution of TMSNTf₂ (47 mg, 0.132 mmol) in CH₂Cl₂ was added dropwise. As the solution of TMSNTf₂ was added the solution turned from a pale yellow colour to a darker yellow colour. The reaction was stirred for 30 minutes at room temperature at which point volatiles were removed under vacuum, and pentane (30 mL) was added to the remaining solid. This suspension was then filtered in a swivel-frit apparatus yielding a pale yellow solid, compound **5^H** (55mg, 0.088 mmol, 67%). ¹H

NMR (500 MHz, Methylene Chloride-d₂) δ 8.29 (d, J = 5.7 Hz, 1H), 8.13 (td, J = 7.9, 1.5 Hz, 1H), 7.57 – 7.49 (m, 2H), 7.48 – 7.42 (m, 7H), 7.39 – 7.34 (m, 3H), 7.18 – 7.05 (m, 5H). ¹³C NMR (126 MHz, CD₂Cl₂) δ 160.23, 159.03, 144.29, 142.34, 139.60, 138.47, 135.43, 133.26, 131.78, 130.14, 129.23, 128.87, 128.73, 128.18, 127.93, 127.76, 127.53, 127.17, 121.78 (q, -CF₃), 119.71. *note: one Carbon from the NTF₂ anion is not visible due to high coupling and crowding in the aromatic region.* ¹⁹F NMR (471 MHz, CD₂Cl₂) δ -79.02 (Br). ¹¹B NMR (161 MHz, CD₂Cl₂) δ 10.96. Elemental analysis calculated for C₂₇H₁₉BF₆N₂O₄S₂: C 51.94%, H 3.07%, N 4.49%, found C 51.38%, H 3.22%, N 4.39%. While the C% is slightly outside the allowable limit for analytical purity, these values are provided to illustrate the best values obtained to date.

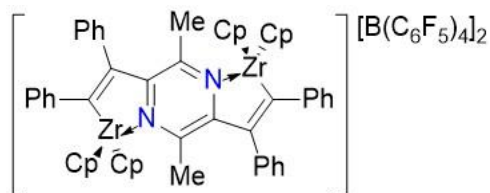
Synthesis of **6^H**:



To a solution of chloroborane **4^H** (150 mg, 0.395 mmol) in THF (10 mL), solid KC₈ (107 mg, 0.790 mmol) was added, causing the pale yellow solution to turn a dark orange colour with the simultaneous formation of black graphite precipitate. This solution was stirred for 5 minutes then filtered through a swivel frit apparatus. After volatiles were removed under vacuum, benzene (10mL) was added, yielding an orange solid with a dark orange supernatant, which was filtered through the swivel-frit apparatus. The solid was washed several times with pentane (10 ml) and dried under vacuum yielding a bright orange solid **6^H** (60 mg, 0.156 mmol, 39%). Crystals suitable for X-ray Diffraction were acquired through the addition of 0.16 mmol of 2,2,2-cryptand to a THF solution of **6^H**, yielding single crystals at room temperature after one hour. ¹H NMR (500 MHz,

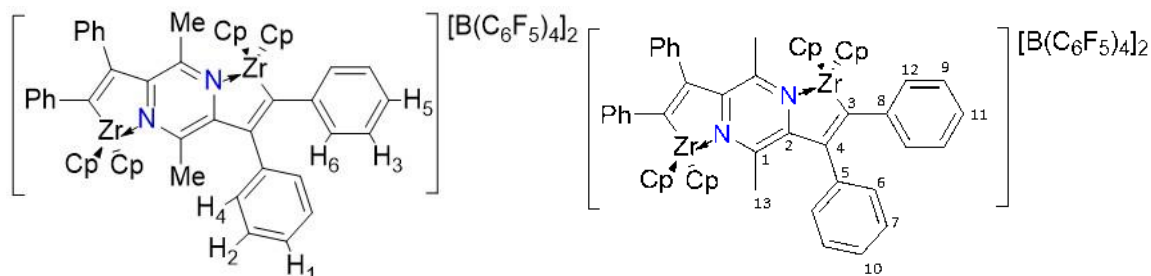
THF- d_8) δ 7.77 (dd, $J = 7.0, 1.3$ Hz, 1H, **Py-H**), 7.59 – 7.51 (m, 2H), 7.23 – 7.16 (m, 2H), 7.15 – 7.04 (m, 5H, 1 **Py-H**), 7.04 – 6.95 (m, 3H), 6.94 – 6.87 (m, 1H), 6.78 (t, $J = 7.7$ Hz, 2H), 6.60 – 6.52 (m, 1H), 5.67 (ddd, $J = 8.8, 5.9, 1.2$ Hz, 1H, **Py-H**), 5.59 (ddd, $J = 7.1, 5.7, 1.4$ Hz, 1H, **Py-H**). ^{13}C NMR (126 MHz, THF) *note: carbons attached to boron not visible in NMR spectra* δ 147.09, 142.19, 134.80, 131.16, 130.71, 128.01, 127.67, 127.58, 127.47, 127.11, 124.49, 122.83, 119.91, 118.97, 117.24, 108.73, 106.36. Elemental analysis calculated for $\text{C}_{25}\text{H}_{19}\text{BKN}$ C 78.33%, H 5.00%, N 3.65%, found C 78.45%, H 4.68%, N 3.34%.

Synthesis of **7^H**:

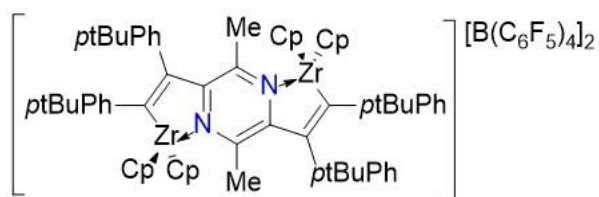


A solution of $\text{Ph}_3\text{CB}(\text{C}_6\text{F}_5)_4$ (1.10 g, 1.20 mmol) in PhCl (5.0 mL) was added drop-wise to a solution of dimethyl zirconocene (300 mg, 1.20 mmol) in PhCl (5.0mL) while stirring under an argon atmosphere on a swivel-frit apparatus. 2,5-dimethylpyrazine (65 mg, 0.60 mmol) in PhCl (1.0 mL) was then added drop-wise to the reaction mixture with stirring, turning the solution from a dark brown colour to a pale yellow and causing a yellow solid to precipitate, which was stirred at room temperature for one hour. To this suspension, diphenylacetylene (214 mg, 1.20 mmol) in PhCl (5.0 mL) was added and the reaction was heated at 80 C for 12 hours yielding a purple solution that upon cooling to room temperature precipitated a dark purple solid which was then filtered and rinsed several times with pentane (25 mL) to yield compound **7^H** as a dark purple solid (1.28 g, 0.57 mmol, 95%). Crystals suitable for X-ray diffraction analysis were grown through slow diffusion of pentane into a concentrated chlorobenzene solution of compound **7^H**. ^1H NMR

(500 MHz, THF-d₈) δ 7.27 (d, J = 1.7 Hz, 2H, H₁), 7.26 (d, J = 2.1 Hz, 4H, H₂), 7.15 (dd, J = 8.2, 7.4 Hz, 4H, H₃), 7.08 – 7.03 (m, 4H, H₄), 7.02 – 6.95 (m, 2H, H₅), 6.85 (dd, J = 8.2, 1.3 Hz, 4H, H₆), 6.69 (s, 20H, Cp-H), 0.95 (s, 6H, Me-H). ¹³C NMR (126 MHz, THF-d₈) δ 151.55 (C1), 149.15(C2), 148.88 (dm, B(C₆F₅)₄), 145.70 (C3), 138.87 (dm, B(C₆F₅)₄), 138.59 (C4), 138.43 (C5), 136.78 (dm, B(C₆F₅)₄), 130.65 (C6), 129.51 (C7), 128.98 (C8), 128.89 (C9), 128.84 (C10), 126.50 (C11), 125.83 (C12), 124.90 (m, B(C₆F₅)₄), 117.52 (Cp), 22.72 (Me). Elemental analysis calculated for C₁₀₂H₄₆B₂F₄₀N₂Zr₂ C 54.12%, H 2.05%, N 1.24%, found C 53.79%, H 1.92%, N 1.19%.



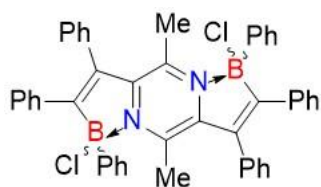
Synthesis of 7^{tBu}:



A solution of Ph₃CB(C₆F₅)₄ (2.121 g, 2.30 mmol) in PhCl (5.0 mL) was added drop-wise to a solution of dimethyl zirconocene (575 mg, 2.30 mmol) in PhCl (20 mL) with stirring under an argon atmosphere on a swivel-frit apparatus. 2,5-dimethylpyrazine (125 mg, 1.15 mmol) in PhCl (1.0 mL) was then added drop-wise to the reaction mixture with stirring, turning the solution from a dark brown colour to pale yellow and causing a yellow solid to precipitate. To this suspension,

di(*p*-tBuphenyl)acetylene (700 mg, 2.41 mmol) in PhCl (10 mL) was added and the reaction was heated at 80 C for 12 hours yielding a purple solution that upon cooling precipitated a dark purple solid which was then filtered and rinsed several times with pentane (25 mL) to yield compound **7^{tBu}** as a dark purple solid (1.75 g, 0.74 mmol, 64%). ¹H NMR (500 MHz, THF-d₈) δ 7.26 (d, *J* = 8.4 Hz, 4H), 7.16 (d, *J* = 8.5 Hz, 4H), 6.92 (d, *J* = 8.4 Hz, 4H), 6.72 (d, *J* = 8.4 Hz, 4H), 6.68 (s, 20H, Cp), 1.23 (s, 18H), 1.20 (s, 18H), 1.09 (s, 6H). ¹³C NMR (126 MHz, THF) δ 152.17, 151.35, 149.54, 149.19, 148.87 (dm, B(C₆F₅)₄), 143.00, 138.86 (dm, B(C₆F₅)₄), 138.76, 136.81 (dm, B(C₆F₅)₄), 135.90, 130.33, 125.99, 125.84, 125.41, 124.82 (m, B(C₆F₅)₄), 117.28, 35.02, 34.71, 31.23, 31.21, 23.10. ¹⁹F NMR (471 MHz, THF-d₈) δ -132.97 – -134.53 (m), -165.54 (t, *J* = 20.3 Hz), -169.13 (t, *J* = 19.1 Hz). Elemental analysis: calculated for C₁₁₈H₇₈B₂F₄₀N₂Zr: C 56.97%, H 3.16%, N 1.13%, Found: C 56.60%, H 3.22%, N 1.15%.

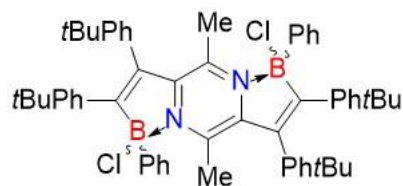
Synthesis of **8^H**:



A 100 mL round bottom flask was charged with Zirconocene **7^H** (1.00 g, 0.423 mmol) and [nBu₄N][PhBCl₃] (0.370 g, 0.846 mmol). Under an argon atmosphere this was attached to a reflux condenser and 50 mL of DCM was vacuum transferred at -78 C, allowed to warm to room temperature, and stirred for 2 hours. Upon addition of dichloromethane and subsequent warming to room temperature, the dark purple solution turned a pale yellow colour. The reaction was then heated at 50 C for 12 hours, during which the mixture turned a fluorescent pink colour. The product was then be purified by silica gel chromatography using DCM:Hex (3:5), where a pink fraction

was collected containing both the *cis* and *trans* isomers in a roughly 50:50 ratio, with a yield of 180 mg (60%). It was then possible to isolate near pure samples of each isomer through selective recrystallization. Crystals of mostly the *trans* isomer were grown through slow diffusion of hexanes (12mL) into a solution of the isomers (100 mg) in DCM (8 mL). While mostly one isomer was crystallized it proved impossible in our hands to isolate completely pure *trans*. When the supernatant of the recrystallization was placed in the -35 C freezer for 4 days single crystals of approx. 98% of the *cis* isomer were formed. NMR data for only the *cis* isomer is listed, but ^1H spectra of the mixture is also given. ^1H NMR (500 MHz, Methylene Chloride- d_2) δ 7.49 – 7.41 (m, 8H), 7.41 – 7.37 (m, 2H), 7.33 (td, J = 7.5, 1.6 Hz, 2H), 7.32 – 7.25 (m, 4H), 7.23 (t, J = 7.7 Hz, 2H), 7.10 – 7.04 (m, 2H), 7.03 (dd, J = 7.1, 1.5 Hz, 2H), 6.97 (td, J = 7.6, 1.7 Hz, 4H), 6.81 – 6.74 (m, 4H), 2.16 (s, 6H). ^{13}C NMR (126 MHz, CD_2Cl_2) δ 175.23 (br), 151.07, 147.19, 138.47 (br), 136.77, 134.86, 133.58, 131.02, 129.55, 129.46, 128.28, 128.02, 127.70, 127.56, 126.84, 126.76, 19.21. Elemental analysis of mixture of two isomers, calculated for $\text{C}_{46}\text{H}_{36}\text{B}_2\text{Cl}_2\text{N}_2$ C 77.89%, H 5.12%, N 3.95%, found: C 78.00%, H 5.42%, N 3.93%.

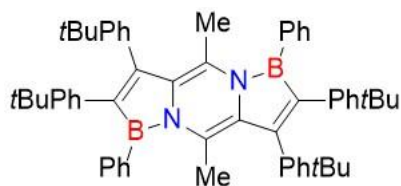
Synthesis of 8^{tBu} :



A 100 mL round bottom flask was charged with Zirconocene 7^{tBu} (1.75 g, 0.740 mmol) and $[\text{nBu}_4\text{N}][\text{PhBCl}_3]$ (0.647 g, 1.40 mmol). Under an inert atmosphere this was attached to a reflux condenser and 50 mL of DCM was added at -78 C, allowed to warm to room temperature, and allowed to stir for 2 hours. Upon addition of dichloromethane the dark purple solution turned a

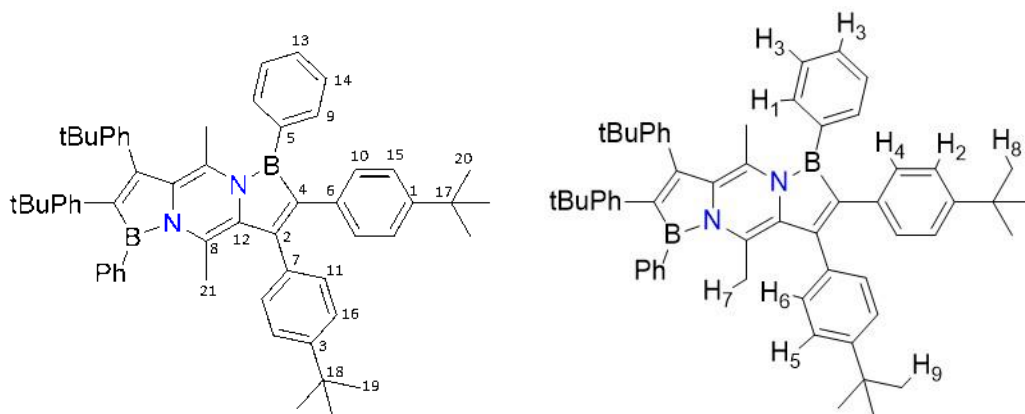
pale yellow colour. The reaction was then heated at 50 C for 12 hours, during which the mixture turned a fluorescent purple colour, and forming some dark purple precipitate. After heating, the reaction mixture was filtered to give a dark purple solid which was one of the two possible isomer (called here isomer a) in a yield of 210 mg (30%). The remaining supernatant from filtration was then purified through column chromatography using silica gel and DCM:Hex (3:1) to give mostly isomer b, with minor amounts of isomer a present in a yield of 160 mg (23%), and an overall yield for both isomer of 370 mg (53%). NMR data for isomer b, as it was the only with high enough solubility to make characterization possible.. ^1H NMR (500 MHz, Methylene Chloride- d_2) δ 7.53 (t, J = 6.7 Hz, 3H), 7.37 – 7.25 (m, 5H), 7.06 (d, J = 8.2 Hz, 1H), 7.02 (dd, J = 8.6, 1.7 Hz, 2H), 6.85 – 6.80 (m, 2H), 2.14 (d, J = 1.4 Hz, 3H), 1.35 (d, J = 1.7 Hz, 9H), 1.19 (d, J = 1.6 Hz, 9H). ^{13}C NMR (126 MHz, CD_2Cl_2) δ 174.00 (br), 152.21, 151.89, 151.38, 147.97, 140.46 (br), 134.54, 134.07, 133.44, 131.99, 130.12, 129.62, 128.54, 127.60, 126.43, 124.76, 34.99, 34.75, 31.45, 31.17, 19.99. Elemental analysis of mixture of two isomers, calculated for $\text{C}_{62}\text{H}_{68}\text{B}_2\text{Cl}_2\text{N}_2$ C 79.75%, H 7.34%, N 3.00%, found: C 79.51%, H 7.36%, N 2.93%.

Synthesis of 9^{tBu} :



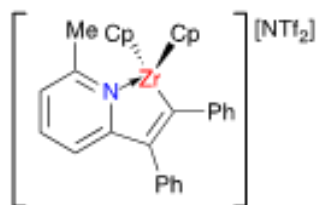
A 50mL round bottom flask was charged with 8^{tBu} (80 mg, 0.086 mmol) in THF (15 mL), and KC_8 (23 mg, 0.17 mmol) was added the round bottom attached to a swivel-frit apparatus. Immediately upon addition of KC_8 the bright purple solution turns a dark yellow colour. This was allowed to stir under an argon atmosphere for 1 hour and then filtered through the swivel frit and washed with

THF three times. Pentane (20mL) was then vacuum transferred into the swivel frit apparatus and a yellow solid precipitated. This was filtered back through the frit, washed several times with pentane and all solvent removed in vacuo yielding a yellow solid (35 mg, 47%). Crystal suitable for x-ray diffraction analysis were grown through the slow diffusion of pentane into a concentrated THF solution of **9^{tBu}**. ¹H NMR (500 MHz, THF-d₈) δ 7.32 (dd, *J* = 6.3, 3.0 Hz, H₁, 4H), 7.27 (d, *J* = 7.9 Hz, H₂, 4H), 7.20 – 7.13 (m, H₃, 6H), 7.07 (d, *J* = 7.8 Hz, H₄, 4H), 6.85 (d, *J* = 8.1 Hz, H₅, 4H), 6.57 (d, *J* = 8.4 Hz, H₆, 4H), 1.64 (s, H₇, 6H), 1.26 (s, H₈, 18H), 1.12 (s, H₉, 18H). ¹³C NMR (126 MHz, THF) δ 150.71 (C1), 150.02 (C2), 147.85 (C3), 146.56 (br, C4), 141.10 (br, C5), 136.48 (C6), 136.44 (C7), 132.65 (C8), 132.60 (C9), 130.13 (C10), 129.80 (C11), 129.46 (C12), 127.98 (C13), 127.78 (C14), 125.50 (C15), 124.14 (C16), 34.96 (C17), 34.56 (C18), 31.44 (C19), 31.41 (C20), 20.36 (C21). ¹¹B NMR (161 MHz, THF) δ 42.3. Elemental analysis calculated for C₆₂H₆₈B₂N₂ C 86.30%, H 7.94%, N 3.25%, found: C 85.93%, H 7.85%, N 3.36%.



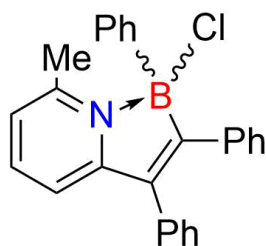
6.3 Experimental Details for Chapter 3

Synthesis of $2^{\text{Me}}\bullet\text{NTf}_2$



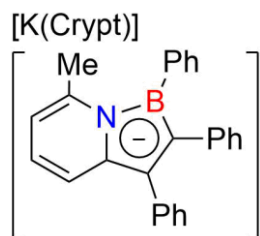
A two neck 100 mL round-bottom flask attached to a swivel frit apparatus was charged with HNTf_2 (1.0 g, 3.56 mmol), and a Teflon stirbar. To this, 50 mL of chlorobenzene was vacuum transferred, and a solution of 2-methylpyridine (0.35 mL, 3.56 mmol) in chlorobenzene (5mL). This was allowed to stir for 1 hour at room temperature, after which a solution of Cp_2ZrMe_2 (895 mg, 3.56 mmol) was added dropwise yielding effervescence of methane and a colour change from clear to pale yellow. After stirring at room temperature for 16 hours a solution of diphenylacetylene (700 mg, 3.92 mmol) in chlorobenzene (5 mL) was added to the reaction and heated to 80 for 16 hours under a flow of argon producing a dark orange solution. The solvent was condensed to approximately 25 mL and pentane (25 mL) was then vacuum-transferred into the flask with stirring, producing an orange precipitate which was filtered through the swivel frit. The solid was then washed with pentane again (2×15 mL), after which it was dried in vacuo, yielding the product $2^{\text{Me}}\bullet\text{NTf}_2$ as an orange solid (2.20 g, 2.85 mmol, 80%). ^1H NMR (500 MHz, THF-d_8) δ 7.88 (t, $J = 7.9$ Hz, 1H), 7.27 (d, $J = 7.7$ Hz, 1H), 7.19 (dd, $J = 8.3, 6.9$ Hz, 2H), 7.16 – 7.09 (m, 5H), 7.01 – 6.92 (m, 3H), 6.92 – 6.85 (m, 1H), 6.81 (s, 10H), 1.99 (s, 3H). ^{13}C NMR (126 MHz, THF) δ 211.80, 159.68, 157.45, 145.67, 141.75, 138.42, 137.46, 129.70, 127.34, 127.20, 126.12, 124.87, 123.92, 122.39, 121.03, 119.47 (q 124 Hz, $-\text{CF}_3$), 116.39, 20.63. Elemental analysis calculated C 49.79, H 3.40, N 3.63, Found C 49.81, H 3.35, N 3.53.

Synthesis of 4^{Me}:



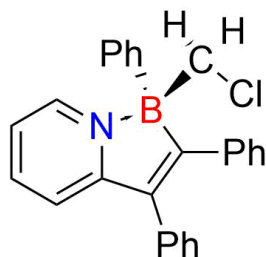
A 50ml round bottom flask was charged with **2^{Me}•NTf₂** (1.0 g, 1.30 mmol), [nBu₄N][PhBCl₃] (982 mg, 1.30 mmol), dichloromethane (30ml), and a Teflon stirbar, producing an orange solution. The mixture was refluxed under argon for 16h producing a pale-yellow solution. The mixture was then run through a silica/dichloromethane plug under atmospheric conditions, where a faint yellow band passed through and was collected. The solvent of the collected solution was then removed *in vacuo*, yielding the product as a bright yellow powder (220 mg, 0.56mmol, 43%). ¹H NMR (500 MHz, Methylene Chloride-*d*₂) δ 7.86 (t, *J* = 7.9 Hz, 1H, PyH), 7.50 (d, *J* = 7.1 Hz, 2H), 7.44 (d, *J* = 7.2 Hz, 2H), 7.34 (d, *J* = 7.4 Hz, 2H), 7.25 (dd, *J* = 14.0, 8.0 Hz, 4H), 7.10 (d, *J* = 7.8 Hz, 2H), 7.06 (m, 5H), 2.53 (s, 3H, PyMeH). ¹³C NMR (126 MHz, CD₂Cl₂) δ 167.36 (br), 160.76, 156.30, 141.66, 137.34, 134.50, 134.31, 131.34, 129.32, 128.53, 128.32, 127.18, 126.98, 126.80, 126.38, 125.99, 122.55, 116.07, 20.20 *Note: one carbon attached to boron is not observed.* ¹¹B NMR (161 MHz, CD₂Cl₂) δ 7.17. Elemental analysis calculated C 79.32, H 5.38, N 3.56, Found C 79.19, H 5.40, N 3.53.

Synthesis of **6^{Me}**:



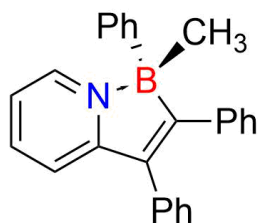
To a solution of chloroborane **4^{Me}** (200 mg, 0.508 mmol) in THF (10 mL), solid KC_8 (144 mg, 1.067 mmol) was added, causing the pale yellow solution to turn a dark orange colour with the simultaneous formation of black graphite precipitate. This solution was stirred for 5 minutes then filtered through a swivel frit apparatus. After filtration a solution of 2,2,2-cryptand (192 mg, 0.508 mmol) in THF (2 mL) was added and the solution allowed to sit at room temperature for two hours. During this time the product crystalized into bright orange crystals that were then collected by filtration to give **6^{Me}** (350 mg, 0.453 mmol, 89%) ^1H NMR (500 MHz, THF-d_8) δ 7.60 – 7.52 (m, 2H, ArH), 7.23 (dd, J = 8.1, 1.4 Hz, 2H, ArH), 7.05 (t, J = 7.7 Hz, 2H, ArH), 7.03 – 6.92 (m, 4H, Ar/PyH), 6.78 (dd, J = 8.3, 1.4 Hz, 2H, ArH), 6.55 (dd, J = 8.3, 7.1 Hz, 2H, ArH), 6.34 – 6.27 (m, 1H, PyH), 5.49 (dd, J = 8.8, 5.9 Hz, 1H, PyH), 5.28 (dt, J = 5.9, 1.2 Hz, 1H, PyH), 3.45 (s, 12H, CryptH), 3.43 – 3.38 (m, 12H, CryptH), 2.46 – 2.40 (m, 12H, CryptH), 1.87 (s, 3H, MeH). ^{13}C NMR (126 MHz, THF-d_8) δ 146.92, 142.77, 136.08, 134.67, 130.47, 129.24, 127.68, 125.72, 124.83, 123.87, 122.27, 120.38, 116.57, 116.47, 115.84, 105.06, 104.65, 69.67, 66.85, 53.17, 24.81. ^{11}B NMR (161 MHz, THF-d_8) δ 26.5. Elemental analysis calculated C 68.20, H 7.54, N 5.42, Found C 68.55, H 7.75, N 5.19.

Synthesis of **10^H**:



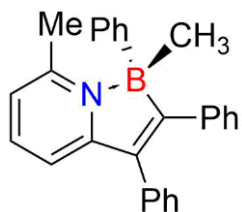
In a glovebox, a 50ml two-neck round bottom flask was charged with **6^H** (100 mg, 0.263 mmol) in 15 mL of THF. K₂C₈ (75 mg, 0.552 mmol) was added and the flask attached to a swivel frit apparatus. The reaction was allowed to stir under argon for 10 minutes. CH₂Cl₂ was vacuum transferred into the flask, turning the dark orange solution into a clear colorless solution. Graphite was filtered off through the frit and solvent removed giving a pale yellow solid. This was then passed through a silica plug using dichloromethane to yield **10^H** as a white solid (76 mg, 0.20 mmol, 74%). ¹H NMR (500 MHz, Methylene Chloride-d₂) δ 8.36 (dd, *J* = 5.7, 1.3 Hz, 1H, PyH), 7.99 (ddd, *J* = 8.7, 7.5, 1.5 Hz, 1H, PyH), 7.48 (d, *J* = 8.2 Hz, 1H, PyH), 7.43 – 7.30 (m, 6H, ArH), 7.25 – 7.16 (m, 5H, ArH/ PyH), 7.11 – 7.08 (m, 3H, ArH), 6.98 – 6.95 (m, 2H, ArH), 3.62 (d, *J* = 12.5 Hz, 1H, CH₂Cl), 3.48 (d, *J* = 12.5 Hz, 1H, CH₂Cl). ¹³C NMR (126 MHz, CD₂Cl₂) δ 161.03, 141.90, 140.42, 139.07, 135.29, 134.77, 131.48, 129.43, 128.11, 127.78, 127.09, 126.97, 126.83, 125.91, 125.60, 119.58, 118.45, 40.90 (br). ¹¹B NMR (161 MHz, CD₂Cl₂) δ 1.89. Elemental analysis calculated C 79.32; H 5.38; N 3.56, Found, C 79.44, H 5.26, N 3.55.

Synthesis of **11^H**:



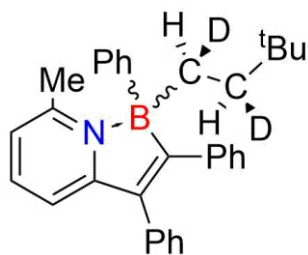
In a glovebox, a 50ml two-neck round bottom flask was charged with **4^H** (106 mg, 0.279 mmol) in 15 mL of THF. KC_8 (75 mg, 0.558 mmol) was added and the flask attached to a swivel frit apparatus. The reaction was allowed to stir under argon for 10 minutes. MeI (0.1 mL, 1.61 mmol) was added dropwise to the reaction, turning the dark orange solution into a clear colorless solution. Solvent was removed under vacuum and 10mL of dichloromethane was added. Graphite and KCl were filtered off through the frit and solvent removed to yield **11^H** as a white solid (62 mg, 0.17mmol, 62%). ^1H NMR (500 MHz, Methylene Chloride- d_2) δ 8.20 (d, $J = 5.6$ Hz, 1H, PyH), 7.92 – 7.85 (m, 1H, PyH), 7.45 – 7.39 (m, 3H ArH/PyH), 7.39 – 7.32 (m, 3H ArH), 7.29 – 7.25 (m, 2H), 7.24 – 7.16 (m, 4H, ArH/PyH), 7.15 – 7.10 (m, 1H ArH), 7.08 – 7.03 (m, 2H, ArH), 7.01 – 6.98 (m, 2H, ArH), 0.43 (s, 3H, BMeH). ^{13}C NMR (126 MHz, CD_2Cl_2) δ 179.78(br), 160.04, 149.54(br), 141.57, 139.30, 135.52, 132.95, 132.46, 131.41, 129.52, 128.15, 128.09, 126.83, 126.81, 126.62, 125.75, 124.98, 119.15, 118.21, 5.48(br). ^{11}B NMR (161 MHz, CD_2Cl_2) δ 1.96. Elemental analysis calculated C 86.92; H 6.17; N 3.90, Found C 86.57, H 6.15, N 3.76.

Synthesis of **11^{Me}**:



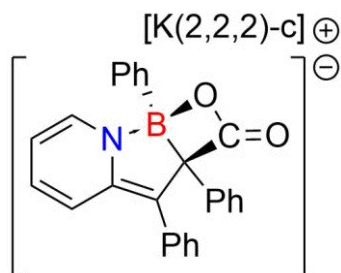
In the glovebox, a 50ml two-neck round bottom flask was charged with **4^{Me}** (92 mg, 0.234 mmol) in 15 mL of THF. KC_8 (66 mg, 0.491 mmol) was added and the flask attached to a swivel frit apparatus. The reaction was allowed to stir under argon for 10 minutes. MeI (0.1 mL, 1.61 mmol) was added dropwise to the reaction, turning the dark orange solution into a clear colorless solution. Solvent was removed under vacuum and 10mL of dichloromethane was added. Graphite and KCl were filtered off through the frit and solvent removed to yield **11^{Me}** as a white solid (55 mg, 0.15mmol, 63%). ^1H NMR (500 MHz, $\text{THF-}d_8$) δ 7.85 (t, $J = 7.8$ Hz, 1H, PyH), 7.36 – 7.30 (m, 3H), 7.30 – 7.24 (m, 4H, Ar/PyH), 7.21 (d, $J = 6.7$ Hz, 2H, ArH), 7.15 (td, $J = 8.1, 7.7, 6.2$ Hz, 2H, ArH), 7.11 – 7.06 (m, 2H, ArH), 6.94 – 6.90 (m, 2H, Ar/PyH), 6.75 (m, 2H, ArH), 2.38 (s, 3H, PyMeH), 0.38 (s, 3H, BMeH). ^{13}C NMR (126 MHz, $\text{THF-}d_8$) δ 161.26, 154.71, 139.18, 135.73, 132.69, 132.53, 131.49, 129.64, 127.91, 127.58, 126.77, 126.59, 126.40, 125.28, 124.65, 120.66, 115.56, 20.14, 1.63 MeC *Note: Two of the carbons attached to boron are not observed.* ^{11}B NMR (161 MHz, $\text{THF-}d_8$) δ 2.86. Elemental analysis calculated C 86.87; H 6.48; N 3.75, Found C 86.81, H 6.40, N 3.69

Synthesis of **12^{Me}**:



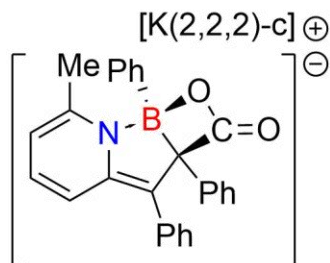
In a two-neck 50 mL round bottom flask **4^{Me}** (50 mg, 0.13 mmol) was taken up in THF (15 mL). To this was added solid KC_8 (37mg, 0.27 mmol), turning the pale yellow solution a dark orange with a black precipitate of graphite forming immediately. The flask was then attached to a swivel frit apparatus and the reaction allowed to stir under argon for 10 minutes. A solution of the dideuterated neohexyl stereoprobe (24mg, 0.14 mmol) in THF (2 mL) was added via syringe turning the dark orange solution a more pale yellow. This was heated at 60 C for three hours before the solvent was removed in vacuo and taken back up into CH_2Cl_2 (25 mL) and filtered through the swivel frit to remove the graphite. The collected solution was passed through a silica plug with CH_2Cl_2 in the atmosphere, which after removal of solvent yielded **12^{Me}** as a white solid (25 mg, 0.056 mmol, 43%). ^1H NMR (500 MHz, Benzene- d_6) δ 7.50 (d, J = 7.2 Hz, 2H, ArH), 7.33 (dd, J = 8.3, 7.1 Hz, 2H, ArH), 7.27 – 7.20 (m, 3H), 7.16 – 6.99 (m, 5H), 6.96 – 6.86 (m, 3H), 6.86 – 6.74 (m, 2H), 6.08 – 6.03 (m, 1H), 2.07 (d, J = 1.6 Hz, 3H), 1.50 (m, 0.5H, BCHD), 1.30 (m, 0.5H, BCHD), 1.16 (m, 0.5H, CHDCHDtBu), 0.89 (s, 9H, tBuH), 0.63 (m, 0.5H, CHDCHDtBu). ^{13}C NMR (126 MHz, C_6D_6) δ 161.84, 154.26, 147.39(br), 139.88, 138.47, 135.73, 133.54, 131.75, 129.78, 128.00, 127.81, 126.30, 125.72, 125.22, 119.73, 115.03, 38.61(br), 30.05, 28.71, 19.63, 11.28(br) *Note: Two of the carbons attached to boron are not observed.* ^{11}B NMR (161 MHz, C_6D_6) δ 4.05. Elemental analysis calculated C 86.28, H 8.15, N 3.14, Found C 85.98, H 8.03, N 3.28.

Synthesis of **13^H**:



In a J young NMR tube, **6^H** (10 mg) was taken up in THF-*d*₈ (0.7 mL). The solution was degassed and placed under one atmosphere of CO₂. After shaking the NMR tube for 5 minutes the sparingly soluble **6^H** was completely dissolved and the dark orange solution had turned a dark red colour, NMR of this showed quantitative conversion to **13^H**. When the THF solution was layered with pentane in the glove box, X-ray quality crystals of **13^H** were obtained (8 mg, 80% yield). ¹H NMR (500 MHz, THF-*d*₈) δ 7.56 – 7.47 (m, 2H, Ar**H**), 7.29 – 7.22 (m, 2H, Ar**H**), 6.96 – 6.92 (m, 4H), 6.88 (td, *J* = 8.6, 7.2 Hz, 3H, Ar/Py**H**), 6.78 – 6.69 (m, 3H, Ar/Py**H**), 6.61 – 6.47 (m, 3H), 6.22 (ddd, *J* = 9.6, 5.9, 1.6 Hz, 1H, Py**H**), 4.94 (td, *J* = 6.2, 1.2 Hz, 1H, Py**H**), 3.55 (s, 12H, Crypt**H**), 3.53 – 3.46 (m, 12H, Crypt**H**), 2.55 – 2.49 (m, 12H, Crypt**H**). ¹³C NMR (126 MHz, THF-*d*₈) δ 176.48(CO₂ C), 147.25, 143.70, 140.97, 139.54, 132.21, 129.83, 126.02, 125.94, 125.48, 125.18, 125.16, 123.81, 120.41, 118.66, 114.61, 100.07, 97.16, 69.72, 66.94, 53.30 *Note: two carbons attached to boron are not observed.* ¹¹B NMR (161 MHz, THF-*d*₈) δ 5.30. IR (KBr pellet) 1708.97 cm⁻¹. Elemental analysis calculated C 65.74, H 6.90, N 5.23, Found C 65.48, H 6.99, N 5.50.

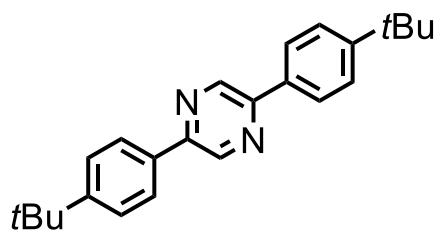
Synthesis of **13^{Me}**:



In a J young NMR tube, **6^{Me}** (10 mg) was taken up in THF-*d*₈ (0.7 mL). The solution was degassed and placed under one atmosphere of CO₂. After shaking the NMR tube for <1 minute the sparingly soluble **6^{Me}** was completely dissolved and the bright orange solution had turned a dark red colour, NMR of this showed quantitative conversion to **13^{Me}**. When the THF solution was layered with pentane in the glove box, small needlelike crystals formed (5 mg, 50%). ¹H NMR (500 MHz, THF-*d*₈) δ 7.49 – 7.42 (m, 3H, ArH), 6.84 (m, 5H, ArH, PyH), 6.72 (m, 3H, ArH), 6.61 (m, 3H, ArH), 6.52 – 6.45 (m, 1H, ArH), 6.43 – 6.37 (m, 1H, ArH), 6.13 (dd, *J* = 9.5, 6.0 Hz, 1H, PyH), 4.77 (d, *J* = 5.9 Hz, 1H, PyH), 3.54 (s, 12H, CryptH), 3.52 – 3.47 (m, 12H, CryptH), 2.54 – 2.49 (m, 12H, CryptH), 1.42 (s, 3H, MeH). ¹³C NMR (126 MHz, THF-*d*₈) δ 173.01, 149.43, 143.90, 141.18, 130.05, 125.91, 125.82, 125.51, 125.25, 125.08, 124.35, 123.03, 120.22, 118.37, 112.33, 109.40, 98.70, 83.22, 69.73, 67.02, 53.56, 21.49. *Note: two carbons attached to boron are not observed* ¹¹B NMR (161 MHz, THF-*d*₈) δ 5.41 IR (KBr Pellet) 1709.63 cm⁻¹. Elemental analysis calculated C 66.09, H 7.03, N 5.14, Found C 65.96, H 6.92, N 5.28.

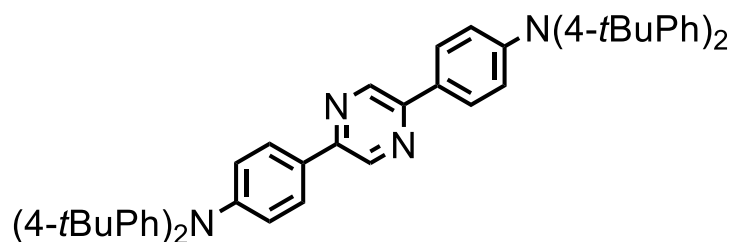
Experimental Details for Chapter 4

Synthesis of 14^{tBu}



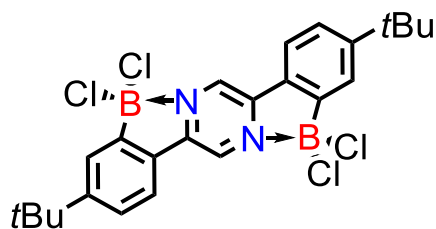
Synthesis adapted from Williams et al.² 4-*t*Butylphenylboronic acid (4.45g, 25.0 mmol) and 2,5-dibromopyrazine (2.29g, 9.6 mmol) were dissolved in 1,4-dioxane (75mL) and the mixture degassed by bubbling through argon for 10 minutes. A solution of K₂CO₃ (7.96g, 57.6 mmol) in 25 mL of water and tetrakis(triphenylphosphine)palladium (6%, 666mg, 0.58 mmol) were added and the reaction mixture was again degassed for 10 minutes. The reaction was heated at 95°C for 16 hours. Upon cooling a solid precipitated which was collected by filtration. The solid was then recrystallized from hot ethanol yielding 2,5-di(4-*t*Buphenyl)pyrazine (2.76g, 8.0 mmol, 83% yield). ¹H NMR (500 MHz, CDCl₃) δ 9.06 (s, 2H), 8.01 (d, *J* = 8.5 Hz, 4H), 7.56 (d, *J* = 8.5 Hz, 4H), 1.39 (s, 18H). ¹³C NMR (126 MHz, CDCl₃) δ 152.43, 149.75, 140.47, 132.97, 125.87, 125.47, 34.25, 30.69. Elemental Analysis: Calculated C 83.68 H 8.19 N 8.13, Found C 83.25 H 8.01 N 7.98.

Synthesis of 14N^{Ar}:



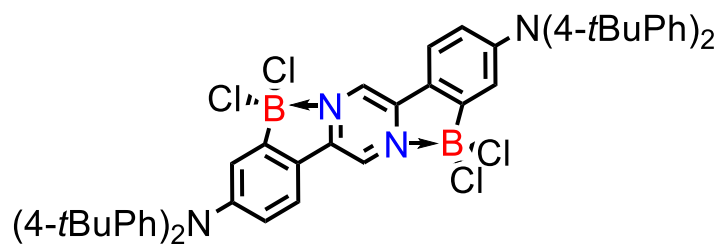
Synthesis adapted from Williams et al.² bis(4-*t*Butylphenyl)aminophenylboronic acid (630mg, 1.6 mmol) and 2,5-dibromopyrazine (150mg, 0.63 mmol) were dissolved in 1,4-dioxane (30mL) and the mixture degassed by bubbling through argon for 10 minutes. A solution of K₂CO₃ (520mg, 3.76 mmol) in 5 mL of water and tetrakis(triphenylphosphine)palladium (6%, 43 mg, 0.04 mmol) were added and the reaction mixture was again degassed for 10 minutes. The reaction was heated at 95°C for 16 hours. Upon cooling a bright yellow solid precipitated which was collected by filtration. The solid was then recrystallized from hot ethanol yielding 2,5-di(bis4-*t*Buphenylaminophenyl)pyrazine (452mg, 0.56 mmol, 91% yield). ¹H NMR (500 MHz, CDCl₃) δ 8.95 (s, 2H), 7.89 (d, *J* = 8.8 Hz, 4H), 7.30 (d, *J* = 8.7 Hz, 8H), 7.14 (d, *J* = 8.8 Hz, 4H), 7.09 (d, *J* = 8.6 Hz, 8H), 1.33 (s, 36H). ¹³C NMR (126 MHz, CDCl₃) δ 148.97, 148.82, 145.89, 143.87, 139.82, 128.22, 126.65, 125.61, 124.08, 121.29, 33.79, 30.86. Elemental Analysis: Calculated C 85.02 H 7.90 N 7.08. Found C 85.31 H 7.54 N 7.23.

Synthesis of **15^{tBu}**:



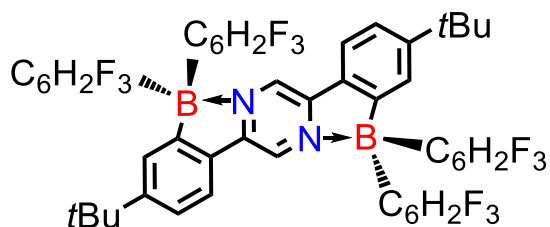
Synthesis adapted from Crossley *et al*³. A two neck round bottom flask was charged with **14^{tBu}** (400mg, 1.16mmol) and tri-tert-butylpyridine (574 mg, 2.32 mmol), and dichloromethane (50mL) was added via vacuum transfer. A solution of borontrichloride in dichloromethane (1.0M, 2.9 mL) was slowly added and the colour changed from clear and colourless to a bright orange. Solid aluminum chloride (619mg, 4.64 mmol) was added to the flask causing an immediate colour change to dark purple. This was stirred at room temperature for 16 hours, before tetramethylammonium chloride (254mg, 2.32 mmol) was added and allowed to stir for 1 hour. The solvent was then removed in vacuo yielding a dark orange solid. Water was added to the flask turning the solid a brighter orange colour and the product was collected by filtration before being washed with more water (150 mL) and hexanes (150 mL) before being dried under high vac yielding a bright orange solid **15^{tBu}** (510 mg, 1.0 mmol, 87% yield). ¹H NMR (500 MHz, CDCl₃) δ 9.26 (s, 2H), 7.90 (d, *J* = 1.8 Hz, 2H), 7.84 (d, *J* = 8.2 Hz, 2H), 7.59 (dd, *J* = 8.2, 1.8 Hz, 2H), 1.42 (s, 18H). ¹³C NMR (126 MHz, CDCl₃) δ 159.12, 149.61, 134.26, 127.46, 127.29, 126.92, 122.19, 35.31, 30.56. (Carbon attached to boron not observed) ¹¹B NMR (161 MHz, CDCl₃) δ 8.39. Elemental Analysis: Calculated C 56.98 H 5.18 N 5.54, Found C 57.27 H 5.26 N 5.44.

Synthesis of **15**^{NAr}:



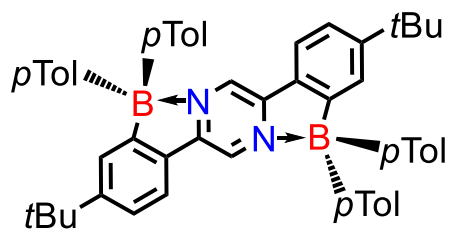
Synthesis adapted from Crossley *et al.* A two neck round bottom flask was charged with **14**^{NAr} (500mg, 0.63mmol) and tri-tert-butylpyridine (313 mg, 1.26 mmol), and dichloromethane (50mL) was added via vacuum transfer. A solution of borontrichloride in dichloromethane (1.0M, 1.6 mL) was slowly added and the colour changed from fluorescent yellow to dark purple. Solid aluminum chloride (340mg, 2.53 mmol) was added to the flask causing a colour change to darker purple-blue. This was stirred at room temperature for 16 hours, before tetramethylammonium chloride (275mg, 2.51 mmol) was added and allowed to stir for 1 hour. The solvent was then removed in vacuo yielding a dark green solid. Water was added to the flask turning the solid a brighter green colour and the product was collected by filtration before being washed with more water (150 mL) and hexanes (150 mL) before being dried under high vac yielding a dark green solid **BN2-Cl** (402 mg, 0.42 mmol, 68% yield). ¹H NMR (500 MHz, CDCl₃) δ 8.80 (s, 2H), 7.47 (d, *J* = 8.7 Hz, 2H), 7.37 (d, *J* = 8.6 Hz, 8H), 7.34 (d, *J* = 2.3 Hz, 2H), 7.13 (d, *J* = 8.6 Hz, 8H), 6.91 (dd, *J* = 8.7, 2.3 Hz, 2H), 1.35 (s, 36H). ¹³C NMR (126 MHz, CDCl₃) δ 153.12, 148.05, 146.39, 142.35, 133.47, 126.10, 125.59, 122.90, 121.19, 119.30, 118.86, 33.99, 30.82. (Signal for carbon attached to boron not observed). ¹¹B Signal not observed. Elemental Analysis: Calculated: C 70.61 H 6.35 N 5.88. Found C 70.55 H 6.30 N 5.91.

Synthesis of **16^{tBu}**:



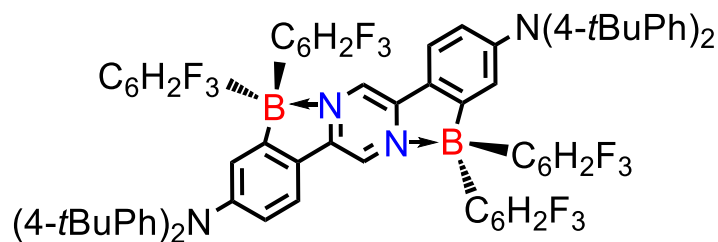
A round bottom flask was charged with **15^{tBu}** (103mg, 0.20mmol) and $\text{Zn}(\text{C}_6\text{H}_2\text{F}_3)_2$ (167 mg, 0.51 mmol) and dichloromethane (20mL). The solution immediately turned a bright fluorescent yellow colour and was stirred at room temperature for 10 minutes. The solution was then passed through a silica plug with dichloromethane and the dried under high vacuum yielding **16^{tBu}** as a bright orange solid (134 mg, 0.42 mmol, 74% yield). ^1H NMR (500 MHz, CDCl_3) δ 9.24 (s, 2H), 7.84 (d, $J = 1.7$ Hz, 2H), 7.77 (d, $J = 8.3$ Hz, 2H), 7.45 (dd, $J = 8.3, 1.8$ Hz, 2H), 6.52 (t, $J = 8.5$ Hz, 8H), 1.33 (s, 18H). ^{13}C NMR (126 MHz, CDCl_3) δ 164.81(dt, $^1J_{\text{CF}} = 243$ Hz, $^3J_{\text{CF}} = 17$ Hz) 161.47(dt, $^1J_{\text{CF}} = 247$ Hz, $^3J_{\text{CF}} = 17$ Hz), 159.25, 156.22, 150.56, 135.38, 128.66, 127.23, 124.28, 120.85, 114.77(br), 99.47(dd, $^2J_{\text{CF}} = 34$ Hz, $^2J_{\text{CF}} = 24$ Hz), 34.88, 30.59.(Signal for carbon attached to boron on phenylpyrazine core not observed). ^{11}B NMR (161 MHz, CDCl_3) δ 0.15. (Elemental Analysis: Calculated C 64.89 H 3.86 N 3.15. Found C 65.10 H 4.18 N 3.09.

Synthesis of **17^{tBu}**:



A round bottom flask was charged with **15^{tBu}** (77mg, 0.15mmol), $\text{Zn}(\text{ptol})_2$ (94 mg, 0.38 mmol) and dichloromethane (20mL). The solution immediately turned a dark yellow colour and was stirred at room temperature for 10 minutes. The solution was then passed through a silica plug with dichloromethane and the dried under high vacuum yielding **1-Tol₂** as a dark yellow solid (58 mg, 0.08 mmol, 53% yield). ^1H NMR (500 MHz, CDCl_3) δ 9.05 (s, 2H), 7.78 (d, $J = 1.8$ Hz, 2H), 7.75 (dd, $J = 8.3, 1.6$ Hz, 2H), 7.41 (d, $J = 8.3$ Hz, 2H), 7.20 – 7.14 (m, 8H), 7.13 – 7.07 (m, 8H), 2.33 (s, 12H), 1.34 (s, 8H). ^{13}C NMR (126 MHz, CDCl_3) δ 163.09(br), 155.55, 149.90, 144.58 (br), 135.44, 134.37, 132.49, 129.60, 128.17, 127.13, 123.88, 34.90, 30.75, 20.65. (signal for carbon attached to boron on phenylpyrazine not observed), ^{11}B NMR (161 MHz, CDCl_3) δ 6.34 Elemental Analysis: Calculated C 85.72 H 7.47 N 3.84. Found C 85.70 H 7.40 N 3.66.

Synthesis of **16^{NAr}**:



A round bottom flask was charged with **15^{NAr}** (60mg, 0.06mmol) and $\text{Zn}(\text{C}_6\text{H}_2\text{F}_3)_2$ (52 mg, 0.16 mmol) and dichloromethane (20mL). The solution immediately turned a darker green colour, and

(s, 12H), 1.33 (s, 36H). ^{13}C NMR (126 MHz, CDCl_3) δ 163.95, 151.03, 147.74, 146.47, 144.95, 143.47, 135.21, 133.69, 132.43, 128.00, 125.60, 124.71, 122.01, 121.35, 118.60, 33.83, 30.85, 20.66. (^{13}C signal attached to B not observed). ^{11}B Signal not observed. Elemental Analysis: Calculated C 85.85 H 7.55 N 4.77. Found C 85.65 H 7.30 N 4.88.

Crystallographic data collection and refinement parameters of isolated compounds

Table 6-1. Crystal Data Collection and Refinement Parameters for Complex 2B(C₆F₅)₄.

	2B(C₆F₅)₄.
formula	C ₂₄ B ₄ F ₂₀ C ₂₉ H ₂₄ NZr
<i>fw</i>	1156.76
crystal system	tetragonal
space group	P43
<i>a</i> (Å)	11.57510(10)
<i>b</i> (Å)	11.57510(10)
<i>c</i> (Å)	34.2480(5)
<i>α</i> (deg)	90
<i>β</i> (deg)	90
<i>γ</i> (deg)	90
<i>V</i> (Å³)	4588.65(10)
<i>Z</i>	4
<i>T</i> (K)	173(2)
Wavelength (Å)	1.54178
<i>ρ</i>_{caled} (g·cm⁻³)	1.674
<i>F</i>(000)	2296
<i>μ</i> (mm⁻¹)	3.073
crystal size, mm³	0.27×0.15×0.15
transmission factors	0.6 – 0.65
<i>θ</i> range (deg)	3.819 – 66.626
data/restraints/param	7737/1/685
GOF	1.069
<i>R</i>₁ [<i>I</i> > 2σ(<i>I</i>)]	0.0338
w<i>R</i>₂ [all data]	0.0814
residual density, e/Å³	0.621 and -0.383

Table 6-2. Crystal Data Collection and Refinement Parameters for Complex 3.

	3
formula	C ₂₉ H ₂₄ ClNZr
<i>fw</i>	513.16
crystal system	monoclinic
space group	P21/c
<i>a</i> (Å)	14.7014(7)
<i>b</i> (Å)	20.2371(15)
<i>c</i> (Å)	7.7474(4)
<i>α</i> (deg)	90
<i>β</i> (deg)	104.290(4)
<i>γ</i> (deg)	90
<i>V</i> (Å³)	2233.6(2)
<i>Z</i>	4
<i>T</i> (K)	173(2)
Wavelength (Å)	1.54178
ρ_{calcd} (g·cm⁻³)	1.526
<i>F</i>(000)	1048
μ (mm⁻¹)	5.253
crystal size, mm³	0.10×0.08×0.06
transmission factors	0.628 – 0.725
θ range (deg)	3.102 – 72.564
data/restraints/param	4307/0/289
GOF	1.014
<i>R</i>₁ [<i>I</i> > 2σ(<i>I</i>)]	0.0370
w<i>R</i>₂ [all data]	0.0976
residual density, e/Å³	0.667 and -0.631

Table 6-3. Crystal Data Collection and Refinement Parameters for Complex 4^H.

	4^H
formula	C ₂₅ H ₁₉ BClN
<i>fw</i>	379.67
crystal system	monoclinic
space group	P21/c
<i>a</i> (Å)	7.5793(5)
<i>b</i> (Å)	20.7341(11)
<i>c</i> (Å)	12.3247(5)
<i>α</i> (deg)	90
<i>β</i> (deg)	94.596(4)
<i>γ</i> (deg)	90
<i>V</i> (Å³)	1930.60(18)
<i>Z</i>	4
<i>T</i> (K)	173(2)
Wavelength (Å)	1.54178
<i>ρ</i>_{calcd} (g·cm⁻³)	1.306
<i>F</i>(000)	792
<i>μ</i> (mm⁻¹)	1.806
crystal size, mm³	0.10×0.10×0.05
transmission factors	0.835 – 0.914
<i>θ</i> range (deg)	4.183 – 66.453
data/restraints/param	3317/0/253
GOF	1.053
<i>R</i>₁ [<i>I</i> > 2σ(<i>I</i>)]	0.0478
w<i>R</i>₂ [all data]	0.1269
residual density, e/Å³	0.345 and -0.247

Table 6-4. Crystal Data Collection and Refinement Parameters for Complex 5^H.

	5^H
formula	C27H19BF6N2O4S2
<i>fw</i>	1248.74
crystal system	triclinic
space group	P-1
<i>a</i> (Å)	10.0900(3)
<i>b</i> (Å)	15.4860(4)
<i>c</i> (Å)	18.2577(5)
<i>α</i> (deg)	75.063(2)
<i>β</i> (deg)	80.627(2)
<i>γ</i> (deg)	89.752(2)
<i>V</i> (Å³)	2717.51(13)
<i>Z</i>	2
<i>T</i> (K)	173(2)
Wavelength (Å)	1.54178
ρ_{calcd} (g·cm⁻³)	1.526
<i>F</i>(000)	1272
μ (mm⁻¹)	2.498
crystal size, mm³	0.20×0.20×0.10
transmission factors	0.6385 – 0.7533
θ range (deg)	2.540 – 64.483
data/restraints/param	8769/399/943
GOF	1.001
<i>R</i>₁ [<i>I</i> > 2σ(<i>I</i>)]	0.0812
w<i>R</i>₂ [all data]	0.2509
residual density, e/Å³	1.002 and -0.539

Table 6-5. Crystal Data Collection and Refinement Parameters for Complex 6^H.

	6^H
formula	C18H36KN2O6,C25H19BN
<i>fw</i>	1013.08
crystal system	orthorhombic
space group	Pbca
<i>a</i> (Å)	19.31(2)
<i>b</i> (Å)	17.619(14)
<i>c</i> (Å)	24.71(2)
<i>α</i> (deg)	90
<i>β</i> (deg)	90
<i>γ</i> (deg)	90
<i>V</i> (Å³)	8408(14)
<i>Z</i>	6
<i>T</i> (K)	173(2)
Wavelength (Å)	1.54178
ρ_{calcd} (g·cm⁻³)	1.201
<i>F</i>(000)	3248
μ (mm⁻¹)	1.493
crystal size, mm³	0.20×0.20×0.20
transmission factors	0.742 – 0.780
θ range (deg)	3.578 – 69.730
data/restraints/param	7897/555/487
GOF	1.027
<i>R</i>₁ [<i>I</i> > 2σ(<i>I</i>)]	0.0612
w<i>R</i>₂ [all data]	0.1776
residual density, e/Å³	0.404 and -0.361

Table 6-6. Crystal Data Collection and Refinement Parameters for Complex 7^H.

	7^H
formula	C106H54B2Cl8F40N2Zr2
<i>fw</i>	2603.17
crystal system	triclinic
space group	P-1
<i>a</i> (Å)	12.6013(2)
<i>b</i> (Å)	14.2473(2)
<i>c</i> (Å)	15.7688(2)
<i>α</i> (deg)	63.9930(10)
<i>β</i> (deg)	86.3180(10)
<i>γ</i> (deg)	80.9800(10)
<i>V</i> (Å³)	2512.88(7)
<i>Z</i>	1
<i>T</i> (K)	173(2)
Wavelength (Å)	1.54178
ρ_{calcd} (g·cm⁻³)	1.720
<i>F</i>(000)	1290
μ (mm⁻¹)	4.793
crystal size, mm³	0.12×0.08×0.07
transmission factors	0.702 – 0.767
θ range (deg)	3.118 – 67.489
data/restraints/param	8791/31/750
GOF	1.023
<i>R</i>₁ [<i>I</i> > 2σ(<i>I</i>)]	0.0416
w<i>R</i>₂ [all data]	0.1147
residual density, e/Å³	0.782 and -0.448

Table 6-7. Crystal Data Collection and Refinement Parameters for Complex *cis*-8^H.

	<i>cis</i> -8 ^H
formula	C ₄₆ H ₃₆ B ₂ Cl ₂ N ₂
<i>fw</i>	354.64
crystal system	triclinic
space group	P-1
<i>a</i> (Å)	14.4818(3)
<i>b</i> (Å)	14.8376(3)
<i>c</i> (Å)	15.0664(5)
<i>α</i> (deg)	112.9650(10)
<i>β</i> (deg)	113.3580(10)
<i>γ</i> (deg)	100.9890(10)
<i>V</i> (Å ³)	2497.76(11)
<i>Z</i>	4
<i>T</i> (K)	173(2)
Wavelength (Å)	1.54178
ρ_{calcd} (g·cm⁻³)	0.943
<i>F</i>(000)	740
μ (mm⁻¹)	1.367
crystal size, mm³	0.3×0.2×0.2
transmission factors	0.756 – 0.761
θ range (deg)	3.544 – 72.829
data/restraints/param	9422/450/471
GOF	1.067
R₁ [I > 2σ(I)]	0.0345
wR₂ [all data]	0.1020
residual density, e/Å³	0.285 and -0.210

Table 6-8. Crystal Data Collection and Refinement Parameters for *trans*-8^H.

	<i>trans</i> -8 ^H
formula	C ₄₆ H ₃₆ B ₂ Cl ₂ N ₂
<i>fw</i>	709.29
crystal system	monoclinic
space group	P2 ₁ /c
<i>a</i> (Å)	6.2200(2)
<i>b</i> (Å)	18.2840(4)
<i>c</i> (Å)	16.2870(5)
<i>α</i> (deg)	90.0000(15)
<i>β</i> (deg)	96.7120(13)
<i>γ</i> (deg)	90.0000(15)
<i>V</i> (Å ³)	1839.57(9)
<i>Z</i>	2
<i>T</i> (K)	293(2)
Wavelength (Å)	0.71073
ρ_{calcd} (g·cm⁻³)	1.281
<i>F</i>(000)	740
μ (mm⁻¹)	0.213
crystal size, mm³	0.23×0.21×0.18
transmission factors	0.954 – 0.964
θ range (deg)	2.518 – 27.507
data/restraints/param	4199/0/236
GOF	1.217
R₁ [I > 2σ(I)]	0.0571
wR₂ [all data]	0.1836
residual density, e/Å³	0.772 and -0.537

Table 6-9. Crystal Data Collection and Refinement Parameters for Complex 9^{tbu}.

	9^{tbu}
formula	C62H68B2N2
<i>fw</i>	431.40
crystal system	triclinic
space group	P-1
<i>a</i> (Å)	10.8060(4)
<i>b</i> (Å)	12.3580(3)
<i>c</i> (Å)	21.0340(7)
<i>α</i> (deg)	88.301(2)
<i>β</i> (deg)	79.2670(10)
<i>γ</i> (deg)	68.171(2)
<i>V</i> (Å³)	2559.46(15)
<i>Z</i>	4
<i>T</i> (K)	153(2)
Wavelength (Å)	0.71073
ρ_{calcd} (g·cm⁻³)	1.120
<i>F</i>(000)	928
μ (mm⁻¹)	0.063
crystal size, mm³	0.2×0.1×0.1
transmission factors	0.992 – 0.994
θ range (deg)	1.777 – 25.000
data/restraints/param	8951/0/609
GOF	1.152
<i>R</i>₁ [<i>I</i> > 2σ(<i>I</i>)]	0.0714
w<i>R</i>₂ [all data]	0.2449
residual density, e/Å³	0.758 and -0.393

Table 6- 10. Crystal Data Collection and Refinement Parameters for Complex 10^H.

	10^H
chemical formula	C ₂₆ H ₂₂ BN
crystal colour	Yellow
<i>F</i>w; <i>F</i>(000)	359.25; 760
<i>T</i> (K)	173(2)
wavelength (Å)	1.54178
space group	P21/c
<i>a</i> (Å)	7.58320(10)
<i>b</i> (Å)	20.8464(3)
<i>c</i> (Å)	12.6521(2)
<i>α</i> (deg)	90
<i>β</i> (deg)	94.8090(10)
<i>γ</i> (deg)	90
<i>Z</i>	4
<i>V</i> (Å³)	1993.03(5)
<i>ρ</i>_{calcd} (g·cm⁻³)	1.197
<i>μ</i> (mm⁻¹)	0.515
<i>θ</i> range (deg); completeness	4.098 – 67.497; 1.000
collected reflections; <i>R</i>_σ	25390; 0.0192
unique reflections; <i>R</i>_{int}	25390; 0.0350
<i>R</i>1^a; <i>wR</i>2^b [<i>I</i> > 2σ(<i>I</i>)]	0.0419; 0.1125
<i>R</i>1; <i>wR</i>2 [all data]	0.0467; 0.1172
GOF	1.033
largest diff peak and hole	0.293 and -0.210

Table 6-11. Crystal Data Collection and Refinement Parameters for Complex 13^H.

	13^H
chemical formula	C ₂₆ H ₁₉ BN ₂ O ₂ ,C ₁₈ H ₃₆ KN ₂ O ₆
crystal colour	Yellow
<i>F</i>w; <i>F</i>(000)	401.91; 1712
<i>T</i> (K)	173(2)
wavelength (Å)	1.54178
space group	P21/c
<i>a</i> (Å)	10.55710(10)
<i>b</i> (Å)	17.9054(2)
<i>c</i> (Å)	22.7508(3)
<i>α</i> (deg)	90
<i>β</i> (deg)	102.3040(10)
<i>γ</i> (deg)	90
<i>Z</i>	8
<i>V</i> (Å³)	4201.78(8)
<i>ρ</i>_{calcd} (g·cm⁻³)	1.271
<i>μ</i> (mm⁻¹)	1.560
<i>θ</i> range (deg); completeness	3.169 – 70.175; 0.989
collected reflections; <i>R</i>_σ	27471; 0.0496
unique reflections; <i>R</i>_{int}	27471; 0.0479
<i>R</i>1^a; <i>wR</i>2^b [<i>I</i> > 2σ(<i>I</i>)]	0.0585; 0.1496
<i>R</i>1; <i>wR</i>2 [all data]	0.0781; 0.1664
GOF	1.006
largest diff peak and hole	0.595 and -0.317

Table 6-12. Crystal Data Collection and Refinement Parameters for Complex 15^{tBu}.

	15^{tBu}
chemical formula	C ₂₄ H ₂₆ B ₂ N ₂ Cl ₄
crystal colour	Yellow
<i>F</i>_w; <i>F</i>(000)	505.89; 262
<i>T</i> (K)	173(2)
wavelength (Å)	0.71073
space group	P-1
<i>a</i> (Å)	5.8598(9)
<i>b</i> (Å)	6.8679(10)
<i>c</i> (Å)	17.032(3)
<i>α</i> (deg)	92.380(7)
<i>β</i> (deg)	94.987(7)
<i>γ</i> (deg)	108.870(6)
<i>Z</i>	1
<i>V</i> (Å³)	644.37(17)
<i>ρ</i>_{calcd} (g·cm⁻³)	1.304
<i>μ</i> (mm⁻¹)	0.474
<i>θ</i> range (deg); completeness	3.612 – 27.642; 0.978
collected reflections; <i>R</i>_σ	6197; 0.1271
unique reflections; <i>R</i>_{int}	6197; 0.0813
<i>R</i>1^a; <i>wR</i>2^b [<i>I</i> > 2σ(<i>I</i>)]	0.0804; 0.1887
<i>R</i>1; <i>wR</i>2 [all data]	0.1213; 0.2176
GOF	1.002
largest diff peak and hole	0.940 and -0.647

Table 6-13. Crystal Data Collection and Refinement Parameters for Complex 16^{tBu}.

	1
chemical formula	C ₂₄ H ₁₇ BF ₆ N
crystal colour	orange
<i>F</i>w; <i>F</i>(000)	444.19; 908
<i>T</i> (K)	173
wavelength (Å)	1.54178
space group	P121/c1
<i>a</i> (Å)	9.0824(4)
<i>b</i> (Å)	22.2704(10)
<i>c</i> (Å)	10.3537(4)
<i>α</i> (deg)	90
<i>β</i> (deg)	90.631(4)
<i>γ</i> (deg)	90
<i>Z</i>	4
<i>V</i> (Å³)	2094.10(15)
<i>ρ</i>_{calcd} (g·cm⁻³)	1.409
<i>μ</i> (mm⁻¹)	1.026
<i>θ</i> range (deg); completeness	1.984 – 68.245; 0.954
collected reflections; <i>R</i>_σ	15951; 0.0580
unique reflections; <i>R</i>_{int}	15951; 0.0627
<i>R</i>1^a; <i>wR</i>2^b [<i>I</i> > 2σ(<i>I</i>)]	0.0787; 0.2218
<i>R</i>1; <i>wR</i>2 [all data]	0.0874; 0.2292
GOF	1.120
largest diff peak and hole	0.271 and -0.440

APPENDIX: PERMISSIONS

Permission from the Royal Society of Chemistry:

Author reusing their own work published by the Royal Society of Chemistry

You do not need to request permission to reuse your own figures, diagrams, etc, that were originally published in a Royal Society of Chemistry publication. However, permission should be requested for use of the whole article or chapter except if reusing it in a thesis. If you are including an article or book chapter published by us in your thesis please ensure that your co-authors are aware of this.

Reuse of material that was published originally by the Royal Society of Chemistry must be accompanied by the appropriate acknowledgement of the publication. The form of the acknowledgement is dependent on the journal in which it was published originally, as detailed in 'Acknowledgements'.

Permission from the American Chemical Society:



[Home](#) [Create Account](#) [Help](#)



Title: Zirconocene-Based Methods for the Preparation of BN-Indenes: Application to the Synthesis of 1,5-Dibora-4a,8a-diaza-1,2,3,5,6,7-hexaaryl-4,8-dimethyl-s-indacenes
Author: Matthew M. Morgan, Evan A. Patrick, J. Mikko Rautiainen, et al
Publication: Organometallics
Publisher: American Chemical Society
Date: Jul 1, 2017
Copyright © 2017, American Chemical Society

[LOGIN](#)

If you're a [copyright.com](#) user, you can login to RightsLink using your copyright.com credentials. Already a [RightsLink](#) user or want to [learn more?](#)

PERMISSION/LICENSE IS GRANTED FOR YOUR ORDER AT NO CHARGE

This type of permission/license, instead of the standard Terms & Conditions, is sent to you because no fee is being charged for your order. Please note the following:

- Permission is granted for your request in both print and electronic formats, and translations.
- If figures and/or tables were requested, they may be adapted or used in part.
- Please print this page for your records and send a copy of it to your publisher/graduate school.
- Appropriate credit for the requested material should be given as follows: "Reprinted (adapted) with permission from (COMPLETE REFERENCE CITATION). Copyright (YEAR) American Chemical Society." Insert appropriate information in place of the capitalized words.
- One-time permission is granted only for the use specified in your request. No additional uses are granted (such as derivative works or other editions). For any other uses, please submit a new request.

References

1. Anthony, J. E. *Chemical Reviews* **2006**, *106*, 5028-5048.
2. Anthony, J. E. *Nature Materials* **2014**, *13*, 773-775.
3. Elbing, M.; Bazan, G. C. *Angewandte Chemie International Edition* **2008**, *47*, 834-838.
4. Usta, H.; Facchetti, A.; Marks, T. J. *Accounts of Chemical Research* **2011**, *44*, 501-510.
5. Shigehiro, Y.; Kohei, T. *Chemistry Letters* **2005**, *34*, 2-7.
6. Entwistle, C. D.; Marder, T. B. *Chemistry of Materials* **2004**, *16*, 4574-4585.
7. Entwistle, C. D.; Marder, T. B. *Angewandte Chemie-International Edition* **2002**, *41*, 2927-2931.
8. Araneda, J. F.; Neue, B.; Piers, W. E. *Angewandte Chemie-International Edition* **2012**, *51*, 9977-9979.
9. Yamaguchi, S.; Xu, C. H.; Tamao, K. *Journal of the American Chemical Society* **2003**, *125*, 13662-13663.
10. Baumgartner, T. *Accounts of Chemical Research* **2014**, *47*, 1613-1622.
11. Ren, Y.; Baumgartner, T. *Dalton Transactions* **2012**, *41*, 7792-7800.
12. Wakamiya, A.; Mori, K.; Yamaguchi, S. *Angewandte Chemie International Edition* **2007**, *46*, 4273-4276.
13. Kaloni, T. P.; Giesbrecht, P. K.; Schreckenbach, G.; Freund, M. S. *Chemistry of Materials* **2017**, *29*, 10248-10283.
14. Hissler, M.; Dyer, P. W.; Reau, R. *Coordination Chemistry Reviews* **2003**, *244*, 1-44.
15. Stock, A.; Pohland, E. *Berichte Der Deutschen Chemischen Gesellschaft* **1926**, *59*, 2210-2215.
16. Dewar, M. J. S.; Kubba, V. P.; Pettit, R. *Journal of the Chemical Society* **1958**, 3073-3076.
17. Morgan, M. M.; Piers, W. E. *Dalton Trans.* **2016**, *45*, 5920-5924.
18. Bosdet, M. J. D.; Piers, W. E. *Canadian Journal of Chemistry* **2009**, *87*, 8-29.
19. Bosdet, M. J. D.; Piers, W. E.; Sorensen, T. S.; Parvez, M. *Angewandte Chemie-International Edition* **2007**, *46*, 4940-4943.
20. Jaska, C. A.; Emslie, D. J. H.; Bosdet, M. J. D.; Piers, W. E.; Sorensen, T. S.; Parvez, M. *Journal of the American Chemical Society* **2006**, *128*, 10885-10896.
21. Neue, B.; Araneda, J. F.; Piers, W. E.; Parvez, M. *Angewandte Chemie International Edition* **2013**, *52*, 9966-9969.
22. Liu, Z.; Marder, T. B., B-N versus C-C: How similar are they? In *Angewandte Chemie - International Edition* 2008; Vol. 47, pp 242-244.
23. Campbell, P. G.; Campbell, P. G.; Marwitz, A. J. V.; Liu, S.-Y., Recent Advances in Azaborine Chemistry. In *Angewandte Chemie.*, Internatio ed.: Weinheim/Bergstr :, 2012; Vol. 51, pp 6074-6092.
24. Wang, T.; Dou, C.; Liu, J.; Wang, L. *Chemistry - A European Journal* **2018**, *24*, 13043-13048.
25. Krieg, M.; Reicherter, F.; Haiss, P.; Stroebale, M.; Eichele, K.; Treanor, M.-J.; Schaub, R.; Bettinger, H. F. *Angewandte Chemie-International Edition* **2015**, *54*, 8284-8286.
26. Xu, S.; Zakharov, L. N.; Liu, S.-Y. *Journal of the American Chemical Society* **2011**, *133*, 20152-20155.

27. Braunschweig, H.; Damme, A.; Jimenez-Halla, J. O. C.; Pfaffinger, B.; Radacki, K.; Wolf, J. *Angewandte Chemie International Edition* **2012**, *51*, 10034-10037.
28. Liu, X.; Zhang, Y.; Li, B.; Zakharov, L. N.; Vasiliu, M.; Dixon, D. A.; Liu, S.-Y. *Angewandte Chemie International Edition* **2016**, *55*, 8333-8337.
29. Ashe, A. J.; Fang, X. D. *Organic Letters* **2000**, *2*, 2089-2091.
30. Abbey, E. R.; Lamm, A. N.; Baggett, A. W.; Zakharov, L. N.; Liu, S.-Y. *Journal of the American Chemical Society* **2013**, *135*, 12908-12913.
31. Baggett, A. W.; Guo, F.; Li, B.; Liu, S.-Y.; Jaekle, F. *Angewandte Chemie-International Edition* **2015**, *54*, 11191-11195.
32. Pan, J.; Kampf, J. W.; Ashe, A. J., III. *Organic Letters* **2007**, *9*, 679-681.
33. McConnell, C. R.; Haeffner, F.; Baggett, A. W.; Liu, S.-Y. *Journal of the American Chemical Society* **2019**.
34. Brown, A. N.; Li, B.; Liu, S.-Y. *Journal of the American Chemical Society* **2015**, *137*, 8932-8935.
35. Braunschweig, H.; Kupfer, T. *Chemical Communications* **2011**, *47*, 10903-10914.
36. Braunschweig, H.; Hoerl, C.; Mailaender, L.; Radacki, K.; Wahler, J. *Chemistry-a European Journal* **2014**, *20*, 9858-9861.
37. Couchman, S. A.; Thompson, T. K.; Wilson, D. J. D.; Dutton, J. L.; Martin, C. D. *Chemical Communications* **2014**, *50*, 11724-11726.
38. Braunschweig, H.; Celik, M. A.; Hupp, F.; Krummenacher, I.; Mailaender, L. *Angewandte Chemie-International Edition* **2015**, *54*, 6347-6351.
39. Braunschweig, H.; Hupp, F.; Krummenacher, I.; Mailaender, L.; Rauch, F. *Chemistry-a European Journal* **2015**, *21*, 17844-17849.
40. Braunschweig, H.; Geetharani, K.; Jimenez-Halla, J. O. C.; Schaefer, M. *Angewandte Chemie-International Edition* **2014**, *53*, 3500-3504.
41. Zhao, P.; Nettleton, D. O.; Karki, R. G.; Zecri, F. J.; Liu, S.-Y. *Chemmedchem* **2017**, *12*, 358-361.
42. Boknevit, K.; Italia, J. S.; Li, B.; Chatterjee, A.; Liu, S.-Y. *Chemical Science* **2019**.
43. Dewar, M. J. S.; Dietz, R. *Journal of the Chemical Society* **1959**, 2728-2730.
44. Dewar, M. J. S.; Kubba, V. P. *Journal of Organic Chemistry* **1960**, *25*, 1722-1724.
45. Dewar, M. J. S.; Jones, R. *Journal of the American Chemical Society* **1968**, *90*, 2137-&.
46. Ishibashi, J. S. A.; Marshall, J. L.; Maziere, A.; Lovinger, G. J.; Li, B.; Zakharov, L. N.; Dargelos, A.; Graciaa, A.; Chrostowska, A.; Liu, S.-Y. *Journal of the American Chemical Society* **2014**, *136*, 15414-15421.
47. Wisniewski, S. R.; Guenther, C. L.; Argintaru, O. A.; Molander, G. A. *Journal of Organic Chemistry* **2014**, *79*, 365-378.
48. Davies, G. H. M.; Zhou, Z.-Z.; Jouffroy, M.; Molander, G. A. *Journal of Organic Chemistry* **2017**, *82*, 549-555.
49. Paetzold, P.; Stanescu, C.; Stubenrauch, J. R.; Bienmuller, M.; Englert, U. *Zeitschrift Fur Anorganische Und Allgemeine Chemie* **2004**, *630*, 2632-2640.
50. Zhuang, F.-D.; Han, J.-M.; Tang, S.; Yang, J.-H.; Chen, Q.-R.; Wang, J.-Y.; Pei, J. *Organometallics* **2017**, *36*, 2479-2482.
51. Molander, G. A.; Wisniewski, S. R.; Amani, J. *Organic Letters* **2014**, *16*, 5636-5639.
52. Molander, G. A.; Amani, J.; Wisniewski, S. R. *Organic Letters* **2014**, *16*, 6024-6027.
53. Molander, G. A.; Wisniewski, S. R. *Journal of Organic Chemistry* **2014**, *79*, 6663-6678.

54. Molander, G. A.; Wisniewski, S. R.; Traister, K. M. *Organic Letters* **2014**, *16*, 3692-3695.
55. Dewar, M. J. S.; Hashmall; Kubba, V. P. *Journal of Organic Chemistry* **1964**, *29*, 1755-&.
56. Dou, C.; Long, X.; Ding, Z.; Xie, Z.; Liu, J.; Wang, L. *Angewandte Chemie International Edition* **2016**, *55*, 1436-1440.
57. Liu, Z.; Ishibashi, J. S. A.; Darrigan, C.; Dargelos, A.; Chrostowska, A.; Li, B.; Vasiliu, M.; Dixon, D. A.; Liu, S.-Y. *Journal of the American Chemical Society* **2017**, *139*, 6082-6085.
58. Wang, X.-Y.; Narita, A.; Feng, X.; Muellen, K. *Journal of the American Chemical Society* **2015**, *137*, 7668-7671.
59. Hatakeyama, T.; Hashimoto, S.; Seki, S.; Nakamura, M. *Journal of the American Chemical Society* **2011**, *133*, 18614-18617.
60. Hatakeyama, T.; Hashimoto, S.; Oba, T.; Nakamura, M. *Journal of the American Chemical Society* **2012**, *134*, 19600-19603.
61. Wang, X.-Y.; Lin, H.-R.; Lei, T.; Yang, D.-C.; Zhuang, F.-D.; Wang, J.-Y.; Yuan, S.-C.; Pei, J. *Angewandte Chemie-International Edition* **2013**, *52*, 3117-3120.
62. Wang, X.-Y.; Zhuang, F.-D.; Wang, R.-B.; Wang, X.-C.; Cao, X.-Y.; Wang, J.-Y.; Pei, J. *Journal of the American Chemical Society* **2014**, *136*, 3764-3767.
63. Wang, X.-Y.; Wang, J.-Y.; Pei, J. *Chemistry-a European Journal* **2015**, *21*, 3528-3539.
64. Sun, C.-J.; Wang, N.; Peng, T.; Yin, X.; Wang, S.; Chen, P. *Inorganic Chemistry* **2019**, *58*, 3591-3595.
65. Wang, X.-Y.; Zhuang, F.-D.; Wang, X.-C.; Cao, X.-Y.; Wang, J.-Y.; Pei, J. *Chemical Communications* **2015**, *51*, 4368-4371.
66. Ma, C.; Zhang, J.; Li, J.; Cui, C. *Chemical Communications* **2015**, *51*, 5732-5734.
67. Li, G.; Zhao, Y.; Li, J.; Cao, J.; Zhu, J.; Sun, X. W.; Zhang, Q. *Journal of Organic Chemistry* **2015**, *80*, 196-203.
68. Liu, X.; Wu, P.; Li, J.; Cui, C. *Journal of Organic Chemistry* **2015**, *80*, 3737-3744.
69. Su, B.; Li, Y.; Ganguly, R.; Lim, J.; Kinjo, R. *Journal of the American Chemical Society* **2015**, *137*, 11274-11277.
70. Wang, S.; Yang, D.-T.; Lu, J.; Shimogawa, H.; Gong, S.; Wang, X.; Møllerup, S. K.; Wakamiya, A.; Chang, Y.-L.; Yang, C.; Lu, Z.-H., In Situ Solid-State Generation of (BN) 2 - Pyrenes and Electroluminescent Devices. Internatio ed.: Weinheim/Bergstr :, 2015; Vol. 54, pp 15074-15078.
71. Fagan, P. J.; Nugent, W. A. *Journal of the American Chemical Society* **1988**, *110*, 2310-2312.
72. Ma, W.; Yu, C.; Chen, T.; Xu, L.; Zhang, W.-X.; Xi, Z. *Chemical Society Reviews* **2017**, *46*, 1160-1192.
73. Fagan, P. J.; Nugent, W. A.; Calabrese, J. C. *Journal of the American Chemical Society* **1994**, *116*, 1880-1889.
74. Freeman, W. P.; Tilley, T. D.; Liable-Sands, L. M.; Rheingold, A. L. *Journal of the American Chemical Society* **1996**, *118*, 10457-10468.
75. Hay, C.; Hissler, M.; Fischmeister, C.; Rault-Berthelot, J.; Toupet, L.; Nyulászi, L.; Réau, R. *Chemistry – A European Journal* **2001**, *7*, 4222-4236.
76. Crassous, J.; Réau, R. *Dalton Transactions* **2008**, 6865-6876.

77. Rosenthal, U.; Ohff, A.; Baumann, W.; Tillack, A.; Görls, H.; Burlakov, V. V.; Shur, V. B. *Zeitschrift für anorganische und allgemeine Chemie* **1995**, 621, 77-83.
78. Fan, C.; Piers, W. E.; Parvez, M. *Angewandte Chemie International Edition* **2009**, 48, 2955-2958.
79. Houghton, A. Y.; Karttunen, V. A.; Piers, W. E.; Tuononen, H. M. *Chemical Communications* **2014**, 50, 1295-1298.
80. Houghton, A. Y.; Hurmalainen, J.; Mansikkamäki, A.; Piers, W. E.; Tuononen, H. M. *Nature Chemistry* **2014**, 6, 983.
81. Rolf Gleiter, G. H., *Aromaticity and Other Conjugation Effects*. Wiley-VCH: Weinheim Germany, 2012.
82. Krygowski, T. M.; Cyrański, M. K. *Chemical Reviews* **2001**, 101, 1385-1420.
83. Krygowski, T. M.; Szatylowicz, H.; Stasyuk, O. A.; Dominikowska, J.; Palusiak, M. *Chemical Reviews* **2014**, 114, 6383-6422.
84. Cyrański, M. K.; Krygowski, T. M.; Katritzky, A. R.; Schleyer, P. v. R. *The Journal of Organic Chemistry* **2002**, 67, 1333-1338.
85. Roberts, J. D.; Streitwieser, A.; Regan, C. M. *Journal of the American Chemical Society* **1952**, 74, 4579-4582.
86. Schleyer, P. v. R.; Maerker, C.; Dransfeld, A.; Jiao, H.; van Eikema Hommes, N. J. R. *Journal of the American Chemical Society* **1996**, 118, 6317-6318.
87. Juselius, J.; Sundholm, D.; Gauss, J. *Journal of Chemical Physics* **2004**, 121, 3952-3963.
88. Fliegl, H.; Taubert, S.; Lehtonen, O.; Sundholm, D. *Physical Chemistry Chemical Physics* **2011**, 13, 20500-20518.
89. Morgan, M. M.; Patrick, E. A.; Rautiainen, J. M.; Spasyuk, D. M.; Tuononen, H. M.; Piers, W. E. *Organometallics* **2017**, 36, 2541-2551.
90. Emslie, D. J. H.; Piers, W. E.; Parvez, M. *Angewandte Chemie-International Edition* **2003**, 42, 1252-1255.
91. Wang, X.; Zhang, F.; Liu, J.; Tang, R.; Fu, Y.; Wu, D.; Xu, Q.; Zhuang, X.; He, G.; Feng, X. *Organic Letters* **2013**, 15, 5714-5717.
92. Mueller, M.; Maichle-Moessmer, C.; Bettinger, H. F. *Angewandte Chemie-International Edition* **2014**, 53, 9380-9383.
93. Mueller, M.; Behnle, S.; Maichle-Moessmer, C.; Bettinger, H. F. *Chemical Communications* **2014**, 50, 7821-7823.
94. Wang, B. J.; Groziak, M. P., Recent Developments in the Chemistry of Boron Heterocycles. In *Advances in Heterocyclic Chemistry, Vol 118*, Scriven, E. F. V.; Ramsden, C. A., Eds. 2016; Vol. 118, pp 47-90.
95. Tasiar, M.; Gryko, D. T. *Journal of Organic Chemistry* **2016**, 81, 6580-6586.
96. Huang, H.; Pan, Z.; Cui, C. *Chemical Communications* **2016**, 52, 4227-4230.
97. Baggett, A. W.; Vasiliu, M.; Li, B.; Dixon, D. A.; Liu, S.-Y. *Journal of the American Chemical Society* **2015**, 137, 5536-5541.
98. Wan, W.-M.; Baggett, A. W.; Cheng, F.; Lin, H.; Liu, S.-Y.; Jakle, F. *Chemical Communications* **2016**, 52, 13616-13619.
99. Zhao, R.; Dou, C.; Xie, Z.; Liu, J.; Wang, L. *Angewandte Chemie-International Edition* **2016**, 55, 5313-5317.
100. Knack, D. H.; Marshall, J. L.; Harlow, G. P.; Dudzik, A.; Szaleniec, M.; Liu, S.-Y.; Heider, J. *Angewandte Chemie-International Edition* **2013**, 52, 2599-2601.

101. Liu, L.; Marwitz, A. J. V.; Matthews, B. W.; Liu, S.-Y. *Angewandte Chemie-International Edition* **2009**, *48*, 6817-6819.
102. Lee, H.; Fischer, M.; Shoichet, B. K.; Liu, S.-Y. *Journal of the American Chemical Society* **2016**, *138*, 12021-12024.
103. Helten, H. *Chemistry-a European Journal* **2016**, *22*, 12972-12982.
104. Ishida, N.; Narumi, M.; Murakami, M. *Organic Letters* **2008**, *10*, 1279-1281.
105. Yuan, K.; Suzuki, N.; Mellerup, S. K.; Wang, X.; Yamaguchi, S.; Wang, S. *Organic Letters* **2016**, *18*, 720-723.
106. Hafner, K.; Stowasser, B.; Krimmer, H. P.; Fischer, S.; Bohm, M. C.; Lindner, H. J. *Angewandte Chemie-International Edition in English* **1986**, *25*, 630-632.
107. Nendel, M.; Goldfuss, B.; Houk, K. N.; Hafner, K. *Journal of Molecular Structure-Theochem* **1999**, *461*, 23-28.
108. Tobe, Y. *Chemical Record* **2015**, *15*, 86-96.
109. Frederickson, C. K.; Zalcharov, L. N.; Haley, M. M. *Journal of the American Chemical Society* **2016**, *138*, 16827-16838.
110. Jordan, R. F.; Taylor, D. F. *Journal of the American Chemical Society* **1989**, *111*, 778-779.
111. Guram, A. S.; Jordan, R. F. *Organometallics* **1991**, *10*, 3470-3479.
112. Jordan, R. F.; Guram, A. S. *Organometallics* **1990**, *9*, 2116-2123.
113. Chien, J. C. W.; Tsai, W. M.; Rausch, M. D. *Journal of the American Chemical Society* **1991**, *113*, 8570-8571.
114. Montavon, T. J.; Tuerkmen, Y. E.; Shamsi, N. A.; Miller, C.; Sumaria, C. S.; Rawal, V. H.; Kozmin, S. A. *Angewandte Chemie-International Edition* **2013**, *52*, 13576-13579.
115. Antoniotti, S.; Dalla, V.; Dunach, E. *Angewandte Chemie-International Edition* **2010**, *49*, 7860-7888.
116. Luinstra, G. A. *Journal of Organometallic Chemistry* **1996**, *517*, 209-215.
117. Sheikh, S. U. *Journal of Thermal Analysis* **1980**, *18*, 299-306.
118. Ishida, N.; Moriya, T.; Goya, T.; Murakami, M. *Journal of Organic Chemistry* **2010**, *75*, 8709-8712.
119. Shaikh, A. C.; Ranade, D. S.; Thorat, S.; Maity, A.; Kulkarni, P. P.; Gonnade, R. G.; Munshi, P.; Patil, N. T. *Chemical Communications* **2015**, *51*, 16115-16118.
120. Piers, W. E.; Bourke, S. C.; Conroy, K. D. *Angewandte Chemie-International Edition* **2005**, *44*, 5016-5036.
121. Wang, C. C.; Tang, T. H.; Wu, L. C.; Wang, Y. *Acta Crystallographica a-Foundation and Advances* **2004**, *60*, 488-493.
122. Dunitz, J. D.; Kruger, C.; Irngartinger, H.; Maverick, E. F.; Wang, Y.; Nixdorf, M. *Angewandte Chemie-International Edition in English* **1988**, *27*, 387-389.
123. Hertwig, R. H.; Holthausen, M. C.; Koch, W.; Maksic, Z. B. *Angewandte Chemie-International Edition* **1994**, *33*, 1192-1194.
124. Moroni, L.; Gellini, C.; Salvi, P. R. *Journal of Molecular Structure-Theochem* **2004**, *677*, 1-5.
125. Hafner, K.; Krimmer, H. P. *Angewandte Chemie-International Edition in English* **1980**, *19*, 199-201.
126. Bachmann, R.; Gerson, F.; Gescheidt, G.; Hafner, K. *Magnetic Resonance in Chemistry* **1995**, *33*, S60-S65.

127. Cary, D. R.; Green, J. C.; O'Hare, D. *Angewandte Chemie-International Edition* **1997**, *36*, 2618-2620.
128. Bheemireddy, S. R.; Ubaldo, P. C.; Rose, P. W.; Finke, A. D.; Zhuang, J.; Wang, L.; Plunkett, K. N. *Angewandte Chemie-International Edition* **2015**, *54*, 15762-15766.
129. Rose, B. D.; Sumner, N. J.; Filatov, A. S.; Peters, S. J.; Zakharov, L. N.; Petrukhina, M. A.; Haley, M. M. *Journal of the American Chemical Society* **2014**, *136*, 9181-9189.
130. Ly, H. V.; Tuononen, H. M.; Parvez, M.; Roesler, R. *Chemical Communications* **2007**, 4522-4524.
131. Ghosh, D.; Periyasamy, G.; Pati, S. K. *Physical Chemistry Chemical Physics* **2011**, *13*, 20627-20636.
132. Morgan, M. M.; Rautiainen, J. M.; Piers, W. E.; Tuononen, H. M.; Gendy, C. *Dalton Transactions* **2018**, *47*, 734-741.
133. Belanger-Chabot, G.; Braunschweig, H.; Roy, D. K. *European Journal of Inorganic Chemistry* **2017**, 4353-4368.
134. Abbey, E. R.; Liu, S.-Y. *Organic & Biomolecular Chemistry* **2013**, *11*, 2060-2069.
135. Baggett, A. W.; Liu, S.-Y. *Journal of the American Chemical Society* **2017**, *139*, 15259-15264.
136. Lamm, A. N.; Garner, E. B., III; Dixon, D. A.; Liu, S.-Y. *Angewandte Chemie-International Edition* **2011**, *50*, 8157-8160.
137. Xu, S.; Mikulas, T. C.; Zakharov, L. N.; Dixon, D. A.; Liu, S.-Y. *Angewandte Chemie-International Edition* **2013**, *52*, 7527-7531.
138. Ishibashi, J. S. A.; Dargelos, A.; Darrigan, C.; Chrostowska, A.; Liu, S.-Y. *Organometallics* **2017**, *36*, 2494-2497.
139. Frederickson, C. K.; Rose, B. D.; Haley, M. M. *Accounts of Chemical Research* **2017**, *50*, 977-987.
140. Marshall, J. L.; O'Neal, N. J.; Zakharov, L. N.; Haley, M. M. *Journal of Organic Chemistry* **2016**, *81*, 3674-3680.
141. Rudebusch, G. E.; Zafra, J. L.; Jorner, K.; Fukuda, K.; Marshall, J. L.; Arrechea-Marcos, I.; Espejo, G. L.; Ponce Ortiz, R.; Gomez-Garcia, C. J.; Zakharov, L. N.; Nakano, M.; Ottosson, H.; Casado, J.; Haley, M. M. *Nature Chemistry* **2016**, *8*, 753-759.
142. Zhu, C.; Guo, Z.-H.; Mu, A. U.; Liu, Y.; Wheeler, S. E.; Fang, L. *Journal of Organic Chemistry* **2016**, *81*, 4347-4352.
143. Segawa, Y.; Suzuki, Y.; Yamashita, M.; Nozaki, K. *Journal of the American Chemical Society* **2008**, *130*, 16069-16079.
144. Segawa, Y.; Yamashita, M.; Nozaki, K. *Science* **2006**, *314*, 113-115.
145. Pécharman, A.-F.; Colebatch, A. L.; Hill, M. S.; McMullin, C. L.; Mahon, M. F.; Weetman, C. *Nature Communications* **2017**, *8*, 15022-15022.
146. Braunschweig, H.; Chiu, C.-W.; Radacki, K.; Kupfer, T. *Angewandte Chemie-International Edition* **2010**, *49*, 2041-2044.
147. Monot, J.; Solov'yev, A.; Bonin-Dubarle, H.; Derat, E.; Curran, D. P.; Robert, M.; Fensterbank, L.; Malacria, M.; Lacote, E. *Angewandte Chemie-International Edition* **2010**, *49*, 9166-9169.
148. Meurling, L. *Acta Chemica Scandinavica Series B-Organic Chemistry and Biochemistry* **1974**, *B 28*, 295-300.

149. Bock, P. L.; Boschett, D. J.; Rasmussen, Jr.; Demers, J. P.; Whiteside, G. M. *Journal of the American Chemical Society* **1974**, *96*, 2814-2825.
150. Igau, A.; Gladysz, J. A. *Organometallics* **1991**, *10*, 2327-2334.
151. Bertermann, R.; Braunschweig, H.; Dewhurst, R. D.; Hoerl, C.; Kramer, T.; Krummenacher, I. *Angewandte Chemie-International Edition* **2014**, *53*, 5453-5457.
152. Moemming, C. M.; Otten, E.; Kehr, G.; Froehlich, R.; Grimme, S.; Stephan, D. W.; Erker, G. *Angewandte Chemie-International Edition* **2009**, *48*, 6643-6646.
153. Taylor, J. W.; McSkimming, A.; Guzman, C. F.; Harman, W. H. *Journal of the American Chemical Society* **2017**, *139*, 11032-11035.
154. Villiers, C.; Dognon, J.-P.; Pollet, R.; Thuery, P.; Ephritikhine, M. *Angewandte Chemie-International Edition* **2010**, *49*, 3465-3468.
155. von Wolff, N.; Lefèvre, G.; Berthet, J. C.; Thuéry, P.; Cantat, T. *ACS Catalysis* **2016**, *6*, 4526-4535.
156. Voss, T.; Mahdi, T.; Otten, E.; Froehlich, R.; Kehr, G.; Stephan, D. W.; Erker, G. *Organometallics* **2012**, *31*, 2367-2378.
157. Wang, B.; Li, Y.; Ganguly, R.; Hirao, H.; Kinjo, R. *Nature Communications* **2016**, *7*.
158. Wu, D.; Kong, L.; Li, Y.; Ganguly, R.; Kinjo, R. *Nature Communications* **2015**, *6*.
159. Methcohn, O.; Gronowit, S. *Chemical Communications* **1966**, 81-&.
160. Pietruszka, J.; Simon, R. C.; Kruska, F.; Braun, M. *European Journal of Organic Chemistry* **2009**, 6217-6224.
161. Wöhrle, D.; Meissner, D. *Advanced Materials* **1991**, *3*, 129-138.
162. Beaujuge, P. M.; Fréchet, J. M. J. *Journal of the American Chemical Society* **2011**, *133*, 20009-20029.
163. Dennler, G.; Scharber, M. C.; Brabec, C. J. *Advanced Materials* **2009**, *21*, 1323-1338.
164. Günes, S.; Neugebauer, H.; Sariciftci, N. S. *Chemical Reviews* **2007**, *107*, 1324-1338.
165. Mishra, A.; Bäuerle, P. *Angewandte Chemie International Edition* **2012**, *51*, 2020-2067.
166. Thompson, B. C.; Fréchet, J. M. J. *Angewandte Chemie International Edition* **2008**, *47*, 58-77.
167. He, Z.; Zhong, C.; Huang, X.; Wong, W.-Y.; Wu, H.; Chen, L.; Su, S.; Cao, Y. *Advanced Materials* **2011**, *23*, 4636-4643.
168. Duan, C.; Huang, F.; Cao, Y. *Journal of Materials Chemistry* **2012**, *22*, 10416-10434.
169. Dou, L.; You, J.; Hong, Z.; Xu, Z.; Li, G.; Street, R. A.; Yang, Y. *Advanced Materials* **2013**, *25*, 6642-6671.
170. Zhang, S.; Ye, L.; Zhao, W.; Liu, D.; Yao, H.; Hou, J. *Macromolecules* **2014**, *47*, 4653-4659.
171. Po, R.; Bernardi, A.; Calabrese, A.; Carbonera, C.; Corso, G.; Pellegrino, A. *Energy & Environmental Science* **2014**, *7*, 925-943.
172. Zhang, G.; Zhao, J.; Chow, P. C. Y.; Jiang, K.; Zhang, J.; Zhu, Z.; Zhang, J.; Huang, F.; Yan, H. *Chemical Reviews* **2018**, *118*, 3447-3507.
173. Wadsworth, A.; Moser, M.; Marks, A.; Little, M. S.; Gasparini, N.; Brabec, C. J.; Baran, D.; McCulloch, I. *Chemical Society Reviews* **2019**, *48*, 1596-1625.
174. Zhang, J.; Tan, H. S.; Guo, X.; Facchetti, A.; Yan, H. *Nature Energy* **2018**, *3*, 720-731.
175. Jadhav, T.; Misra, R.; Biswas, S.; Sharma, G. D. *Physical Chemistry Chemical Physics* **2015**, *17*, 26580-26588.
176. Liu, W.; Yao, J.; Zhan, C. *Chinese Journal of Chemistry* **2017**, *35*, 1813-1823.

177. Ding, Z.; Long, X.; Meng, B.; Bai, K.; Dou, C.; Liu, J.; Wang, L. *Nano Energy* **2017**, *32*, 216-224.
178. Grandl, M.; Schepper, J.; Maity, S.; Peukert, A.; von Hauff, E.; Pammer, F. *Macromolecules* **2019**, *52*, 1013-1024.
179. Crossley, D. L.; Cade, I. A.; Clark, E. R.; Escande, A.; Humphries, M. J.; King, S. M.; Vitorica-Yrezabal, I.; Ingleson, M. J.; Turner, M. L. *Chemical Science* **2015**, *6*, 5144-5151.
180. Crossley, D. L.; Cid, J.; Curless, L. D.; Turner, M. L.; Ingleson, M. J. *Organometallics* **2015**, *34*, 5767-5774.
181. Sen, R.; Singh, S. P.; Johari, P. *The Journal of Physical Chemistry A* **2018**, *122*, 492-504.
182. Sonar, P.; Singh, S. P.; Leclère, P.; Surin, M.; Lazzaroni, R.; Lin, T. T.; Dodabalapur, A.; Sellinger, A. *Journal of Materials Chemistry* **2009**, *19*, 3228-3237.
183. Terao, J.; Nakamura, M.; Kambe, N. *Chemical Communications* **2009**, 6011-6013.
184. Goh, K. K. K.; Sinha, A.; Fraser, C.; Young, R. D. *RSC Advances* **2016**, *6*, 42708-42712.
185. Henne, A. L.; Newman, M. S. *Journal of the American Chemical Society* **1938**, *60*, 1697-1698.
186. Saito, T.; Nishiyama, H.; Tanahashi, H.; Kawakita, K.; Tsurugi, H.; Mashima, K. *Journal of the American Chemical Society* **2014**, *136*, 5161-5170.
187. Noguchi, M.; Suzuki, K.; Kobayashi, J.; Yurino, T.; Tsurugi, H.; Mashima, K.; Yamashita, M. *Organometallics* **2018**, *37*, 1833-1836.
188. Yamamoto, K.; Chan, K. W.; Mougél, V.; Nagae, H.; Tsurugi, H.; Safonova, O. V.; Mashima, K.; Copéret, C. *Chemical Communications* **2018**, *54*, 3989-3992.
189. Lee, J.; Back, H.; Kong, J.; Park, D.-W.; Lee, K. *Solar Energy Materials and Solar Cells* **2012**, *98*, 208-211.
190. Nazari, M.; Cielechowicz, E.; Welsh, T. A.; Welch, G. C. *New Journal of Chemistry* **2019**, *43*, 5187-5195.
191. Sun, Y.; Seo, J. H.; Takacs, C. J.; Seifert, J.; Heeger, A. J. *Advanced Materials* **2011**, *23*, 1679-1683.
192. Huang, J.; Li, Y. *Frontiers in Chemistry* **2018**, *6*, 1-22.
193. Dash, B. P.; Hamilton, I.; Tate, D. J.; Crossley, D. L.; Kim, J.-S.; Ingleson, M. J.; Turner, M. L. *Journal of Materials Chemistry C* **2019**, *7*, 718-724.
194. Zhang, F.; Hu, Y.; Schuettfort, T.; Di, C.-a.; Gao, X.; McNeill, C. R.; Thomsen, L.; Mannsfeld, S. C. B.; Yuan, W.; Sirringhaus, H.; Zhu, D. *Journal of the American Chemical Society* **2013**, *135*, 2338-2349.
195. Sugiyama, F.; Kleinschmidt, A. T.; Kayser, L. V.; Rodriguez, D.; Finn, M.; Alkhadra, M. A.; Wan, J. M. H.; Ramírez, J.; Chiang, A. S. C.; Root, S. E.; Savagatrup, S.; Lipomi, D. J. *Polymer Chemistry* **2018**, *9*, 4354-4363.
196. Rozema, M. J.; Sidduri, A.; Knochel, P. *The Journal of Organic Chemistry* **1992**, *57*, 1956-1958.
197. Kim, J. H.; Ko, Y. O.; Bouffard, J.; Lee, S.-g. *Chemical Society Reviews* **2015**, *44*, 2489-2507.
198. Turkoglu, G.; Cinar, M. E.; Ozturk, T. *Topics in Current Chemistry* **2017**, *375*, 84.
199. Frederickson, C. K.; Barker, J. E.; Dressler, J. J.; Zhou, Z.; Hanks, E. R.; Bard, J. P.; Zakharov, L. N.; Petrukhina, M. A.; Haley, M. M. *Synlett* **2018**, *29*, 2562-2566.
200. Nishida, J.-i.; Tsukaguchi, S.; Yamashita, Y. *Chemistry – A European Journal* **2012**, *18*, 8964-8970.

201. Sbargoud, K.; Mamada, M.; Marrot, J.; Tokito, S.; Yassar, A.; Frigoli, M. *Chemical Science* **2015**, *6*, 3402-3409.
202. Hu, P.; Lee, S.; Herng, T. S.; Aratani, N.; Gonçalves, T. P.; Qi, Q.; Shi, X.; Yamada, H.; Huang, K.-W.; Ding, J.; Kim, D.; Wu, J. *Journal of the American Chemical Society* **2016**, *138*, 1065-1077.
203. Dressler, J. J.; Zhou, Z.; Marshall, J. L.; Kishi, R.; Takamuku, S.; Wei, Z.; Spisak, S. N.; Nakano, M.; Petrukhina, M. A.; Haley, M. M. *Angewandte Chemie International Edition* **2017**, *56*, 15363-15367.
204. Dressler, J. J.; Teraoka, M.; Espejo, G. L.; Kishi, R.; Takamuku, S.; Gómez-García, C. J.; Zakharov, L. N.; Nakano, M.; Casado, J.; Haley, M. M. *Nature Chemistry* **2018**, *10*, 1134-1140.
205. Giustra, Z. X.; Liu, S.-Y. *Journal of the American Chemical Society* **2018**, *140*, 1184-1194.
206. Coropceanu, V.; Cornil, J.; da Silva Filho, D. A.; Olivier, Y.; Silbey, R.; Brédas, J.-L. *Chemical Reviews* **2007**, *107*, 926-952.
207. Park, S. K.; Jackson, T. N.; Anthony, J. E.; Mourey, D. A. *Applied Physics Letters* **2007**, *91*, 063514.
208. Ishibashi, J. S. A.; Darrigan, C.; Chrostowska, A.; Li, B.; Liu, S.-Y. *Dalton Transactions* **2019**, *48*, 2807-2812.
209. Chen, M.; Nie, H.; Song, B.; Li, L.; Sun, J. Z.; Qin, A.; Tang, B. Z. *Journal of Materials Chemistry C* **2016**, *4*, 2901-2908.
210. Lalancette, J. M.; Rollin, G.; Dumas, P. *Canadian Journal of Chemistry* **1972**, *50*, 3058-3062.
211. Dunsford, J. J.; Clark, E. R.; Ingleson, M. J. *Angewandte Chemie International Edition* **2015**, *54*, 5688-5692.
212. Sheikh, S. U. *Journal of thermal analysis* **1980**, *18*, 299-306.